The Dissertation Committee for Hoang Vi Tran
Certifies that this is the approved version of the following dissertation:

MATERIALS FOR ADVANCED MICROLITHOGRAPHY: POLYMERS FOR 157 NM LITHOGRAPHY AND ACID DIFFUSION MEASUREMENTS

Committee:

C. Grant Willson, Supervisor

Brent L. Iverson

Eric V. Anslyn

David A. Vanden Bout

Jeffrey D. Byers

Materials for Advanced Microlithography: Polymers for 157 nm Lithography and Acid Diffusion Measurements

by

Hoang Vi Tran, B.S., M.A.

Dissertation

Presented to the Faculty of the Graduate School of

The University of Texas at Austin

in Partial Fulfillment

of the Requirements

for the Degree of

Doctor of Philosophy

The University of Texas at Austin

May 2002

Acknowledgements

The work presented in this dissertation would not have been completed without the help and support of the many people involved. I have been extremely fortunate to be able to work with my supervisor, Professor C. Grant Willson. His continuous support, encouragement, guidance, and friendship have helped me develop both personally and professionally and made my days as a graduate student in Austin exceedingly memorable. I could not have imagined myself working for any other man.

Many thanks are due to the graduate students and post-doc with whom I have had the pleasure of working directly in one or more projects: Michael Stewart, Sergei Postnikov, Raymond Hung, and Peter Tattersall. I gratefully acknowledge Tsutomo Shimokawa, David Medeiros, Kyle Patterson, Shintaro Yamada, Sungseo Cho, Takashi Chiba, Timo Rager, and Scott MacDonald for their numerous insightful discussions and advice. I thank all the talented members of the Willson research group for teaching me how to be a team player, and I am forever indebted to Kathleen Sparks for all of her support throughout the years.

I have had the pleasure of working with Dr. Stephen Webber on the fluorescence experiments. Without his help, this part of the acid diffusion project would not be possible. Dr. Douglas Loy and Dr. David Wheeler are gratefully acknowledged for their help and guidance during my stay at Sandia National

Laboratories. I have learned an exceptional amount of silicon chemistry from them and owe them my sincerest gratitude. I am also grateful to the members of my dissertation committee, Professor Eric Anslyn, Professor Brent Iverson, Professor David Vanden Bout, and Dr. Jeffrey Byers, for their careful review of this document and their insightful suggestions. International SEMATECH and the Semiconductor Research Corporation are acknowledged for their generous funding of the projects. Will Conley is also acknowledged for the help he has given the group as our SEMATECH project leader. The employees of International SEMATECH, Danny Miller, Vicky Graffenberg, and Shashi Patel are gratefully acknowledged for their help with the tools used for imaging.

Last, but not least, I thank my friends and family for their unending support. I thank my parents for their love and encouragement. Their guidance and unwavering support has brought me to where I am today.

Materials for Advanced Microlithography: Polymers for 157 nm Lithography and Acid Diffusion Measurements

Publication No._____

Hoang Vi Tran, Ph.D.

The University of Texas at Austin, 2002

Supervisor: C. Grant Willson

In order to print the sub-micron features that are required for advanced integrated circuits, new materials must be designed. This dissertation will focus on the design, synthesis, and evaluation of several novel compounds and polymers for advanced microlithography. Some of these materials are made and evaluated in a photoresist formulation. Others are made to carefully examine the diffusion of photogenerated acid through a thin polymer film in order to study the effects of acid diffusion on linewidth spread as feature sizes shrink.

Several siloxanes and silsesquioxanes have been designed, synthesized, and evaluated as potential polymers for 157 nm lithography. Their low absorbance at this wavelength make this class of polymers particularly attractive. Unfortunately, the low glass transition temperatures of these polymers hinder

their immediate use in resist applications. Several methods are presented to make siloxane and silsesquioxane polymers with higher glass transition temperatures while still retaining their low absorption at 157 nm. These new materials are evaluated lithographically and their potential use in a bilayer resist process is discussed.

Several other materials have been designed and synthesized for acid diffusion studies. These polymers contain groups that are reactive to acid molecules and can also be monitored spectroscopically. One set of polymers contains a covalently-bound acridine molecule that undergoes a dramatic shift in fluorescence when protonated, and therefore the presence of acid can be monitored by fluorescence spectroscopy. Another set of polymers can be monitored by infrared spectroscopy because the presence of acid either causes the lost or formation of a carbonyl group. Sandwich experiments used to measure and study the diffusion of acid molecules are discussed. Diffusion of acid molecules was found to be highly dependent on the glass transition temperature of the matrix polymer. A mechanism for acid migration and quenching is discussed. Several polymer-bound photoacid generators have been made to further study the effects of acid diffusion.

TABLE OF CONTENTS

LIST OF TABLES

LIST OF FIGURES

CHAPTER 1: *INTRODUCTION AND BACKGROUND*

All great inventions change society in such a dramatic fashion that it takes many years to fully comprehend their true impact. Consider how the automobile transformed modern life, changing the way we view distance and time. New industries were formed because transporting goods from one city to another was possible and required less time. Other great inventions such as gunpowder, the atomic bomb, the radio, the telephone, the television, and the airplane, have all transformed our lives in one way or another. The introduction of the world's first "computer on a chip" in 1971, the microprocessor, had the same effect, although a more subtle one. By their presence in objects ranging in sophistication from a simple toaster to a personal computer, microprocessors have improved existing products as well as given us the capability to design new, more advanced products. We are now, at the beginning of this century, only beginning to appreciate the impact of the microprocessor on society. *Fortune* magazine, in 1975, realized this[1]:

> The microprocessor is one of those rare innovations that simultaneously cuts manufacturing costs and adds to the value and capabilities of the product. As a result, the microprocessor has invaded a host of existing products and created new products never before possible.

The story of the microprocessor began with the independent invention of the integrated circuit by Jack Kilby of Texas Instruments and Robert Noyce of

[1] Malone, M. S. *The Big Score: The Billion Dollar Story of Silicon Valley*; Doubleday: New York, 1985; p 141.

Fairchild Semiconductor in 1959. Their invention paved the way for others in the field. The notion was in the air that rather than having single, discrete transistors, it was possible to link several transistors on a single piece of semiconductor material to make an integrated circuit. By the late 1960s, the idea of integrating the components of a calculator onto one general purpose chip was put forth. These chips could then be programmed for specific applications, such as for arithmetic calculations. In fact, the first real application for the microprocessor was the calculator. The idea of a "CPU on a chip" came to reality only through the hard work of Ted Hoff, Federico Faggin, and numerous other engineers at Intel in 1971 who created the world's first microprocessor: the Intel 4004 (Figure 1.1). Through the years numerous other microprocessors have been fabricated by Intel as well as a host of other companies such as AMD, Motorola, Cyrix, and IBM. Each successive processor generation has been more complex than the previous one. The Intel 4004 was fabricated using 10 μm technology and had 2250 transistors. Today's Intel Pentium 4 and AMD Athlon processors are fabricated using 0.18 μm technology and contain over 37 million transistors. Today's microprocessors have over 100 times the computing power of personal computers of just a decade ago.[2] Over a time span of 30 years, the complexity of these processors has grown at a tremendous rate and continues to grow. This rate is made possible by the ability of device manufacturers to cram more components in a given area, thus allowing them to make complex chips with improved capacity, size, speed, and price.

[2] Malone, M. S. *The Microprocessor: A Biography*; Springer-Verlag: New York, 1995; p 10-20.

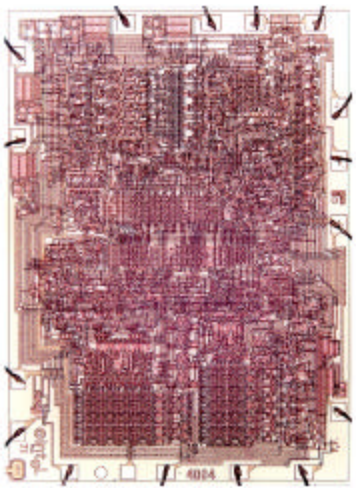

Figure 1.1: The world's first microprocessor, the Intel 4004.[3]

MOORE'S LAW

The number of transistors in an integrated circuit doubles every 18 to 24 months. This trend of increasing circuit density was first observed and predicted by Gordon E. Moore, co-founder of Intel, in 1965.[4] Impressed by the rate at which memory chips improved in capacity, Moore decided to plot the logarithm of the number of transistors in each new generation of chips against time. To his amazement, the graph turned out to be a straight line (Figure 1.2). Moore had originally predicted this trend up to 1975, but Moore's Law has been maintained to this day because of both innovations in semiconductor technology and economic pressures on the industry to produce faster, lower costing chips. Moore's Law is significant not because it correctly predicts the growth in capacity

[3] Photograph obtained from www.intel.com

[4] Moore, G. E. *Electronics* **1965**, *38*, 1.

of chips over the years, but because it provides a guideline for the industry in the years to come. Aside from an unforeseen technological roadblock, companies today could devise business plans five, ten, or even twenty years from now, taking into consideration what new generations of technology are needed in order to maintain the growth seen in Moore's Law. Much of this new technology is driven by advances in microlithography.

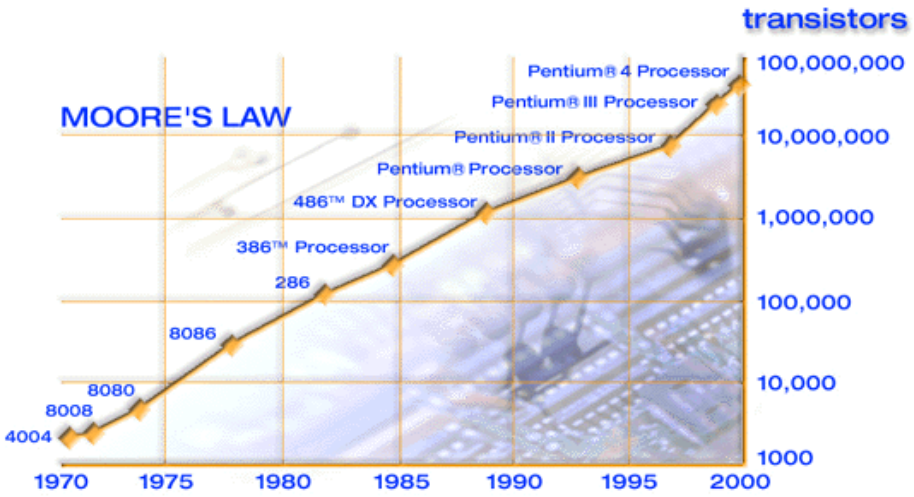

Figure 1.2: Moore's Law – doubling the number of transistors every 18 to 24 months.[3]

MICROLITHOGRAPHY

Microlithography is the process by which intricate circuit patterns on a mask are transferred to a semiconductor substrate. Many cycles of lithographic imaging, metallization, etching, and semiconductor doping are required to form the three-dimensional circuit patterns that are contained in a microprocessor. The sequence of steps for the formation of a Metal Oxide Semiconductor Field Effect Transistor (MOSFET) is outlined in Figure 1.3. A lightly doped P-type silicon is

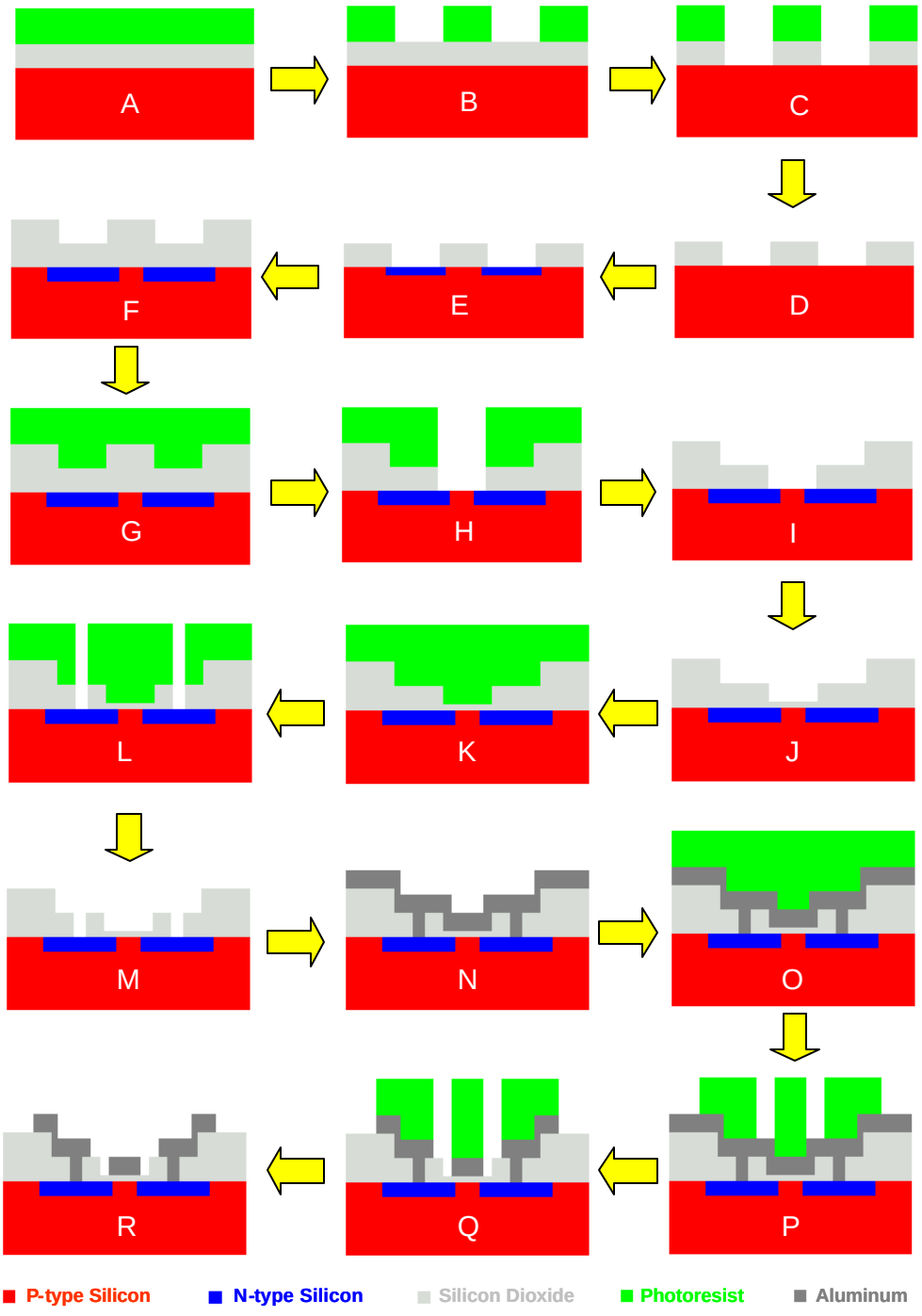

Figure 1.3: Many lithographic steps are required in the fabrication of a MOSFET.

first oxidized, forming a thin silicon dioxide top layer, which is subsequently coated with a photoresist (A). The photoresist is patterned (B) using photolithography (post-apply bake, exposure, post-exposure bake, and development, as explained in the next section), the exposed oxide layer is etched by hydrofluoric acid (C), and the resist is stripped (D) with a solvent or by plasma oxidation, leaving a patterned oxide layer that is the same pattern as the opaque areas on the mask. Phosphorous deposition into the P-type silicon creates N-type silicon for the source and drain regions (E). An oxide layer is formed from another thermal oxidation step (F), followed by another lithographic step to form a gate region (G, H, I). A very thin gate oxide layer is then grown by thermal oxidation (J). In another lithographic step (K, L, M), contact holes to the N-type silicon are formed. Aluminum is then deposited over the entire surface (N), and in a final lithographic step (O, P, Q, R), the MOSFET is formed that contains electrical contacts made of aluminum. Millions of transistors must be linked together through vertical interconnects between layers and horizontal interconnects across each layer of a chip. The final chip is connected to an integrated circuit package through tiny wires, sealed, tested, and sold as a complete microprocessor.[2]

Photolithography

As one can see from the description above of the fabrication of a microprocessor, many lithographic steps are required. There are many techniques available for transferring the image from the mask to the substrate. These include, and are not limited to, x-ray lithography, electron-beam lithography, ion-

beam lithography, extreme-UV lithography, and photolithography.[5] The use of ultraviolet light to pattern images is called photolithography, and this is the predominant technique used today. Photolithography involves several steps, as shown in Figure 1.4. A semiconductor substrate is first spin-coated with a photoresist, a photosensitive material that changes its solubility when exposed to light. The uniform resist layer is heated to a specified temperature and time (depending on the type of resist material), in a post-apply baking (PAB) step, to drive off the coating solvent and promote adhesion to the semiconductor substrate. This step is also called the soft bake step. The resist-coated wafer is then positioned and aligned under a photomask, which contains transparent and opaque regions that define the desired circuit pattern to be imaged. Shining light through this mask onto the photoresist causes the exposed regions of the resist to undergo a chemical change that modifies the solubility of the region to an aqueous base developer. The wafer is subsequently baked at a certain temperature in the post-exposure baking (PEB) step to complete the solubility-switching chemistry. In the development step, the wafer is washed with aqueous base developer (usually 0.26 *N* tetramethylammonium hydroxide – TMAH) to dissolve either the exposed areas or the unexposed areas, depending on the type of resist used. When the exposed areas are developed away, the resist is called a positive-tone resist, because the indented pattern is a replica of the transparent regions in the photomask. Positive-tone resists, therefore, contain materials that typically become more polar after exposure to light, causing the region to become

[5] Thompson, L. F.; Willson, C. G.; Bowden, M. J. *Introduction to Microlithography*, 2nd ed.; American Chemical Society: Washington DC, 1994.

more soluble in an aqueous base developer. Negative-tone resists, on the other hand, contain materials that become less polar, creating regions that do not dissolve in aqueous base developer. Typically, but not always, this is done by a crosslinking reaction that is initiated upon exposure to light.

The regions that are not covered by resist are selectively etched away by free radicals and reactive ions in a plasma etching step. The areas covered by polymer "resist" the etchant, hence the term photoresist. This resist is then removed, or stripped, by dissolution in a solvent such as acetone or by plasma oxidation, leaving a positive or negative-tone relief image in the underlying substrate.

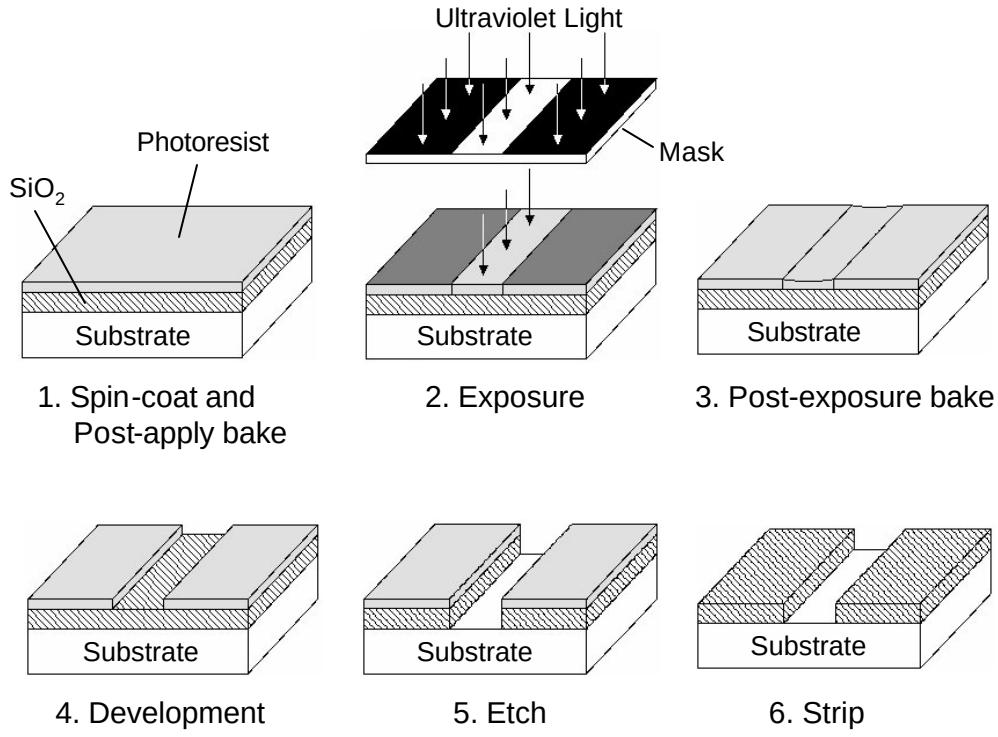

Figure 1.4: Formation of positive-tone images by the photolithographic process.

The number of transistors that can be put into an integrated circuit depends, in a large part, on the size of the features attainable from the lithographic process. In projection photolithography, the image of light transmitted through the mask is focused onto a resist-coated wafer using a complex system of lenses. The minimum resolution (R), therefore, in this type of lithography is governed by the relation

$$R = k_1 l / NA \tag{1}$$

where λ is the wavelength of the exposing light, k_1 is a process-dependent parameter in the range of 0.4-1, and NA is the numerical aperture, equal to the refractive index of the surrounding medium (~1 for air) times the sine of the angle subtended by the objective lens of the system.[5,6] The depth of focus (DOF) is given by the equation

$$DOF = k_2 l / (NA)^2 \tag{2}$$

where k_2 is a process-dependent parameter on the order of 0.5-1 and λ and NA are wavelength and numerical aperture. The depth of focus, to the resist chemist, defines how rapidly the aerial image decays as a function of distance from perfect focus. Because the region of perfect focus is confined to a plane, a large depth of focus is desired because it increases the tolerance of the system as the image plane departs from the plane of perfect focus.[5,7]

To achieve smaller features, one must improve resolution while maintaining a maximum DOF. Increasing the NA (currently 0.6-0.8) of the projection lens system will improve resolution, but this results in a quadratic

---

6 Born, M.; Wolf, E. *Principles of Optics*, 6th ed.; Pergamon Press: Oxford, 1983; pp 415, 441.
7 Wallraff, G. M.; Hinsberg, W. D. *Chem. Rev.* **1999**, *99*, 1801-1821.

decrease in the DOF. Therefore most lithographers prefer to improve resolution by decreasing the exposing wavelength, which only causes a linear decrease in DOF.

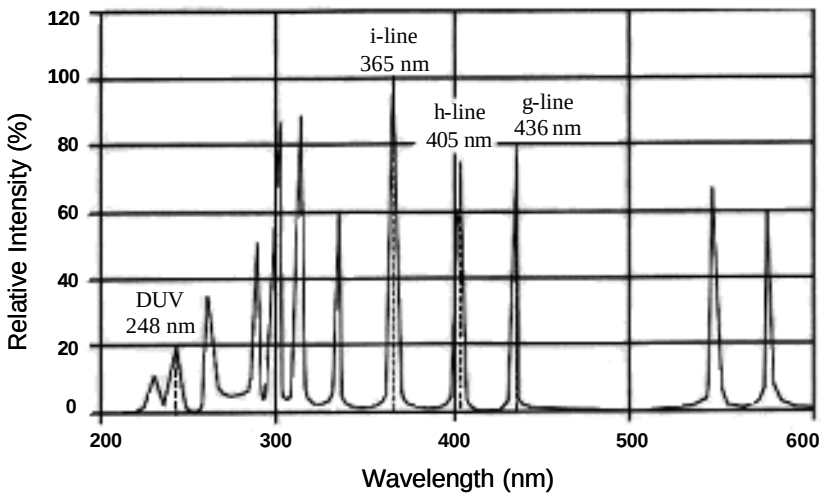

Figure 1.5: Emission spectrum of a high-intensity mercury arc lamp.[8]

Over the past few decades, the industry has moved to shorter and shorter wavelengths of ultraviolet light for exposure. The first exposure tools were equipped with high pressure mercury discharge lamps which produced UV wavelengths of 436 nm (g-line) and 365 nm (i-line) at adequate intensities, Figure 1.5.[8] Today, integrated circuits with device geometries as small as 250 nm have been manufactured using i-line exposure. When the industry decided to shift to a smaller exposure wavelength (248 nm) to improve resolution, the mercury lamps could not be used anymore because of their low emission intensity at this wavelength. Instead, a krypton fluoride (KrF) excimer laser was chosen as the

[8] Quirk, M.; Serda, J. *Semiconductor Manufacturing Technology*; Prentice-Hall: Upper Saddle River, 2001; p 373.

high intensity light source. This laser emits radiation at a characteristic wavelength of 248 nm (deep UV) that is about five times more intense than the output of a mercury arc lamp at the same wavelength. The move to this shorter wavelength has allowed the industry to produce device geometries below 200 nm in size. Higher resolution images using projection lithography will demand the use of argon fluoride (ArF, 193 nm) and fluorine (F_2, 157 nm) excimer lasers as light sources (Table 1.1).[5]

Table 1.1: Characteristic emission wavelengths for several excimer lasers.

Laser	XeF	N_2	XeCl	KrF	ArF	F_2
Wavelength (nm)	351, 353	337	308	248	193	157

Photoresists

Each movement to a shorter wavelength requires new advances in resist technology to allow efficient imaging at that particular wavelength. Since photoresists are responsible for providing the solubility-switching chemistry that occurs during exposure and for resisting the etchants during etching, designing and formulating a workable resist at the imaging wavelength is critical. For example, resists that have been designed to work efficiently using 436 nm radiation may not function using 365 nm radiation because the formulation is opaque or the photoactive compound (PAC) contained in the resist formulation no longer bleaches at the shorter wavelength. The move to 193 nm lithography will require new resists because the current polymers used for 248 nm lithography are too absorbing at the new exposing wavelength, capturing all the light that the photoactive species present in the matrix needs to undergo a chemical

transformation. Understanding the history of photoresists, therefore, may provide insight on how the components (polymer, photoactive compound, solvent, and other additives) in a resist formulation are chosen.

Bis(arylazide)-rubber Resists

The first resists to earn widespread use in the microelectronics industry were the negative-tone resists developed by Eastman Kodak in the 1960s.[9] These are based on cyclized poly(cis-isoprene) as the matrix polymer and a bis(arylazide) as the photoactive compound (Figure 1.6). Exposure of this two-component resist system using 365 nm radiation causes the bisazide to decompose to nitrogen gas and a reactive intermediate, a nitrene. This nitrene undergoes a variety of reactions, but the reaction of relevance is insertion into the unsaturated matrix polymer which results in a crosslinked polymer network. Therefore, crosslinking occurs in the exposed areas, and the unexposed areas are selectively washed away by an organic developer in a subsequent development step to give a negative-tone image.

The negative-tone resists described above were used to fabricate many of the early integrated circuits. However, the move from *contact alignment* (the mask is pressed firmly against the resist-coated wafer) to *projection alignment* (the mask is positioned at a certain distance above the wafer and the image is transferred by projection optics) created a new problem for the bisazide-rubber resists. The aerial image of the projectors used at the time was poor, so an imaging material of high contrast was needed to print features with sharp edges.

---

[9] Reiser, A. *Photoreactive Polymers: The Science and Technology of Resists*; John Wiley & Sons: New York, 1989.

The bisazide-rubber resists were inadequate because of their low contrast and because they tended to swell during development, making it nearly impossible to print features below 1 μm in diameter. A new resist system was needed.

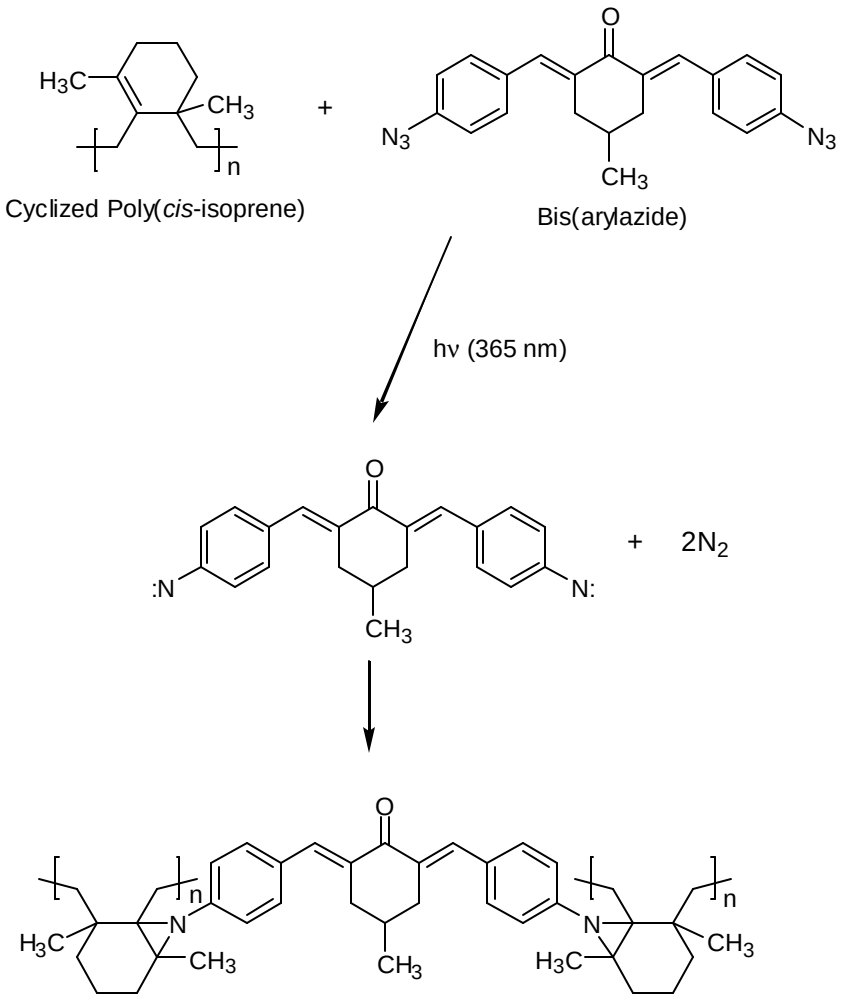

Figure 1.6: Eastman Kodak's negative-tone resist based on crosslinking of cyclized poly(*cis*-isoprene) by nitrene insertion.

Diazoquinone-Novolac Resists

In 1972, AZ resists were introduced by the Azoplate Corporation.[9] These resists have replaced the negative-tone rubber resists because they provide enhanced sensitivity (high contrast) and as a bonus, offer greater resistance to dry etching environments. The two-component resist system is composed of a low molecular weight novolac matrix resin and a diazoquinone photoactive compound or sensitizer. These are positive-tone resists because the exposed regions are rendered more soluble in an alkali developer. Images obtained from these resists have resolutions below 1 μm.

Novolac is a condensation polymer of *m*-cresol and formaldehyde. It dissolves in common organic solvents and can be coated to form fine films with excellent adhesion to the substrate. Since novolac contains the phenol functionality ($pK_a \sim 10$), it is easily ionized in dilute aqueous base and therefore dissolves readily. However, when an additive such as diazonaphthoquinone is added to the resin, the dissolution rate of the novolac film in aqueous base is decreased significantly. The diazonaphthoquinone photoactive compound, therefore, acts as a "dissolution inhibitor" in its initial form.[10] The interaction between novolac and diazoquinones is still an area of active research.[9,11,12] It is known that the photochemistry of the photoactive compound is affected solely by the ring system while the sulfonate, or "ballast", group on the aromatic ring

---

[10] Dammel, R. *Diazonaphthoquinone-based Resists*; Tutorial Texts in Optical Engineering, v. TT 11; SPIE Optical Engineering Press: Bellingham, WA, 1993.

[11] Uenishi, K.; Kawabe, Y.; Kokubo, T.; Slater, S.; Blakeney, A. *Proc. SPIE Int. Soc. Opt. Eng.* **1991**, *1466*, 102.

[12] McAdams, C. L.; Tsiartas, P.; Willson, C. G. *Polym. Mater. Sci. Eng.* **1997**, *77*, 437-438.

determines the dissolution inhibition efficiency. Explanations on why diazoquinones are able to retard the dissolution of novolac so efficiently are numerous, and much research in this area is needed to fully understand this interaction.

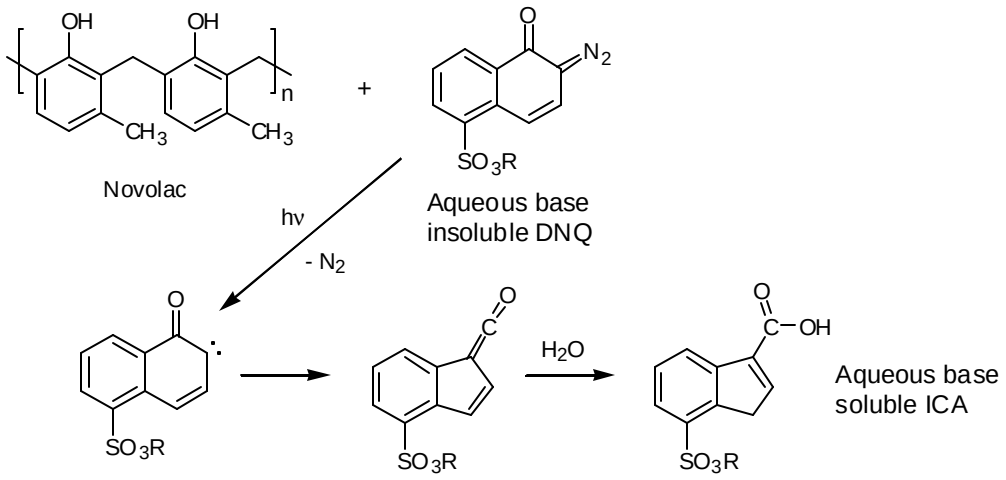

Figure 1.7: Diazonaphthoquinone-novolac resist. Novolac is blended with diazonaphthoquinone (DNQ), which undergoes photolysis to produce an indenecarboxylic acid (ICA) via carbene and ketene intermediates.

When the diazonaphthoquinone sensitizer is exposed to UV radiation, an extremely reactive carbene is formed along with the evolution of nitrogen gas (Figure 1.7). Through the Wolff rearrangement, the carbene intermediate is transformed to a ketene. Water in the resist film or from the environment then reacts with the ketene to form the final carboxylic acid. This indenecarboxylic acid is base soluble and promotes the dissolution of the matrix resin in aqueous base (Figure 1.8). In summary, a base-insoluble compound that inhibits the

dissolution of the matrix polymer is photochemically converted to a base-soluble compound that accelerates the dissolution of the matrix resin. This is one way of inducing a solubility differential in positive-tone resists. The other way is described in a later section.

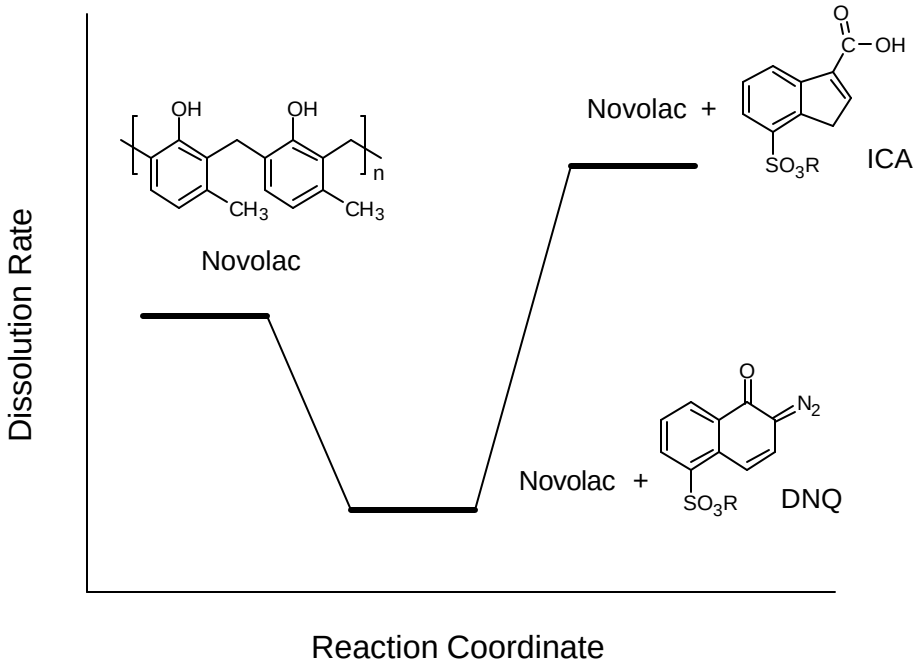

Figure 1.8: Graph depicting the effect of DNQ and ICA on the dissolution rate of novolac in aqueous base.

The widely used diazonaphthoquinone-novolac resists have provided device geometries as small as 350 nm. In order to print smaller features, the semiconductor industry needed to use a shorter wavelength of exposing light, as described by equation (1). The gain in resolution by using deep-UV exposure, however, is not without cost. Several problems had to be solved. The power

available from the high-pressure mercury arc lamps primarily used for 365 nm exposure was not sufficient for 248 nm exposure. At 248 nm, the emission intensity of the mercury lamps is very weak (Figure 1.5), so a new high-intensity, deep-UV light source was required. The introduction of rare gas halide excimer lasers in the late 1970s made deep-UV lithography a reality. By combining the excited states of a rare gas such as krypton and a halogen atom such as fluorine, a KrF excimer is formed that radiates at a characteristic wavelength (248 nm) on dissociation. These excimer lasers became the light source of choice because of their high average power, high brightness, and excellent frequency stability.[5]

The DNQ-novolac system that had been predominantly used for i-line exposure was no longer suitable for use at deep-UV wavelengths. The novolac resin is highly absorbing at wavelengths below 300 nm, causing nonuniform distributions of indenecarboxylic acid throughout the depth of the film. These resists, therefore, had low sensitivity and poor contrast at shorter wavelengths. Attempts to modify the DNQ-novolac system by using more transparent matrix polymers and alternative dissolution inhibitors have not brought much success.[13] This may be due to the difficulty of optimizing the dissolution properties of the polymer/dissolution inhibitor pair, since much research is needed to fully understand this complex interaction.[12,14] New resist materials with low absorbance and high sensitivity at 248 nm had to be designed.

---

[13] Willson, C. G.; Yueh, W.; Leeson, M. J.; Steinhausler, T.; McAdams, C. L.; Dammel, R. R.; Sounik, J. R.; Aslam, M.; Vicari, R.; Sheehan, M. T. *Proc. SPIE-Int. Soc. Opt. Eng.* **1997**, *3049*, 226-237.

[14] Wallraff, G. M.; Hinsberg, W. D. *Chem. Rev.* **1999**, *99*, 1801-1821.

Chemically-amplified Resists and Development of 248 nm Resists

In the early 1980s, researchers at IBM demonstrated a "chemically amplification" concept in which radiation is used to photochemically generate an initiating species or catalyst that is active in subsequent reactions.[15-17] The species generated is an acid molecule that catalyzes a deprotection reaction that transforms an initially base-insoluble polymer to a base-soluble polymer (Figure 1.9). A typical resist consists of poly(hydroxystyrene) (PHOST) partially protected by *tert*-butoxycarbonyl (*t*-BOC) pendent groups as the matrix resin and an onium salt photoacid generator (PAG) as the photoactive compound. PHOST and novolac are similar polymers with the same phenol functional group, but the absorbance of PHOST at deep-UV wavelengths is about an order of magnitude lower than that of novolac. This property makes PHOST a suitable polymer for 248 nm imaging. Instead of having a separate molecule to inhibit the dissolution of PHOST in aqueous base, the dissolution inhibition of PHOST is provided by the *t*-BOC groups that are pendent on the polymer.

Irradiation of the two-component resist film generates a low concentration of a strong Brönsted acid. Upon heating, this photogenerated acid is responsible for fragmenting the *t*-BOC groups into carbon dioxide and a tertiary carbocation intermediate that undergoes elimination to regenerate an acid molecule. There is no net consumption of acid in the reaction. However, the acid is eventually quenched by a variety of methods. It has been estimated that the number of *t*-

---

15 Ito, H.; Willson, C. G. *Polym. Eng. Sci.* **1982**, *23*, 1021.
16 Frechet, J. M. J.; Ito, H.; Willson, C. G. *Proc. Microcircuit. Eng.* **1982**, *82*, 260.
17 Ito, H. *IBM J. Res. Develop.* **1997**, *41*, 69-80.

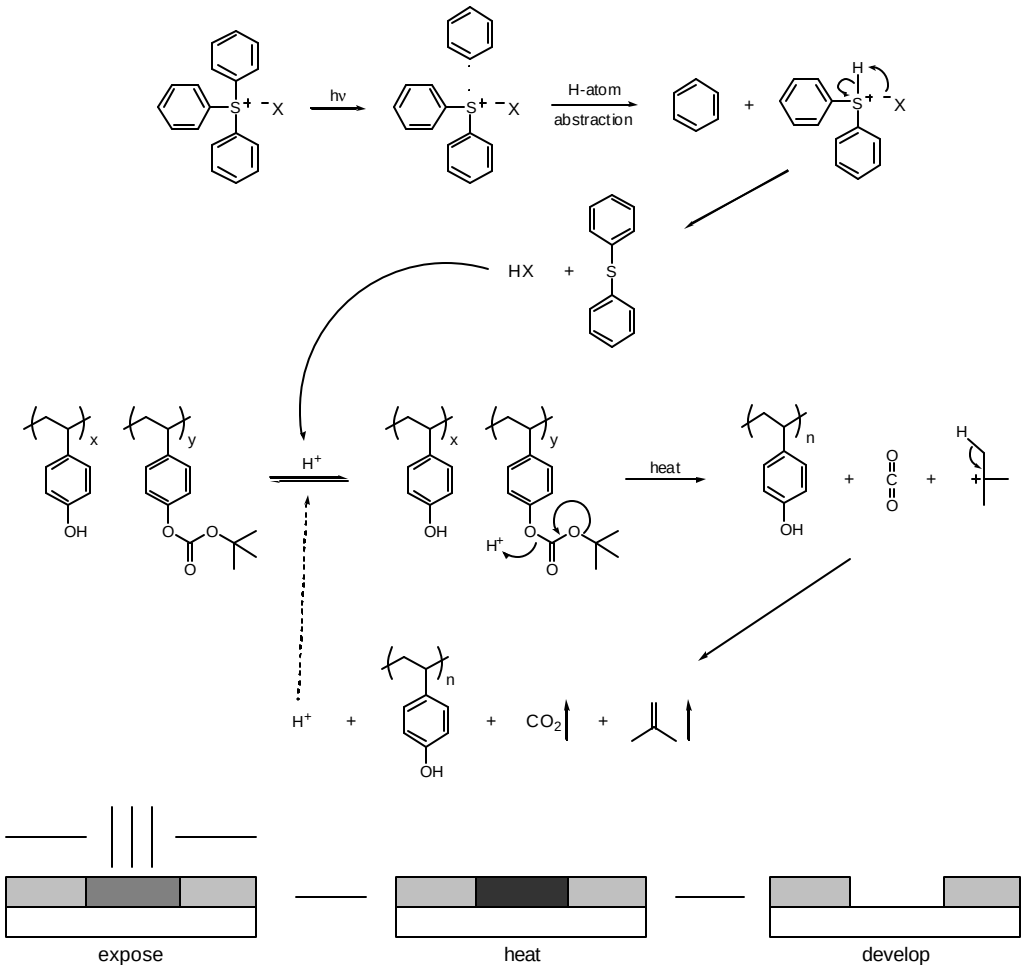

Figure 1.9: Photodecomposition of a photoacid generator to produce a strong acid that deprotects the *t*-BOC groups upon heating to produce a base-soluble polymer. The tertiary carbocation undergoes elimination to regenerate acid that catalyzes further reactions.

BOC groups cleaved per photogenerated acid is in the range of 1000.[18] This concept of generating a species photochemically that catalyzes many other reactions is called "chemical amplification". Resists based on this chemical

[18] McKean, D.; Schaedili, U.; MacDonald, S. *Polymers in Microlithography*, In *ACS Symposium Series 412*; Reichmanis, E.; MacDonald, S.; Iwayanagi, T., Eds.; American Chemical Society: Washington, DC, 1989; p 27.

amplification concept are much more sensitive than the DNQ-novolac resists discussed earlier. The quantum yield for the Wolff rearrangement shown in Figure 1.7 is about 0.1-0.3.[10] This translates to an i-line exposure energy of 100-200 mJ/cm^2.[14] Resists based on the chemical amplification concept, on the other hand, are much more sensitive and typically require doses in the range of 20-30 mJ/cm^2 at 248 nm. Doses as small as 1 mJ/cm^2 have been used.

The matrix polymer in the exposed areas is thus converted to a more polar polymer after deprotection of the protection groups. Development of the newly unprotected regions in aqueous base thus provides positive-tone images. This represents the second method of inducing a solubility differential in positive-tone resists. To date, many positive-tone resists based on chemical amplification have been introduced. Most of them are based on a relatively nonpolar polymer that is converted to a more polar polymer by photogenerated acid through the deprotection of a protecting group. The protecting groups have varied from *t*-BOC groups to acetal and *t*-butyl ester groups. All these groups are acid-labile to take advantage of acid catalysis.

A variety of photoacid generators have been used in chemically-amplified resists. Both nonionic[19] and ionic PAG's can be used, but the onium salts first developed by Crivello[20-23] have gained wide-spread use because of their high quantum yields of acid production, good absorption properties at 248 nm, and

---

19 Reichmanis, E.; Houlihan, F.; Nalamasu, O.; Neehan, T. *Chem. Mater.* **1991**, *3*, 394.
20 Crivello, J. V. *J. Polym. Sci., Part A: Polym. Chem.* **1999**, *37*, 4241-4254.
21 Crivello, J. V., In *Radiation Curing in Polymer Science and Technology: Photoinitiating Systems*; Fouassier, J. P.; Rabek, J. F., Eds.; Elsevier: New York, 1993; Vol. II, Chapter 8.
22 Crivello, J. V.; Lam, J. H. W. *Macromolecules* **1977**, *10*, 1307.
23 Crivello, J. V.; Lam, J. H. W. *J. Org. Chem.* **1978**, *43*, 305.

good solubility and thermal stability in resists films.[14] Because of their ease of synthesis through metathesis reactions, many onium salts have been made. The acid counterion can be modified to provide photogenerated acids with various pK_a's, volatilities, and sizes.[24-26] The photodecomposition of PAG's is complex and still not fully understood. In the case of a sulfonium salt, it is generally believed that irradiation causes the homolytic cleavage of the sulfur-carbon bond to generate a radical cation. This radical then abstracts a proton from the surrounding medium (polymer, solvent, or water) to provide the protonated sulfonium cation-counteranion pair which eventually dissociates into a sulfide and the acid molecule (Figure 1.9).[20,27]

Development of 193 nm Resists

Optimized 248 nm resist formulations based on the chemical amplification concept described above have been used to print devices with features less than 200 nm in diameter. As the industry moves to imaging at shorter wavelengths (most likely 193 nm imaging using the ArF excimer laser), new resists must be prepared because the current resists are too absorbing at the new wavelength. However, much of what has been learned from designing 248 nm resists can be applied to the development of 193 nm resists. For example, all of the protecting

---

[24] Allen, R. D.; Wallraff, G. M.; Hinsberg, W. D.; Simpson, L.; Kunz, R. *Polymers for Microelectronics*, In *ACS Symposium Series 537*; Thompson, L. F.; Willson, C. G.; Tagawa, S., Eds.; American Chemical Society: Washington, DC, 1994; Chapter 11.

[25] Nakano, K.; Maeda, K.; Iwasa, S.; Hasegawa, E. *Proc. SPIE Int. Soc. Opt. Eng.* **1995**, *2438*, 433.

[26] Houlihan, F. M.; Kometani, J. M.; Timko, A. G.; Hutton, R. S.; Gabor, A.; Medina, A.; Biafore, J.; Slater, S. *Proc. SPIE Int. Soc. Opt. Eng.* **1998**, *3333*, 73.

[27] Hacker, N., In *Radiation Curing in Polymer Science and Technology: Photoinitiating Systems*; Fouassier, J. P.; Rabek, J. F., Eds.; Elsevier: New York, 1993; Vol. II, Chapter 9.

groups and aqueous-base soluble functional groups may be borrowed from the polymers used in 248 nm resists. Much progress has been made in designing 193 nm resists.[28-30] Researchers have demonstrated line/space patterns as small as 80 nm.[30] When considering the design of these new resists, it is helpful to understand several important concepts, as described in the next few sections.

Absorbance

The major obstacle in using the current 248 nm polymers for 193 nm imaging is their high absorbance at 193 nm. A highly absorbing resist material will cause "footing" problems during imaging because all the incident radiation is absorbed in the resist film before reaching the bottom of the film (Figure 1.10). Acid is therefore only generated near the top of the film. This part is the only part that is developed away after the post-exposure baking step, leaving residual resist material in the exposed regions. In a more transparent resist, the light is able to penetrate to the bottom of the resist film, thus generating acid that is evenly distributed throughout the exposed areas. Baking and development of these areas results in a "cleared" resist profile.

Since poly(*p*-hydroxystyrene) is used as the resin material in a majority of the 248 nm resists, these resists are not suitable for 193 nm imaging because of the polymer's strong absorbance at 193 nm (Figure 1.11).[31] This absorbance is

---

[28] Okoroanyanwu, U.; Shimokawa, T.; Byers, J.; Medeiros, D. R.; Willson, C. G. *Proc. SPIE Int. Soc. Opt. Eng.* **1997**, *3049*, 92.

[29] Wallow, T. I.; Houlihan, F. M.; Nalamasu, O.; Chandross, E. A.; Neenan, T. X.; Reichmanis, E. *Proc. SPIE Int. Soc. Opt. Eng.* **1996**, *2724*, 255.

[30] Patterson, K.; Okoroanyanwu, U.; Shimokawa, T.; Cho, S.; Byers, J.; Willson, C. G. *Proc. SPIE Int. Soc. Opt. Eng.* **1998**, *3333*, 425-437.

[31] Allen, R. D.; Wallraff, G. M.; Hofer, D. C.; Kunz, R. R. *IBM J. Res. Develop.* **1997**, *41*, 95.

due to the presence of aromatics in the polymer (π to π^* transitions). This problem may be solved by using non-aromatic polymers such as polyacrylates, which are significantly more transparent than the aromatic polymers at 193 nm. Even though the polyacrylates contain π systems (carbonyl groups), their absorbance is not high at 193 nm. This has led many researchers to pursue resist materials based on this acrylate platform.[31-35]

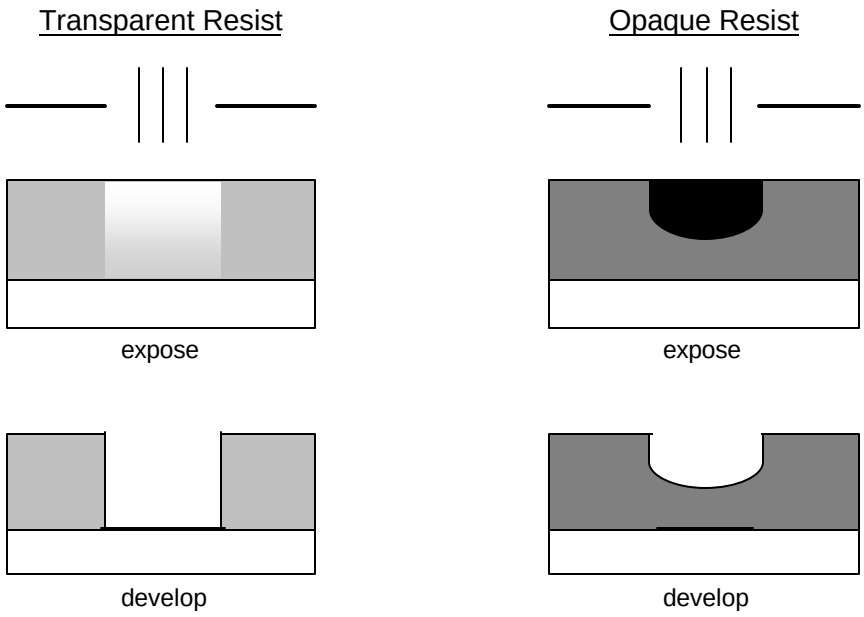

Figure 1.10: The effect of optical density on the shape of the final resist profile.

[32] Allen, R. D.; Wallraff, G. M.; Hinsberg, W. D.; Simpson, L. *J. Vac. Sci. Technol. B* **1991**, *9*, 3357.

[33] Kaimoto, Y.; Nozaki, K.; Takechi, S.; Abe, N. *Proc. Soc. Photo-Opt. Instrum. Eng.* **1992**, *1672*, 66.

[34] Allen, R. D.; Wallraff, G. M.; Hinsberg, W. D.; Conley, W. *J. Photopolym. Sci. Technol.* **1993**, *6*, 575.

[35] Kunz, R.; Allen, R. D.; Hinsberg, W. D.; Wallraff, G. M. *Proc. Soc. Photo-Opt. Instrum. Eng.* **1993**, *1925*, 167.

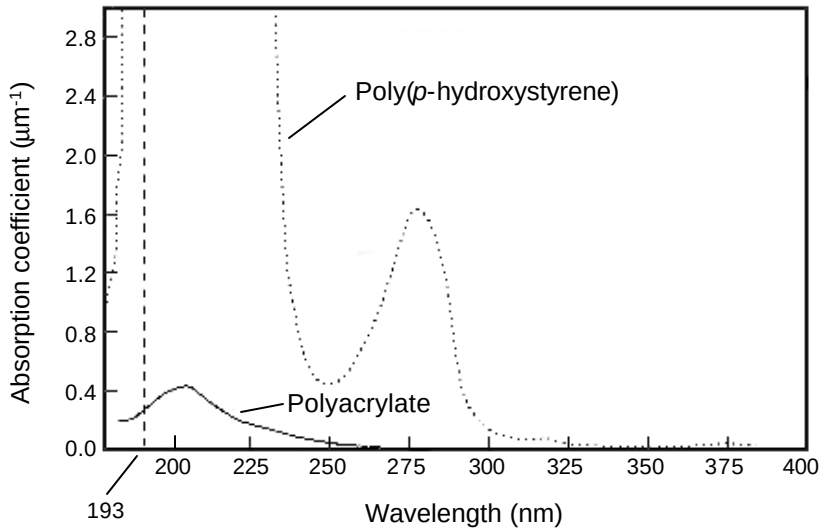

Figure 1.11: Absorption spectra of poly(*p*-hydroxystyrene vs. poly(methyl methacrylate).

Etch Resistance

Another factor taken into consideration when designing a new resist material is plasma etch resistance. The resist must not only be able to provide high resolution images, but also be able to resist the etchant so that the desired circuit pattern can be transferred to the underlying substrate layer. In early lithographic processes, liquid chemical etchants such as HF were used to etch patterns into the substrate. Since this process is inherently isotropic (the substrate is etched at the same rate in all directions), parts of the substrate underneath the resist profile were also etched (undercutting).[36] This did not become a problem until features less than 1 μm were required. As the desired dimensions became

[36] Mucha, J. A.; Hess, D. W.; Aydil, E. S., In *Introduction to Microlithography*; 2nd ed.; Thompson, L. F.; Willson, C. G.; Bowden, M. J., Eds.; American Chemical Society: Washington, DC, 1994; Chapter 5.

smaller, undercutting became much more significant in altering the pattern size and thus was intolerable (Figure 1.12).

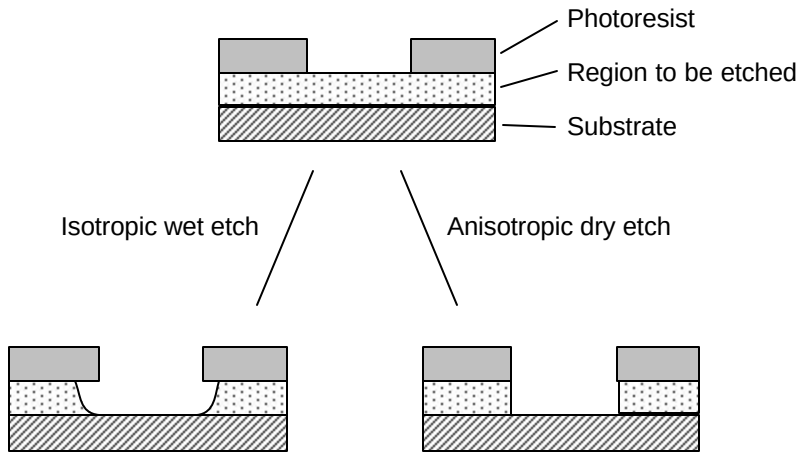

Figure 1.12: The isotropic nature of a wet etch, leading to undercutting, as compared to the anisotropic nature of a dry etch (little undercutting).

Dry etching, or plasma etching, techniques have almost completely replaced wet etching techniques because they offer an etching reaction that proceeds faster in the vertical direction than in the horizontal direction (anisotropic etch). This provides minimal undercutting, and is the preferred pattern transfer method for small features. Plasma etching involves placing the wafer in a reactive ion etching (RIE) chamber that contains two parallel-plate electrodes. An electric field is applied that excites the gas of choice, leading to high-energy collisions between free electrons with the gas molecules to produce reactive ions, radicals, and molecular fragments. The ions and electrons establish

a potential within the chamber that leads to the bombardment of positive ions on the wafer surface, anisotropically etching the substrate.[36]

The chemical makeup of the photoresist is crucial in determining etch rate. Studies have shown that the plasma etch rate of organic materials is highly dependent on the carbon content of the material. This empirically-derived relationship, called the Ohnishi parameter,[37] directly relates the plasma etch resistance of a polymer to the ratio of carbon and hydrogen atoms contained in the polymer:

$$R \propto \frac{N_T}{N_C - N_O} \tag{3}$$

where R is the observed etch rate, N_T is the total number of atoms, N_C is the total number of carbon atoms, and N_O is the total number of oxygen atoms.

It was observed that polymers containing a high carbon to hydrogen/oxygen ratio provided a better barrier to reactive ion etching processes. Since a high carbon to hydrogen ratio suggests unsaturation and aromaticity, designing polymers that contain aromatic groups greatly increases etch resistance. It is therefore not surprising that resists used for i-line and 248 nm lithography offer high plasma etch resistance because they contain aromatic resin polymers, while the new resists designed for 193 nm lithography that are based on acrylic polymers offer little etch resistance. Research has been done to improve the etch resistance of these polymers by incorporating pendent alicyclic groups[33] such as

[37] Gokan, H.; Esho, S.; Ohnishi, Y. *J. Electrochem. Soc.: Solid State Sci. Tech.* **1983**, *130*, 143.

norbornane or adamantine, but these resists are still inferior to i-line and 248 nm resists in terms of plasma etch resistance.

By designing new polymers that contain alicyclic compounds as the repeat unit in the polymer backbone, researchers have demonstrated that 193 nm resists are capable of achieving almost the same etch selectivity as the i-line and 248 nm resists. These new polymers were made by the free-radical polymerization, ring-opening metathesis polymerization (ROMP), or vinyl addition polymerization of various cycloolefin monomers.[30,38] Radical polymerizations of norbornene monomers with pendent acid-labile functionalities and a comonomer such as maleic anhydride have provided polymers that have been used to image very small features.[30] Images from polymers made from ROMP and vinyl addition polymerization have also been demonstrated, but these polymers are not in the forefront because of several factors, including low glass transition temperature (ROMP polymers), swelling (vinyl addition polymers), and the fear of metal contamination (both).

Metal Contamination

Device manufacturers are fearful of metal contamination because trace levels of metals in photoresist formulations can drastically reduce the yields of semiconductor devices. Even parts-per-billion (ppb) levels of metals are disastrous because the trace metals can leach into the semiconductor substrate, creating many functional problems that are nearly impossible to fix once the device is completed. Since the vinyl-addition polymers and ROMP polymers are

---

[38] Okoroanyanwu, U.; Shimokawa, T.; Byers, J.; Willson, C. G. *Chem. Mater.* **1998**, *10*, 3319-3327.

made by using a metal catalyst, removal of this catalyst to the sub-ppb levels is crucial. The most effective way to screen out metals is to not use them at all, and this unfortunately precludes the use of vinyl addition polymers and ROMP polymers as 193 nm photoresists. However, these polymers will find use when the technology becomes available for trace-metal removal to the sub-ppb range.

Airborne Amine Contamination

Chemically-amplified resists to date have provided high contrast, high resolution images with feature dimensions below 200 nm in size. This luxury, however, comes at a cost. It has been observed that features obtained from chemically-amplified resists often show a T-topped profile, commonly known as "T-topping" (Figure 1.13). A large amount of time was spent on experiments to find the exact cause of this phenomenon. Finally, through several air-filtration experiments, the cause of the T-topping was linked to airborne amine that was present in the atmosphere during resist processing.[39-42] Diffusion of this amine onto the resist surface after exposure quenches the just-formed acid at the surface, leading to T-topped profiles after development (Figure 1.14). Even amine levels in the ppb range may cause undesired T-topping.

Several steps have been taken to alleviate this problem. The air is now chemically filtered to reduce airborne amines. The resist polymer may be

---

[39] MacDonald, S. A.; Hinsberg, W. D.; Wendt, H. R.; Clecak, N. J.; Willson, C. G.; Snyder, C. D. *Chem. Mater.* **1993**, *5*, 348-356.

[40] Hinsberg, W. D.; MacDonald, S. A.; Clecak, N. J.; Snyder, C. D. *Chem. Mater.* **1994**, *6*, 481-488.

[41] Hinsberg, W.; MacDonald, S.; Clecak, N.; Snyder, C. *J. Photopolym. Sci. Technol.* **1993**, *6*, 535-546.

[42] Hinsberg, W. D.; MacDonald, S. A.; Clecak, N. J.; Snyder, C. D.; Ito, H. *Proc. SPIE-Int. Soc. Opt. Eng.* **1993**, *1925*, 43-52.

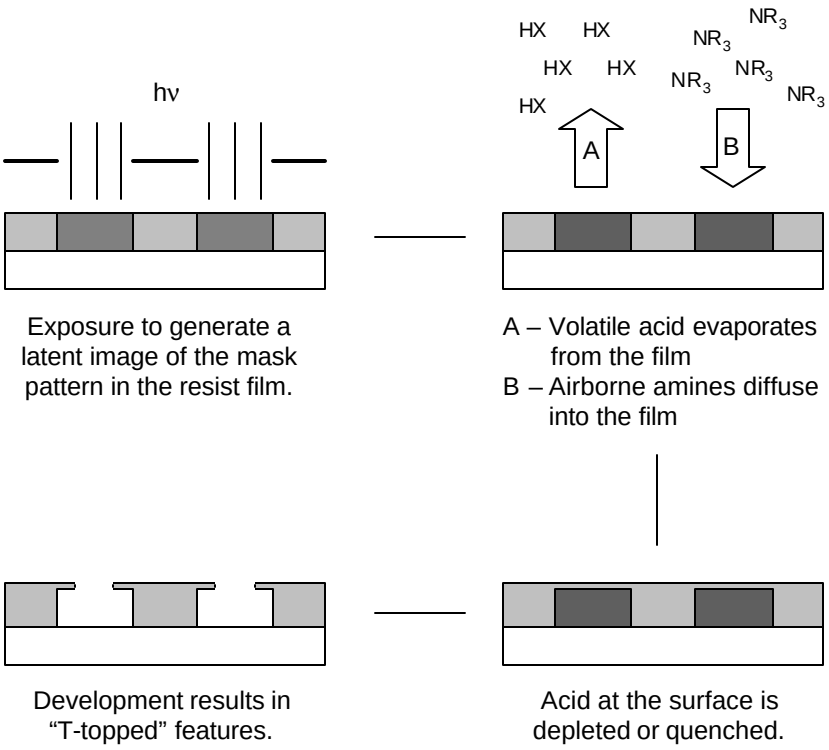

Figure 1.13: T-topped resist features resulting from evaporation of acid during post-exposure baking and quenching of acid due to airborne amine contamination

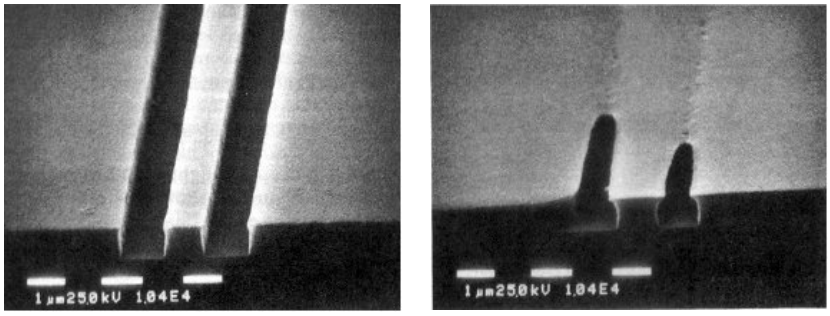

No amine contamination Airborne amine contamination

Figure 1.14: SEMs showing the effects of airborne amine contamination during resist processing.[39]

annealed before exposure to reduce free volume, hence reducing diffusion of airborne contaminants.[43] Preventing airborne diffusion may also be accomplished by using a transparent protective overcoat at the resist surface.[44] Finally, the method that is mostly used in addition to air filtration is to deliberately add a known amount of basic compound into the resist formulation.[45] This extra base is usually only 10% of the photoacid generator present in the formulation, but is enough to soften the impact of airborne amine contamination. This makes the effect of diffused airborne amine negligible on the final resist profile. The sensitivity of the resist is reduced, but this is an acceptable loss if T-topping is alleviated.

Another cause of depleted acid at the resist surface is the evaporation of photogenerated acid with low boiling points. During the post-exposure baking step, small acid molecules may evaporate from the surface, especially if the baking temperature is close to or higher than the boiling point of the photogenerated acid. This problem may be controlled by using larger acid molecules that are less volatile.

---

[43] Ito, H.; Breyta, G.; Sooriyakumaran, R.; Hofer, D. C. *J. Photopolym. Sci. Technol.* **1995**, *8*, 505.

[44] Oikawa, A.; Hatakenaka, Y.; Ikeda, Y.; Kokubo, Y.; Miyata, S.; Santoh, N.; Abe, N. J. *J. Photopolym. Sci. Technol*. **1995**, *8*, 519.

[45] Przybilla, K. J.; Kinoshita, Y.; Kudo, T.; Masuda, S.; Okazaki, H.; Padmanaban, M.; Pawlowski, G.; Roeschert, H.; Spiess, W.; Suehiro, N. *Proc. SPIE Int. Soc. Opt. Eng.* **1993**, *1925*, 76.

CHAPTER 2: *157 NM PHOTOLITHOGRAPHY*

The extension of optical lithography by using 157 nm light, the characteristic output wavelength of the F_2 excimer laser, has been gaining widespread support throughout the semiconductor industry. The Semiconductor Industry Association (SIA), a group that evaluates and assesses future imaging technologies, predicts that gate lengths of 35 nm will be needed by 2007.[46] In order to obtain features this small, several candidate imaging technologies have been proposed. These next-generation lithography (NGL) techniques include, and are not limited to, X-ray lithography, extreme-UV (EUV) lithography, ion-projection lithography (IPL), and e-beam lithography (SCALPEL – SCattering with Angular Limitation Projection Electron Beam Lithography or PREVAIL – Projection Reduction Exposure with Variable Axis Immersion Lenses). Each of these techniques has demonstrated high resolution images, but requires many engineering and technological advances before being production-worthy. Optical lithography using 157 nm radiation has its own challenges and problems, but may be easier to implement due to the abundance of knowledge gained within the last 30 years. Therefore, this technique is viewed by some as the transitional technology to use before the NGL technologies are implemented.

ABSORBANCE AT 157 NM

In addition to requiring improvements in optical materials, optical coatings, mask materials, and pellicles, 157 nm lithography will require

[46] The International Technology Roadmap for Semiconductors (ITRS) may be obtained at http://public.itrs.net.

significant innovations in resist material. Current resists used for 248 nm lithography, as well as resists that have been proposed for 193 nm lithography, are not suitable for use at 157 nm lithography because of their strong absorption at the new wavelength. An early survey of the absorbance of several polymers by researchers at MIT Lincoln Labs demonstrated that most polymers are highly absorbing at 157 nm.[47-51] As shown in Table 2.1, a typical 248 nm resist has an absorbance of close to 7 per micron of resist film. This is also true of a typical 193 nm resist. This high absorbance makes imaging very difficult (as described in Chapter 1). If these resists are used for 157 nm imaging, they would have to be coated very thin (< 100 nm), and this is not a feasible solution because the defect levels associated with using ultra-thin resists makes imaging very difficult.

Table 2.1: The absorbance of several materials at 157 nm.

	Wavelength (nm)		
	157	**193**	**248**
248 nm Resist	6.84 μm^{-1}	---	0.37
193 nm Resist	6.86	0.47	---
Poly(methyl methacrylate)	5.69	---	---
Poly(norbornene)	6.10	---	---
Poly(styrene)	6.20	---	---
Teflon AF	0.70	---	---
Hydridosilsesquioxane	0.02	---	---

47 Bloomstein, T. M.; Horn, M. W.; Rothschild, M.; Kunz, R. R.; Palmacci, S. T.; Goodman, R. B. *J. Vac. Sci. Technol., B* **1997**, *15*, 2112-2116.

48 Bloomstein, T. M.; Rothschild, M.; Kunz, R. R.; Hardy, D. E.; Goodman, R. B.; Palmacci, S. T. *J. Vac. Sci. Technol., B* **1998**, *16*, 3154-3157.

49 Rothschild, M.; Bloomstein, T. M.; Curtin, J. E.; Downs, D. K.; Fedynyshyn, T. H.; Hardy, D. E.; Liberman, V.; Sedlacek, J. H. C.; Uttaro, R. S.; Bates, A. K.; Van Peski, C. *J. Vac. Sci. Technol. B* **1999**, *17*, 3262-3266.

50 Kunz, R. R.; Bloomstein, T. M.; Hardy, D. E.; Goodman, R. B.; Downs, D. K.; Curtin, J. E. *J. Vac. Sci. Technol., B* **1999**, *17*, 3267-3272.

51 Fedynyshyn, T. H.; Kunz, R. R.; Doran, S. P.; Goodman, R. B.; Lind, M. L.; Curtin, J. E. *Proc. SPIE Int. Soc. Opt. Eng.* **2000**, *3999*, 335.

Simple polymers such as poly(methyl methacrylate), poly(norbornene), and poly(styrene) all are strongly absorbing at 157 nm. It was concluded that simple hydrocarbons, aromatic groups, and carbonyl groups all contribute strongly to the absorption at 157 nm. Polymers that have bonds that are able to undergo π to π^* transitions (for example, C=C or C=O) are especially absorbing. The two general classes of compounds that have been found to be sufficiently transparent at 157 nm are fluorinated hydrocarbon polymers and siloxane polymers. Teflon AF, a polymer that is mostly poly(tetrafluoroethylene), has an absorbance of about 0.70 μm^{-1}, while poly(hydridosilsesquioxane) has an absorbance of 0.02 μm^{-1}. The results from these early studies may be used to guide the design of transparent resist materials for 157 nm lithography. Potential building blocks for lower absorbing polymers, therefore, may be monomers containing the more transparent carbon-fluorine bonds or a high degree of silicon-oxygen bonding.

HYDROFLUOROCARBON MONOMERS AND POLYMERS

Our research group has focused attention on building and designing transparent monomers and polymers containing an increased degree of carbon-fluorine bonding.[52-58] There are several very important discoveries made from

---

[52] Patterson, K.; Yamachika, M.; Hung, R.; Brodsky, C.; Yamada, S.; Somervell, M.; Osborn, B.; Hall, D.; Dukovic, G.; Byers, J.; Conley, W.; Willson, C. G. *Proc. SPIE Int. Soc. Opt. Eng.* **2000**, *3999*, 365-374.

[53] Brodsky, C.; Byers, J.; Conley, W.; Hung, R.; Yamada, S.; Patterson, K.; Somervell, M.; Trinque, B.; Tran, H. V.; Cho, S.; Chiba, T.; Lin, S. H.; Jamieson, A.; Johnson, H.; Vander Heyden, A.; Willson, C. G. *J. Vac. Sci. Technol. B* **2000**, *18*, 3396-3401.

[54] Chiba, T.; Hung, R.; Yamada, S.; Trinque, B.; Yamachika, M.; Brodsky, C.; Patterson, K.; Vander Heyden, A.; Jamieson, A.; Lin, S. H.; Somervell, M.; Byers, J.; Conley, W.; Willson, C. G. *J. Photopolym. Sci. Technol.* **2000**, *13*, 657-664.

these studies. The reader is referred to the references for a more detailed account of the 157 nm research progress to date.

The hexafluoroisopropanol group was identified early as a transparent base-soluble group. Because of inductive stabilization of the conjugate base by the adjacent electron-withdrawing trifluoromethyl groups, the pKa of such a group is near that of phenol, around 11.[59] This group may be protected by common alcohol protecting groups to provide the solubility-switching mechanism. The presence of adjacent electron-withdrawing moieties not only increases the acidities of groups such as hydroxyls or carboxylic acids but decreases their absorbance at 157 nm as well. It was demonstrated that α-trifluoromethyl carboxylic acids, in their ester form, are much more transparent than their non-fluorinated analogs. These two pieces of information guided the design of the first transparent, functional monomers for 157 nm lithography.

The transition from alicyclics and acrylates that are predominant in 193 nm resists to 157 nm structures may be accomplished by fluorination of the 193

---

[55] Hung, R. J.; Tran, H. V.; Trinque, B. C.; Chiba, T.; Yamada, S.; Sanders, D. P.; Connor, E. F.; Grubbs, R. H.; Kopp, J.; Frechet, J. M. J.; Thomas, B. H.; Shafer, G. J.; DesMarteau, D. D.; Conley, W.; Willson, C. G. *Proc. SPIE* **2001**, *4345*, 385-395.

[56] Tran, H. V.; Hung, R. J.; Chiba, T.; Yamada, S.; Mrozek, T.; Hsieh, Y. T.; Chambers, C. R.; Osborn, B. P.; Trinque, B. C.; Pinnow, M. J.; Sanders, D. P.; Connor, E. F.; Grubbs, R. H.; Conley, W.; MacDonald, S. A.; Willson, C. G. *J. Photopolym. Sci. Technol.* **2001**, *14*, 669-674.

[57] Sanders, D. P.; Connor, E. F.; Grubbs, R. H.; Hung, R. J.; Osborn, B. P.; Tran, H. V.; MacDonald, S.; Willson, C. G. *Macromolecules* **2002**, submitted for publication.

[58] Tran, H. V.; Hung, R. J.; Chiba, T.; Yamada, S.; Mrozek, T.; Hsieh, Y. T.; Chambers, C. R.; Osborn, B. P.; Trinque, B. C.; Pinnow, M. J.; MacDonald, S. A.; Willson, C. G. *Macromolecules* **2002**, submitted for publication.

[59] Grandler, J. R.; Jencks, W. P. *J. Am. Chem. Soc.* **1982**, *104*, 1937.

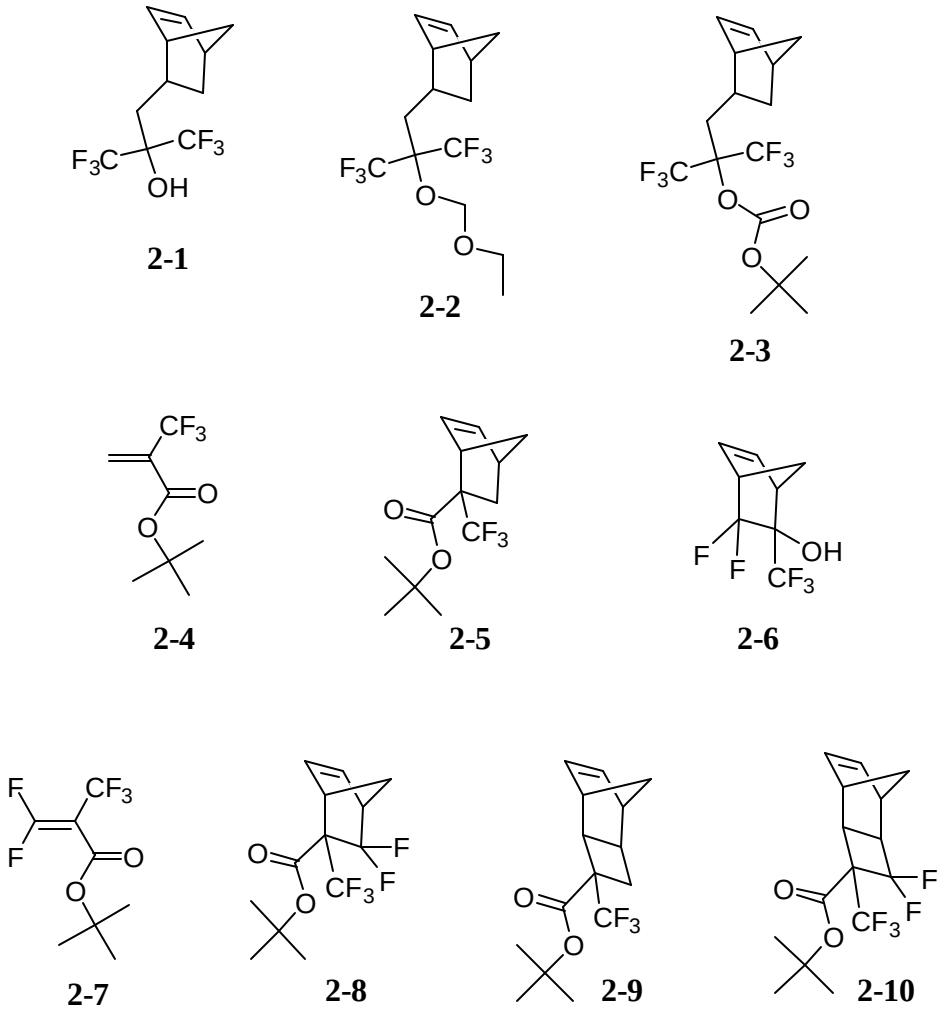

Figure 2.1: Structures of several candidate monomers for 157 nm lithography.

nm structures. This may seem like a straightforward task at first, but studies have shown that selective fluorination, rather than perfluorination, of those same structures is enough to significantly lower the compound's absorbance at 157 nm. Perfluorination is not necessary, and in fact, is probably not desired since the resulting polymer's adhesion to the substrate and plasma etch resistance would be

significantly reduced with increased fluorine content. Considerable work has been done on the synthesis and gas-phase VUV absorbance measurements of partially fluorinated norbornane structures. It is envisioned that these structures, when functionalized with appropriate transparent acid-labile groups, would provide the etch-resistant backbone for a 157 nm resist. All of these studies have helped to guide the design of several candidate monomers that could be incorporated into a 157 nm resist (Figure 2.1). Polymerization of these monomers using various polymerization methods such as free-radical polymerization, vinyl-addition polymerization, and ring-opening metathesis polymerization has provided relatively transparent polymers. These polymers, when formulated into a 157 nm resist, have shown the capability of producing high resolution images. Features as small as 70 nm have been demonstrated.

SILOXANES AND SILSESQUIOXANES

The second class of polymers that has been found to be relatively transparent at 157 nm, besides the hydrofluorocarbon polymers, is the siloxane polymers. For reasons that are still under investigation, polymers that contain large amounts of silicon-oxygen bonding are more transparent than other polymers. These siloxanes and their cross-linked analogs, the silsesquioxanes, have not been widely used for resist applications because their glass transition temperatures (T_g) are well below typical resist processing temperatures. The T_gs of several siloxanes and silsesquioxanes are shown in Table 2.2. It is because of these discouragingly low T_g values that not much effort and time have been dedicated to the silicon-containing resist project. However, the remarkable

transparency of these polymers at 157 nm is difficult to ignore. In the last three years or so, we have shown that it is possible to synthesize siloxanes with T_g values above 100°C.

Table 2.2: Glass transition temperatures of some siloxanes and silsesquioxanes.[60]

Siloxanes			**Silsesquioxanes**	
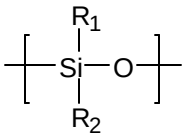			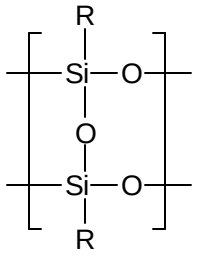	
R_1	**R_2**	**Tg (°C)**		
CH_3	H	-138		
CH_3	CH_3	-125		
CH_3	CH_2CH_3	-135		
CH_3	$CH_2CH_2CH_3$	-120	**R**	**Tg (°C)**
CH_3	$CH_2CH_2CF_3$	-70	CH_3	~95
CH_3	Phenyl	-90 to -75	PhOH	~120
Phenyl	Phenyl	50 to 100	CyclohexylCOOH	~100

The low glass transition temperatures of the linear siloxanes are due to two main reasons. The Si-O skeletal bond is unusually long (1.63 Å) as compared to 1.42 Å for a typical C-O bond or 1.54 Å for a typical C-C bond. Also, the Si-O-Si bond angle of ~143° is much more open than the usual tetrahedral bonding occurring at ~110°.[61] These two characteristics allow the polymer chains to be highly flexible. The chains, therefore, have the ability to dynamically change their spatial arrangements by rotations around the long skeletal bonds. This is

[60] Clarson, S. J.; Semlyen, J. A. *Siloxane Polymers*; Prentice Hall: Englewood Cliffs, 1993.
[61] Mark, J. E. *Polym. Prepr. (Am. Chem. Soc., Div. Polym. Chem.)* **1998**, *39*, 437-438.

especially true when there are small groups attached to the silicon atom, and is the reason for poly(dimethylsiloxane)'s low glass transition temperature of -125°C, which is the lowest recorded for any common polymer. It is not too surprising, therefore, that the glass transition temperatures of these linear siloxanes may be increased by the incorporation of bulkier groups onto the silicon atom. As seen in Table 2.2, substitution of a methyl group in poly(dimethylsiloxane) by a phenyl group to produce poly(methylphenylsiloxane) increases the T_g of the new polymer by about 35-50°C. When both methyl groups are substituted by phenyl groups, the new polymer's T_g becomes 50-100°C. This is very encouraging news for the resist chemist since it is possible to design siloxane polymers with T_gs close to or above photoresist processing temperatures.

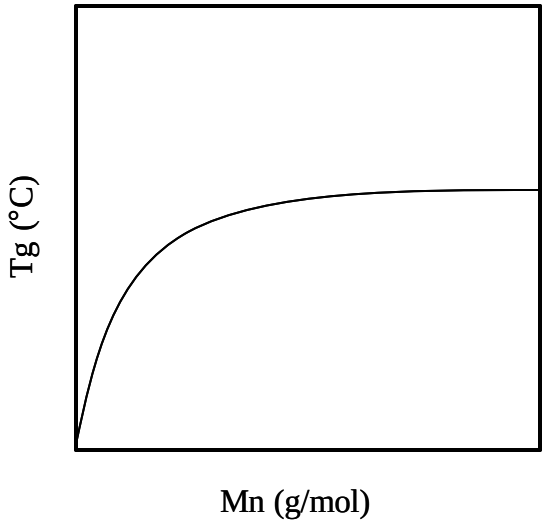

Figure 2.2: Dependence of glass transition temperature on molecular weight for linear siloxanes.

The wide range for the T_g of poly(diphenylsiloxane) depends on the molecular weight of the polymer itself. As shown in Figure 2.2, the glass transition temperatures of linear siloxanes are greatly dependent on their molecular weights.[60] Therefore, as one increases the molecular weight of the linear polymer, the glass transition temperature is increased due to the difficulty of segmental motion associated with longer chains as compared to shorter chains. Also noteworthy in Table 2.2 is the observation that a polymer with increased fluorine content in one of the side groups ($CH_2CH_2CF_3$ instead of $CH_2CH_2CH_3$) has a higher Tg than the same polymer without fluorine content. This may be due to the increased polarity of the polymer, which results in an increased Tg. One can also take advantage of hydrogen bonding to raise glass transition temperatures by incorporating phenol or carboxylic acid groups.

Silsesquioxanes, which are polymers that have, on average, one and a half oxygen atom to every silicon atom ($RSiO_{3/2}$, hence the prefix *silsesqui*), generally have higher T_gs than their siloxane counterparts. This is due to the decreased segmental motion resulting from the crosslinked chains. For example, poly(methylsilsesquioxane) has a T_g of approximately 95°C, much higher than the T_g of poly(dimethylsiloxane). When bulkier groups are used, the glass transition temperature is increased further.

Siloxanes and silsesquioxanes are useful as 157 nm resists not only because of their relative transparency at this wavelength, but also because silicon-containing polymers such as these have been found to be highly etch resistant to oxygen reactive ion etching. One of the largest concerns for using highly

fluorinated polymers is their low etch resistance towards halogen plasma reactive ion etching. One may increase the etch resistance of these polymers by incorporating alicyclics to modify the polymer's carbon ratio (see the discussion on the Ohnishi parameter in Chapter 1), but adding such groups raises the absorbance of these polymers significantly. On the other hand, silicon-containing polymers are highly etch resistant towards oxygen reactive ion etching, and the addition of more Si-O to the polymer not only lowers the polymer's absorbance but also increases its oxygen reactive ion etch resistance. This is a major advantage to using siloxanes and silsesquioxanes for 157 nm lithography. These polymers, under these etching conditions, act as a "hard mask" and very effectively protect the underlying substrate from the etchants.

From the data presented thus far, it is clear that hydrofluorocarbon polymers, siloxane/silsesquioxane polymers, or a mixture of both will be useful polymers for 157 nm lithography. Much progress has been made on fluorinated polymers. The next two chapters will discuss the research thus far on the design and synthesis of siloxane-based polymers for 157 nm lithography.

CHAPTER 3: *SILOXANES FOR 157 NM LITHOGRAPHY*

Siloxanes, or silicones $(R_1R_2SiO)_n$, are widely used for a broad variety of applications because of their many important properties.[62] Much has been learned about silicone chemistry since the early twentieth century. Many excellent books[60,63] and reviews[64-67] have been published on this subject. In general, silicones are exceptionally thermally stable in the absence of acidic or basic catalysts. Dimethylsiloxane oils only begin to degrade at temperatures above 350°C. Phenylsiloxanes are stable at higher temperatures, which is why they are used in seals for kitchen appliances, hair dryers, and other devices that require materials with high thermal stability. Besides their high thermal stability, silicones are also very resistant to electricity. This property makes silicones especially useful as materials for wire coatings, motor insulators, and transformers. Their exceptional hydrophobicity allows these silicone materials to be used as moisture barriers such as tents, waxes, sealants, etc. Because of their low surface energy, silicones are widely used as release agents to prevent

---

62 Voronkov, M. G.; Yuzhelevskii, Y. A.; Mileshkevich, V. P. *Russ. Chem. Rev.* **1975**, *44*, 355.

63 Noll, W. *Chemistry and Technology of Silicones*; Academic Press: New York, 1968.

64 Drake, R.; MacKinnon, I.; Taylor, R. *Recent Advances in the Chemistry of Siloxane Polymers and Copolymers*, In *The Chemistry of Organic Silicon Compounds*; Rappoport, Z.; Apeloig, Y., Eds.; Wiley: Chichester, UK, 1998; Vol. 2, Chap. 38, p 2217.

65 Stark, F. O.; Falender, J. R.; Wright, A. P. *Silicones*, In *Comprehensive Organometallic Chemistry*; Wilkinson, G.; Stone, F. G. A.; Abel, E. W., Eds.; Pergamon: Oxford, 1982; Chap. 9.3; p 305.

66 *Silicon Compounds (Silicones)*, In *Kirk-Othmer Encyclopedia of Chemical Technology*; 4th ed.; Kroschwitz, J. I.; Howe-Grant, M., Eds.; Wiley: New York, 1997; Vol. 22, p 1.

67 Burger, C.; Kreuzer, F. H. *Polysiloxanes and Polymers Containing Siloxane Groups*, In *Silicon in Polymer Synthesis*; Kricheldorf, H. R., Ed.; Springer: Berlin, 1996; Chap. 3; p 113.

adhesion in a variety of applications. One such application is the backing of adhesive labels.[68]

Although silicones are useful for many applications due to their unique properties as described above, some of the same properties hinder their use for lithography applications. Their low glass transition temperatures, low adhesion to many substrates, and extreme hydrophobicity make them unlikely candidates for resist applications. Polymers for resist applications need to have high T_gs to withstand the high processing temperatures, otherwise the small features may melt together. Good adhesion to the substrate is needed to prevent peeling of the features, and some hydrophilicity is also needed to help wet the polymer during aqueous-base development. The siloxanes' only true advantage is their relatively low absorbance at 157 nm. If the aforementioned problems are overcome, then siloxanes will be useful candidates for 157 nm lithography. This chapter will describe our efforts in making this goal possible. The T_gs of the siloxanes should be raised by incorporation of bulky substituents (see Chapter 2). The hydrophilicity of the siloxanes should be improved by incorporating hydrophilic groups. This should promote both adhesion and wetting by aqueous base.

CONDENSATION POLYMERIZATION

Siloxanes are normally made by the condensation polymerization of dialkyldichlorosilanes or dialkyldialkoxysilanes. Hydrolysis of chlorosilanes is the most common method of preparing silicones (Figure 3.1). The mechanism for this condensation reaction is believed to first begin with the hydrolysis of the

---

[68] Brook, M. A. *Silicones*, In *Silicon in Organic, Organometallic, and Polymer Chemistry*; Wiley: New York, 2000; Chap. 9.

starting dichlorosilane to silanediols. The silanols then condense with each other or with more chlorosilanes to produce disiloxanes, trisiloxanes, etc. The rates of hydrolysis of chlorosilanes, condensation of silanols with chlorosilanes, and silanol-silanol condensation depend greatly on the pH of the reaction (Figure 3.2). The rate of condensation polymerization between silanols is greater under basic or acidic conditions than neutral conditions. The products from these condensation reactions include linear oligomers, hexaalkylcyclotrisiloxanes (D_3), octaalkylcyclotetrasiloxanes (D_4), and other larger cyclics. The most thermodynamically stable cyclic, D_4, predominates.

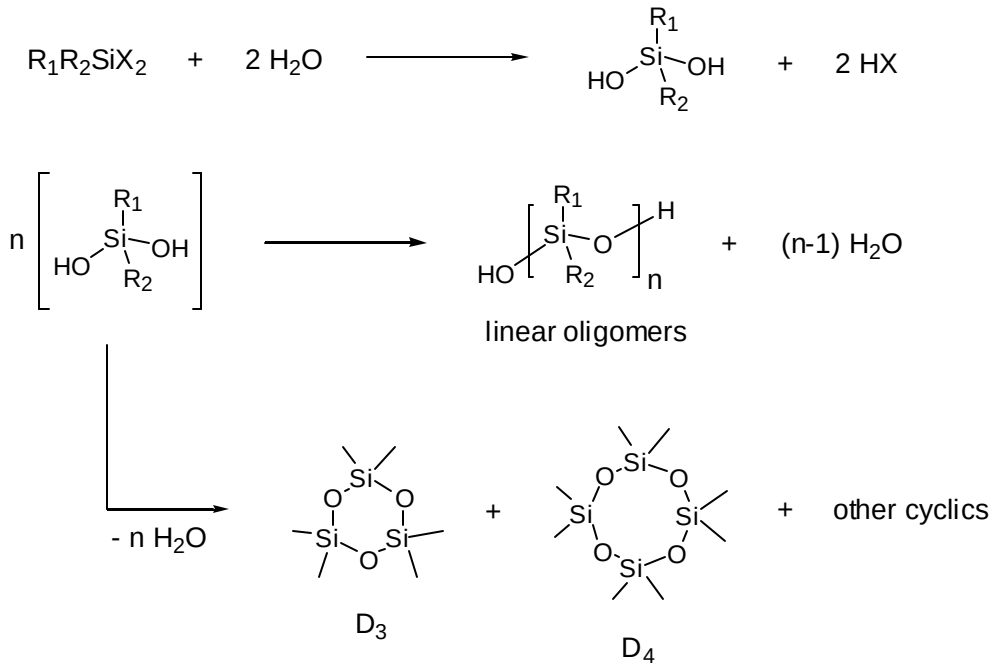

Figure 3.1: Condensation of silanols to give linear and cyclic siloxanes.

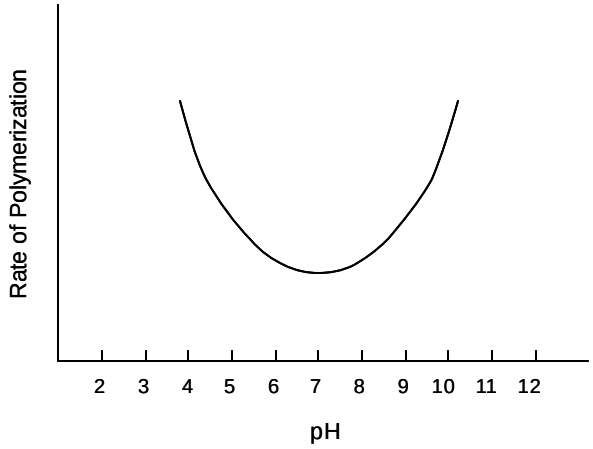

Figure 3.2: Rate of polymerization of silanols is faster under acidic or basic conditions than neutral conditions.

When the amount of water is low, chlorosilanols are produced that immediately dimerize to produce 1,3-dichlorodisiloxanes. This chloro-terminated molecule may then undergo a series of reactions with itself or with other chlorosilanols in the presence of water to produce linear oligomers, D_3, D_4, and other larger cyclics. When the polymerization is carried out in organic solvents with little water, the formation of linear siloxanes can be almost completely suppressed.

Dialkyldialkoxysilanes may also be hydrolyzed to produce polysiloxanes. However, the rate of reaction is much slower because no catalytic reagents (e.g., HCl) are produced during the condensation. The reaction rate may be increased by the use of acid or base catalysis. Linear oligomers and cyclic siloxanes are also formed.

The condensation polymerization of chlorosilanes and alkoxysilanes depends on a number of factors, some of which have already been discussed. The amount of water used is important. The type of solvent, reaction temperature, bulkiness of the alkyl group on silicon, time of reaction, type of catalyst, and pH of the reaction solution are other important factors. The reader is referred to other sources[60,68] for a more in-depth discussion.

RING-OPENING POLYMERIZATION

Linear siloxanes may also be prepared by the ring-opening polymerization of cyclic siloxanes by either acidic or basic catalysis. The D_3 cyclics reacts more rapidly than the other cyclics because of the release of ring strain (12-15 kcal/mol).[69] Under these nonequilibrating conditions (kinetic control), it is possible to prepare silicones with narrow polydispersity and very high molecular weight. Anionic initiators such as metal trimethylsilanolates may be used to initiate ring-opening polymerization (Figure 3.3). During propagation, mostly linear polymers are formed, but the living silanolate may react with existing polymer in an intramolecular (backbiting) or intermolecular fashion. Termination of the reaction is caused by end-capping the silanolate with a chlorosilane to give a stable polymer. In cationic ring-opening polymerization (Figure 3.4), protic acids, Lewis acids, or other electrophiles may be used for initiation. An oxonium ion is first produced when the initiating electrophile adds to an oxygen lone pair. Nucleophilic attack by monomer on silicon adjacent to the oxonium ion opens the ring, leading to polymerization. As with anionic polymerization, backbiting or

---

[69] Davidson, I. M. T.; Thompson, J. F. *J. Chem. Soc., Chem. Commun.* **1971**, 251.

intermolecular reactions may also occur, leading to a broad polydispersity. Termination occurs when the oxonium ion is consumed by nucleophiles such as water.

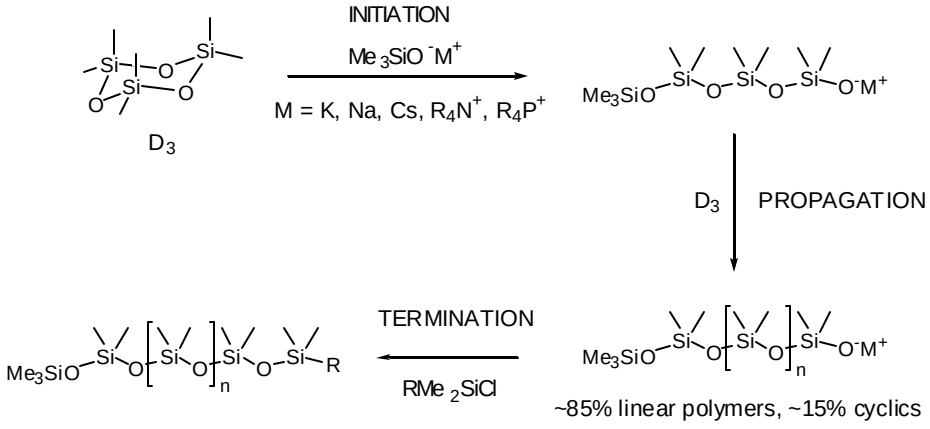

Figure 3.2: Anionic ring-opening polymerization of D_3 cyclics.

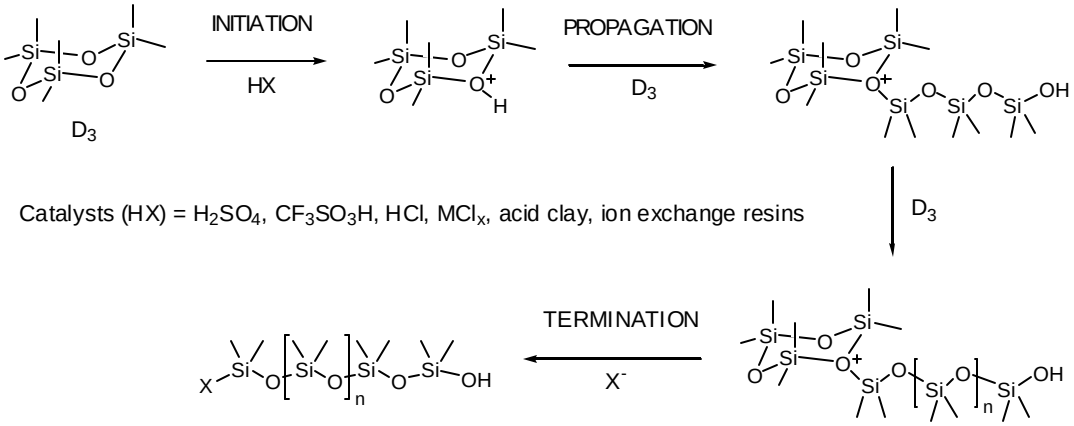

Figure 3.3: Cationic ring-opening polymerization of D_3 cyclics.

SILICON-CARBON BOND FORMATION

In order to prepare functional organosilanes, one must know how to form silicon-carbon bonds. There are no known organosilicon species produced in nature, therefore one must rely on known synthetic methods for silicon-carbon bond formation. Two of the most common methods for silicon-carbon bond formation is the nucleophilic attack of Grignard and lithium reagents onto silicon halides or silicon alkoxides and hydrosilylation of alkenes or alkynes onto silicon-hydride bonds. These two methods will be discussed in turn. These techniques, as well as other methods, have been reviewed, and the reader is referred to these reviews[68,70-72] for a more detailed discussion.

Grignard and Lithium Reactions

One of the most convenient and efficient methods for preparing organosilanes is the nucleophilic substitution reaction between carbanions and chlorosilanes. This S_N2 reaction occurs readily because the bonds to silicon are longer, making the silicon nucleus more accessible. Also, the silicon atom is more electrophilic than an analogous carbon atom because silicon usually has a partial positive charge (silicon is often polarized in the opposite sense to carbon).

Organomagnesium and alkyllithium reagents are frequently used for these substitution reactions. The most active and widely used electrophiles are chlorosilanes and alkoxysilanes, but other leaving groups on silicon may also be

---

[70] McGrath, M.; Sall, E.; Tremont, S. *Chem. Rev.* **1995**, *95*, 381.

[71] Eaborn, C.; Bott, R. W. *Synthesis and Reaction of the Silicon-Carbon Bond*, In *The Bond to Carbon*; MacDiarmid, A. G., Ed.; Dekker: New York, 1968; Vol. 1, p 105.

[72] Petrov, A. D.; Mironov, B. F.; Ponomarenko, V. A.; Chernyshev, E. A. *Synthesis of Organosilane Monomers*; Consultants Bureau: New York, 1964.

used. In general, the ease of displacement follows the pattern: Si-CN > Si-Cl > Si-OR > Si-OSi > Si-H.[73] Among the silicon halides, the rate of displacement is: Si-F > Si-Cl > Si-Br > Si-I. This is unusual since silicon-halogen bond strengths follow the same pattern. Bond strengths are often reported as bond dissociation energies for homolytic cleavage. This is an unusual reaction for silicon. Silicon usually undergoes ionic reactions. The Si-F bond is the most reactive towards nucleophilic substitution because it is a kinetically reactive bond under ionic conditions. In fact, F^- is a catalyst for cleavage of more Si-X bonds.

Hydrosilylation

The second most common method for silicon-carbon bond formation is the hydrosilylation reaction. Hydrosilylation involves the addition of a Si-H bond across a π bond (an alkene or alkyne). The reaction can be initiated radically by a free-radical initiator or by the use of a transition metal catalyst. An azo compound such as azobis(isobutyronitrile) (AIBN) or a peroxide such as di-*tert*-butyl peroxide may be used to initiate the radical hydrosilylation reaction, although the abstraction of hydrogen from R_3SiH is favored thermodynamically by about 20 kcal/mol over a carbon radical. The silyl radical then adds across the double bond in an *anti*-Markovnikov fashion, generating a carbon radical which may abstract another hydrogen from R_3SiH (Figure 3.4).[74] The efficiency of radical hydosilylation depends on the reactivity of the alkene and the hydrosilane. Terminal alkenes react much more rapidly than internal alkenes. Hydrosilanes

---

[73] Arkles, B. *Silanes*, In *Handbook of Grignard Reagents*; Silverman, G.; Rakita, P., Eds.; Marcel Dekker: New York, 1996; Chap. 32; p 667.

[74] Marciniec, B.; Gulinski, J.; Urbaniak, W.; Kornetka, Z. W. *Comprehensive Handbook on Hydrosilylation Chemistry*; Pergamon: Oxford, 1992.

containing electron-withdrawing groups are much more reactive than those containing electron-donating groups. The order of hydrosilane reactivity toward radical hydrosilylation is: $HSiCl_3 > HSiRCl_2 > HSiR_2Cl > HSiR_3$.[74] Radical hydrosilylation cannot be used with olefins that are easily polymerized free-radically, such as styrene and the acrylates.

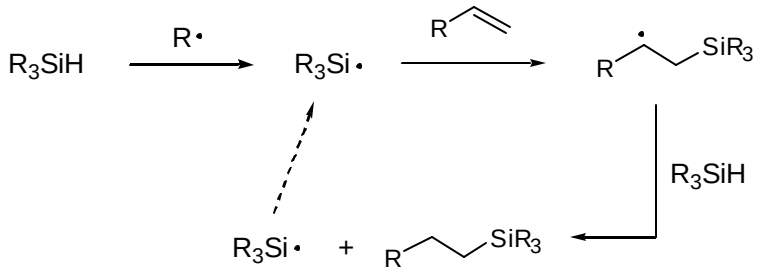

Figure 3.4: Radical hydrosilylation between an olefin and a hydrosilane.

Hydrosilylation by transition metal catalysts has become more popular than radical hydrosilylation. This is due to the discovery of extremely efficient metal catalysts based on Pt. Other catalysts such as Rh, Co, and Ni have also been used, but Pt is by far the most efficient and most studied catalyst. Less than 1 ppm of Pt catalyst is needed for complete hydrosilylation in some reactions. The efficiency and rate of hydrosilylation depends on the type and properties of the catalyst, olefin, and hydrosilane.

Three classes of platinum catalysts were studied in this project. Platinum catalysts at the zero oxidation state [Karstedt's catalyst, which is Pt^0 complexed by a divinylsiloxane species, $Pt_2(H_2C{=}CHSiMe_2OSiMe_2CH{=}CH_2)_n$], as well as

those at higher oxidation states such as Pt^{IV} (Speier's catalyst, H_2PtCl_6) and Pt^{II} (cyclopentadienyldichloroplatinum, $CpPtCl_2$), have all been studied. Each of these catalysts has its own advantages and disadvantages depending on the reaction conditions. Several reviews[74-77] have been written describing these differences.

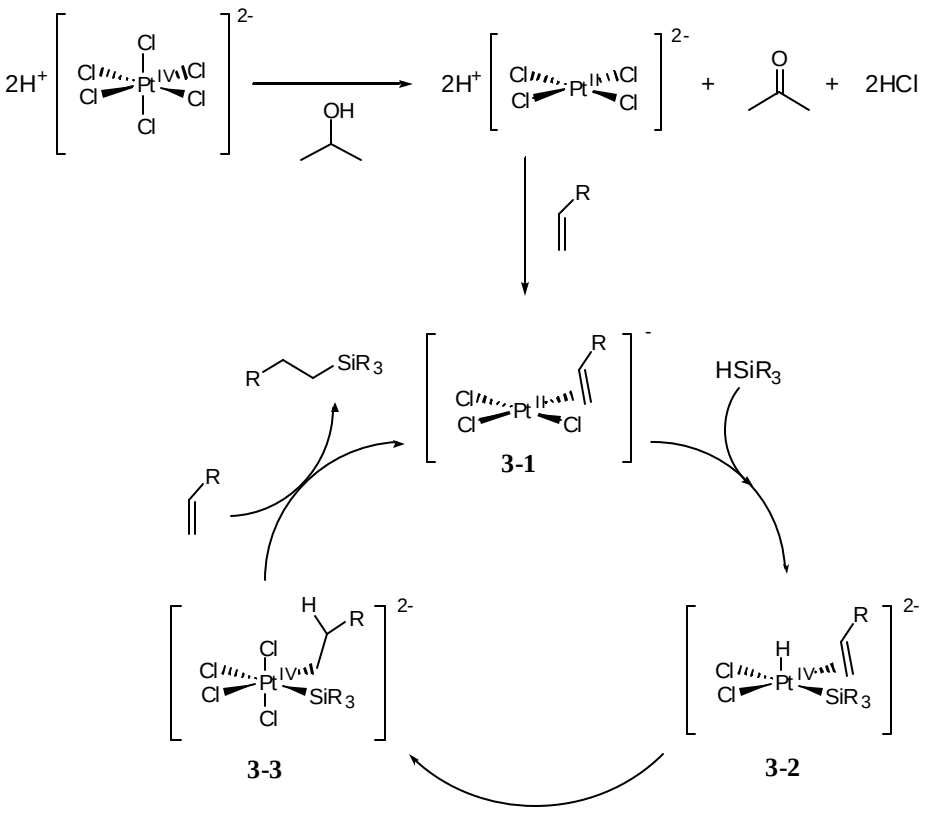

Figure 3.5: Proposed mechanism for platinum-catalyzed hydrosilylation.

---

75 Ojima, I.; Li, Z.; Zhu, J. *Recent Advances in the Hydrosilylation and Related Reactions*, In *The Chemistry of Organic Silicon Compounds*; Rappoport, Z.; Apeloig, Y., Eds.; Wiley: Chichester, UK, 1998; Vol. 2, Chap. 29, p 1687.

76 Ojima, I. *The Hydrosilylation Reaction*, In *The Chemistry of Organic Silicon Compounds*; Patai, S.; Rappoport, Z., Eds.; Wiley: Chichester, UK, 1989; Vol. 1, Chap. 25, p 1479.

77 Hiyama, T.; Kusumoto, T. *Hydrosilylation of C=C and C°C*, In *Comprehensive Organic Synthesis*; Trost, B. M.; Fleming, I., Eds.; Pergamon: Oxford, 1991; Vol. 8, Chap. 3.12, p 763.

The proposed mechanism for platinum-catalyzed hydrosilylation, first brought forth by Chalk and Harrod in 1965, involves the sequence of steps outlined in Figure 3.5.[74,78] Reduction of the catalyst by isopropanol converts the starting Pt^{IV} species to a Pt^{II} species. Coordination of the olefin provides the complex **3-1**. Oxidative addition of $HSiR_3$ gives the hexacoordinated species **3-2**, and migratory insertion of hydrogen onto the double bond changes the π complex to a σ complex **3-3**. Reductive *syn* elimination results in the desired, hydrosilylated product.

During hydrosilylation, it is known that platinum is reduced: $Pt^{IV} \rightarrow Pt^{II} \rightarrow Pt^{0} \rightarrow$ Pt colloids. The formation of Pt colloids turns the reaction medium from a yellow color to a dark brown color, so one can visually observe the completion of the reaction. The platinum catalyst can tolerate a variety of functional groups, but groups that are good ligands for platinum (e.g., amines, phosphines, and sulfoxides) poison the catalyst because they coordinate more strongly to the platinum center than the olefin. It has also been observed that the presence of O_2 accelerates the reaction (O_2 is a co-catalyst).[79] As with radical hydrosilylation, terminal olefins react faster than internal olefins in platinum-catalyzed hydrosilylation (steric factor). Electron-rich olefins react more rapidly than electron-poor olefins (electronic factor). Hydrosilanes with electron-withdrawing groups react more rapidly than hydrosilanes with electron-donating

---

78 Chalk, A. J.; Harrod, J. F. *J. Am. Chem. Soc.* **1965**, *87*, 16.

79 Brook, M. A. *Formation of Si-C Bonds: The Synthesis of Functional Organosilanes*, In *Silicon in Organic, Organometallic, and Polymer Chemistry*; Wiley: New York, 2000; Chap. 12.

groups, as seen in the trend: $HSiCl_3$ > $HSiEtCl_2$ > $HSiEt_3$ > $HSi(OEt)_2Et$ > $HSi(OEt)_3$.

EARLY STUDIES ON AROMATIC SILOXANES

Near the beginning of the 157 nm project, a large effort was put into identifying transparent materials. Several researchers measured the absorbance of many polymers using variable angle spectroscopic ellipsometry (VASE) – see Chapter 2. In addition to these measurements, our group also started to measure the absorbance of several monomers in the gas phase.[53] If these compounds were found to be transparent in the gas phase, then the polymers that are made from these monomers should be transparent as well.

Preliminary screening of several compounds using gas-phase vacuum UV spectrometry showed that aromatic siloxanes are relatively transparent at 157 nm, when compared to norbornane and 2,2-difluoronorbornane (Figure 3.6). This observation is surprising considering that the π to π^* transition of the aromatic ring would cause these compounds to absorb strongly in the vacuum UV region. This data may be a little suspicious, considering that thin film absorbance measurements showed that poly(methylphenylsiloxane) has an absorbance of 2.7 mm^{-1} at 157 nm. Also, in the gas-phase spectra shown in Figure 3.6, the large absorbance at ~200 nm typical of aromatic compounds is missing. This later led us to question the accuracy of the gas-phase data. In spite of these problems, we decided to pursue the synthesis of aromatic siloxane polymers for two reasons. First, we wanted to learn and optimize the methods for synthesizing silicon-carbon bonds by Grignard addition. The use of aromatic Grignards provided the

most facile pathway. In addition, we wanted to determine how high we could increase the glass transition temperature of these siloxanes by incorporating bulky substituents such as benzene.

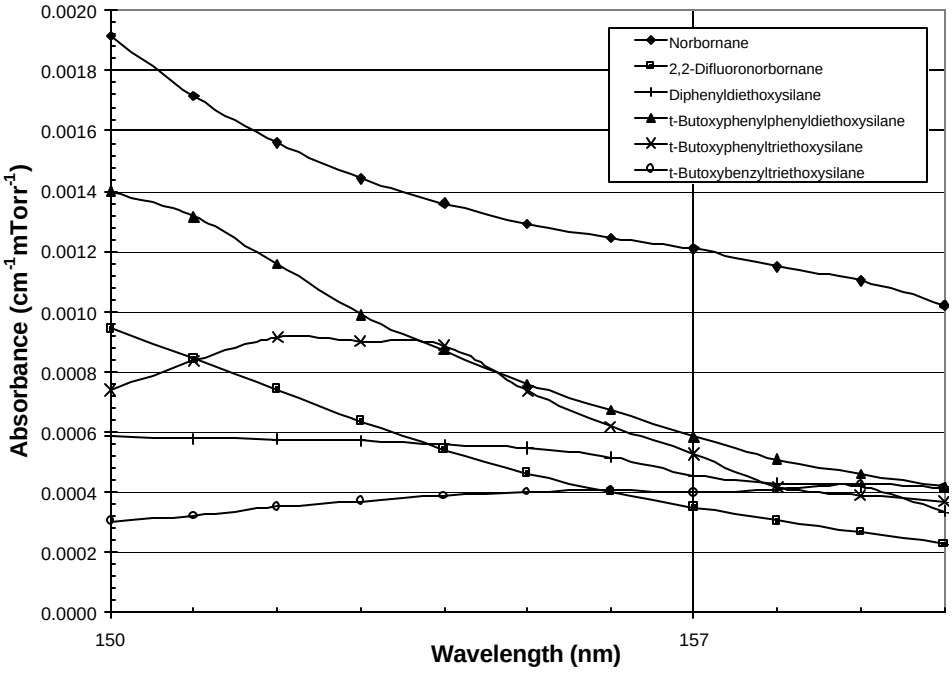

Figure 3.6: Gas-phase vacuum UV spectra of several ethoxysilanes. Each is compared to the absorbance of norbornane and the relatively transparent 2,2-difluoronorbornane.

Several Grignard reactions were performed in an attempt to make *tert*-butoxyphenylsilanes. The tert-butyl protecting group was chosen because of its higher resistance to acid as compared with an acetal or *t*-BOC protecting group. This is important, as shown later, when one wants to make functionalized chlorosilanes. The synthesis of *t*-butoxyphenyldiethoxysilane (**3-4**) was

attempted by the Grignard addition of *t*-butoxyphenylmagnesium bromide to triethoxysilane (Figure 3.7). This product was chosen because hydrosilylation of other bulky, fluorinated olefins onto the silicon-hydrogen bond could provide access to a polymer with a high glass transition temperature. However, the synthesis of this monomer is not as easy as it looks. Normally, the aqueous workup step after a Grignard addition is used to purify the product, which is usually more soluble in the organic phase, from water soluble impurities and ions. When an aqueous workup was used in this reaction, a gel was obtained instead of the desired product.

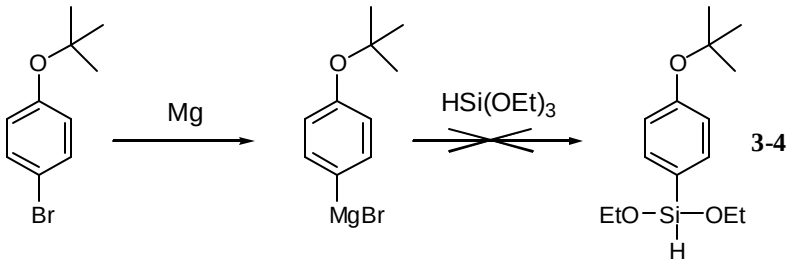

Figure 3.7: Attempted synthesis of *tert*-butoxyphenyldiethoxysilane.

Since the addition of water to the reaction mixture would quench any excess Grignard reagent to create hydroxide anions, the basic aqueous medium would cause the formation of silanols (hydrolysis of ethoxy groups), leading to polymerization of the monomer. Neutral water alone will also cause this, albeit at a much slower rate. This is not so undesired, since the final target would need to be polymerized by aqueous acid or base anyway. However, what also happens in this aqueous base medium is the cleavage of the silicon-hydride bond. It is

known that this bond is very susceptible to aqueous base hydrolysis.[80] Infrared analysis of the gel did not show the characteristic peak of the Si-H bond at ~2100 cm^{-1}.

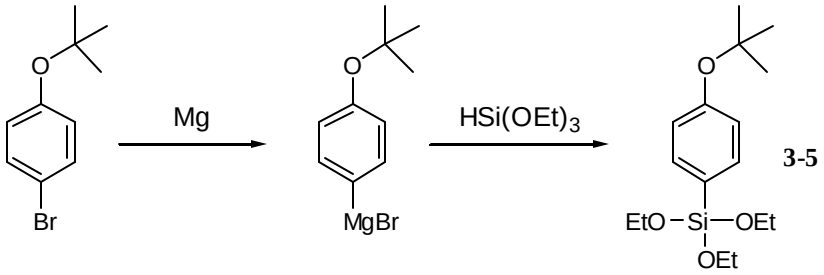

Figure 3.8: Unexpected synthesis of *tert*-butoxyphenyltriethoxysilane.

Due to the problems presented, the reaction shown in Figure 3.7 was performed using nonaqueous workup conditions with Schlenck techniques. The THF was evaporated and hexane was added to precipitate inorganic salts and dissolve the product. Filtration, followed by evaporation, should have provided the desired product **3-4**, but instead the major product was determined to be **3-5** (Figure 3.8). A likely explanation for this observation is that the reaction does not undergo a true S_N2 pathway. Since silicon's coordination shell is easily expanded due to its low-lying d-orbitals, attack of the carbanion may lead to a pentacoordinated silicon intermediate. In a sense, the hydrosilane is activated by a silaphilic nucleophile such as DMSO, fluoride, amines, alkoxides, and hydroxides. In this case the carbanion is the silaphilic nucleophile. A ligand on extracoordinate silicon is often more nucleophilic than the same ligand on tetracoordinate silicon. Therefore, hydrosilanes that undergo coordination

[80] Brook, M. A. *Hydrosilanes as Reducing Agents*, In *Silicon in Organic, Organometallic, and Polymer Chemistry*; Wiley: New York, 2000; Chap. 7.

expansion in the presence of added nucleophiles become strong reducing agents. The hydride can participate in other reactions such as the reduction of carbonyl groups or abstraction of acidic protons to produce hydrogen gas. An example of such a reaction is shown in Figure 3.9.[80] The base-catalyzed redistribution of oligomethylhydridosiloxane to form a crosslinked polymer is shown in Figure 3.10.[81] The hydroxide anion in aqueous base acts as the silaphilic catalyst, expanding the coordination shell of the hydrosilane. The hydride abstracts a proton from water, producing hydrogen gas and regenerating hydroxide which reacts with the hydrosilane again. Both of these examples help to explain the redistribution of the Si-H bond seen in the Grignard reactions.

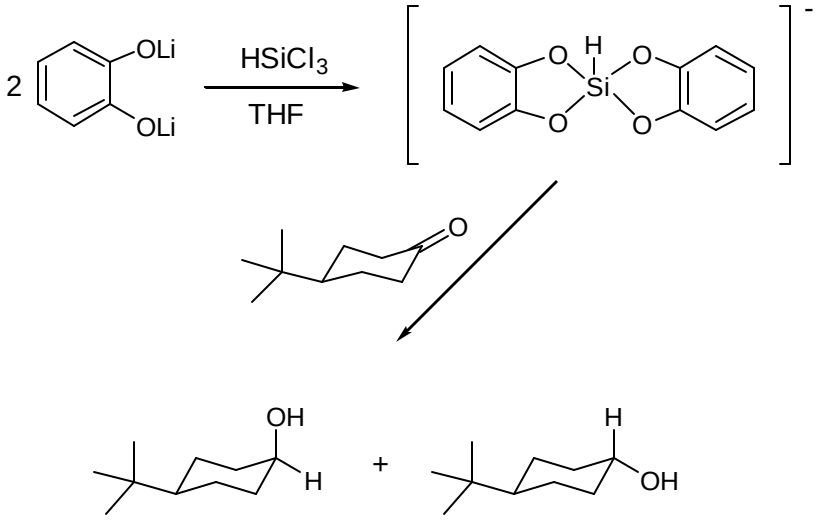

Figure 3.9: Extracoordinated hydrosilanes are strong reducing agents.

[81] Rahimian, K.; Assink, R. A.; Loy, D. A. *Polym. Prepr. (Am. Chem. Soc., Div. Polym. Chem.)* **2000**, *41*, 512-513.

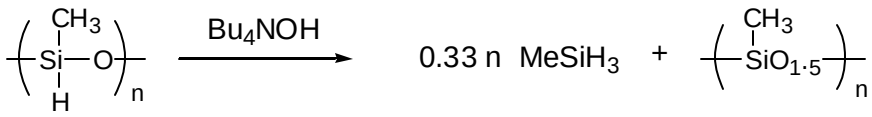

Figure 3.10: Base-catalyzed redistribution of oligomethylhydridosiloxane to form polymethylsilsesquioxane.

Instead of triethoxysilane, which led to all the problems discussed above, we decided to use phenyltriethoxysilane as the electrophile. The Grignard addition of *t*-butoxyphenylmagnesium bromide to this compound provided the expected monomer after nonaqueous workup (Figure 3.11). Large quantities of this monomer were made for polymerization studies. These alkoxysilanes may be polymerized using either aqueous acid or aqueous base, as discussed earlier. Aqueous acid will most likely cleave the *t*-butyl ether protecting group, so in this case aqueous base was the only other option. The polymerization was studied with three different bases: 1 *M* NaOH, 30% NH_4OH in water, and 40% $N(Bu)_4OH$ in water. All the polymerizations were done under neat (no solvent) conditions to minimize the formation of cyclics. The final polymers were not end-capped with a trimethylsilyl group for these studies, but would need to be end-capped for imaging studies to prevent redistributions of the Si-O bond. Table 3.1 lists the effect of each base on the polymerization.

Tetrabutylammonium hydroxide is the most efficient of the three bases tested. Polymerization occured at room temperature and a white solid precipitate is seen only after a few hours. When sodium hydroxide or ammonium hydroxide

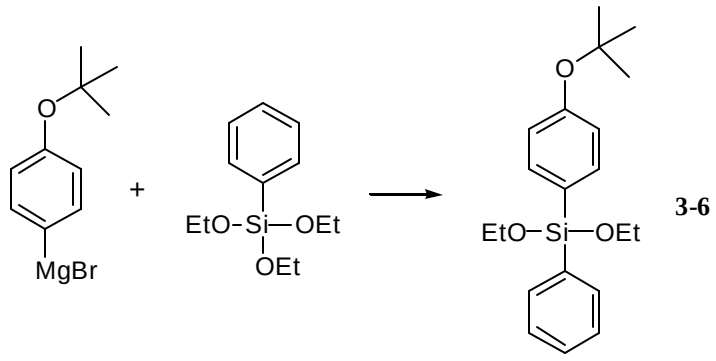

Figure 3.11: Successful synthesis of a functionalized alkoxysilane.

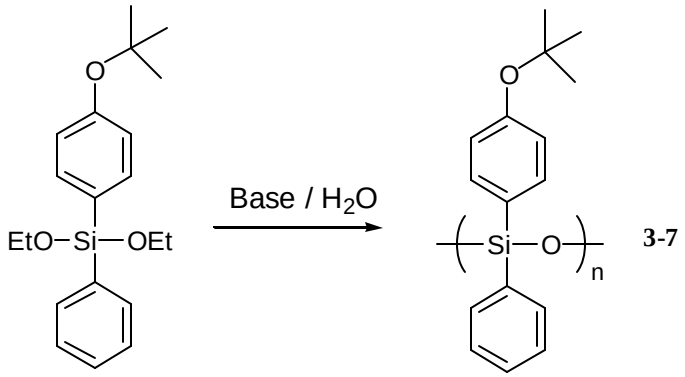

Table 3.1: Polymerization results of a dialkoxysilane using different bases.

Base	GPC Analysis
1 *M* NaOH	Mn = 6,000 + cyclics
30% NH_4OH	Mn = 10,000 + cyclics
40% $N(Bu)_4OH$	Mn = 17,000 + cyclics

is used as the base, heating is necessary to obtain higher molecular weight polymer. This difference may be due to tetrabutylammonium hydroxide's higher solubility in the monomer. The other two bases may not be as efficient because of their lower solubilities.

Grignard addition to chlorosilanes is much more facile than that with alkoxysilanes. When trichlorosilane is used as the electrophile, side reactions such as the redistribution of Si-H do not happen because chlorine is a good leaving group. In this case the reaction acts more like a typical S_N2 reaction. The synthesis of *t*-butoxyphenyldichlorosilane (**3-8**) is shown in Figure 3.12. Polymerization of compound **3-8** using either aqueous acid or base is problematic. The addition of water would cause the generation of HCl, cleaving the *t*-butyl ether protecting group. Aqueous base would cause the redistribution of the Si-H bond. A way around this dilemma is shown in Figure 3.13.

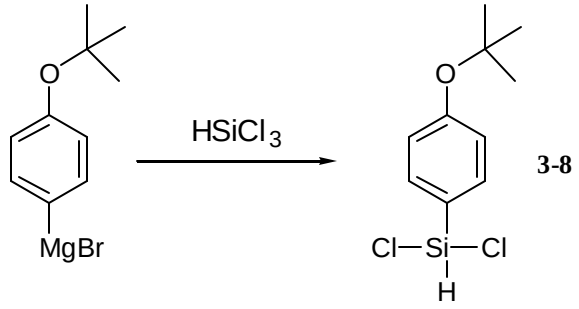

Figure 3.12: Synthesis of a dichlorosilane.

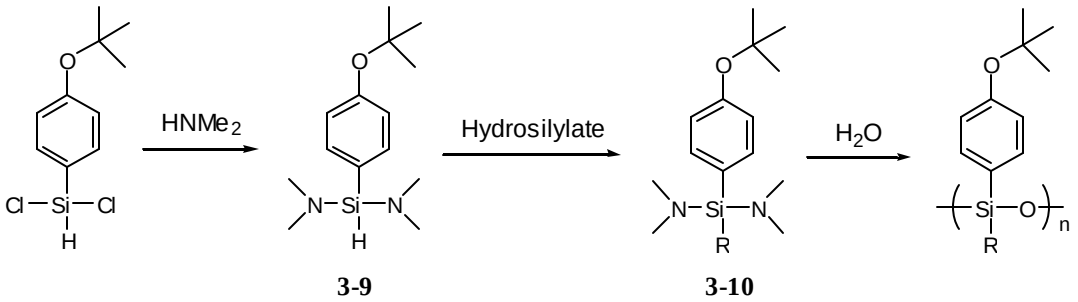

Figure 3.13: Alternative pathway to a hydrosilylated siloxane.

Bubbling dimethylamine gas into the reaction mixture containing chlorosilane (**3-8**) would produce the dimethylamino adduct **3-9**. Hydrosilylation of the desired olefin would give **3-10**. Hydrosilylation of compound **3-9** is chosen rather than hydrosilylation of the starting dichlorosilane because the hydrosilylation reaction proceeds much more easily with electron-donating groups on silane. The addition of water to **3-10** would liberate dimethylamine and form a siloxane polymer.

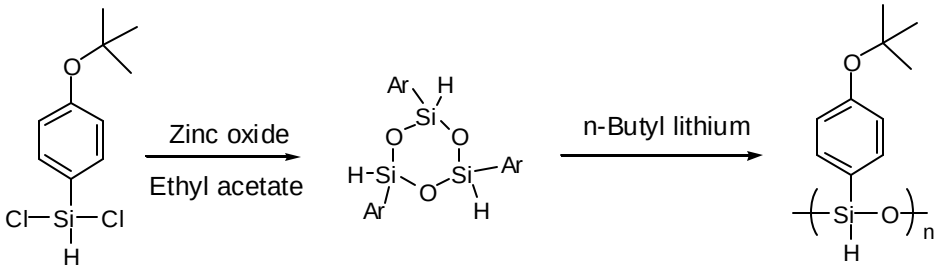

Figure 3.14: Pathway to a functionalized linear hydridosiloxane.

Another pathway for polymerizing compounds like **3-8** is to form D_3 cyclics and polymerize those strained cyclics (Figure 3.14). The reaction of dichlorosilanes and zinc oxide produces cyclic siloxanes of different sizes. The D_3 cyclic can be isolated by crystallization. The anionic ring-opening polymerization of these strained cyclics by *n*-butyl lithium should provide polymers containing Si-H bonds.

Two other aromatic silicon-containing polymers were made early in the project for initial evaluation. These are the aromatic silsesquioxanes. More will be discussed about the silsesquioxanes in the next chapter, but the aromatic

silsesquioxanes are included here for completeness. The synthesis of these two polymers is shown in Figure 3.15. The procedures that had been worked out for synthesizing the siloxanes were used to make these polymers. The organolithium reagent was prepared by cleavage of the corresponding methylbenzyl ether.[82-84] Both the Grignard reagent and organolithium reagent were added to tetraethylorthosilicate, forming a triethoxysilane that was polymerized in aqueous base to give the respective silsesquioxane.

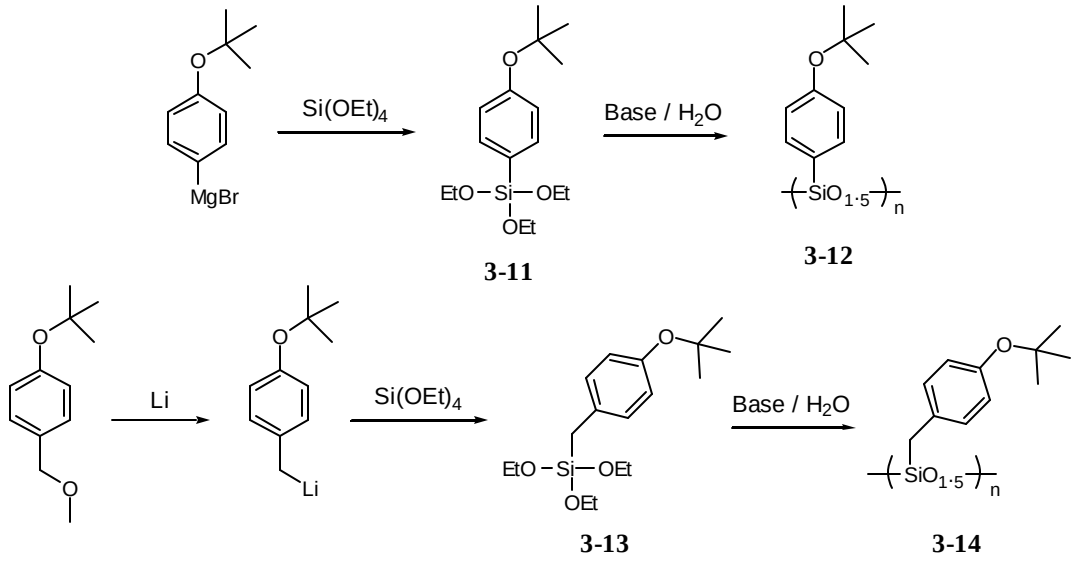

Figure 3.15: Synthesis of functionalized aromatic silsesquioxanes.

Thin films of polymers **3-7**, **3-12**, and **3-14** were coated onto silicon wafers and their vacuum UV absorbance was determined. Figure 3.16 shows the spectra of these three polymers. All the polymers are strongly absorbing at 157

82 Gilman, H.; McNinch, H. A. *J. Org. Chem.* **1961**, *26*, 3723-3729.
83 Maercker, A. *Angew. Chem. Int. Ed. Engl.* **1987**, *26*, 972-989.
84 Wakefield, B. J. *Organolithium Methods*; Academic Press: London, 1988; p 47-49.

nm. Polymer **3-7** has an absorbance of 7 μm^{-1}, while both polymers **3-12** and **3-14** have an absorbance of 5 μm^{-1}. These numbers are much higher than the target of 1-2 μm^{-1} for a 157 nm resist. Also, this data contradicts the data seen in the gas-phase spectra for the alkoxysilane monomers used to make these polymers (Figure 3.6). In Figure 3.16, the typical aromatic absorption is evident in the large absorption peak at approximately 195 nm. This data is therefore more reliable than the gas-phase data reported earlier, in which no aromatic absorption peaks were seen. Unfortunately, the tail of this absorption only "dips" as far as 5 μm^{-1} at 157 nm, making these aromatic siloxane and silsesquioxane polymers unsuitable for use as 157 nm resists.

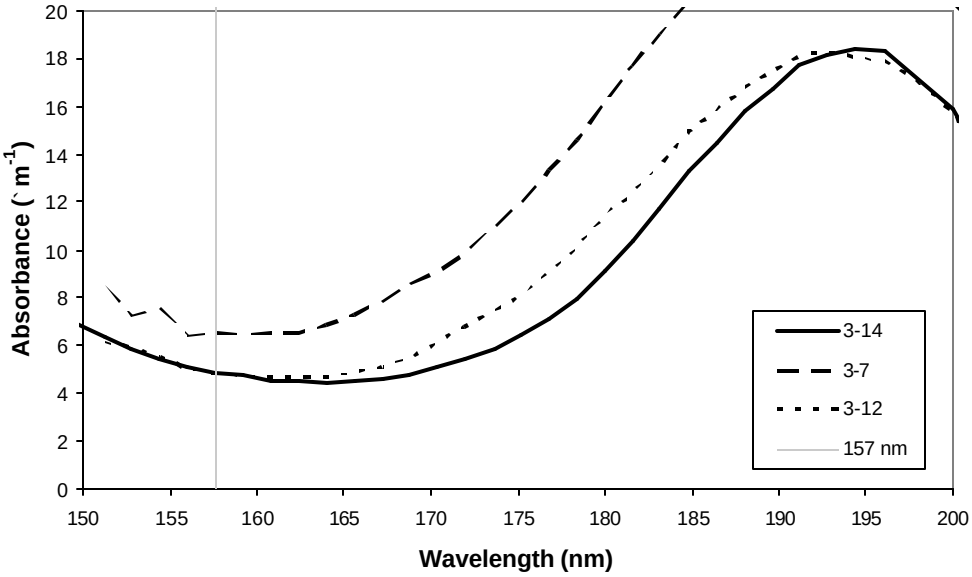

Figure 3.16: Vacuum UV absorbance of aromatic siloxane polymers.

Table 3.2 provides a summary of the properties of polymers **3-7**, **3-12**, and **3-14**. The siloxane polymer (**3-7**) has a Tg well below typical resist baking temperatures. However, the aromatic silsesquioxane polymers (**3-12** and **3-14**) have very reasonable Tg's. Unfortunately their absorbance at 157 nm is too high, so other polymers must be designed that possess these high Tg characteristics but are lower absorbing at 157 nm.

Table 3.2: Properties of three aromatic siloxane polymers.

Polymer	Mw	Tg (°C)	A_{157} (μm^{-1})
3-7	10,000	56	6.45
3-12	3,650	111	4.72
3-14	2,760	95	4.88

EARLY STUDIES ON ALICYCLIC SILOXANES

Although much has been learned about the synthesis of aromatic siloxanes through Grignard and organolithium addition to chlorosilanes or alkoxysilanes, the absorbance of these polymers is unfortunately high. A pathway to less absorbing polymers may be the use of alicyclic substituents to replace the aromatic substituents. This has been done before when 193 nm resists were designed to replace 248 nm resists. As we move to the 157 nm wavelength, fluorinated alicyclics are needed.

Early studies on the synthesis of alicyclic siloxanes involved the hydrosilylation of norbornene or dinorbornene alicyclics onto commercially available poly(methylhydridosiloxane) using an appropriate platinum catalyst.

Several polymers were made using this method (Figure 3.17).[85,86] The first polymer, **3-15**, has a Tg of about 6°C, making it unsuitable for imaging. However, by incorporating bulkier groups such as dinorbornene onto the polymer chain, the Tg's of these siloxanes may be increased significantly. For instance, the other three polymers all have glass transition temperatures above room temperature. Polymers **3-17** and **3-18** have glass transition temperatures of 74°C and 100°C, respectively. The imaging characteristics of each was tested using contact printing with 248 nm radiation. Each system showed positive-tone images, which suggests that these siloxanes are good candidates as 157 nm resists.

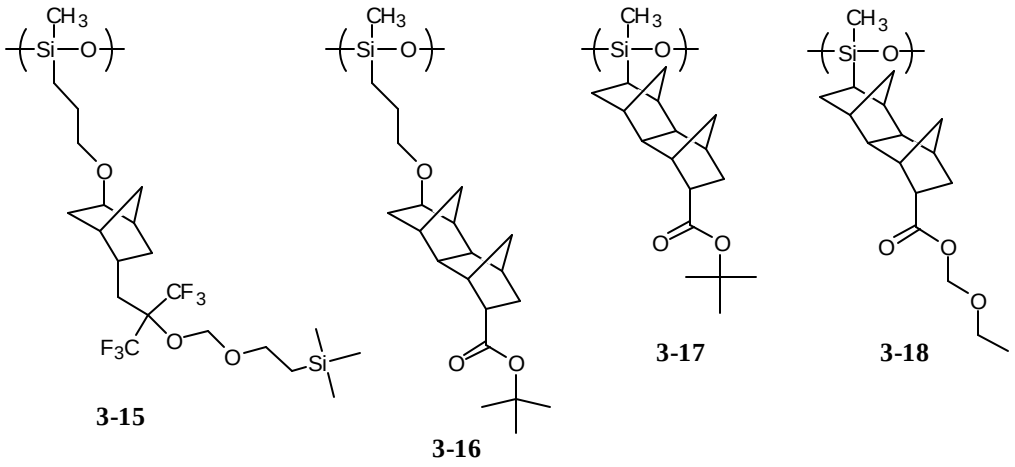

Figure 3.17: Early siloxane polymers made for 157 nm imaging.

Because the last three of these linear alicyclic siloxanes have many C-C and C-H bonds and do not incorporate any fluorine, they are highly absorbing at 157 nm. Polymer **3-17**, for example, has an absorbance of 6 μm^{-1}. This is not

[85] Patterson, K. Ph.D. Dissertation, University of Texas at Austin, 2000.
[86] Hung, R. J. Ph.D. Dissertation, University of Texas at Austin, 2001.

acceptable, so fluorines must be incorporated into this polymer to decrease absorbance at 157 nm.

Another problem that arose during initial imaging of these linear siloxanes is their hydrophobicity. These polymers are very hydrophobic and do not wet well during aqueous base development. As a result, the exposed areas are not cleanly dissolved away, and adhesion failure is observed in the smallest features. The best way to fix this problem, besides adding a surfactant to the base developer, is to incorporate more hydrophilic groups onto the side chain.

FLUORINATED ALICYCLIC SILOXANES

A pathway to more hydrophilic polymers is the hydrosilylation of monomers such as 3-(bicycle[2.2.1]hept-5-en-2-yl)-1,1,1-trifluoro-2-(trifluoromethyl)propan-2-ol (NBHFA, **2-1**) or its dinorbornene analog onto poly(methylhydridosiloxane). Hydrosilylation of free alcohols is problematic because hydrosilanes will react with reactive hydrogens such as OH to produce H_2 gas and alkoxysilanes (Figure 3.18). This reaction is often slower than the hydrosilylation reaction itself, but its occurrence would drastically lower hydrosilylation yields. Free alcohols may also suppress the catalytic activity of platinum complexes by competing for the platinum center with the olefin to be hydrosilylated. When platinum catalysts such as Karstedt's catalyst [$Pt_2(H_2C{=}CHSiMe_2OSiMe_2CH{=}CH_2)n$] or dicyclopentadienyldichloroplatinum is used to hydrosilylate the hexafluoroisopropanol monomers, the yields obtained are often low. However, when Speier's catalyst (H_2PtCl_6) is used, hydrosilylation occurs in good yield. This high reactivity towards hindered alcohols may be due

to the acidic nature of the catalyst. The alcohol is most likely protonated during the reaction, preventing its interference with hydrosilylation and reaction with the hydrosilane.

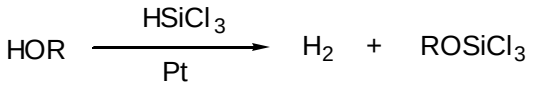

Figure 3.18: Side reaction of alcohol and hydrosilane to produce hydrogen gas and an alkoxysilane.

Speier's catalyst, therefore, was used to synthesize both polymers **3-20** and **3-22** (Figure 3.19). Each alicyclic monomer was heated with poly(methylhydridosiloxane) in toluene at 100°C with a catalytic amount of hexachloroplatinic acid. After an induction time of several minutes, the reaction solution turned a dark brown color, indicating the formation of active platinum colloids. The workup step involves the addition of activated carbon to the reaction mixture to grab residual platinum and filtering the solids through diatomaceous earth (Dicalite). Further purification involves bubbling the reaction mixture with hydrogen gas to reduce and unbind any platinum species that are still coordinated to the polymer. Stirring with activated carbon and filtering through Dicalite, followed by precipitation to remove excess monomer, provides a white polymer with platinum contamination in the ppm range (according to elemental analysis). Analysis of the final polymers revealed that the hexafluoroisopropanol moiety was not consumed in the reaction (infrared shows a significant amount of OH). Due to the acidic nature of this reaction (if THF is used as the solvent, poly(tetramethyleneoxide), or poly(THF), is formed), one

might suspect the cleavage of Si-O backbone in the polymer. This, in fact, is not observed because little to no water is present in the reaction medium, preventing the redistribution of the Si-O bonds. Both polymers **3-20** and **3-22** were synthesized in high yields using these reaction conditions.

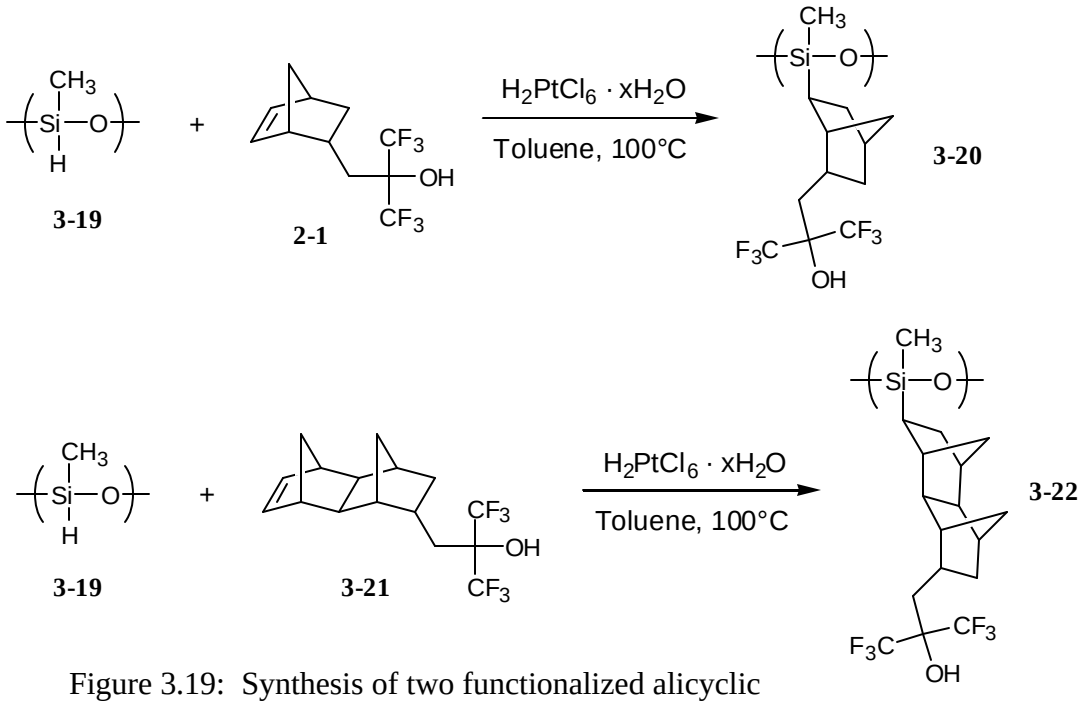

Figure 3.19: Synthesis of two functionalized alicyclic siloxanes by the hydrosilylation reaction.

The large dependence of glass transition temperature on the molecular weight was observed in the synthesis of polymer **3-22**. Two versions of polymer **3-19** may be bought commercially. One has a molecular weight of 400 g/mol while the other has a molecular weight of 2,200 g/mol. Hydrosilylation of monomer **3-21** onto the lower molecular weight polymer provides a polymer (**3-22**) that is a viscous oil at room temperature. On the other hand, hydrosilylation

of monomer **3-21** onto the higher molecular weight polymer provides a polymer (**3-22**) that is a white solid at room temperature. This difference is drastic, and provides evidence that the glass transition temperatures of linear siloxanes can be improved significantly by both incorporating bulky substituents and increasing the molecular weight of the final polymer.

Table 3.3: Properties of two alicyclic linear siloxanes.

Polymer	Mw	Tg (°C)	A_{157} (μm^{-1})
3-20	19,600	43	2.34
3-22	45,400	105	3.09

The absorbance of these two polymers at 157 nm are much higher than expected. Poly(methylhydridosiloxane)'s absorbance could not be measured because the polymer is an oil at room temperature and could not be coated onto a silicon wafer for vacuum UV measurement. Its absorbance is not expected to be high because siloxanes are one of the most transparent materials at 157 nm. The homopolymer of monomer **2-1**, poly(NBHFA), has an absorbance of about 1.2 μm^{-1}. Therefore, by attaching monomer **2-1** onto poly(methylhydridosiloxane), one would not expect such a high absorbance at 2.34 μm^{-1}. This high absorbance may be caused by contaminants in the polymer such as platinum. The platinum content of these two polymers was measured by elemental analysis and found to be < 115 ppm. Although this number may seem low, it is high according to resist standards, which require resists with metal contamination down to the ppb range.

Polymer **3-22** was partially protected with the *tert*-butyloxycarbonyl (*t*-BOC) group by reaction with di-*tert*-butyl dicarbonate (bisBOC) and 4-

dimethylaminopyridine (DMAP) to give copolymer **3-23** (Figure 3.20). The final copolymer ratio was very close to the feed ratio of bisBOC and each monomer unit of polymer **3-22**. An 80/20 ratio was targeted because this would provide a

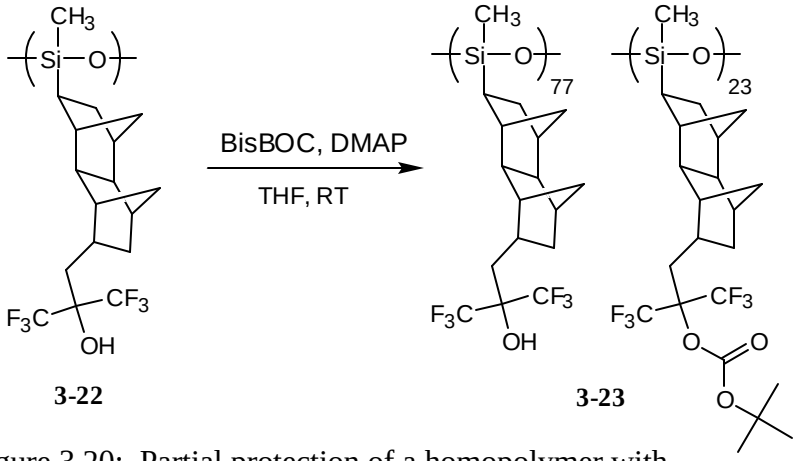

3-22 **3-23**

Figure 3.20: Partial protection of a homopolymer with *t*-BOC to provide a new copolymer.

copolymer with enough protected sites to render it insoluble in the industry standard 0.26 *N* TMAH base developer. This polymer was evaluated lithographically using 248 nm radiation to determine if there are any unforeseen problems that might be encountered when imaging these siloxane polymers. Figure 3.21 shows a representative image from the contact printing experiment, in which the mask was placed directly in contact with the wafer during exposure. About 6 wt% (relative to the weight of the polymer) of triphenylsulfonium nonaflate was used as the photoacid generator. A positive-tone image was obtained. This observation is significant because of the following reason. Siloxanes are generally very stable thermally, but are not very stable hydrolytically, especially in the presence of acids or bases. In such an

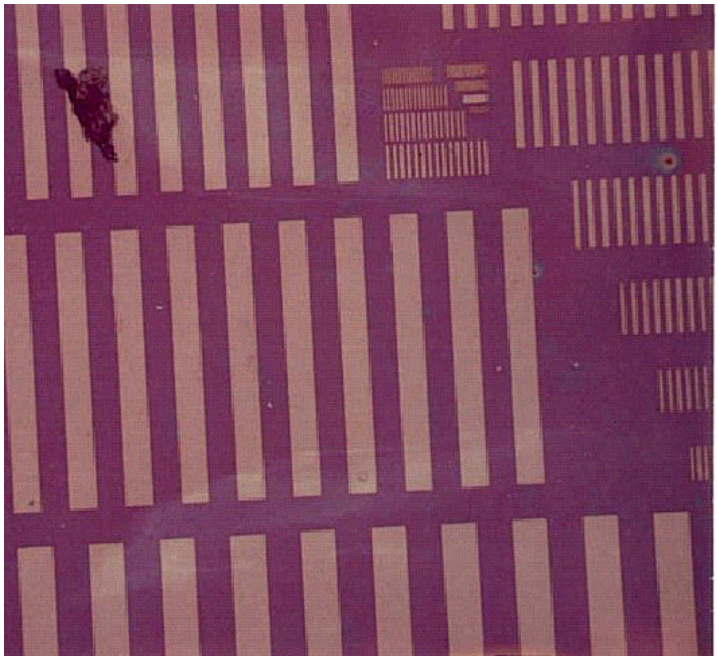

Conditions: PAB: 110°C/90s, Exposure: 23 mJ/cm^2, PEB: 110°C/90s, Develop: 10% v/v IPA in 0.26 *N* TMAH/60s

Figure 3.21: Contact print of polymer **3-23** with 6 wt% triphenylsulfonium nonaflate.

environment, the Si-O bond would cleave and main chain scission occurs. The positive-tone image obtained proves that the dissolution of the polymer in aqueous base is much faster than the cleavage of the Si-O bond, otherwise cleavage would occur, silanols would form, and the entire polymer film would dissolve in the aqueous base developer, leaving no image. This does not occur in the 60 seconds it takes to dissolve the exposed areas in base developer, and a positive-tone image is obtained. Measurement of the thickness of the film in the unexposed areas before and after development showed that no thickness loss occurred.

The partially protected polymer used to obtain the image shown in Figure 3.21 is still very hydrophobic. Development of the exposed areas required addition of at least 10% v/v of isopropyl alcohol (IPA) to the base developer to help wet the polymer and develop away the exposed regions. If IPA had not been used, the aqueous base solvent would not have been able to penetrate the polymer surface for development. In addition, some of the smallest features on the wafer had peeled off due to its hydrophobic nature. To solve this problem, we decided to use unprotected polymers **3-20** and **3-22** with the addition of a dissolution inhibitor to inhibit the dissolution of these polymers in aqueous base. Exposure would cause the dissolution inhibitor to change its solubility and promote the dissolution of the matrix polymer. This concept was explained in Chapter 1 and is shown schematically in Figure 3.22.

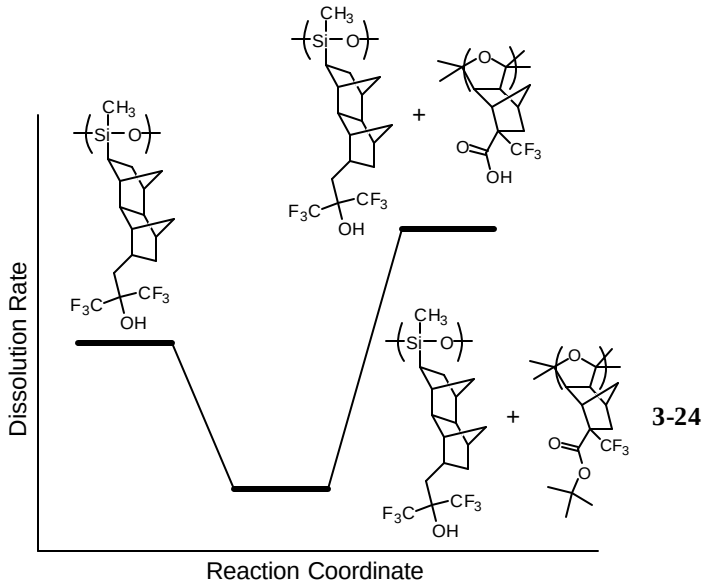

Figure 3.22: The use of a dissolution inhibitor to inhibit and promote the dissolution of a matrix polymer.

Therefore, both polymers **3-20** and **3-22** were blended with a low molecular weight carbon monoxide copolymer **3-24** as the dissolution inhibitor. Since these polymers alone would not provide the solubility switch required for imaging, a dissolution inhibitor was added for this function. Copolymer **3-24** was chosen because it is a low molecular weight polymer (about four units long due to its rod-like nature) and it was shown to efficiently inhibit the dissolution of another aqueous-base soluble polymer.[55,56] The dissolution inhibition efficiency of a certain compound depends greatly on its interaction with the matrix polymer with which it is blended. Some inhibitors may work well with one polymer but may not work as well with other polymers. Experiments with polymer **3-20** and dissolution inhibitor **3-24** were not fruitful because the matrix polymer melted below the lithographic processing conditions required for successful imaging due to its low Tg (43°C). On the other hand, positive-tone images were obtained with polymer **3-22**, 25 wt% of dissolution inhibitor **3-24**, and 5 wt% of triphenylsulfonium nonaflate as the photoacid generator. Figure 3.23 shows a representative image. Even though polymer **3-22** was not protected with any *t*-BOC groups, the addition of 10% v/v IPA was still needed to help wet and dissolve away the exposed areas. In addition, poor adhesion to the bare silicon was observed, indicating the hydrophobicity of the matrix polymer.

In order to improve adhesion and wetting, we envisioned the design of linear siloxanes shown in Figure 3.24. However, the synthesis of such a polymer would be difficult for several reasons. We would have to perform the condensation polymerization ourselves, and separating the cyclics from the linear

polymer would be problematic. Also, no clear, facile pathway to the target polymer could be seen.

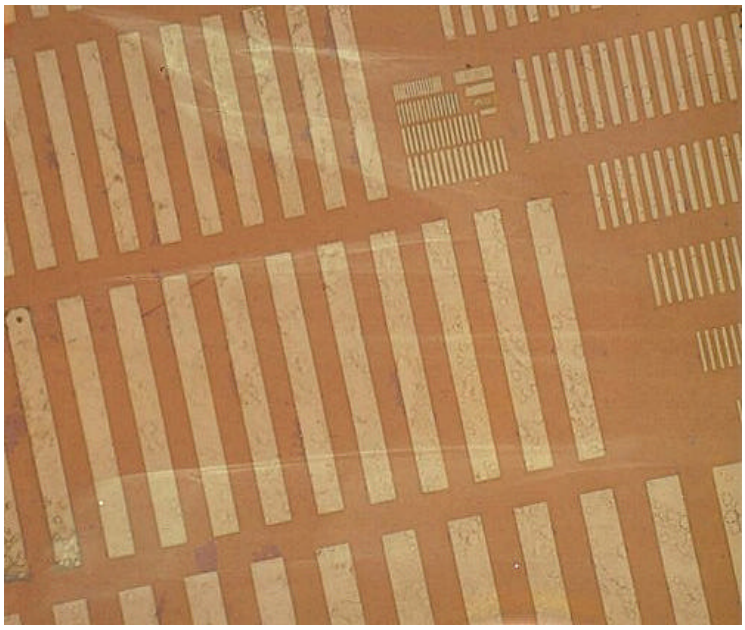

Conditions: PAB: 120°C/90s, Exposure: 23 mJ/cm^2, PEB: 120°C/90s, Develop: 10% v/v IPA in 0.26 *N* TMAH/30s

Figure 3.23: Contact print of polymer **3-22** with 25 wt% of copolymer **3-24** as the dissolution inhibitor and 5 wt% triphenylsulfonium nonaflate.

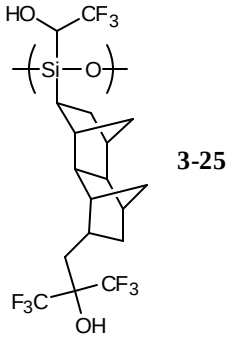

3-25

Figure 3.24: Target for a more hydrophilic, high Tg linear siloxane.

In addition, the transparency of these linear siloxanes has been disappointing. It has been shown empirically that siloxanes in general are higher absorbing than silsesquioxanes. Since siloxanes have two Si-C bonds and silsesquioxanes only have one Si-C bond, one might speculate that the extra Si-C bond is the cause of the higher absorbance. This can be shown experimentally by comparing the absorbance of poly(dimethylsiloxane) with the absorbance of poly(methylsilsesquioxane). However, since poly(dimethylsiloxane) is an oil at room temperature, its absorbance data cannot be taken easily. One may also compare the gas-phase spectra of dimethyldiethoxysilane with that of methyltriethoxysilane. However, we've seen before that the gas-phase analysis of siloxane monomers is suspicious at best (Figure 3.6). Therefore we are left with the original data that hints that siloxanes are in general more absorbing than silsesquioxanes because of the extra Si-C bonds.

We have shown the high-yield synthesis of functionalized linear siloxanes by a one-step hydrosilylation reaction with commercially available poly(methylhydridosiloxane) and fluorinated alicyclic olefins. We have also managed to make linear siloxanes with some of the highest glass transition temperatures known by incorporating bulky alicyclic compounds and shown that these resulting polymers can be used to print images in the positive tone. However, because these linear siloxanes are disappointingly absorbing and the route to a more hydrophilic polymer is difficult, we are abandoning the use of linear siloxanes for 157 nm lithography. We therefore turned our attention to the lower-absorbing and higher Tg silesquioxanes.

CHAPTER 4: *SILSESQUIOXANES FOR 157 NM LITHOGRAPHY*

Silsesquioxanes, as discussed in Chapter 2, are crosslinked analogs of siloxanes. Only one R group is attached to the silicon atom. The other three sites are occupied by oxygen atoms. In a silsesquioxane polymer, there are, on average, one and a half oxygen atoms for every silicon atom. These polymers have much of the same properties as the linear polymers. Their major difference, as already discussed, is that they tend to possess higher glass transition temperatures because of their crosslinked nature. In general, they are also relatively more transparent than linear siloxanes because of the extra Si-O bonds. Their higher Tg and transparency make them more likely candidates for 157 nm lithography. This chapter discusses our synthetic efforts and lithographic evaluation of these silsesquioxanes.

CONDENSATION POLYMERIZATION

Silsesquioxanes are also made by the condensation polymerization of the corresponding trialkoxy- or trichlorosilane monomers. The polymerization rates of these monomers are much the same as those for the dialkoxy- and dichlorosilane monomers discussed in Chapter 3. That is, polymerization rates are catalyzed by acids or bases and depend greatly on the type of substituent on silicon. Small groups have little effect on the polymerization rate while bulky groups hinder the rate. Figure 4.1 shows the condensation polymerization of these trifunctional monomers and the types of products that are formed.

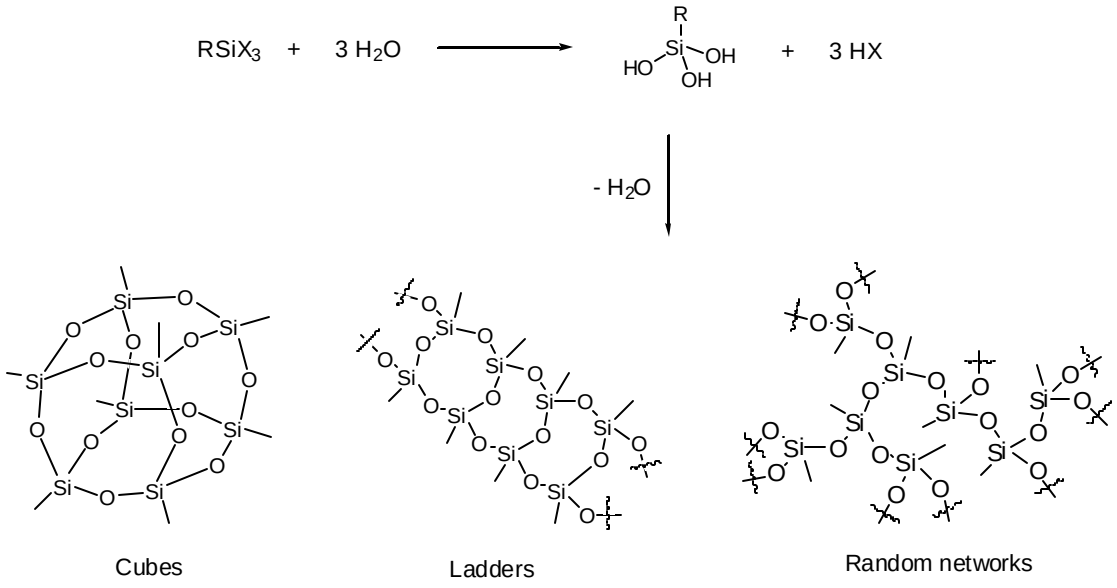

Figure 4.1: Condensation of trisilanols to give silsesquioxanes.

Depending on the reaction conditions (amount of water, type of solvent, reaction temperature, etc.) that are used, several types of products are possible. The major product is the random network of crosslinked silsesquioxane polymer.[87] Some well-defined prismatic cage structures may form to a small extent, but under dilute and well-controlled conditions, these cubes are formed to a larger degree in high yields.[88-92] Several functionalized silsesquioxane cubes are now sold commercially by Aldrich Chemical. Some researchers have proposed the formation of ladder structures[93] shown in Figure 4.1, but others have

87 Loy, D. A.; Shea, K. J. *Chem. Rev. (Washington, D. C.)* **1995**, *95*, 1431-1442.
88 Feher, F. J.; Weller, K. J. *Inorg. Chem.* **1991**, *30*, 880.
89 Feher, F. J.; Weller, K. J.; Ziller, J. W. *J. Am. Chem. Soc.* **1992**, *114*, 9686.
90 Agaskar, P. A. *J. Chem. Soc., Chem. Commun.* **1992**, *63*, 131.
91 Martynova, T. N.; Korchkov, V. P.; Smyannikov, P. P. *J. Organomet. Chem.* **1983**, *258*, 277.
92 Frye, C. L.; Collins, W. T. *J. Am. Chem. Soc.* **1970**, *92*, 5586.
93 Brown, J. F., Jr.; Vogt, J. H., Jr.; Katchman, A.; Eustance, J. W.; Kiser, K. M.; Krantz, D. W. *J. Am. Chem. Soc.* **1960**, *82*, 6194.

questioned the existence of such structures. Their existence is not universally accepted.[94]

SYNTHESIS OF TRIALKOXYSILANE MONOMERS

In the last chapter, the synthesis of aromatic silsesquioxane polymers was discussed. These were made by Grignard or organolithium addition of phenyl or benzyl groups to alkoxysilane monomers followed by base-catalyzed hydrolysis. Since the resulting polymers were found to be highly absorbing at 157 nm due to the aromatic groups, it was decided that other groups such as alicyclic groups needed to be used in place of the aromatic groups. One may attach any of the functionalized norbornene monomers shown in Figure 2.1 onto the silicon atom by a simple hydrosilylation reaction. Although one may also make alicyclic siloxane monomers by addition of the corresponding alicyclic Grignard to silicon, the hydrosilylation reaction is a much more facile pathway to the desired product.

Since the norbornene monomers shown in Figure 2.1 bear highly electron-withdrawing fluorine atoms, this makes the double bond on norbornene very electron-deficient. Coordination of this double bond to the platinum center is less likely to occur, reducing the yields obtained in the hydrosilylation reaction. For example, the yield obtained when monomer **2-5** is hydrosilylated onto triethoxysilane is much less than the yield obtained with the corresponding monomer without the trifluoromethyl group. Hydrosilylation of monomer **2-1**, on the other hand, provides acceptable yields of product because the trifluoromethyl groups are further away from the double bond such that the electron density of the

[94] Frye, C. L.; Klosowski, J. M. *J. Am. Chem. Soc.* **1971**, *93*, 4599.

double bond is not reduced significantly. There is also a steric and coordinating factor during the hydrosilylation reaction. Norbornene monomers with substituents in the *exo* position hydrosilylate faster than those with substituents in the *endo* position, especially when the norbornene monomer possesses a coordinating oxygen atom (C=O) in the *endo* position. This effect has been studied by several researchers, and a platinum complex with an *endo*-coordinated norbornene carboxylic ester has even been isolated.[95] These studies focused on the *endo*/*exo* uptake of functionalized norbornene monomers during vinyl addition polymerization. The results of these metal coordination studies apply to the hydrosilylation reaction as well.

A fluorinated tertiary alcohol, 1,1,1-trifluoro-2-trifluoromethyl-pent-4-ene-2-ol (**4-1**), was protected with ethyl chloromethyl ether to form the desired acetal. This olefin was then hydrosilylated onto triethoxysilane using dicyclopentadienylplatinum (II) chloride as catalyst to form the functionalized triethoxysilane in good yield. The resulting monomer was polymerized using aqueous tetrabutylammonium hydroxide (Figure 4.2). Unfortunately, the final polymer has a glass transition temperature below 25°C, since the polymer was an oil at room temperature. Therefore, bulkier groups such as alicyclics need to be incorporated onto the polymer chain. We then decided to make several norbornene and dinorbornene trialkoxysilane monomers.

---

[95] Hennis, A. D.; Polley, J. D.; Long, G. S.; Sen, A.; Yandulov, D.; Lipian, J.; Benedikt, G. M.; Rhodes, L. F.; Huffman, J. *Organometallics* **2001**, *20*, 2802-2812.

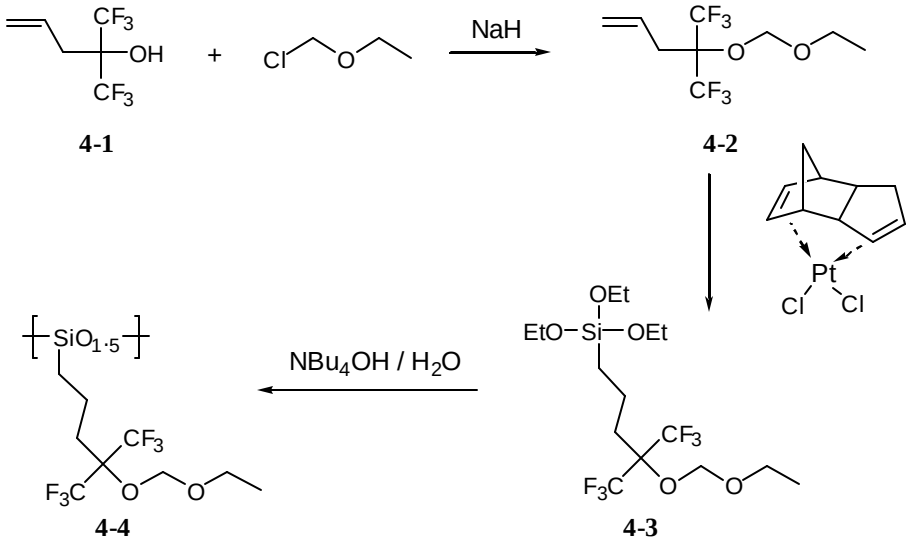

Figure 4.2: Synthesis of a low Tg, functionalized silsesquioxane.

The fluorinated dinorbornene monomer (**4-5**) was therefore hydrosilylated onto triethoxysilane using dicyclopentadienylplatinum (II) chloride as catalyst (Figure 4.3). Normally, purification of the hydrosilylated product involves distillation to remove Pt catalyst. However, in this case the product, **4-6**, has too high of a boiling point for vacuum distillation. Chromatography on silica gel would most likely be unsuccessful because the acidic Si-OH groups of the gel will react with the alkoxy groups on the monomer, especially if the eluent is wet. This would cause condensation polymerization of the monomer in the column. Instead, the crude reaction mixture was stirred with activated carbon to adsorb most of the Pt catalyst, evaporated to remove excess solvent, and filtered to give a light yellow oil.

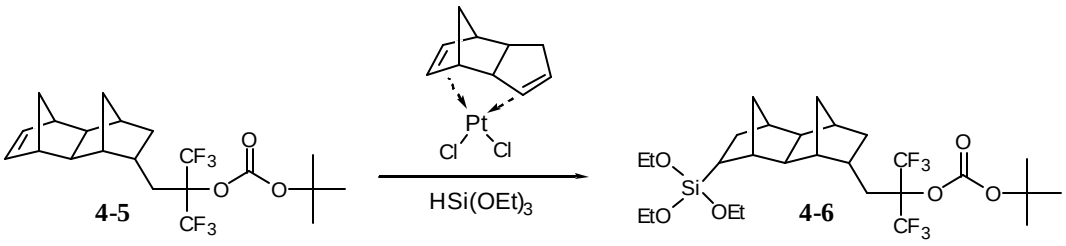

Figure 4.3: Synthesis of a functionalized dinorbornyl triethoxysilane.

Functionalized norbornenes were also hydrosilylated onto triethoxysilane or trimethoxysilane. Figure 4.4 shows an attempted synthesis of compound **4-7** from the hydrosilylation of monomer **2-3** onto triethoxysilane using chloroplatinic acid. However, the *t*-BOC group was cleaved during the reaction and half of the reaction mixture consisted of compound **4-8**. This observation is not very surprising due to the acidic nature of the catalyst. When

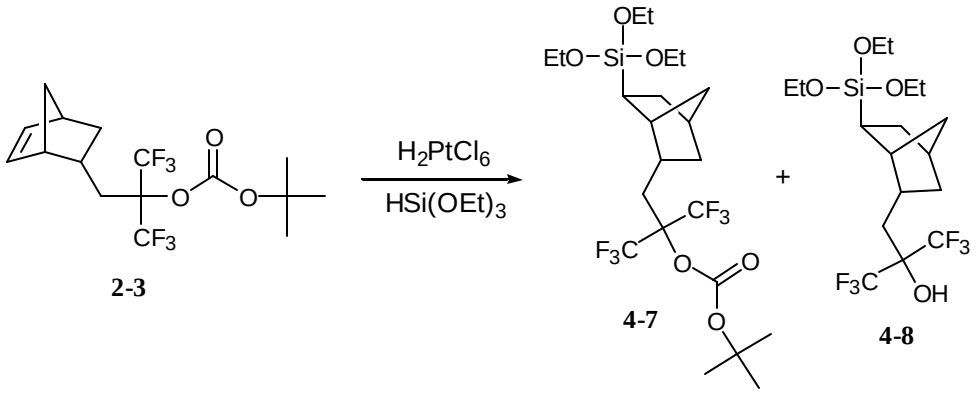

Figure 4.4: Deprotection is observed with chloroplatinic acid.

dicyclopentadienylplatinum (II) chloride or Karstedt's catalyst was used with the same monomer, no deprotection was observed. Karstedt's catalyst is

homogeneous in the reaction medium because the platinum is surrounded by divinylsiloxane units, making the catalyst more soluble in organic solvents. On the other hand, dicyclopentadienylplatinum (II) chloride is considered a heterogeneous catalyst because it is not very soluble in organic solvents. This is the reason why the yields obtained with Karstedt's catalyst is usually higher. Yields of hydrosilylation reactions with non-fluorinated monomers are often higher than those with fluorinated monomers. Figure 4.5 shows the norbornane alkoxysilanes synthesized from the three platinum catalysts. Compound **4-8** was made using Speier's catalyst (hexachloroplatinic acid). The other compounds were made using either Karstedt's catalyst or dicyclopentadienylplatinum (II) chloride. All these compounds were either distilled under vacuum, stirred with activated carbon, or bubbled with hydrogen gas (followed by activated carbon treatment) to remove most, if not all of the platinum catalyst. This step is the most important step because any residual platinum will contaminate the final polymer, therefore increasing its absorbance at 157 nm.

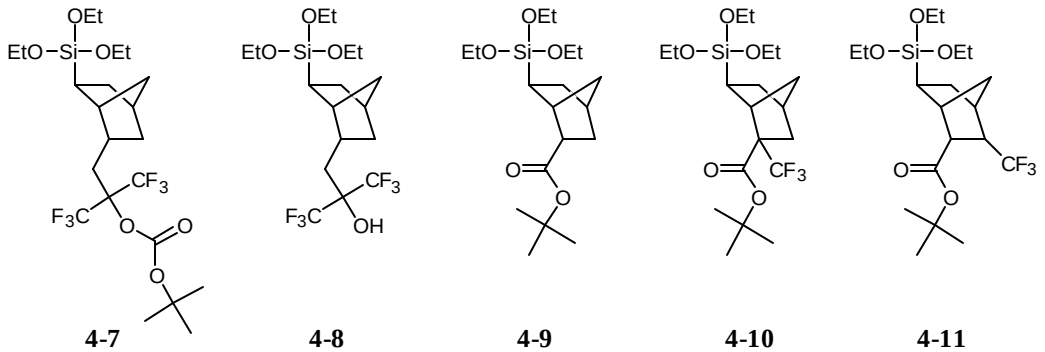

4-7 **4-8** **4-9** **4-10** **4-11**

Figure 4.5: Several functionalized ethoxysilanes synthesized by the hydrosilylation reaction.

POLYMERIZATION AND EVALUATION OF SILSESQUIOXANES

Several of the ethoxysilanes shown in Figure 4.5 were polymerized under aqueous acid and base conditions. Water alone is able to polymerize the monomers, but the condensation is accelerated by acid or base, as discussed in Chapter 3 (Figure 3.2). Aqueous ammonium hydroxide (28%) was first used as the condensation catalyst, but under neat conditions (no solvent), not all of the monomer (**4-9**) was consumed in the first 24 hours at room temperature. This may be due to the poor solubility of the aqueous catalyst in the lipophilic monomer medium. Aqueous tetrabutylammonium hydroxide (40 wt%) was next used under the same neat reaction conditions. This catalyst was able to polymerize all of the monomer in the same time period, producing polymer with a relatively higher molecular weight. The polymerization rate was not significantly affected when THF was used as the solvent. The crude polymer was precipitated into a mixture of water and methanol to isolate the polymer while dissolving any unreacted monomer. ^{1}H-NMR analysis of the polymer revealed the presence of tetrabutylammonium hydroxide. Repeated precipitations into the water/methanol mixture did not fully remove the catalyst. Therefore this catalyst, although very effective, was not used in further polymerizations because of the problems with its removal from the final polymer. Any excess base left in the polymer would quench photogenerated acid and therefore reduce the sensitivity of the resist during processing.

Both of these base catalysts were chosen because it was thought that the catalysts could be removed by thermal decomposition from heating. Ammonium

hydroxide could easily be removed this way, but the catalyst was not very effective during polymerization. Tetrabuylammonium hydroxide required higher temperatures, and we could not heat above 150°C because the *t*-BOC and *t*-butyl ester protecting groups would thermally decompose.

Oxalic acid (HOCOCOOH) was next used as the condensation catalyst. The pH of a 0.1 *M* solution in water is about 1.3, and the acid decomposes to CO_2, CO, formic acid, and water at temperatures above 140°C. This catalyst, therefore, may be removed from the final polymer by heating. However, during polymerization at room temperature some deprotection of the *t*-BOC and *t*-butyl ester groups was observed. Infrared analysis of the crude polymers showed a large peak at about 3400 cm^{-1}. This catalyst is not useful for protected monomers such as **4-7**, **4-9**, **4-10**, and **4-11**, but polymerizes monomers such as **4-8** well.

Aqueous sodium hydroxide has been found to be the most effective condensation catalyst for the ethoxysilanes shown in Figure 4.5. A 0.01 *N* solution of NaOH is sufficient to catalyze the condensation. Polymerizations using this catalyst were performed under neat conditions or with THF or methanol as the solvent. The most effective procedure involves dissolving the monomer into methanol and adding 1.5 equivalents of 1 *N* NaOH. The solution is initially mixed and then allowed to stand, unstirred, at room temperature overnight to allow the monomers to assemble in a random fashion into a network structure. Repeated precipitation of the resulting solution into a water/methanol mixture provides fine, white powder (Figure 4.6). It is important to remove residual

sodium salts because any sodium left in the polymer would be disastrous in terms of absorbance and metal contamination.

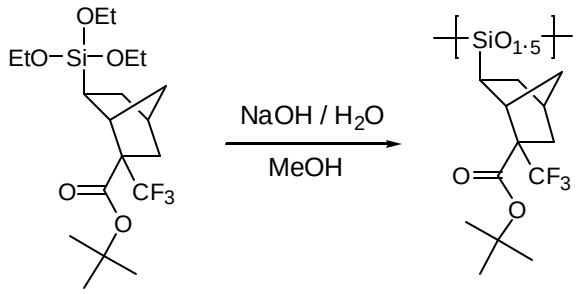

4-10 **4-12**

Figure 4.6: Condensation polymerization of **4-10** by NaOH in methanol to yield **4-12**.

The glass transition temperature of polymer **4-12** was measured (DSC) to be about 42°C and its absorbance at 157 nm was found to be 3.14 μm^{-1} (Figure 4.7). Several batches of polymer were made, and all the polymers had molecular weights in the range of 1500-3000. In this molecular weight range, the T_g's of the polymers were 40-60°C, indicating that the polymers needed to be cured to higher molecular weights to increase their glass transition temperatures. The absorbance is clearly higher than expected because the silsesquioxane backbone should be very transparent at this wavelength, and the norbornane structure should have an absorbance of less than 2 μm^{-1} according to gas-phase measurements. Hydridosilsesquioxane, in comparison, has a measured absorbance of 0.02 μm^{-1}.

The higher absorbance of these polymers may be due to several reasons. Polymerization of the ethoxysilane monomers yields small amounts of crystalline cubic structures of the type shown in Figure 4.1. Other larger cubes may also be

present. Since these crystalline structures are difficult to remove from the final polymers, their presence may scatter the radiation and cause a higher reading of absorbance.

In addition, substitution of the Si-H bond in hydridosilsesquioxane with an alicyclic Si-C bond may significantly increase the absorbance. The polymer shown in Figure 4.6 (**4-12**) was not end-capped, meaning that the Si-OH end groups were not protected. When the end groups in this polymer were protected by reaction with trimethylchlorosilane, the resulting polymer's absorbance was higher than the unprotected polymer. The polymer's absorbance was found to be 4.32 μm^{-1}. Infrared analysis showed the expected decrease in OH vibration from the protection reaction. The higher absorbance may support the hypothesis that creating Si-C bonds would increase 157 nm absorbance.

Residual platinum from the hydrosilylation reaction also contributes to absorption at 157 nm. When a polymer such as **4-12** is dissolved in THF and hydrogen gas in bubbled through the solution, some platinum that was still complexed to the polymer may have been released. Treatment of the solution with activated carbon followed by filtration through celite, precipitation, and isolation provided a polymer with a slightly lower absorbance. The platinum content measured in these polymers was found to be less than 115 ppm by elemental analysis, but even this amount of platinum may contribute significantly to 157 nm absorption.

Even though the glass transition temperature of the silsesquioxane polymer shown in Figure 4.6 is lower than 50°C, preliminary imaging studies

using 193 nm radiation were done to assess the lithographic performance of these functionalized silsesquioxane polymers under typical lithographic processing conditions. The resist solution (polymer **4-12**, triphenylsulfonium nonaflate (TPS-NF) as the PAG, trioctylamine, and THF) was coated onto a thick layer of bottom anti-reflective coating (BARC) on a silicon wafer. After post-apply bake (90°C for 60 sec), exposure at 193 nm, and post-exposure bake (100°C for 90 sec), the resulting image was analyzed using a scanning electron microscope (Figure 4.7). As expected, the polymer imaged in the positive tone, but it seems

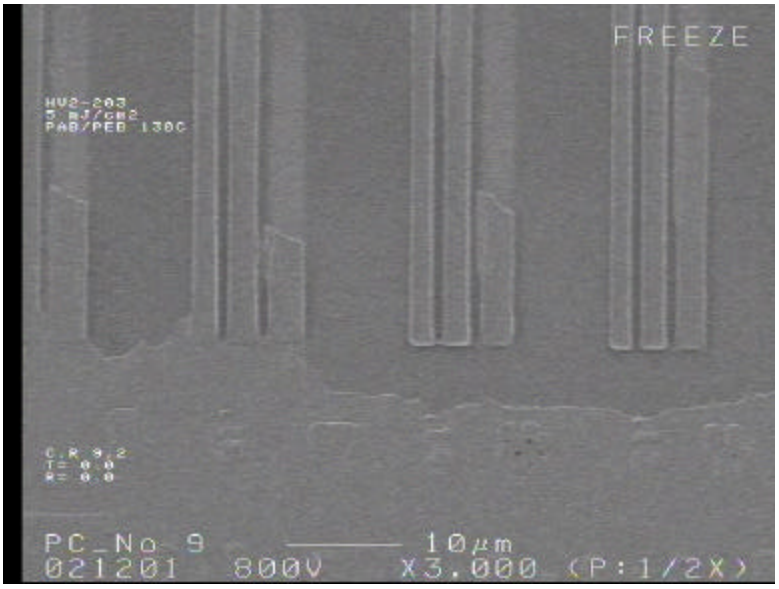

Figure 4.7: SEM image of a resist formulation containing polymer **4-12**, imaged using 193 nm radiation.

that most of the polymer film lost adhesion to the underlying BARC layer and folded over itself. In the regions where some lines were distinguishable, one also notices that most of the lines had fused together due to the "melting" of the low T_g

polymer at high baking temperatures. This was expected, since the post-exposure baking temperature was more than twice the T_g of the polymer. This high processing temperature was needed because the *t*-butyl ester groups had to be cleaved to enable the solubility switch needed. From this preliminary study, it is clear that the glass transition temperatures of these silsesquioxanes needed to be raised a significant degree.

As discussed in Chapter 2, one way to raise the glass transition temperatures of these silsesquioxane polymers is to increase their molecular weights. In order to raise the molecular weights of these condensation polymers, one must either partially crosslink the polymer or further cure the polymer by heating to promote condensation of the end groups. Curing the polymer requires high temperatures, so this method is not very feasible because most of the polymers have protecting groups that are thermally labile above 200°C. In one experiment, a silsesquioxane polymer was heated to 150°C, and the resulting polymer's molecular weight was measured and found to be almost the same as that of the starting polymer. Therefore the other option of crosslinking the polymers has been investigated. Small amounts of crosslinkers such as those shown in Figure 4.8 (**4-13** and **4-14**) were added to monomer **4-10** during polymerization in methanol. Upon addition of NaOH as the catalyst, a white solid was immediately precipitated from the solution. During workup, two different polymers were observed: an amorphous, low T_g polymer and a powdery white solid. This indicated that tetraethylorthosilicate (**4-13**) had polymerized much faster than the more hindered monomer **4-10**. This phase separation occurred

even though as little as 5 mol% of crosslinker was used. In the case of triethoxysilane (**4-14**), the evolution of hydrogen gas was observed during the polymerization. This is due to the spontaneous disproportionation of Si-H in aqueous base to produce hydrogen gas and new Si-O bonds. This crosslinker is much more reactive than the other crosslinker, so phase separation was more prominent when this crosslinker was used. Both crosslinkers produced a separate white SiO_2 powder and did not react with monomer **4-10** to a noticeable degree. One possible way of preventing tetraethylorthosilicate (**4-13**) from crashing out of solution during polymerization is to use LiOH as the catalyst. The lithium silicate that is formed during polymerization may be more soluble in the organic medium, allowing time for reaction with the functionalized triethoxysilane (**4-10**).

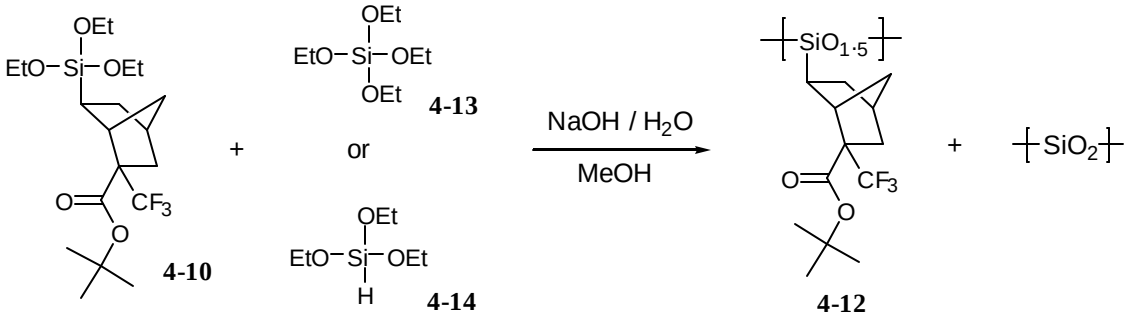

Figure 4.8: Attempted copolymerization of a functionalized triethoxysilane with tetraethylorthosilicate or triethoxysilane.

The path to higher molecular weight polymers presented above was abandoned. We next pursued the synthesis of polyhedral oligomeric silsesquioxane (POSS) cubes. These T_8 cores are well defined, structurally rigid, and thermally resistant. Many research groups have studied these cubes to

develop novel silica particles, zeolite models, sol-gel precursors, and other unique hybrid organic/inorganic materials.[96-103] Aldrich Chemical currently sells many of these functionalized T_8 cores, the most interesting of which are the cubes with

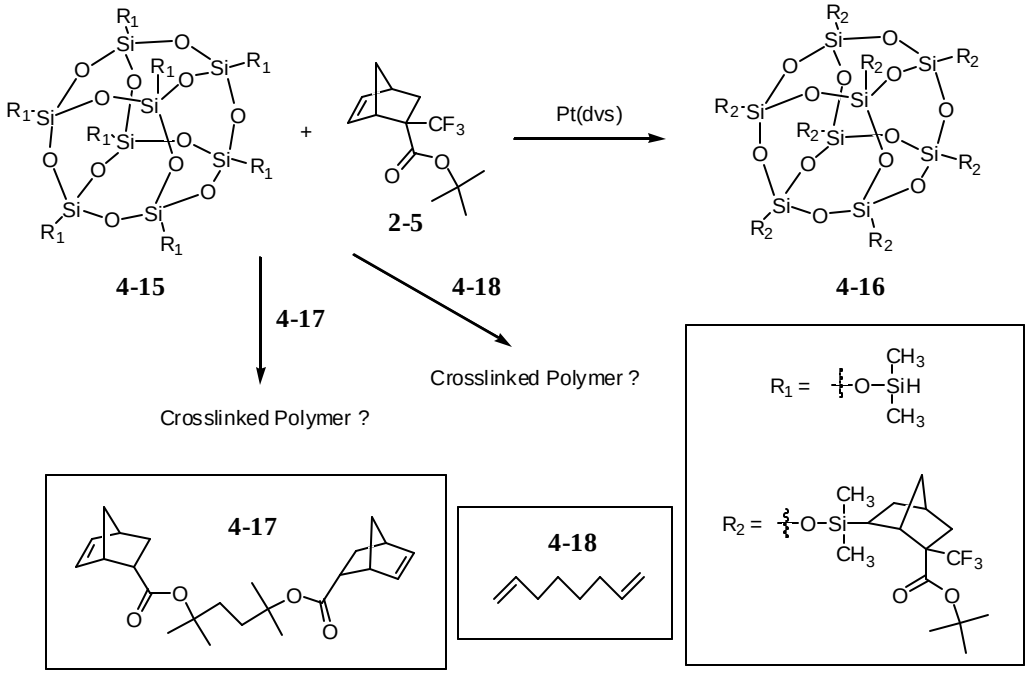

Figure 4.9: Synthesis of functionalized cubic POSS cores and their reaction with two crosslinkers.

96 Feher, F. J.; Budzichowski, T. A.; Blanski, R. L.; Weller, K. J.; Ziller, J. W. *Organometallics* **1991**, *10*, 2526-2528.

97 Agaskar, P. A. *Colloids and Surfaces* **1992**, *63*, 131-138.

98 Laine, R. M.; Sellinger, A. *Macromolecules* **1996**, *29*, 2327-2330.

99 Laine, R. M.; Zhang, C. *J. Organomet. Chem.* **1996**, *521*, 199-201.

100 Laine, R. M.; Sellinger, A. *Chem. Mater.* **1996**, *8*, 1592-1593.

101 Fasce, D. P.; Williams, R. J. J.; Mechin, F.; Pascault, J. P.; Llauro, M. F.; Petiaud, R. *Macromolecules* **1999**, *32*, 4757-4763.

102 Crivello, J. V.; Malik, R. *J. Polym. Sci., Part A: Polym. Chem.* **1997**, *35*, 407-425.

103 Zheng, L.; Farris, R. J.; Coughlin, E. B. *J. Polym. Sci., Part A: Polym. Chem.* **2001**, *39*, 2920-2928.

eight Si-H bonds protruding from each corner of the cube, $(HSiO_{1.5})_8$ and $(HMe_2SiOSiO_{1.5})_8$. Both of these cubes were hydrosilylated with monomer **2-5** using Karstedt's catalyst [Pt(dvs), platinum divinyltetramethyldisiloxane] or dicyclopentadienylplatinum (II) chloride [Pt(dcp)]. Interestingly, the use of Pt(dvs) did not form crosslinked gels from the divinyltetramethyldisiloxane in solution, as reported by Laine *et al*.[98] However, gels were formed when this catalyst was used to hydrosilylate olefins to poly(methylhydridosiloxane) (**3-19**), as previously discussed in Chapter 3. Cubes of $(HSiO_{1.5})_8$ were much less reactive than cubes of $(HMe_2SiOSiO_{1.5})_8$ to the hydrosilylation reaction, which is similar to the findings of Laine *et al*. Figure 4.9 shows the hydrosilylation reaction of cubic $(HMe_2SiOSi_{1.5})_8$ (**4-15**) with monomer **2-5** to form pure white, crystalline cubes **4-16** in good yield.

Compound **4-16** was analyzed by infrared and ^{1}H-NMR spectroscopy, and all eight corners of the cube were shown to be fully "capped" because no Si-H bond was observed. These cubes are only soluble in a few polar solvents such as THF, DMF, and DMSO, and are insoluble in common resist casting solvents such as PGMEA, ethyl lactate, and ketone solvents. No glass transition temperature was observed by DSC analysis. Since these cubes are crystalline in nature, they do not coat well on silicon wafers to form fine films. Blending of these cubes with silsesquioxane polymers such as **4-12** do not work well. When the blends are cast from THF onto a silicon wafer, phase separation of the cubes from the silsesquioxane polymer was observed. Under the microscope, one can see the bumps of the crystalline domains inside the thin film of the silsesquioxane

polymer. In addition, THF is not the most useful solvent for coating applications because the solvent evaporates too fast during spin-coating, leaving very rough films. The limited solubility of the **4-16** cubes in common resist solvents as well as their phase separation from amorphous polymers hinder their use in lithography applications.

Therefore it was decided that small amounts of crosslinkers could be added to the hydrosilylation reaction to link the cubes together. It was hoped that the coating properties of the resulting linked cubes would improve due to their more "polymeric" nature. To this end, two crosslinkers were investigated. Crosslinker **4-17** was first tested. This crosslinker was chosen because it was readily available and worked well in other experiments that will not be discussed here. In addition to the olefin **2-5**, compound **4-17** was added to the hydrosilylation reaction in mol % concentrations (relative to cubes) of 10, 20, and 40. Figure 4.10 shows a plot of the weight-average molecular weight of the resulting "polymers" versus the mol % of crosslinker **4-17** added to the reaction. As seen in the plot, and contrary to what one might predict, the addition of **4-17** did not affect the molecular weight of the final polymer. Even at 40 mol % of added crosslinker, the molecular weight did not seem to change. Infrared and ^{1}H-NMR analysis of the cubes showed no traces of Si-H bonding, indicating that all of the reactive sites were hydrosilylated. NMR analysis of the cubes after precipitation also showed no trace of unreacted olefin. Infrared analysis showed the presence of carbonyl functionality. From these observations, it was concluded that the norbornene monomer **2-5** was hydrosilylated onto the starting POSS cube,

but very little (if any) of crosslinker **4-17** was incorporated because the molecular weight did not change. These observations also indicate that the more electron-rich olefin, **4-17**, hydrosilylated faster than the less electron-rich olefin, **2-5**. This in contrary to most hydrosilylation reactions, in which electron-rich olefins are hydrosilylated faster than electron-poor olefins.

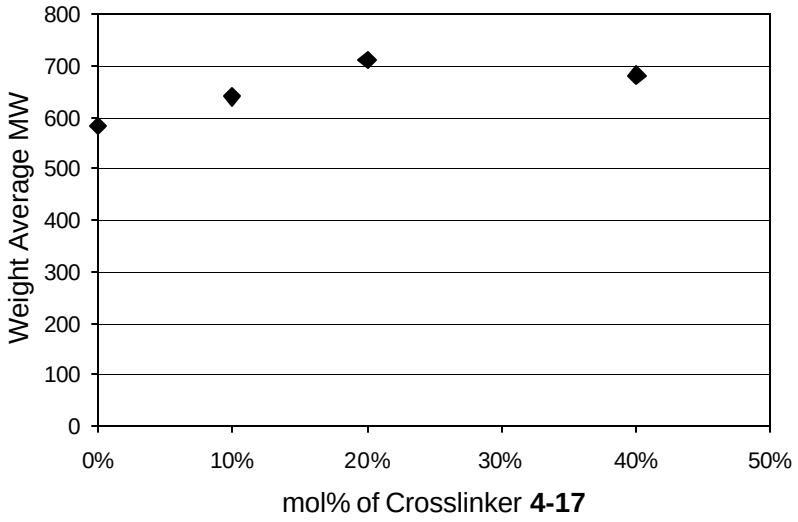

Figure 4.10: Plot of weight-average molecular weight of product vs. concentration of crosslinker **4-17** in the hydrosilylation reaction.

The observations from the above experiment prompted the use of 1,7-octadiene (**4-18**) as the crosslinker. The hydrosilylation of a terminal olefin such as this one should be faster than the more hindered norbornene monomer **2-5**. However, as shown in Figure 4.11, the expected results were not obtained. The molecular weights of the final "polymers" were not significantly affected by increasing concentrations of the crosslinker. These unexpected results were very

discouraging. One possible remedy, which has not been tried, is to "fix" the reaction by changing the order of reactant addition (mode of addition). In previous experiments, both monomers **2-5** and crosslinker **4-17** or **4-18** were added simultaneously to the hydrosilylation reaction. The desired polymer may be obtained if one first adds the crosslinker with the platinum catalyst, allowing time for reaction before addition of the rest of the functionalized monomer.

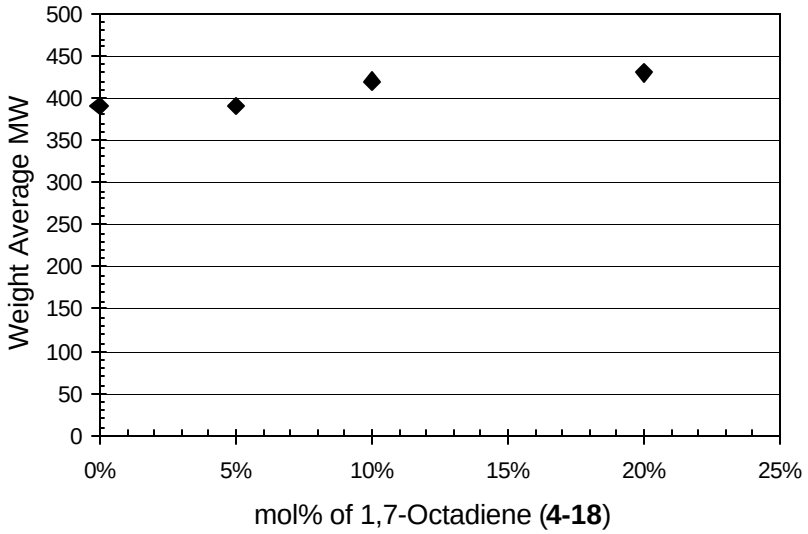

Figure 4.11: Plot of weight-average molecular weight of product vs. concentration of crosslinker **4-18** in the hydrosilylation reaction.

The above path to cage-like network polymers was abandoned due to unsuccessful crosslinking of the cages. We next investigated a commercially available hydrogen silsesquioxane resin $(HSiO_{1.5})_n$ sold by Dow Corning Corporation. Sold under the trade name of FOx Flowable Oxide, this semiconductor grade polymer is used to coat thin uniform films for low-k

dielectric applications. The polymer is usually dissolved in methyl isobutyl ketone (MIBK) as the carrier solvent. Besides their use as a low-k dielectric material, they have found use in other lithography applications. Hydrogen silsesquioxane (HSQ) may be a promising resist material because of its high O_2 reactive ion etch resistance. Negative-tone images have been obtained when this polymer was exposed with e-beam radiation.[104-106] Other researchers have imaged this polymer, also in the negative-tone, by blending the polymer with a photobase generator and radiating select regions with 254 nm light.[107] The photogenerated base acts as a catalyst, with water, to disproportionate the Si-H bonds, forming thermally stable Si-O-Si bonds in the process.

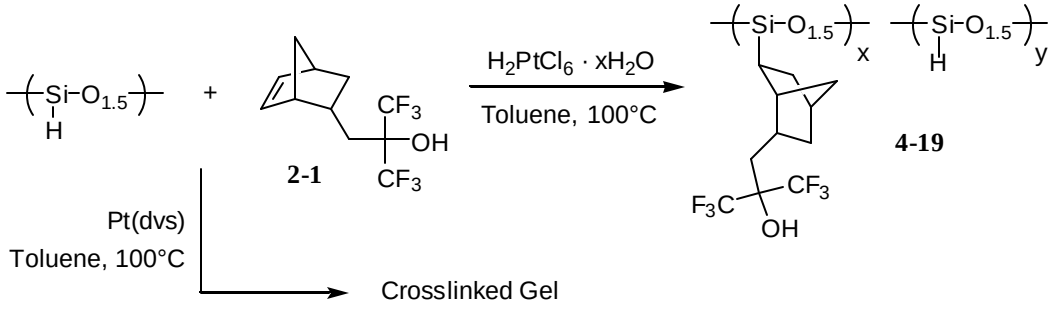

Figure 4.12: Hydrosilylation of **2-1** onto HSQ using both Pt(dvs) and Speier's catalyst.

A positive-tone resist based on the hydrogen silsesquioxane core was investigated in our group. Figure 4.12 shows the hydrosilylation reaction of HSQ

---

104 Namatsu, H.; Yamaguchi, T.; Nagase, M.; Yamazaki, K.; Kurihara, K. *Microelectron. Eng.* **1998**, *41/42*, 331-334.

105 Namatsu, H.; Takahashi, Y.; Yamazaki, K.; Yamaguchi, T.; Nagase, M.; Kurihara, K. *J. Vac. Sci. Technol. B* **1998**, *16*, 69-76.

106 van Delft, F. C. M. J. M.; Weterings, J. P.; van Langen-Suurling, A. K.; Romijn, H. *J. Vac. Sci. Technol. B* **2000**, *18*, 3419-3423.

107 Harkness, B. R.; Takeuchi, K.; Tachikawa, M. *Macromolecules* **1998**, *31*, 4798-4805.

with norbornene **2-1** using both Pt(dvs) and Speier's catalyst. The starting HSQ polymer was purchased as a solution in MIBK, so this solvent had to be evaporated because ketones interfere with the hydrosilyation reaction (the ketone is reduced). The solid obtained was immediately dissolved in dry toluene to prevent degradation of the Si-H bond in oxygen and light. This polymer has a weight average molecular weight of 10,500 g/mol and a polydispersity of 2.5, as measured relative to polystyrene standards (Dow Corning's measurement). When Karstedt's catalyst was added to the HSQ/norbornene solution in toluene and the reaction allowed to stir at 100°C overnight, a crosslinked gel was obtained. Further investigation revealed that the source of the crosslinking came from the catalyst solution. Since Pt(dvs) is a platinum complex with divinyltetramethyldisiloxane in a xylene solvent, it is believed that the divinyltetramethhyldisiloxane is the cause of the crosslinking. Because HSQ is already a random network connected by three sites on the silicon atom, only a small amount of crosslinking at the fourth site, Si-H, is needed to form insoluble gel. This has also been observed when the same catalyst is used to hydrosilylate norbornene structures onto poly(methylhydridosiloxane).

When hexachloroplatinic acid was used, polymer **4-19** was formed instead of an insoluble gel. However, hydrosilylation was not complete, even when the reaction was allowed to continue for five days. It is believed that some Si-H bonds on the polymer is encased by the polymer chains, preventing catalyst from binding to the site and monomer from accessing the site (Figure 4.13). After five days, the polymer was isolated nevertheless, and through integration of the Si-H

peak as compared to the aliphatic hydrogens by ^{1}H-NMR analysis, it is estimated that hydrosilylation is complete only to about 50%. Infrared spectroscopy reveals the slightly reduced Si-H stretch at about 2237 cm^{-1}. The glass transition temperature of the polymer was measured to be 77°C, and the polymer's absorbance at 157 nm is 1.85 μm^{-1}. Its weight average molecular weight was measured to be 7,470 g/mol with a polydispersity of 2.5, relative to polystyrene standards. The T_g of the polymer is still somewhat lower than the target value of 100°C or above, but this may be satisfactory if the polymer is used as a thin top layer in a bilayer resist process. The aborbance of 1.85 μm^{-1} is the lowest seen for a functionalized silsesquioxane polymer. This is high when compared to the absorbance of HSQ (0.02 μm^{-1}), but the higher value is the result of increased absorbance due to the extra C-C, C-H, C-O, and Si-C bonds added.

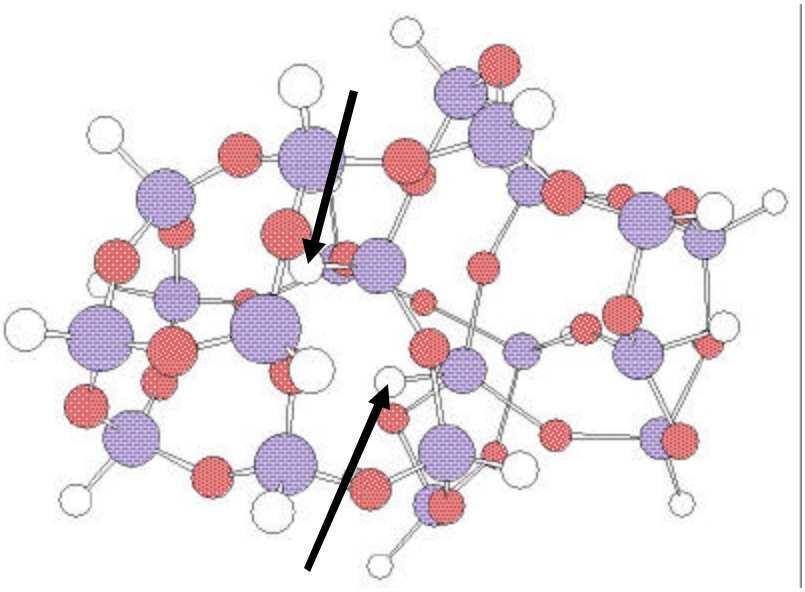

Figure 4.13: Structure of HSQ showing enclosed Si-H bonds, preventing reaction at that site.

Polymer **4-19** was blended with polymer **4-12** as the dissolution inhibitor and a small amount of TPS-NF as the PAG. This blend was coated from PGMEA and imaged using 248 nm radiation (Figure 4.14). Positive-tone images were obtained, and the smallest features were resolved, showing the potential of this system. However, even at 30 wt% loading of the dissolution inhibitor (relative to polymer **4-19**), some thickness loss was seen in the unexposed areas. Polymer **4-19** is very soluble to aqueous base developer (unlike the siloxane polymers discussed in Chapter 3, isopropyl alcohol was not needed to help wet the polymer), and the large amount of dissolution inhibitor was not enough to inhibit the polymer's dissolution. The dissolution inhibitor, therefore, needed to be changed.

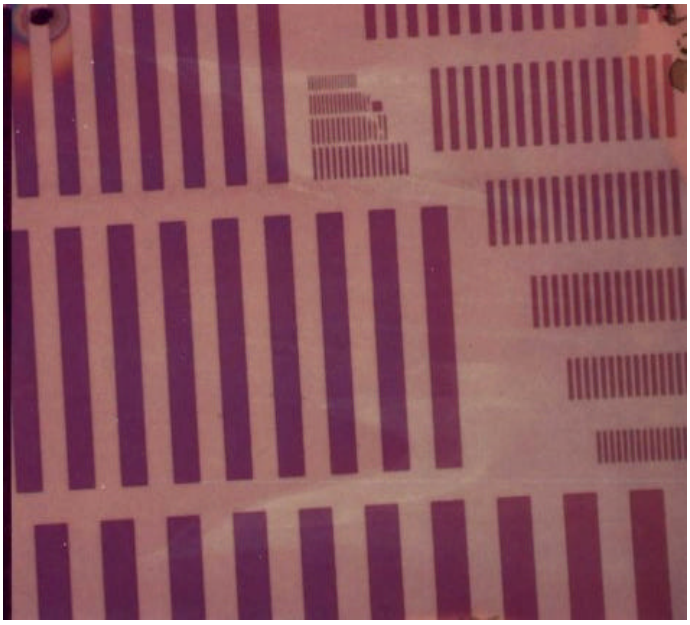

Conditions: PAB: 120°C/90s, Exposure: 24 mJ/cm^2,
PEB: 120°C/90s, Develop: 0.26 *N* TMAH/30s

Figure 4.14: Contact print of polymer **4-19** with 30 wt% **4-12** as the dissolution inhibitor and 6 wt% TPS-NF.

The more effective dissolution inhibitor, **3-24**, was used in the next imaging experiments. Polymer **4-19** was blended with several different amounts (10-30 wt%) of **3-24** and 5 wt% of TPS-NF. These blends were coated from PGMEA to form fine films and imaged at International Sematech on the Exitech 157 nm stepper. Figure 4.15 shows some representative images from these experiments. As can be seen, high resolution images were obtained. Lines as small as 120 nm were resolved, and very little roughness was seen. No thickness loss was observed, indicating that the chosen dissolution inhibitor was effective at inhibiting the dissolution of the matrix polymer in standard base developer. When one examines the "L" bar images, some collapse of the lines is seen. This is due to the low T_g of the matrix polymer. The baking conditions applied were 30-40°C higher than the T_g of the polymer, so the lines were somewhat "soft" and image collapse occurred. This may not be a problem if a thinner layer of this resist system is used for bilayer applications.

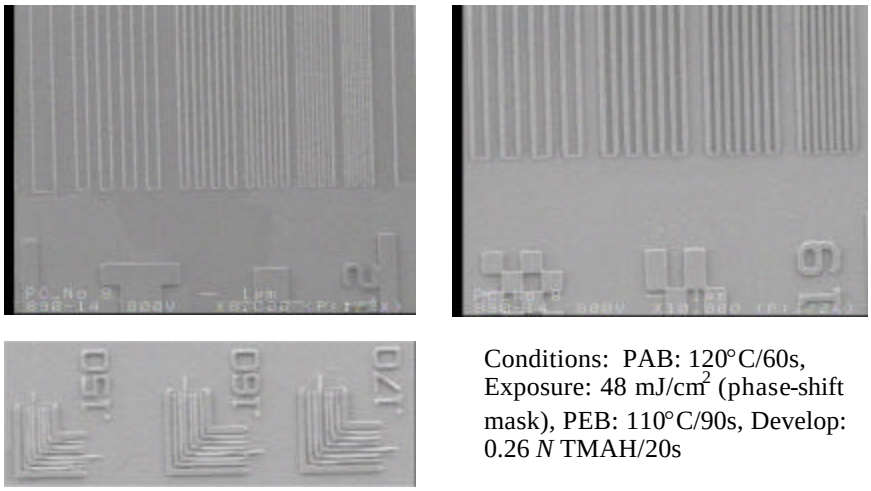

Conditions: PAB: 120°C/60s, Exposure: 48 mJ/cm^2 (phase-shift mask), PEB: 110°C/90s, Develop: 0.26 *N* TMAH/20s

Figure 4.15: SEM images of polymer **4-19** blended with 10-30 wt% **3-24** (DI) and 5 wt% TPS-NF.

FUTURE WORK AND DIRECTION

The silsesquioxane polymers that have been made up to this point have shown promising results during lithographic imaging tests. The polymers coat well from PGMEA and image in the positive tone. Although the highest T_g we have seen for these polymers is 77°C, other researchers have reported T_gs of 120°C for their silsesquioxanes. There is definitely room for improvement. Higher molecular weight polymers are needed by further curing or crosslinking. Other crosslinkers besides the ones shown should be investigated.

An improvement in the absorbance of the silsesquioxane polymers may still be needed. Although 1.85 μm^{-1} is the lowest number we've seen for these functionalized silsesquioxane polymers, small amounts of platinum contamination may have a significant impact on this number. One synthetic method of avoiding metal contaminants in the final polymer is shown in Figure 4.16. Hydrosilylation of norbornene **2-1** onto triethoxysilane, followed by distillation, should provide pure **4-8** that is free of any platinum metal. Polymerization of this monomer in aqueous oxalic acid, rather than aqueous NaOH, will provide a polymer without any sodium contaminants. In addition, oxalic acid may be decomposed and baked off above 140°C. The resulting low molecular weight polymer may then be cured in neat triethylamine to condense pendant Si-OH bonds. Precipitation, followed by water washes, should provide polymer **4-20**. This polymer may then be partially protected with *t*-BOC, for example, or used in conjunction with a dissolution inhibitor in imaging studies.

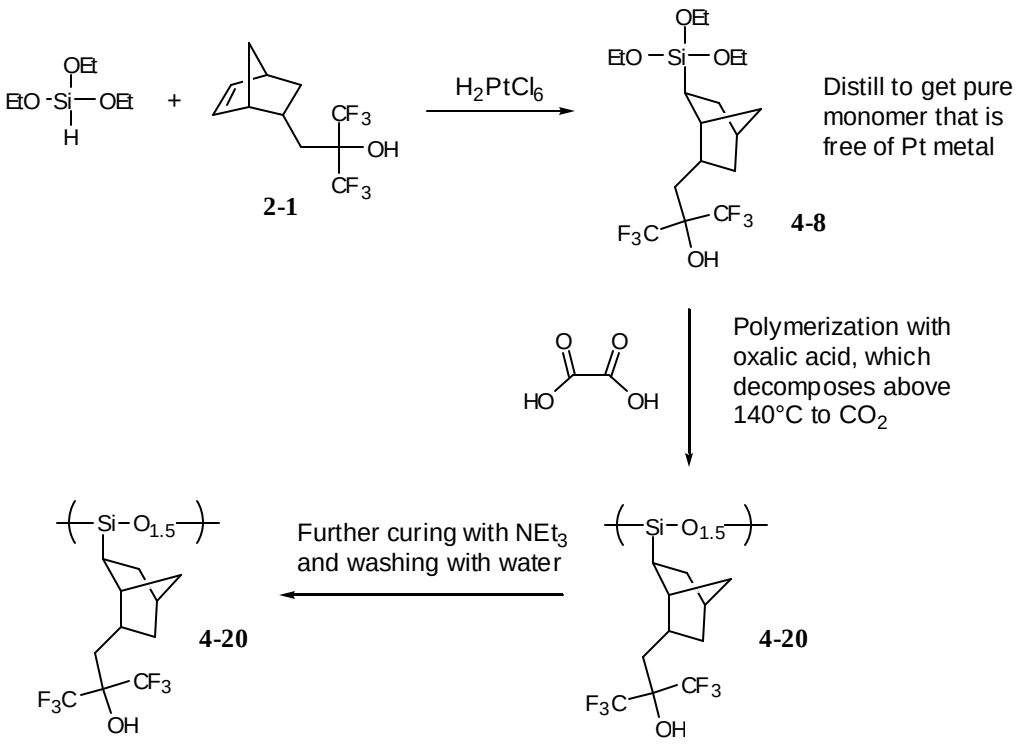

Figure 4.16: Proposed route to a metal-free silsesquioxane polymer.

The oxygen plasma reactive ion etch resistance of these silsesquioxane polymers also needs to be studied. Many reports have been found in the literature comparing the etch rates of silicon-containing compounds to non-silicon compounds. The silicon-containing compounds, especially siloxanes and silsesquioxanes, are far superior at resisting oxygen etching as compared to non-silicon-containing compounds. These numbers need to be obtained for the new silsesquioxanes that have been synthesized.

A major concern for 157 nm lithography is lens contamination from resist outgassing. The photon energy at 157 nm (7.9 eV as compared to 6.4 eV at 193

nm) is large enough to cause cleavage of sigma bonds. The fragments formed during exposure may evaporate and collect on the exposure lens, resulting in transmission loss and severe image distortion. A large amount of effort is underway to design resists that do not outgas during exposure. Outgassed silicon byproducts are especially damaging to the lens system because the layer of SiO_2 that is formed cannot be removed easily by current lens cleaning techniques. Several tests have been performed to determine the amount of outgassing and type of species that are outgassed when silicon-containing resists are used.[108] Polymers that have silicon-containing side chains tend to outgas more silicon byproducts than polymers that contain silicon in the main chain (siloxanes and silsesquioxanes). The silsesquioxanes that we have made need to be tested.

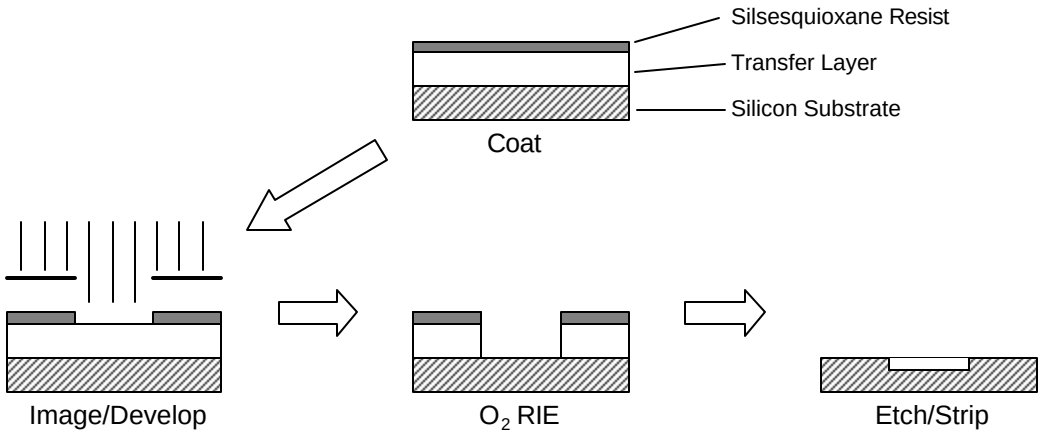

Figure 4.17: A bilayer resist process using a thin silsesquioxane-based resist top layer.

[108] Hien, S.; Angood, S.; Ashworth, D.; Basset, S.; Bloomstein, T. M.; Dean, K. R.; Kunz, R. R.; Miller, D. A.; Patel, S.; Rich, G. *Proc. SPIE Int. Soc. Opt. Eng.* **2001**, *4345*, 439-447.

As discussed previously, the silsesquioxanes that have been made may be useful in bilayer resist applications. A general bilayer scheme is shown in Figure 4.17. A very thin resist composed of a silsesquioxane polymer is coated over a relatively thick transfer layer of carbon-based polymer. Imaging is performed on the thin top layer, and an oxygen reactive ion etch step is added to etch away the transfer layer. The silsesquioxane layer resists the oxygen plasma, and a three-dimensional pattern is obtained. Since the top layer may be coated thin, a lower T_g polymer is tolerable because image collapse is rare due to the lower aspect ratios of the imaged features. The bilayer scheme is advantageous because high aspect ratios may be obtained due to the high oxygen plasma etch resistance of the silsesquioxanes. Fluorocarbon-based, single-layer resists may not have adequate etch resistance to halogen plasma etching.

With these experiments, it is clear that silsesquioxanes have a large potential for 157 nm lithography patterning. In the three to four years allowed for the development of 157 nm photoresists, considerable progress has been made to identify and synthesize functional polymers for this new imaging wavelength. The glass transition temperatures of these polymers have been improved, the absorbance of functionalized silsesquioxane polymers have been reduced below 2 μm^{-1}, and initial imaging has provided promising features below 200 nm. Although much progress still needs to be made (T_g > 140°C, Absorbance < 1 μm^{-1}), these silicon-containing resists show great potential for 157 nm lithography. Since these polymers are highly resistant to oxygen plasma etching, they may also find use as bilayer resists for 193 nm lithography.

CHAPTER 5: *ACID DIFFUSION INTRODUCTION AND BACKGROUND*

As described in Chapter 1, chemically-amplified photoresists were first developed to provide high resolution imaging. The transition to 248 nm lithography required more sensitive resists to replace the conventional diazoqinone/novolac-based resists. Many new classes of chemically-amplified resists have since been developed, all of which utilize a photoacid generator (PAG), i.e., a substance that produces acid as one product of photolysis. Exposure causes the PAG present in the resist film to produce acid. During a subsequent post-exposure baking step, an acid-catalyzed reaction is initiated that cleaves acid-labile groups used to protect the OH of an acidic polymer. Since the protected, nonpolar polymer is thus converted to the more polar, acidic polymer, the solubility of the exposed regions is modified such that the exposed areas are rendered more soluble in an aqueous base developer. This concept is shown in Figure 1.9, in which a triphenylsulfonium salt produces acid upon irradiation, causing the catalytic cleavage of *t*-BOC on the lipophilic (base-insoluble) poly(*p*-*tert*-butyloxycarbonyloxystyrene) (PTBOCST) to give poly(hydroxystyrene) (PHOST) that is base-soluble.

The shape of the final developable latent image of diazonaphthoquinone-novolac resists is determined by the conditions of the initial exposure such as the characteristics of the projected optical image and the optical and photochemical properties of the resist film.[5] With chemically-amplified resists, the structure of the developable latent image also depends on the chemistry and physics that take

place during post-exposure thermal processing. Diffusion of the photogenerated acid during the period of time between exposure and development may cause contrast loss (blurring) and changes in the dimension of the latent image, both of which can lead to linewidth variation (Figure 5.1). This critical dimension (CD) bias, which refers to the difference between a feature's targeted dimension (ideally, the dimension on the mask) and the actual feature dimension printed in the photoresist, becomes much more important as the required feature sizes become smaller and smaller. A bias of 10 nm on each side of the feature profile may not be as significant when the feature is 500 nm wide, but when the required feature width is 70 nm, this bias is disastrous.

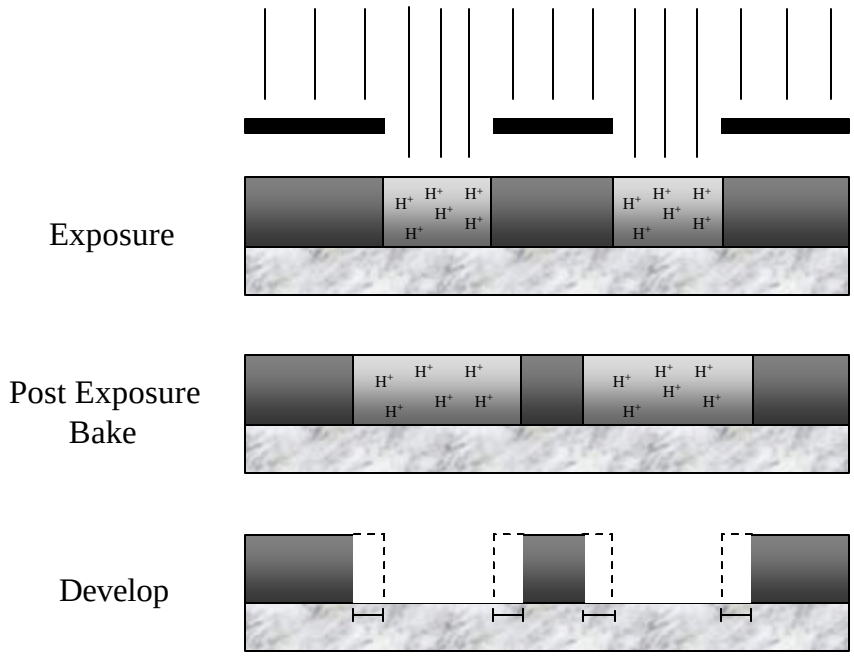

Figure 5.1: Linewidth variation that may be due to diffusion of photogenerated acid during post-exposure baking.

During imaging exposure, a spatially nonuniform distribution of acid is generated in the exposed regions because of constructive and destructive interference of the incoming and reflected radiation. Diffusion of the acid within the exposed areas is necessary and desired to catalyze the deprotection reaction chemistry and smooth out the rough edges that would otherwise form if there was no diffusion. The rate of deprotection of the acid-labile component in a resist depends largely on the concentration of the protonated species. The concentration of the protonated species, in turn, is strongly dependent on the acid diffusion coefficient. An acid with a high diffusion coefficient may increase the rate of deprotection reaction, thereby increasing the sensitivity of the photoresist, but will cause large critical dimension bias due to diffusion outside of the exposed areas. On the other hand, an acid with a low diffusion coefficient will not cause linewidth spread, but may decrease the deprotection reaction kinetics and therefore decrease the sensitivity of the resist. Since most resist chemistry deals with the interaction of a very strong acid with weak bases, the equilibrium protonation of the protecting group is fast and the next defragmentation step to yield unprotected product and volatile byproduct is the rate-limiting step (specific acid catalysis). In this scenario, the reaction is considered to be reaction rate limited.

The close relationship between resist kinetics and acid diffusion makes the study of acid diffusion in resist polymers very difficult. This is the reason why so many experiments have been done to understand the contribution of acid migration to CD bias and the exact acid transport mechanism. What are the acid

diffusion coefficients of each type of photogenerated acid in each type of photoresist material? Is acid diffusion in resist polymers driven solely by a concentration gradient (Fickian diffusion), or is there another transport mechanism that is responsible for this catalyst migration? Finding the answers to these questions may help lithographers design better simulation models of the lithographic process that correctly and accurately predicts final resist feature shapes, dimensions, roughness, etc.[109-112] These simulations save time and money by decreasing the amount of experimental work necessary to predict the best formulation, and the models also provide guidance for the rational design of improved materials.

EARLY EXPERIMENTS

Fick's first law of diffusion states that the flux of matter (J, the number of particles per unit area per unit time) is equal to a diffusion coefficient (D) times the concentration gradient at that point:

$$J(matter) = -D\frac{\partial C}{\partial z} \tag{3}$$

The image blur that is seen when chemically-amplified resists are imaged has typically been attributed to classical Fickian diffusion of the acid catalyst from exposed regions to unexposed regions. Typical diffusion coefficients of

---

109 Zuniga, M.; Neureuther, A. R. *J. Vac. Sci. Technol. B* **1995**, *13*, 2957.

110 Petersen, J. S.; Mack, C. A.; Sturtevant, J.; Byers, J. D.; Miller, D. A. *Proc. SPIE Int. Soc. Opt. Eng.* **1995**, *2438*, 167.

111 Krasnoperova, A. A.; Khan, M.; Rhyner, S.; Taylor, J. W.; Zhu, Y.; Cerrina, F. *J. Vac. Sci. Technol. B* **1994**, *12*, 3900.

112 Petersen, J. S.; Byers, J. D. *Proc. SPIE Int. Soc. Opt. Eng.* **1996**, *2724*, 164.

molecules in solution at 25°C are on the order of 10^{-5} to 10^{-6} cm^2/s.[113] The diffusion coefficients of small molecules in glassy polymers below T_g are on the order of 10^{-10} cm^2/s (10^{-2} $\mu m^2/s$).[7] Many attempts have been made to measure the diffusion coefficients of acid molecules in resist polymers. All of these numbers range between 1 x 10^{-4} and 1 x 10^{-6} $\mu m^2/s$. This is much slower than the values reported for the diffusion of small molecules in glassy polymers and the diffusion of molecules in solution reported above. With these small diffusion coefficients, the protecting-group protonation rate and the overall deprotection reaction rates would be expected to be much slower than those of the same reaction in solution. In addition, diffusion coefficients in this range would translate to a bias of 1 to 10 nm per second of post-exposure bake time. This large bias will become much more significant as feature sizes continue to shrink.

Although the theory of diffusion of gases and small molecules by Fickian diffusion in polymer systems is relatively straight-forward[114], the measurement of acid diffusion through a resist film is quite complex because the photoacids are capable of substantial interactions with the polymer. Diffusion is often coupled with the reaction kinetics of the polymer matrix.[115] As the acid diffuses, acid-catalyzed cleavage reactions can change the polarity of the film, generate volatile byproducts, and cause film shrinkage. These factors can not only change the reaction kinetics, but also can affect diffusion to a significant degree. Since the polymer matrix changes both chemically and physically during thermal

---

113 Gray, D. E., Ed. *American Institute of Physics Handbook*; McGraw-Hill: New York, 1972.

114 Crank, J.; Park, G. *Diffusion in Polymers*; Academic Press: New York, 1968.

115 Hinsberg, W.; Houle, F. A.; Hoffnagle, J.; Sanchez, M.; Wallraff, G.; Morrison, M.; Frank, S. *J. Vac. Sci. Technol., B* **1998**, *16*, 3689-3694.

processing, the study of acid diffusion in a resist system is much more complicated than the study of the diffusion of inert small molecules in a polymer matrix.

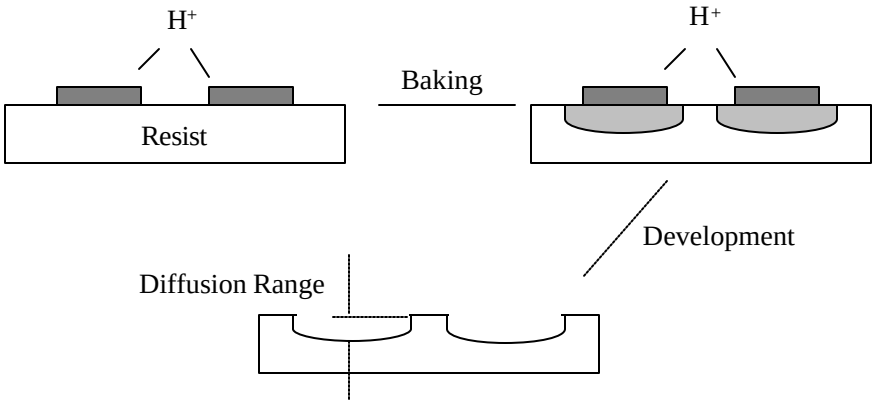

Figure 5.2: One method of measuring acid diffusion coefficients in a resist polymer. The diffusion coefficient is inferred from measurements of the developed resist profile.

Despite these difficulties, many researchers have developed methods for studying acid transport in chemically-amplified resists. Since it is extremely difficult to make optical contact with the acids directly, their location is generally inferred from scanning electron microscopy (SEM) images of developed patterns. Schlegel *et al.* described one such experiment where an acid feeder layer is directly laid over a resist layer (Figure 5.2)[116]. Exposure, followed by baking and development, provided holes in the resist layer. The holes were analyzed under the SEM and their depths measured. Diffusion coefficients were therefore

[116] Schlegel, L.; Ueno, T.; Hayashi, N.; Iwayanagi, T. *J. Vac. Sci. Technol. B* **1991**, *9*, 278.

obtained as a function of the processing conditions. However, the diffusion coefficients obtained are not very accurate because the developed resist profile is complicated by subsequent processes such as resist chemistry, baking, and chemical development. Others have used similar techniques to measure acid diffusion coefficients.[117-121] The diffusion of the catalytic acid in chemically-amplified resists was determined by Schlegel *et al.* to be governed by Fick's law of diffusion. They proposed a model to predict the diffusion of several sulfonic acids. From their model the average diffusion length could be estimated from the equation:

$$L = \sqrt{2Dt} \tag{4}$$

where L is the average diffusion length, D is the diffusion coefficient, and t is the time allowed for diffusion. Their study demonstrated that the larger acid molecules exhibited reduced diffusion distances. In similar studies, Nakamura *et al.* outlined several variables that affect diffusion of acid species in a photoresist.[122] Acid diffusion was shown to have a strong dependence on the polymer structure and processing conditions, concentration of photogenerated acid (controlled by exposure dose and quantum yield of the PAG), size of the photogenerated acid molecule (increasing size reduces mobility), and temperature.

---

117 Yoshiyuki, T.; Nakayama, Y.; Okazaki, S. *J. Vac. Sci. Technol. B* **1992**, *10*, 2615.

118 Cronin, M. F.; Adams, M.; Fedynyshyn, T. H.; Georger, J.; Mori, J. M.; Sinta, R.; Thackeray, J. W. *Proc. SPIE Int. Soc. Opt. Eng.* **1994**, *2195*, 214.

119 Itani, T.; Yoshino, H.; Fujimoto, M.; Kasama, K. *J. Vac. Sci. Technol. B* **1995**, *13*, 3026.

120 Connolly, J.; Chen, K. R.; Kwong, R.; Lawson, M.; Linehan, L.; Moreau, W. *Proc. SPIE Int. Soc. Opt. Eng.* **1998**, *3333*, 1124.

121 Rau, N.; Neureuther, A. R.; Ogawa, T.; Kubena, R.; Stratton, F.; Fields, C.; Willson, C. G. *Proc. SPIE Int. Soc. Opt. Eng.* **1998**, *3333*, 1413.

122 Nakamura, J.; Ban, H.; Tanaka, A. *Jpn. J. Appl. Phys.* **1992**, *31*, 4294-4300.

Several other experiments have been reported in the literature in an attempt to directly quantify photoacid diffusion. Ion conductivity,[123,124] acid volatization correlation,[125] acid vapor absorption,[126] STM measurements,[127] and laser confocal microscopy[128] experiments have all been described. In our own group, several experimental techniques have been designed and tested that are based on capacitance measurements, diffraction grating analysis, and atomic force microscopy.[129] In these experiments, no diffusion of photogenerated acid was observed through PHOST at typical resist processing temperatures. To further validate these experimental results a new technique was devised that is based on the measurement of acid transport between two or more contacted polymer films. One film contains PAG molecules that generate acid upon exposure while another film contains acid-labile or acid-sensitive groups which serve as a detection layer for the transported acid. Similar experiments have been documented in the literature.[130-132] In our case, both fluorescence and infrared spectroscopy will be

---

123 Nakamura, J.; Ban, H.; Deguchi, K.; Tanaka, A. *Jpn. J. Appl. Phys.* **1991**, *10*, 6065.

124 Fedynyshyn, T. H.; Thackeray, J. W.; Georger, J. H.; Denison, M. D. *J. Vac. Sci. Technol. B* **1994**, *12*, 3888.

125 Thackeray, J. W.; Denison, M. D.; Fedynyshyn, T. H.; Kang, D.; Sinta, R. *Microelectronics Technology, Polymers for Advanced Imaging and Packaging*, In *ACS Symposium Series 614*; Reichmanis, E.; Ober, C.; MacDonald, S.; Iwayanagi, T.; Nishikubo, T., Eds.; American Chemical Society: Washington, DC, 1995; p 84.

126 Mueller, K. E.; Koros, W. J.; Mack, C. A.; Willson, C. G. *Proc. SPIE Int. Soc. Opt. Eng.* **1997**, *3049*, 706.

127 Perkins, F. K.; Dobisz, E. A.; Marrian, C. R. K. *J. Vac. Sci. Technol. B* **1993**, *11*, 2597.

128 Zhang, P. L.; Webber, S.; Mendenhall, J.; Byers, J. D.; Chao, K. *Proc. SPIE Int. Soc. Opt. Eng.* **1998**, *3333*, 794.

129 Postnikov, S. V. Ph.D. Dissertation, University of Texas at Austin, 1999.

130 Asakawa, K.; Ushirogouchi, T.; Nakase, M. *Proc. SPIE Int. Soc. Opt. Eng.* **1995**, *2438*, 563.

131 Uchino, S.; Yamamoto, J.; Migitaka, S.; Kojima, K.; Hashimoto, M.; Murai, F.; Shiraishi, H. *J. Photopolym. Sci. Technol.* **1998**, *11*, 555.

132 Sakamizu, T.; Arai, T.; Yamaguchi, H.; Shiraishi, H. *Proc. SPIE Int. Soc. Opt. Eng.* **1997**, *3049*, 448.

used to measure the presence of acidic species in the detector layer. In the former case, the change in fluorescence of a dye molecule upon protonation can be correlated to acid diffusion. In the latter case, the measurement of acid location can be accomplished by correlating the change in absorbance of the relevant peak to acid diffusion. Both of these techniques will be discussed in the next two chapters.

CHAPTER 6: *MEASURING ACID DIFFUSION WITH FLUORESCENCE SPECTROSCOPY*

Fluorescence spectroscopy is a very powerful and convenient tool for monitoring the production and diffusion of photogenerated acids in thin polymer films. Fluorescence techniques are already being used in a wide range of research fields including biochemical, medical, and chemical research, due primarily to the inherent sensitivity of the technique and the favorable time scale of the phenomenon of fluorescence.[133] It is not surprising, therefore, to find many references in which fluorescence spectroscopy has been used for the detection of low acid concentration in thin polymer films.[134-142] Many of these experiments have concentrated on the use of pH-sensitive dyes to quantify the generation of acid molecules during resist exposure. Acid quantification is usually accomplished by the spectrophotometric or spectrofluorometric titration of dyes

---

133 Lackowicz, J. R. *Principles of Fluorescence Spectroscopy*; Plenum Press: New York, 1986; Chapters 1-2.

134 McKean, D. R.; Schaedeli, U.; MacDonald, S. A. *J. Polym. Sci., Part A: Polym. Chem.* **1989**, *27*, 3927.

135 Pohlers, G.; Virdee, S.; Scaiano, J. C.; Sinta, R. *Chem. Mater.* **1996**, *8*, 2654-2658.

136 Eckert, A. R.; Moreau, W. M. *Proc. SPIE-Int. Soc. Opt. Eng.* **1997**, *3049*, 879-887.

137 Cameron, J. F.; Mori, J. M.; Zydowsky, T. M.; Kang, D.; Sinta, R.; King, M.; Scaiano, J.; Pohlers, G.; Virdee, S.; Connolly, T. *Proc. SPIE-Int. Soc. Opt. Eng.* **1998**, *3333*, 680-691.

138 Dentinger, P. M.; Lu, B.; Taylor, J. W.; Bukofsky, S. J.; Feke, G. D.; Hessman, D.; Grober, R. D. *J. Vac. Sci. Technol., B* **1998**, *16*, 3767-3772.

139 Jessop, J. L. P.; Goldie, S. N.; Scranton, A. B.; Blanchard, G. J.; Rangarajan, B.; Capodieci, L.; Subramanian, R.; Templeton, M. K. *Proc. SPIE-Int. Soc. Opt. Eng.* **1999**, *3678*, 914-922.

140 Coenjarts, C.; Cameron, J. F.; Deschamps, N.; Hambly, D.; Pohlers, G.; Scaiano, J. C.; Sinta, R. F.; Virdee, S.; Zampini, A. *Proc. SPIE-Int. Soc. Opt. Eng.* **1999**, *3678*, 1062-1073.

141 Jessop, J. L. P.; Goldie, S. N.; Scranton, A. B.; Blanchard, G. J. *Polym. Mater. Sci. Eng.* **2000**, *82*, 48-49.

142 Feke, G. D.; Grober, R. D.; Pohlers, G.; Moore, K.; Cameron, J. F. *Analytical Chemistry* **2001**, *73*, 3472-3480.

that exhibit a significant change of absorption or fluorescence with respect to acid concentration. On-wafer techniques have been developed that correlate dye fluorescence to acid concentration for *in-situ* measurements, eliminating the destructive developing step required for acid titrations.[138-142]

Although many approaches to measure acid generation and concentration by fluorescence spectroscopy have been documented, not many approaches to measure acid diffusion directly have been reported. In one approach to measure acid diffusion, some researchers have analyzed fluorescent patterns produced by contact printing of polymer films containing a pH-sensitive dye by fluorescence microscopy. Diffusion of acid outside of the exposed regions would deteriorate the images. However, in this study, it is extremely difficult to quantify diffusion lengths by fluorescence microscopy.[140]

EXPERIMENTAL DESIGN

A new approach based on the creation of layers, or "sandwiches", of polymer film was devised for measuring acid transport through thin polymer films (Figure 6.1).[129] In this sandwich technique, the photogenerated acid is allowed to move from one layer to the next layer. The first layer is composed of a polymer matrix that has been blended with a known amount of photoacid generator. Upon ultraviolet exposure (at time = 0), a uniform distribution of acid is produced, generating an acid reservoir layer. Another polymer layer of known thickness is placed over the acid reservoir layer. This layer contains the polymer to be studied (i.e., the polymer through which acid will diffuse). A third layer is then placed over the second layer. This detector layer is composed of a polymer that is

sensitive to the presence of acid and can be analyzed by either infrared or fluorescence spectroscopy. Therefore, acid that is created in the first layer would be expected to diffuse through the intermediate layer and penetrate the detector layer. The time required for this diffusion can be measured and is a function of the thickness of the intermediate layer. Other researchers have reported the use of this sandwich technique to study the diffusion of small molecules in various thin polymer films[143] or polymer-polymer interdiffusion[144], but the use of this technique to monitor acid diffusion is new.

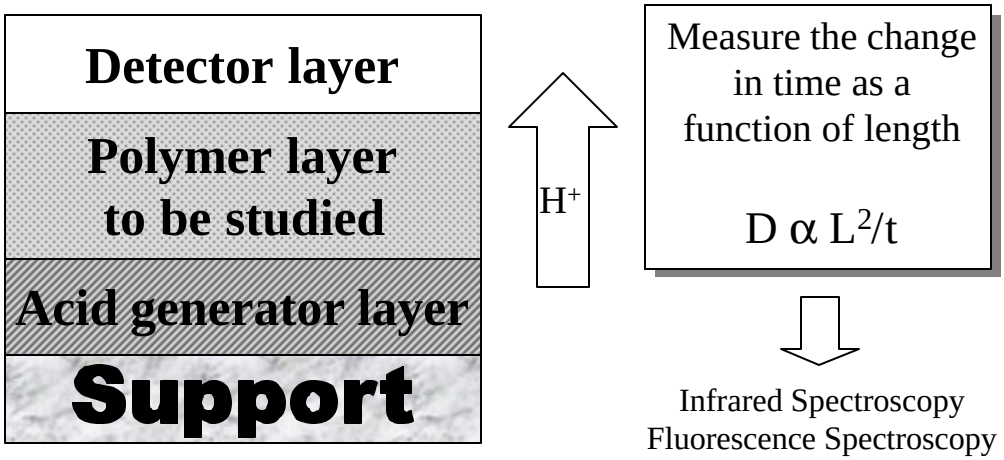

Figure 6.1: The "sandwich" technique used to monitor the diffusion of photogenerated acid molecules.

If Fickian diffusion is observed, than the diffusion coefficient of the acid molecule at a certain temperature is proportional to the length squared (L^2) divided by the time (t) allowed for diffusion. This expression can be derived from

[143] Hall, D. B.; Torkelson, J. M. *Macromolecules* **1998**, *31*, 8817-8825.
[144] Lin, E. K.; Wu, W.-l.; Satija, S. K. *Macromolecules* **1997**, *30*, 7224-7231.

Fick's second law of diffusion, which relates the change of concentration at a point to the spatial variation of the concentration at that point:[145]

$$\frac{\partial C}{\partial t} = D\frac{\partial^2 C}{\partial x^2} \tag{5}$$

Usually, the initial concentration (C_0) of the particle depletes over a distance L in a certain time t in an inhomogeneous region. The concentration at a given point in time after this depletion over distance L is represented by C_t.

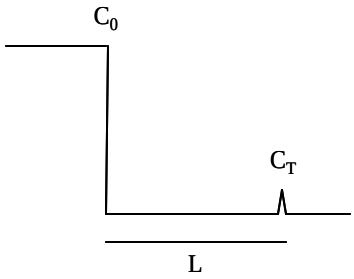

Solving for a concentration C at a point L distance away at time t, one gets:

$$C_t = C_0\left[1 - erf\,\frac{L}{2(Dt)^{0.5}}\right] \tag{6}$$

Since both the initial concentration, C_0, and the concentration at time t, C_t, are constants, then the relation

$$\frac{L}{2(Dt)^{0.5}} \tag{7}$$

must be a constant as well. Therefore, let

[145] Atkins, P. W. *Physical Chemistry*, 5th ed.; W. H. Freeman and Company: New York, 1994; p 851.

$$K = \frac{L}{2(Dt)^{0.5}} \tag{8}$$

Solving for D, we get

$$D = \frac{1}{4K^2} \bullet \frac{L^2}{t} \quad \text{or} \quad D \propto \frac{L^2}{t} \tag{9}$$

Monitoring the diffusion of photogenerated acid using fluorescence spectroscopy requires modifying the trilayer stack shown in Figure 6.1 slightly. The support is a quartz substrate to allow the passage of UV light through the stack. The detector layer is made of a polymer that has a small percentage of pH-sensitive dye molecule bound to the polymer backbone. The dye molecule was bound to the polymer backbone to prevent the diffusion of the dye molecule itself. If the fluorescent molecule was not bound to the polymer structure, then erroneous data would be obtained because acid and dye could diffuse and meet in the middle polymer layer. The fluorescence intensity of the dye can then be monitored with respect to time to produce a graph similar to the one shown in Figure 6.2. The thickness of the middle polymer layer can be measured with a profilometer or ellipsometer. The time allowed for acid diffusion is taken as the difference between the start time (after irradiation of the stack and upon first heating) and the time corresponding to the arrival of the first detectable acid molecule. This end time (when the fluorescence intensity first increases), rather than the time at the inflection point on the curve, is chosen to eliminate variations of acid concentration in the acid front. For example, the slope of the curve shown

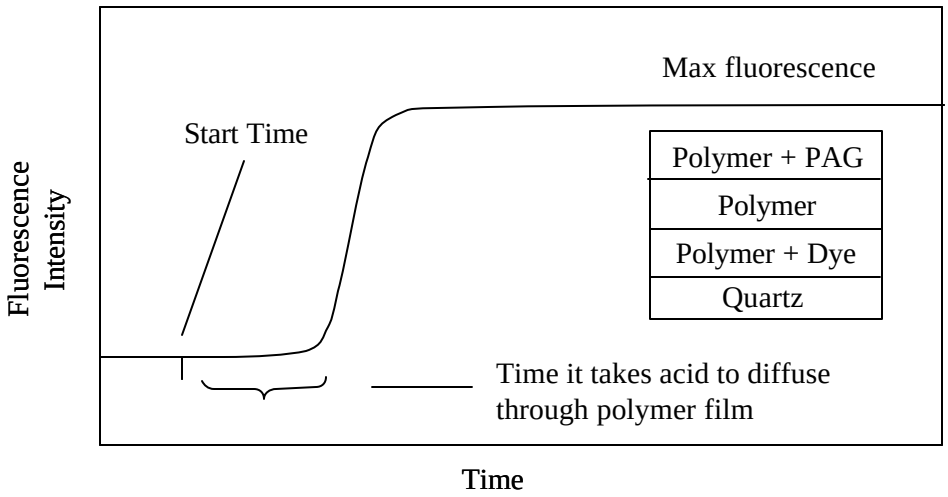

Figure 6.2: Monitoring the fluorescence intensity of the dye molecule with respect to time to extract the diffusion coefficient.

in Figure 6.2 may be shallow in one experiment and steep in the next, depending on the slope of the concentration of the acid front. The time at which the fluorescence intensity first increases will remain the same. By arbitrarily picking this point, we are averaging out these inconsistencies. The diffusion coefficient can then be calculated by using the relationship shown in equation 9.

SYNTHESIS OF POLYMER-BOUND DYES

Many molecules with pH-dependent fluorescence properties are known and used in spectrofluorimetric titrations or as probes for intracellular pH determinations. Some of these fluorophores have dramatically different emission characteristics in their protonated and unprotonated forms.[146-148] For use in resist applications, the ideal acid sensor must possess the following properties:

---

[146] Mataga, N.; Kaifu, Y.; Koizumi, M. *Bull. Chem. Soc. Jpn.* **1956**, *29*, 373.

- Increase in quantum yield or significant shift of fluorescence wavelength upon protonation
- Emission in the visible range of the spectrum ($\lambda > 450$ nm)
- High fluorescence quantum yield
- Thermally stable up to 140°C
- Good photostability
- Good solubility in the commonly used resist solvents
- High extinction coefficient at $\lambda > 300$ nm
- High sensitivity (low pK_b value)

The long-wavelength emission characteristic of the sensor is required to avoid overlap with the fluorescence of the phenolic polymers that are widely used in microlithography. The sensor should also be thermally stable to withstand the high temperatures normally employed in post-exposure baking, and their high sensitivity (low pK_b value) is needed so they are the only species to be protonated in the film. Three possible candidates are the molecules studied by Pohlers *et al.*:[135] 2-phenylpyridine (**6-1**), 2-phenylquinoline (**6-2**), and acridine (**6-3**) (Figure

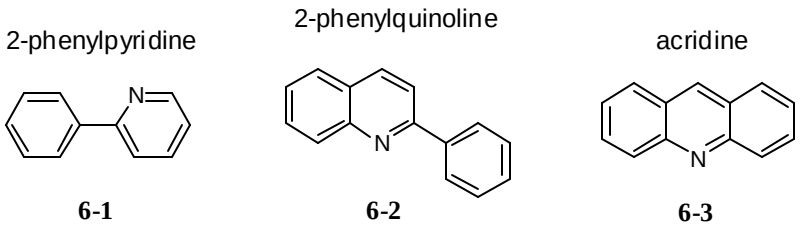

6-1 **6-2** **6-3**

Figure 6.3: Three acid sensor candidates for measuring the diffusion of photogenerated acid by fluorescence spectroscopy.

---

147 Bowen, E. J.; Holder, N. J.; Woodger, G. B. *J. Phys. Chem.* **1962**, *66*, 2491.
148 Diverdi, L. A.; Topp, M. R. *J. Phys. Chem.* **1984**, *88*, 3447-3451.

6.3). These aromatic monoazines have been known for a long time to be essentially nonfluorescent in non-hydrogen-bonding solvents, whereas the protonated forms of these molecules are highly fluorescent. Acridine was chosen in our experiments because it was shown to be the most promising sensor with respect to applications in phenolic polymers. Acridine is not protonated by phenolic groups, and the acridinium ion fluorescence does not overlap with the fluorescence emission of the polymers containing phenolic groups. The large spectral shift upon protonation observed for acridine allows the selective excitation of only the protonated form. Furthermore, the acridinium ion was shown to have the highest fluorescence quantum yield of the three candidates.

As stated earlier, the fluorescent molecule needed to be attached directly to the polymer backbone to prevent diffusion of the sensor molecule. Acridine was therefore incorporated into a poly(styrene) backbone as shown in Figure 6.4. The synthesis of monomer **6-7** began with a Tscherniac-Einhorn reaction using acridine, *N*-hydroxymethylphthalimide (**6-4**), and sulfuric acid as the electrophilic aromatic substitution catalyst.[149] The mono-substituted product, **6-5**, with the substituent at both the 4- and 5-position was obtained. Di-substituted product was also obtained, so separation by column chromatography was necessary. The desired product, 4-phthalimidomethylacridine, was obtained in low yield (19%). Acid-catalyzed hydrolysis and subsequent neutralization yielded the free amine (**6-6**). Dicyclohexylcarbodiimide (DCC) coupling provided the polymerizable monomer **6-7**, and free-radical polymerization of this monomer with styrene using

[149] Hess, F.; Cullen, E.; Grozinger, K. *Tet. Let.* **1971**, *28*, 2591-2594.

2,2'-azobisisobutyronitrile (AIBN) as the initiator gave copolymer **6-8**. Since it was difficult to remove dicyclohexylurea after the coupling reaction, a water-soluble variant of DCC, 1-[3-dimethylamino]propyl]-3-ethylcarbodiimide methiodide (DEC), was used instead which provided a much cleaner reaction. It was important to keep a methylene spacer between the acridine molecule itself and the polymerizable group to prevent modification of the spectroscopic properties of acridine. If acridine was directly linked in conjugation with the polymerizable group, then its absorbance and fluorescence would change.

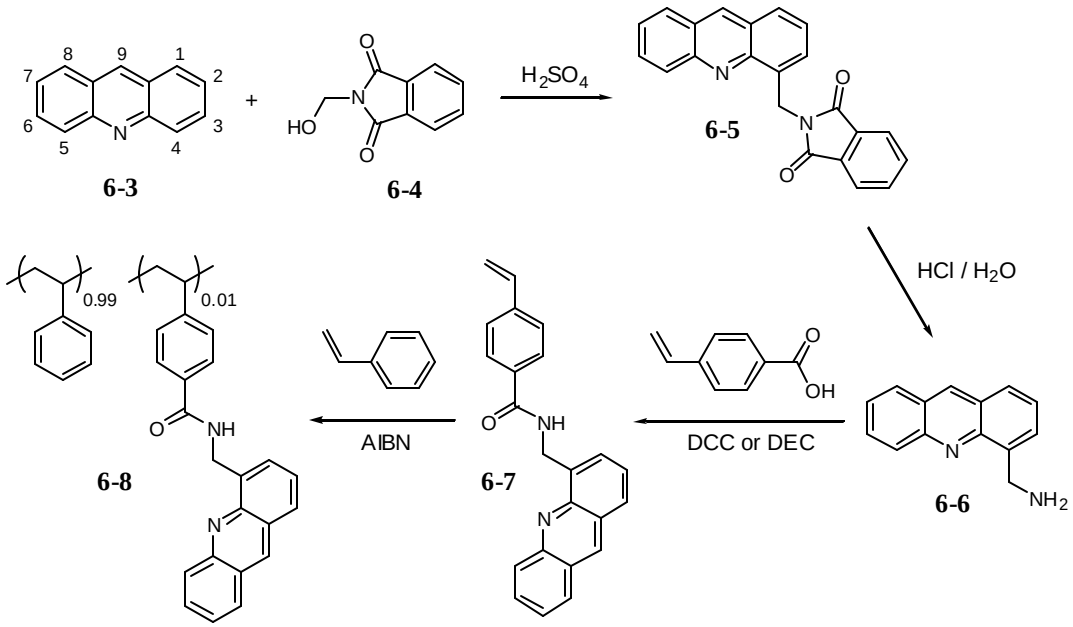

Figure 6.4: Synthesis of an acridine-bound copolymer linked via an amide linkage for trilayer stack fluorescence studies.

Since the yields obtained from the Tscherniac-Einhorn reaction to make molecule **6-5** were unacceptably low, other methods to make a polymer-bound dye were explored. A polystyrene-bound dye linked via an ester functionality was synthesized (Figure 6.5). This pathway provided much higher yields of product. The synthesis of 9-methylacridine (**6-9**) involved a Bernthsen reaction in which a mixture of an aromatic or aliphatic carboxylic acid, diphenylamine, and zinc chloride is heated to 200-270°C in the absence of a solvent.[150-152]

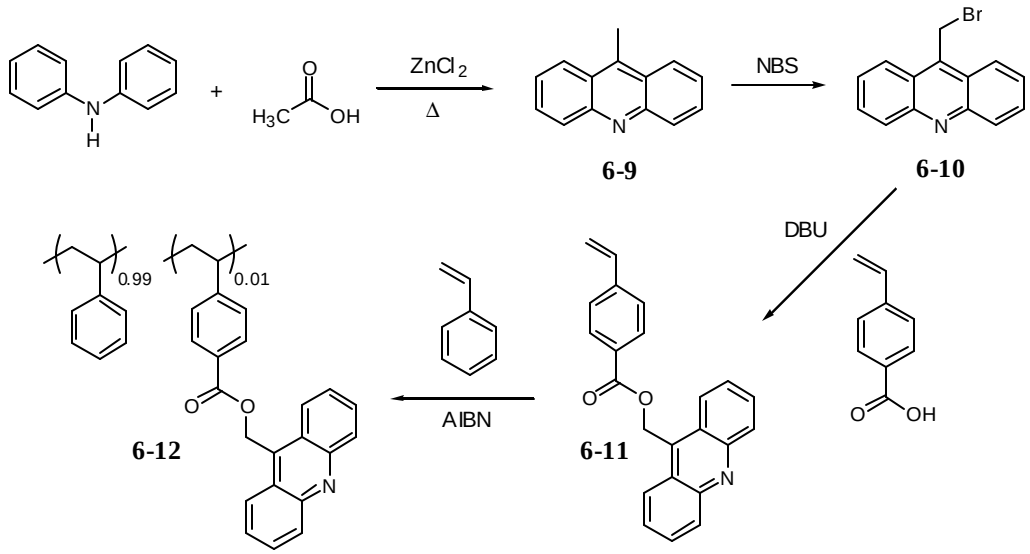

Figure 6.5: Synthesis of an acridine-bound copolymer linked via an ester linkage for trilayer stack fluorescence studies.

Bromination with *N*-bromosuccinimide provided 9-bromomethylacridine (**6-10**) which was converted to the monomer **6-11** via reaction with 4-vinylbenzoic acid

150 Bernthsen, A. *Liebigs Ann. Chem.* **1884**, *224*, 1.
151 Raulins, N. R., In *Acridines*; 2nd ed.; Acheson, R. M., Ed.; John Wiley & Sons: New York, 1973; Chapter 1.
152 Moller, U.; Cech, D.; Schubert, F. *Liebigs Ann. Chem.* **1990**, *12*, 1221-1225.

and 1,8-diazabicyclo[5.4.0]undec-7-ene (DBU). Copolymerization of this monomer with styrene yielded copolymer **6-12**.

A third copolymer was made to compare its results with that of the other two copolymers (Figure 6.6). Bernthsen synthesis provided 9-methylacridine (**6-9**) as before. Refluxing this compound with formaldehyde solution gave 9-(2-hydroxyethyl)acridine (**6-13**)[153], which was attached to a styrene unit by reaction with 4-vinylbenzylchloride and potassium carbonate. Monomer **6-14** should be the most stable (out of the three covalently-attached dye molecules) towards acid cleavage because of its ether linkage. Copolymerization of this monomer with styrene provided copolymer **6-15**.

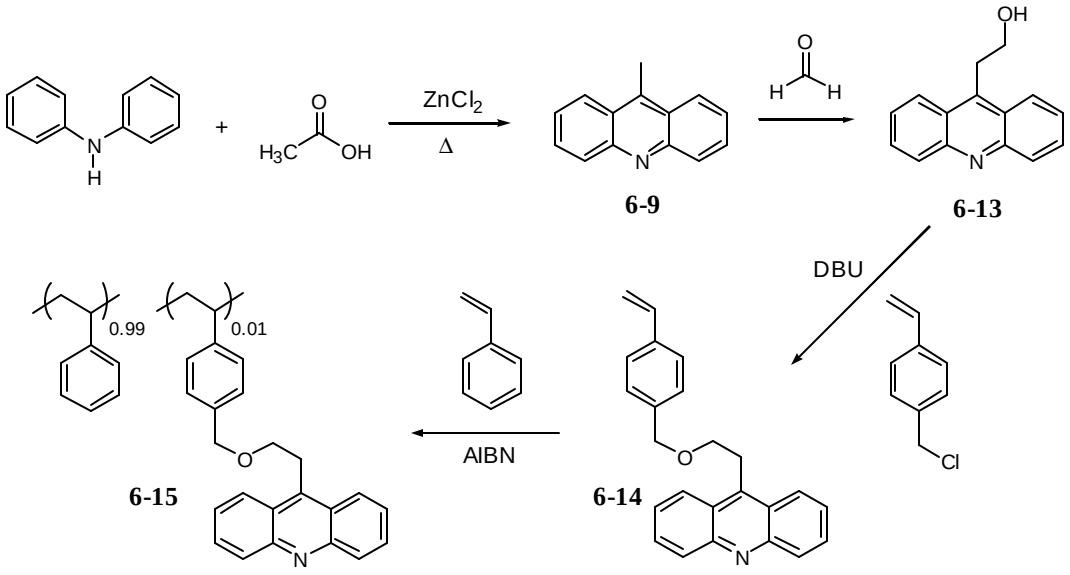

Figure 6.6: Synthesis of an acridine-bound copolymer linked via an ether linkage for trilayer stack fluorescence studies.

[153] Homberger, A. W.; Jensen, H. *J. Am. Chem. Soc.* **1926**, *48*, 800-801.

With all of the copolymers made for the acid diffusion studies, it was important to verify that there was no residual, unbound fluorescent monomer left in the isolated polymers. Any impurities could lead to erroneous readings because the unbound fluorophores would diffuse outside of the detector layer. To verify this, the copolymers were analyzed by a gel permeation chromatograph equipped with both a refractive index detector and a fluorescence detector. If the chromophore is attached to the polymer structure, then the refractive index signal and fluorescence signal should overlap. However, if there are unattached chromophore molecules in the polymer sample, then the two signals should not overlap. As seen in Figure 6.7, both signals overlapped when polymer **6-8** was analyzed, so it was concluded that the chromophore was directly attached to the polymer backbone. The same result was obtained for the other two copolymers.

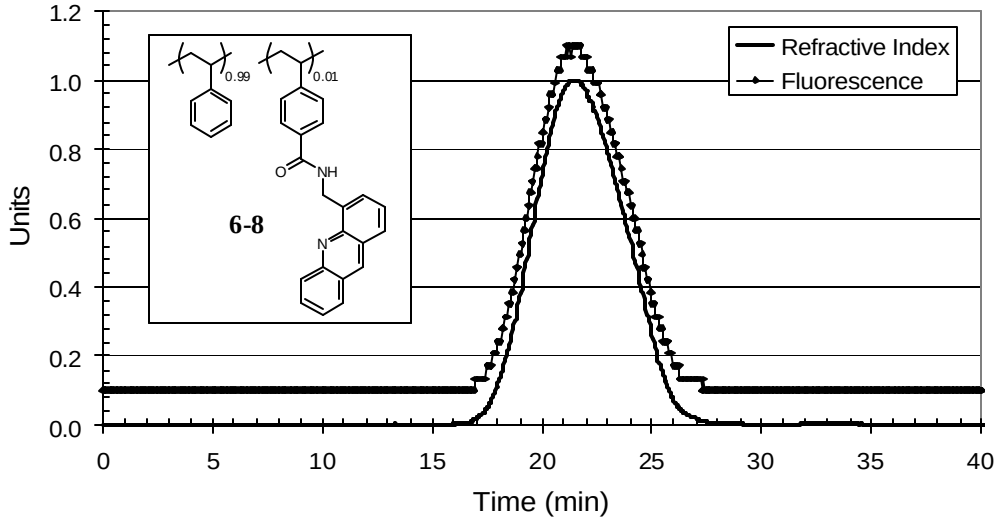

Figure 6.7: GPC trace of overlapped refractive index and fluorescence signals, indicating that the chromophore is directly bound to the polymer backbone.

ACID DIFFUSION STUDIES WITH BOUND FLUOROPHORES

Once the fluorescent copolymers were made for use as the detector layer, acid diffusion experiments were initiated. Bilayer stacks were first made to test the design concept and the sensitivity of the acridine-bound copolymers to acid species. Polymer **6-8** was coated from an appropriate solvent onto a thin quartz disc. Normally, the second polymer layer was spin-coated over the first layer by using a solvent that dissolves the second polymer but not the first. When no solvent could be found that met that requirement, a floating technique was used (Figure 6.8). This involved coating a polymer onto a microscope slide and scraping the edges of the slide to facilitate polymer lift-off. The slide was carefully immersed in a bath of water to lift the polymer film off of the slide. The floated film was then picked up with the dye-coated quartz substrate. The bilayer stack was subsequently dried on a hotplate to drive off residual water.

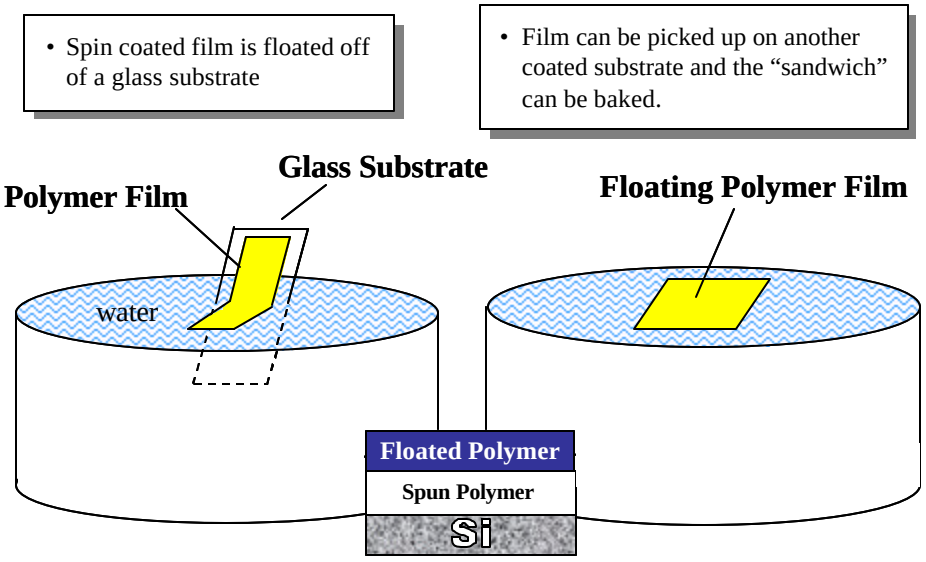

Figure 6.8: Floating technique for making bilayer stacks.

This floating technique was used to make the bilayer stack shown in Figure 6.9. The stack was placed in a spectrofluorometer and time-based fluorescence emission scans were recorded. The attached acridine molecule was excited at a wavelength of 357 nm and fluorescence emission at a wavelength of 480-500 nm was monitored (the maximum emission wavelength of the protonated dye molecule). Neat trifluoroacetic acid was injected into the sample chamber containing the bilayer stack. As seen in the figure, the fluorescence emission

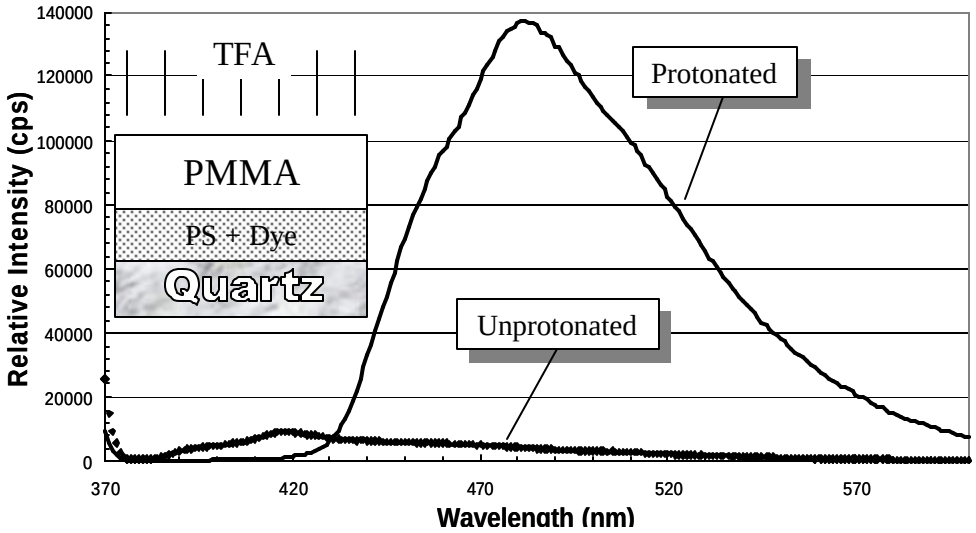

Figure 6.9: Fluorescence emission spectra of protonated and unprotonated forms of acridine.

intensity of the attached dye molecule increased dramatically after acid diffused through the poly(methylmethacrylate) (PMMA) layer. Figure 6.10 shows the time delay for diffusion of trifluoroacetic acid through the PMMA layer. After about 200 sec, the acid had diffused through the polymer film and protonated the

acridine molecule, resulting in an intense increase in fluorescence emission at 480 nm. This experiment shows the viability and sensitivity of this technique for monitoring the diffusion of acid through thin polymer films.

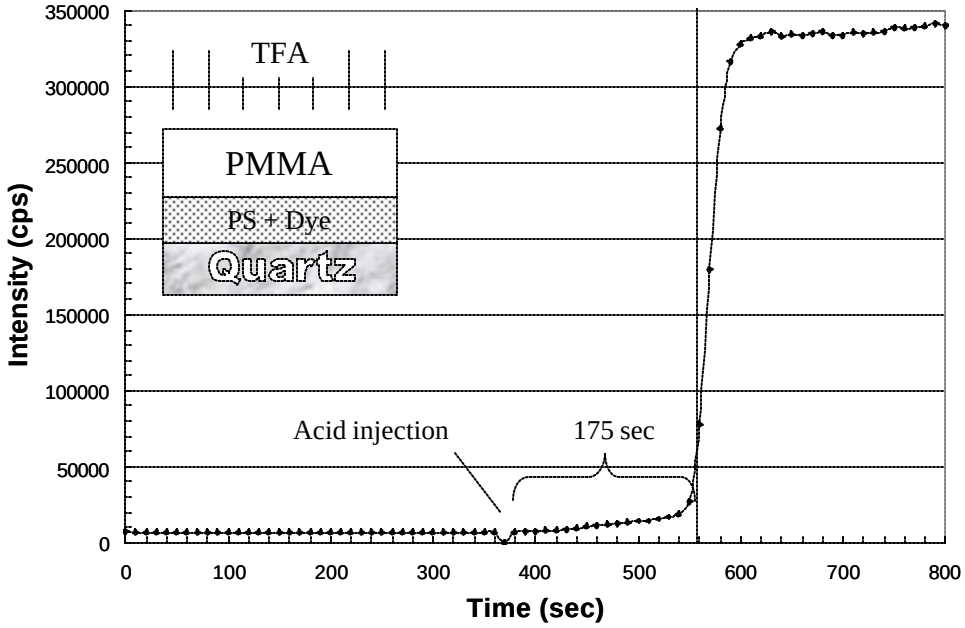

Figure 6.10: Fluorescence intensity vs. time for a bilayer stack experiment showing the intense increase in fluorescence after dye protonation.

The success of these experiments prompted the investigation of trilayer stacks, in which the third, acid generation layer consisted of a polymer that is blended with triphenylsulfonium antimonate (Ph_3SSbF_6). The amount of acid produced in this layer depends on the amount of PAG blended with the matrix polymer, the quantum yield of the PAG, the optical density, and the radiation dose. The middle layer was changed from PMMA to PHOST because PHOST is

a key component of some 248 nm resists, which are copolymers including *p*-hydroxystyrene and *p*-hydroxystyrene protected with *t*-BOC. In addition, PHOST allows study of the diffusion of acid through an inert polymer matrix rather than a reactive polymer matrix (if an actual resist polymer was used). This will allow for more accurate measurement of diffusion coefficients that are decoupled from the reaction kinetics. The detector layer remained the same and was coated onto the quartz substrate by spin-coating. The PHOST layer was spin-coated over this first layer from ethanol, which dissolves PHOST, but not poly(styrene). The third layer, PMMA + PAG, was floated over the stack using the method described previously. After baking to remove residual solvent, this stack was analyzed in

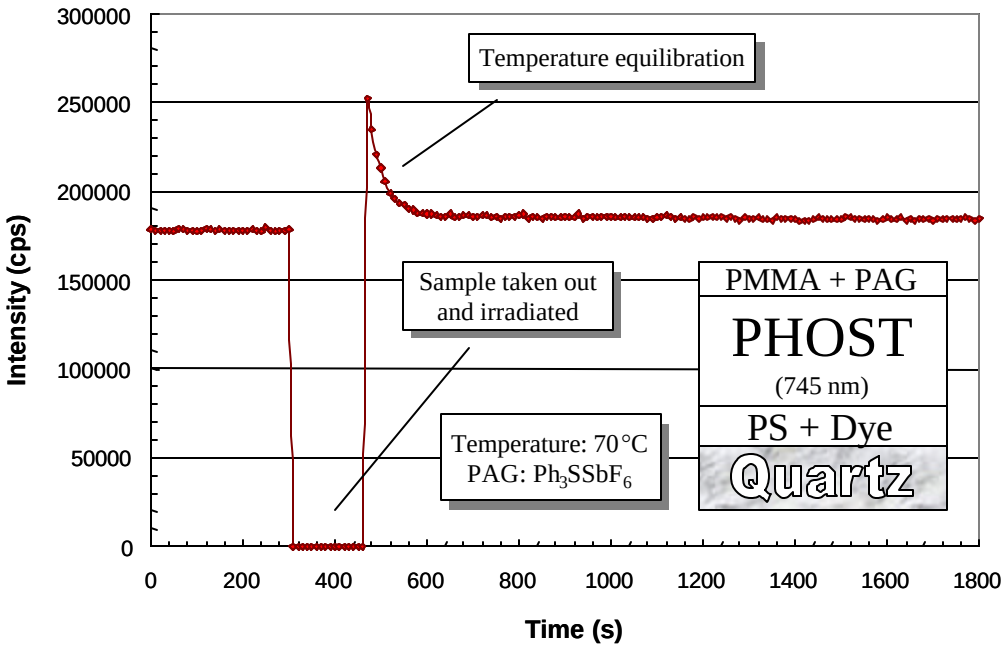

Figure 6.11: Trilayer stack experiment showing that photogenerated acid was not detected after 30 min.

the spectrofluorometer at 70°C (Figure 6.11). The stack was put into the chamber and the initial fluorescence emission was measured. The stack was then taken out, irradiated at a specified dose, and put back into the spectrofluorometer. As seen in the figure, the fluorescence intensity starts higher than the initial intensity and then quickly returns to the same level. This is due to a thermal process in which energy is lost thermally rather than photochemically (fluorescence) from the higher temperature. After several hours at 70°C, no increase in fluorescence intensity was observed.

In order to make sure that acid was indeed produced during exposure and that the acid molecule was able to penetrate the interface between the two different polymers, a bilayer stack was made and analyzed. This bilayer stack consisted of a PMMA + PAG layer that had been floated over a polystyrene + dye layer. The middle PHOST polymer layer was eliminated in this stack. After exposure, the stack was monitored with the spectrofluorometer, and an increase in fluorescence intensity was immediately observed. This experiment showed that acid was indeed produced and was able to diffuse from one polymer layer to the next.

In light of these experiments, we concluded that acid was not able to diffuse through the 745 nm thick layer of PHOST during the time allowed for diffusion. In several other experiments in which the thickness of the PHOST layer was decreased to 200 nm and less, acid was still not detected. This observation will be discussed and explained in more detail in the next chapter.

Many experiments of the type shown in Figure 6.11 were performed. In several instances, the fluorescence intensity was seen to increase with time even before irradiation of the PAG, as shown in Figure 6.12. At first it was thought that the floating technique somehow allows acid contaminant that may be in the

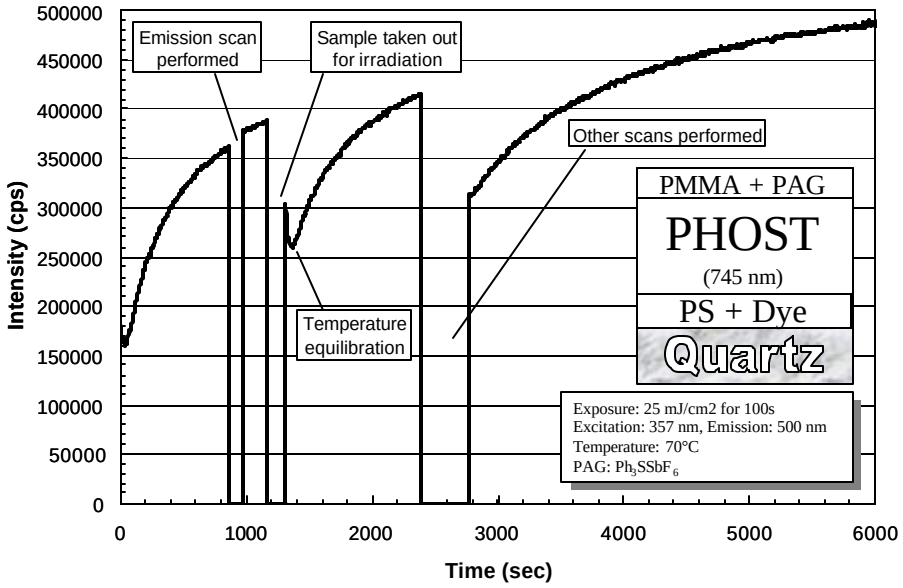

Figure 6.12: Trilayer stack experiment showing increasing fluorescence intensity even before irradiation of the stack.

water to "poison" the dye layer. This was proven not to be true through several control experiments. In one control study the quartz substrate was only coated (by spin-coating) with the poly(styrene) + dye layer. The initial emission spectrum at 70°C looked consistent with an unprotonated spectrum. However, after 10 minutes, the emission spectrum started to look like the spectrum of a protonated species (with the appearance of a shoulder at 500 nm), as seen in Figure 6.13. Trace levels of acid in the spectrofluorometer chamber may be the

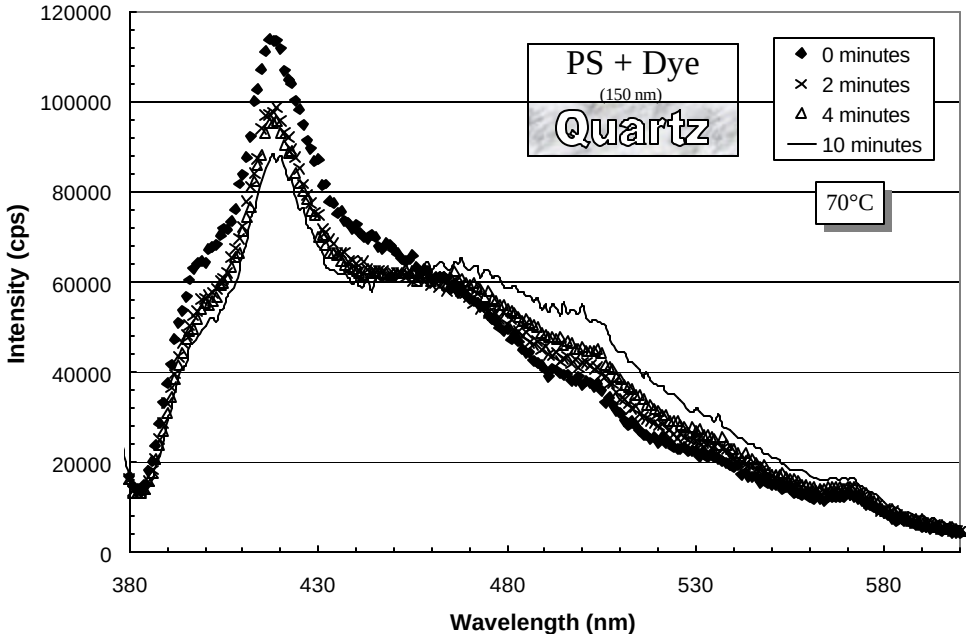

Figure 6.13: Fluorescence spectrum of acridine showing unexplainable drift of fluorescence at 70°C.

cause of this phenomenon, but this phenomenon was still observed after thorough cleaning of the chamber. Because of these inconsistencies from one experiment to the next, the measurement of acid diffusion by fluorescence spectroscopy was abandoned, and efforts were concentrated on monitoring acid diffusion by infrared spectroscopy, which proved to be more reproducible.

CHAPTER 7: *MEASURING ACID DIFFUSION WITH INFRARED SPECTROSCOPY*

The use of infrared spectroscopy to monitor the diffusion of photogenerated acid through thin polymer films has several advantages. An infrared spectrophotometer can be modified such that sample spectra can be collected, *in situ*, in a nitrogen-purged chamber that is attached to a temperature-controlled hotplate. Infrared spectroscopy is sensitive, and poly(4-tert-butyloxycarbonyloxystyrene) (PTBOCST) can be purchased or made easily and used as the detector layer. This eliminates the need to synthesize polymer-bound dye molecules, as in the case for fluorescence spectroscopy. The trilayer stacks, therefore, consist of an acid-generating layer that has been spun on a silicon substrate, a middle polymer layer that is to be studied that is coated over the first layer, and PTBOCST as the detector layer that has been applied by floating over the two layers. When the photogenerated acid reaches the detector layer, it catalyzes cleavage of the *t*-BOC protecting group, releasing carbon dioxide, isobutylene, and another acid molecule that may catalyze other cleavage reactions. Because of this "chemical amplification", this method of detecting acid is very sensitive since even minute amounts of acid cause a strong detector response. The decrease in the absorbance of the carbonyl peak (from the *t*-BOC group) can be monitored in the infrared as acid catalyzes the deprotection of PTBOCST (Figure 7.1).[129,154-156]

---

[154] Postnikov, S. V.; Stewart, M. D.; Tran, H. V.; Nierode, M. A.; Medeiros, D. R.; Cao, T.; Byers, J.; Webber, S. E.; Wilson, C. G. *J. Vac. Sci. Technol., B* **1999**, *17*, 3335-3338.

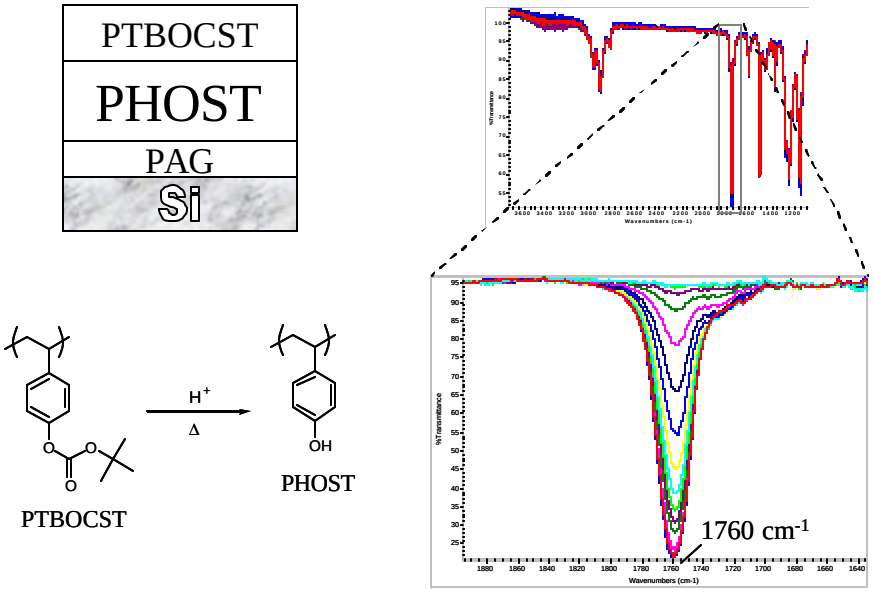

Figure 7.1: Measurement of acid diffusion by infrared spectroscopy. The decrease in absorbance of the carbonyl group is monitored as acid catalyzes the deprotection of PTBOCST

Several limitations of infrared spectroscopy in this application must be mentioned. Since the carbonyl peak of the detector layer is monitored in the IR, the other polymer layers must not contain any carbonyl groups to facilitate analysis. It is possible to have other carbonyl groups, but the sensitivity of this technique then depends on the amount of overlap of the carbonyl peaks. In addition, the presence of acid is measured after a deprotection reaction, so the kinetics of deprotection also plays a role in the sensitivity of this technique. This is in contrast to the fluorescence spectroscopy experiments described in the last

---

155 Stewart, M. D.; Postnikov, S. V.; Tran, H. V.; Medeiros, D. R.; Nierode, M. A.; Cao, T.; Byers, J.; Webber, S. E.; Willson, C. G. *Polym. Mater. Sci. Eng.* **1999**, *81*, 58-59.

156 Stewart, M. D.; Somervell, M. H.; Tran, H. V.; Postnikov, S. V.; Willson, C. G. *Proc. SPIE Int. Soc. Opt. Eng.* **2000**, *3999*, 665-674.

chapter, in which the presence of acid is detected by protonation of the dye molecule. Lastly, the thermal stability of the carbonate polymer (PTBOCST) must be considered because at temperatures above 150°C, uncatalyzed thermolysis of the protecting group occurs at a finite rate. This limits the study of acid diffusion to temperatures below the thermal decomposition temperature of the detector layer.

TRILAYER STACK EXPERIMENTS WITH PHOST

Experiments analogous to the trilayer experiments in the previous chapter were performed. In this case, the detector layer was PTBOCST instead of the poly(styrene) + dye layer, and the stack was analyzed by infrared spectroscopy instead of fluorescence spectroscopy. As shown in Figure 7.2, and in agreement

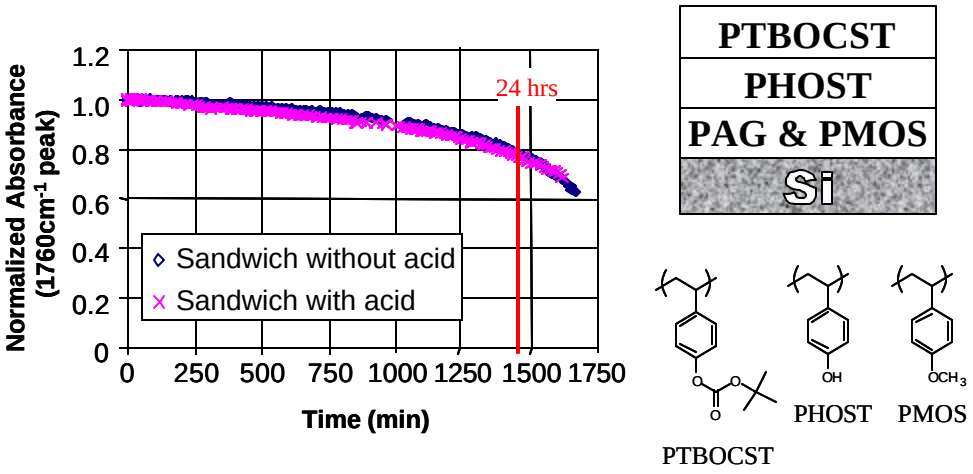

Figure 7.2: Trilayer experiment showing the uncatalyzed thermolysis of PTBOCST with and without acid.

with the results obtained using fluorescence spectroscopy, diffusion of the photogenerated acid through the intermediate PHOST layer was never detected.

After monitoring the detector layer response for over 24 hours, a negative slope in the curve was observed, indicating a diminution in absorbance of the carbonyl peak. This indicates deprotection of the PTBOCST, but a control experiment in which no PAG was added to the feeder layer showed the same response curve. This indicates deprotection by the uncatalyzed thermolysis of PTBOCST at 90°C rather than catalyzed deprotection due to acid arrival. Also evident from the change in the slope of the curve is that the phenolic product is itself a catalyst for *t*-BOC deprotection, albeit a rather inefficient one. Even when the thickness of the intermediate PHOST layer was decreased to form very thin films, when the time allowed for diffusion increased, when the temperature was varied, and when several different PAGs were used, no diffusion of acid through PHOST was ever detected. The diffusion coefficient of the acid at 90°C when PHOST is the medium must be much smaller than reported diffusion coefficients of acid in resist films, which are usually on the order of 10^{-4} to 10^{-6} $\mu m^2/s$. The diffusion coefficients suggested by these experiments are far too small to account for the bias observed during actual resist imaging. Of course, PHOST cannot be compared to an actual resist because the polymer is inert to the diffusing acid whereas a typical resist polymer (PHOST that is 20% protected with *t*-BOC) would be capable of substantial interaction and reaction with the diffusing acid. However, these experiments do provide some important insights into the nature of acid diffusion through polymers at temperatures below T_g (for PHOST, T_g ~ 180°C). This will be discussed in more detail in a later section.

BILAYER STACK EXPERIMENTS WITHOUT PHOST

Experiments were performed on bilayer stacks in which the intermediate PHOST layer was removed.[156] This puts the PTBOCST detector layer in direct contact with the acid feeder layer. The motivation for these experiments came from the desire to determine whether acid was able to traverse between the two polymer films and to explore the effect of acid diffusion through the detector layer. Would diffusion of acid through a reactive polymer matrix be driven solely by a concentration gradient (hence, classical Fickian diffusion), or does interaction with the reactive polymer matrix change the diffusion characteristics such that Fickian diffusion alone cannot account for the behavior?

The results obtained from these experiments were very interesting. For example, in a bilayer stack consisting of 320 nm of PTBOCST coated over a layer of poly(methoxystyrene) containing 10 wt% triphenylsulfonium perfluorobutanesulfonate (420 nm) that has been exposed with 248 nm radiation (60 mJ/cm^2), a very fast diffusion rate was observed in the first few minutes (Figure 7.3). This is followed by a marked decrease in rate which starts to level off after about 3 minutes. The path length calculated for acid diffusion shown on the y-axis may be obtained by the equation shown in Figure 7.4. The initial absorbance, A_0, of the stack at the carbonyl peak and the initial thickness, l_0, of the PTBOCST is known. The absorbance at time t, A_t, is also known, so one can calculate the thickness of the PTBOCST layer at time t, l_t. Path length is defined as l_0 minus l_t. Of course, this assumes that acid does not skip any protected sites and that there is full deprotection in the path length region. Figure 7.3 shows the

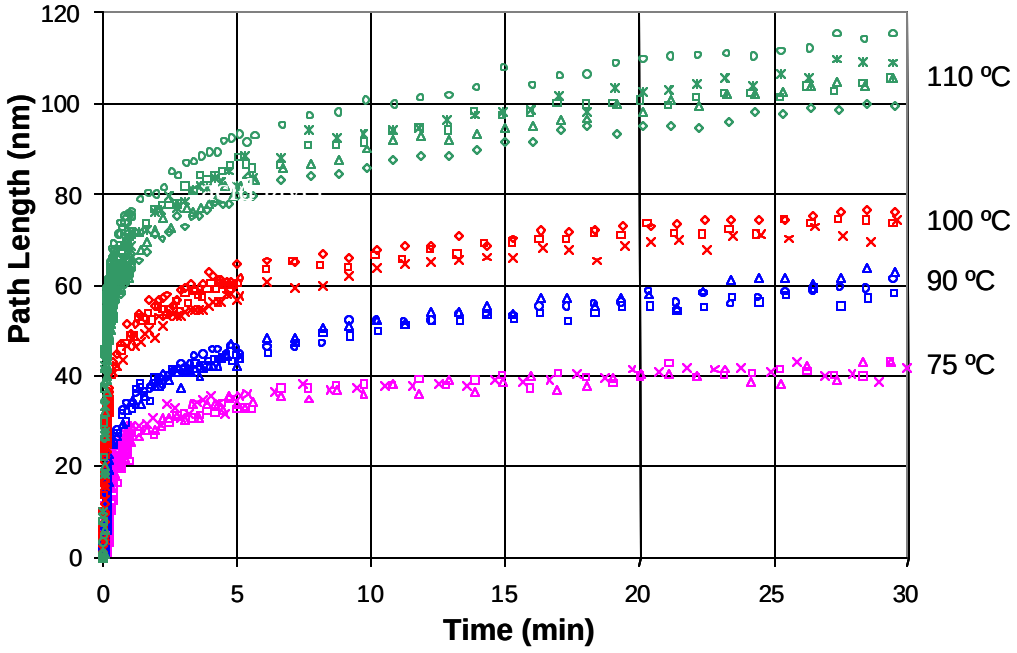

Figure 7.3: Dependence of acid path length in PTBOCST on post-exposure bake temperature for perfluorobutanesulfonic acid.

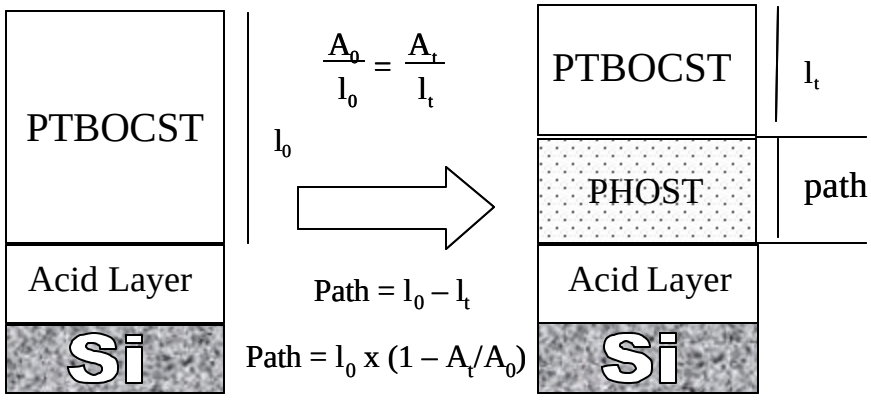

Figure 7.4: Calculation of the path length, assuming full deprotection of PTBOCST in the diffused region.

path length of perfluorobutanesulfonic acid in PTBOCST at four different temperatures. As expected, path length of diffusion is higher with increasing temperature. Bilayer experiments using different PAGs as well as different exposure doses have also been carried out. The curves obtained from these experiments are all similar to those shown in Figure 7.3.[154] The steady increase in path length after 5 minutes is not attributed to acid diffusion, but is instead attributed to the background thermal decomposition of PTBOCST at the elevated temperatures. A control experiment with a bilayer stack containing PAG and the same stack without PAG shows that the slope of the curve after the first few minutes is very similar (Figure 7.5).

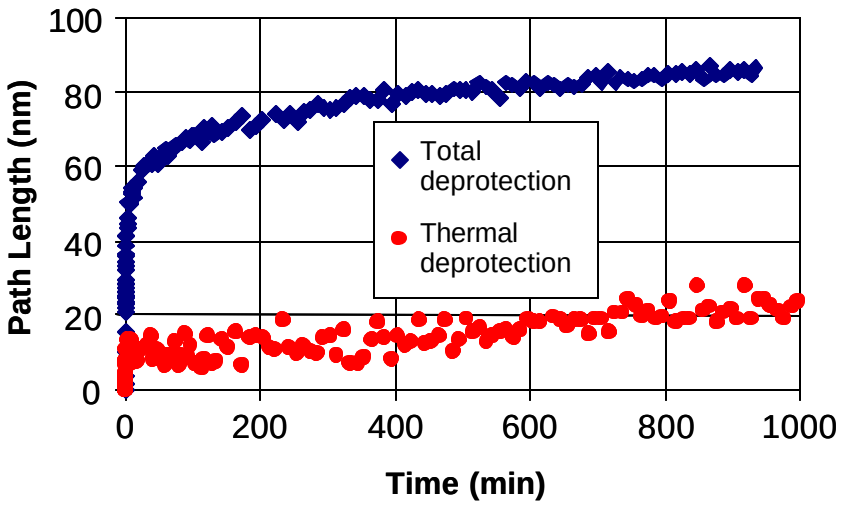

Figure 7.5: Graph showing that the positive slope after 10 minutes is due to the thermal deprotection of PTBOCST.

Simple Fickian diffusion alone cannot explain the behavior shown in Figures 7.3 and 7.5. If diffusion occurred by a pure classical concentration-

gradient diffusion mechanism, then the initial fast rate of diffusion observed in the first 3 seconds would not taper off so drastically. Some mechanism for acid quenching must be incorporated into the model to explain this fast leveling effect. A physical model, termed the reaction front propagation model, was proposed in an attempt to explain this behavior (Figure 7.6).[129] Initial diffusion of acid into the PTBOCST layer is fast because the photogenerated acid molecules present at the polymer-polymer interface react with PTBOCST, generating PHOST, carbon dioxide, isobutylene, and another acid molecule. A reaction zone in which this chemistry occurs is created, and propagates in the positive direction stepwise, layer by layer, leaving a film of PHOST behind. While this chemistry occurs,

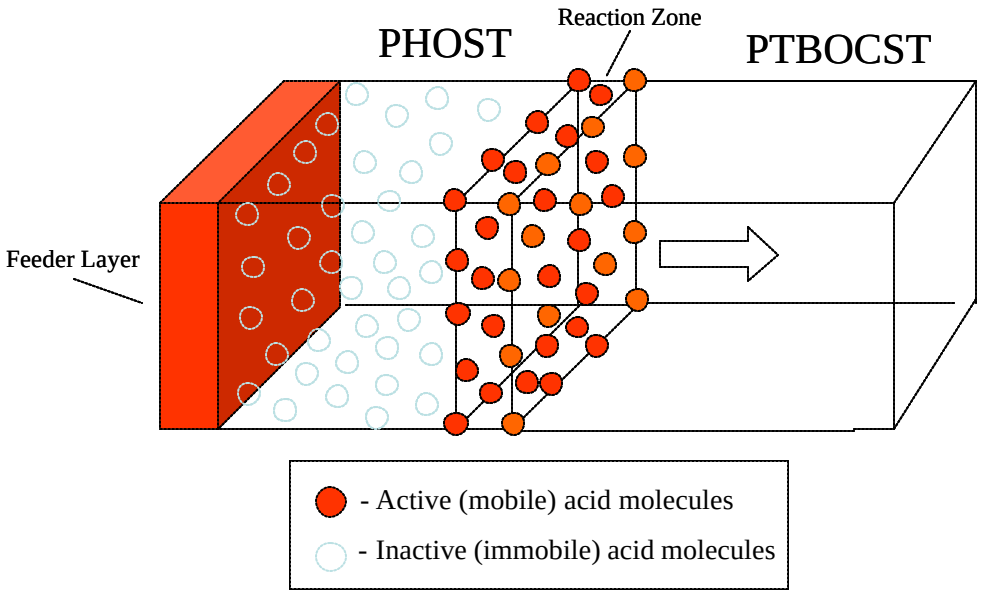

Figure 7.6: Pictorial illustration of the reaction front propagation model. Acid molecules are trapped in the newly formed PHOST layer.

free volume is created in the reaction zone due to the evolution of gaseous products (CO_2 and isobutylene). Acid molecules become trapped in the newly formed PHOST matrix when the film collapses. As we've seen in the trilayer experiments reported earlier, diffusion of acid molecules through PHOST is extremely slow below the polymer's T_g. Therefore, the acid molecules that are trapped in PHOST are considered lost. They are "trapped" in the PHOST matrix and do not further contribute to the chemistry taking place in the reaction zone. Therefore, there is a net loss of acid from this zone with time, and the reaction eventually stops. Apparently, from the data shown in Figure 7.3 and other experiments, the time scale of this occurrence is about 3 minutes. After that, there is no acid to catalyze further deprotection reactions, and only thermolysis of PTBOCST is seen.

If one truncates the data after the first 90 seconds (a typical post-exposure bake time), then the diffusion coefficient is estimated to be on the order of 10^{-4} $\mu m^2/s$ based on the diffusion lengths observed. This is on the same order of magnitude as that reported in the literature for a commercial resist (10^{-4} to 10^{-6} $\mu m^2/s$). This diffusion coefficient is based on a homopolymer of PTBOCST. If a commercial resist was analyzed with this same technique, then the diffusion coefficient would be expected to be smaller (possibly down to 10^{-6} $\mu m^2/s$) because of the increased content of PHOST.

TRILAYER STACK EXPERIMENTS WITH PEMA

Since the diffusion of acid through PHOST was not observed below the polymer's T_g, several experiments were performed to study this transport more

carefully. Much work has been published that describes the dependence of the diffusivity of various penetrants on the glass transition temperature of the polymer medium.[157-159] The permittivity (P) of inert gas molecules or other small molecules in a polymer matrix is defined as the diffusion coefficient (D) times the solubility coefficient (S) of the molecule:

$$P = D \bullet S \tag{10}$$

When the temperatue is below the glass transition temperature of the polymer, the penetrant has to move around the polymer chains (Figure 7.7). When the temperature is above the Tg of the polymer, the penetrant moves in a straighter path because the polymer chains are more easily pushed aside due to the increased

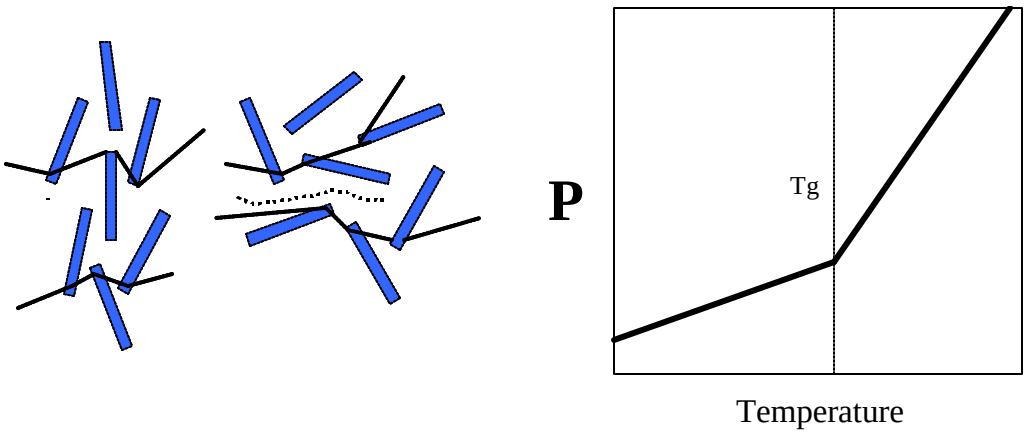

Figure 7.7: The diffusion of inert molecules through a polymer matrix is highly dependent on the glass transition temperature of the polymer.

157 Van Amergedon, G. J. *Rubber Chem. Technol.* **1951**, *24*, 109.
158 Vrentas, J. S.; Liu, H. T.; Lau, M. K. *J. Appl. Polym. Sci.* **1982**, *27*, 3987.
159 Koros, W. J.; Hellums, M. W. *Transport Properties*, In *Encyclopedia of Polymer Science and Engineering*; 2nd ed., 1989.

dynamic motion and free rotation of the chains. The permittivity or diffusion rate of the small molecule through the polymer matrix is therefore increased above the polymer's T_g.

Experiments in which PHOST was replaced with poly(ethyl methacrylate) (PEMA) as the analyzed intermediate layer were performed.[155] PEMA has a glass transition temperature of approximately 68°C, as measured by differential scanning calorimetry (DSC). By using this polymer instead of PHOST, which has a T_g of approximately 180°C, we are able to investigate the diffusion of acid molecules at typical post-exposure baking temperatures (90-150°C) that are above the T_g of the polymer matrix. A trilayer stack consisting of PTBOCST (360 nm), PEMA (740 nm), and PMOS + 5 wt% of $(t\text{-BuPh})_2I^+{}^-O_3SC_4F_9$ was made and analyzed in the IR at 90°C after irradiation at 60 mJ/cm^2 (Figure 7.8). As shown,

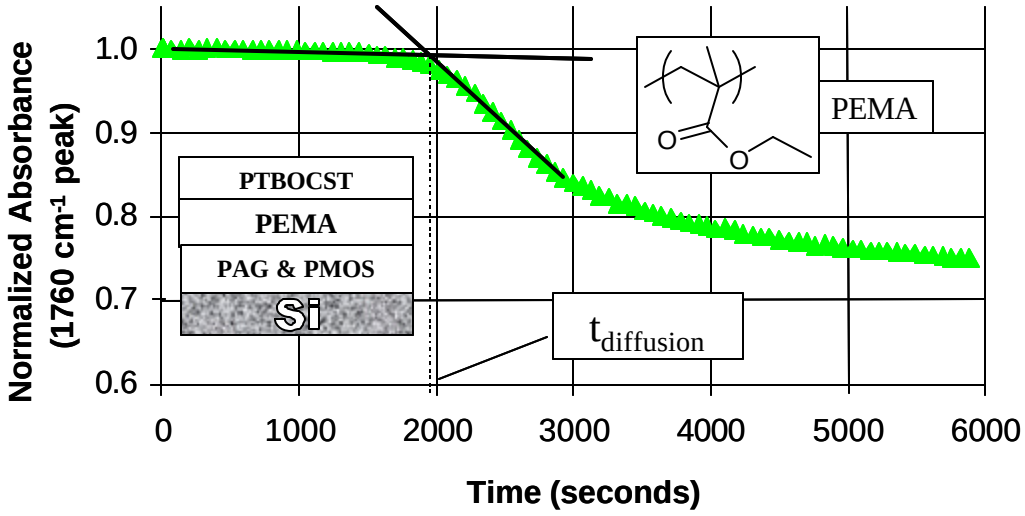

Figure 7.8: Diffusion of photogenerated acid is observed through PEMA above the polymer's T_g.

the absorbance of the carbonyl peak of PTBOCST immediately decreases when the photogenerated acid reaches the detector layer after diffusing through the middle PEMA layer. The PEMA thickness was varied and acid transit time was found to scale linearly with the square of the thickness Figure (7.9). This result is the same as that predicted by equation 9, therefore classical Fickian diffusion is observed at temperatures above the T_g of PEMA. The diffusion coefficient

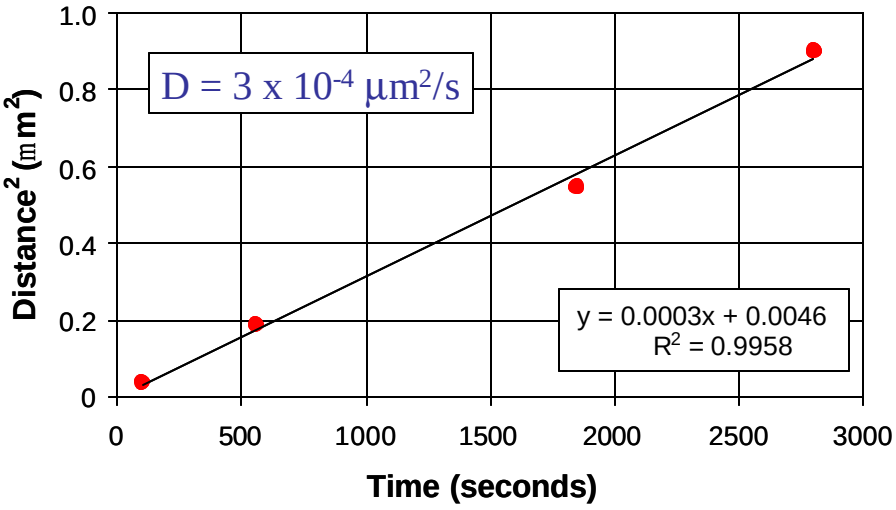

Figure 7.9: Acid transport through PEMA above T_g follows classical Fickian behavior.

calculated from these studies is on the order of 10^{-4} $\mu m^2/s$. When the temperature was varied from 60°C to 95°C in a trilayer stack containing a 150 nm thick PEMA layer, the temperature dependence of diffusion was clearly demonstrated (Figure 7.10). At temperatures below the T_g range of PEMA, diffusion was not observed in the time frame of the experiment. In the softening region of PEMA, diffusion of acid was observed and closely followed Fickian behavior as the

temperature was increased above T_g. These experiments helped us to understand why diffusion was not observed at 90°C when PHOST was used as the intermediate layer. At 90°C, which is 90°C below the Tg of PHOST, diffusion was so slow that acid was never detected, even when the experiment was conducted over a period of a week.

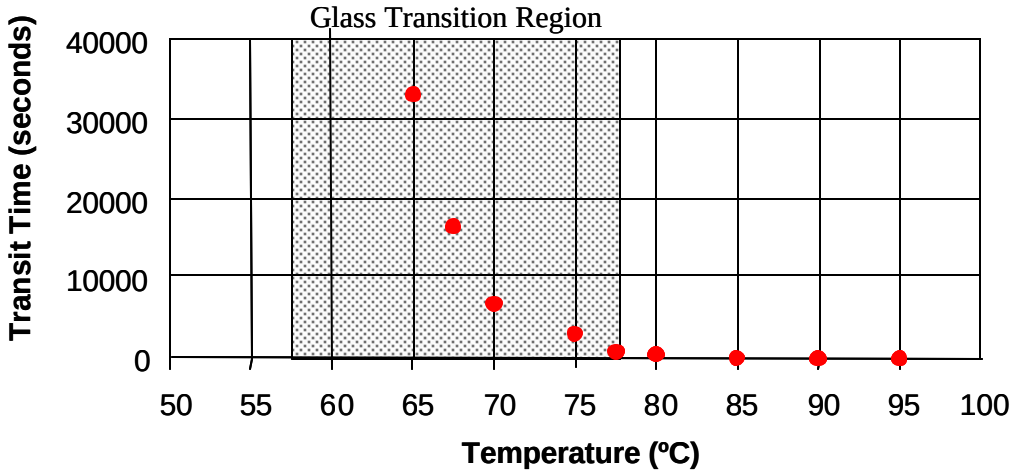

Figure 7.10: Acid transit time decreases markedly as the baking temperature is increased above the T_g region of PEMA.

TRILAYER STACK EXPERIMENTS WITH PHOST ABOVE TG

In order to determine if acid is able to traverse through PHOST near the polymer's T_g, the temperature of analysis needed to be increased to about 180°C. However, the detector layer (PTBOCST), thermally decomposes rapidly above 150°C, as seen in the thermogavimetric analysis (TGA) plot shown in Figure 7.11. This presented a large problem, and demanded establishment of a new detector layer that is thermally stable above 180°C while still reactive to acid.

The new detector polymer also had to be able to undergo a chemical change in the presence of acid that can be detected using infrared spectroscopy. The most effective method so far has been to monitor the increase or decrease of absorbance of a carbonyl peak.

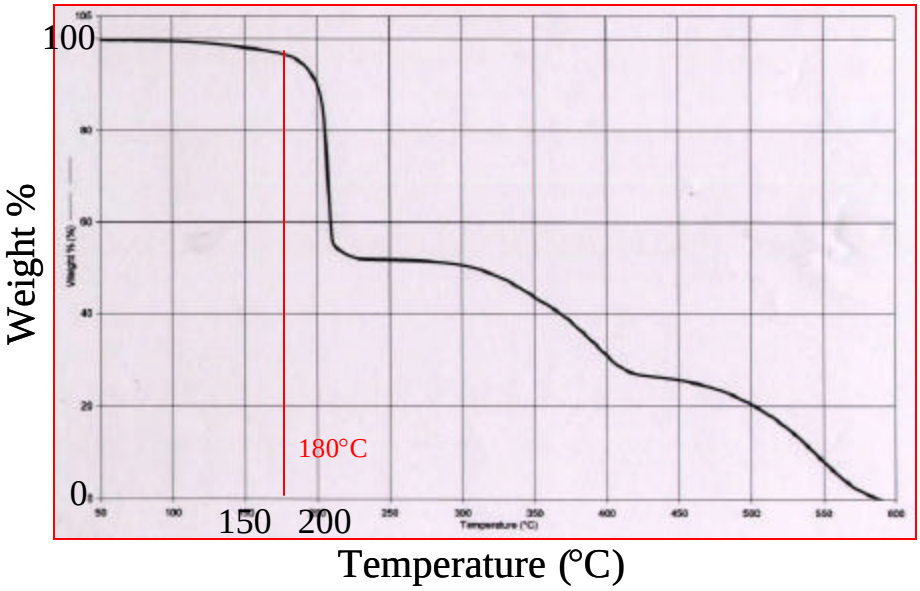

Figure 7.11: Thermogravimetric plot showing the uncatalyzed thermal decomposition of PTBOCST above 150°C.

A series of polycarbonate polymers similar in structure to PTBOCST were synthesized in hope of achieving this goal (Figure 7.12). These polymers were made by the reaction of poly(4-hydroxystyrene) (PHOST) with the appropriate chloroformate using triethylamine as the base. Several chloroformates were available commercially. The ones that were not available were synthesized by the reaction of the corresponding alcohol with excess phosgene. Triethylamine was

added in the preparation of chloroformates of secondary alcohols, but was not needed in the preparation of chloroformates of primary alcohols.

The thermal decomposition of PTBOCST most likely involves decarboxylation and cleavage of the *t*-butyl group to form a stable tertiary carbocation and carbon dioxide gas. One would therefore predict that the thermal

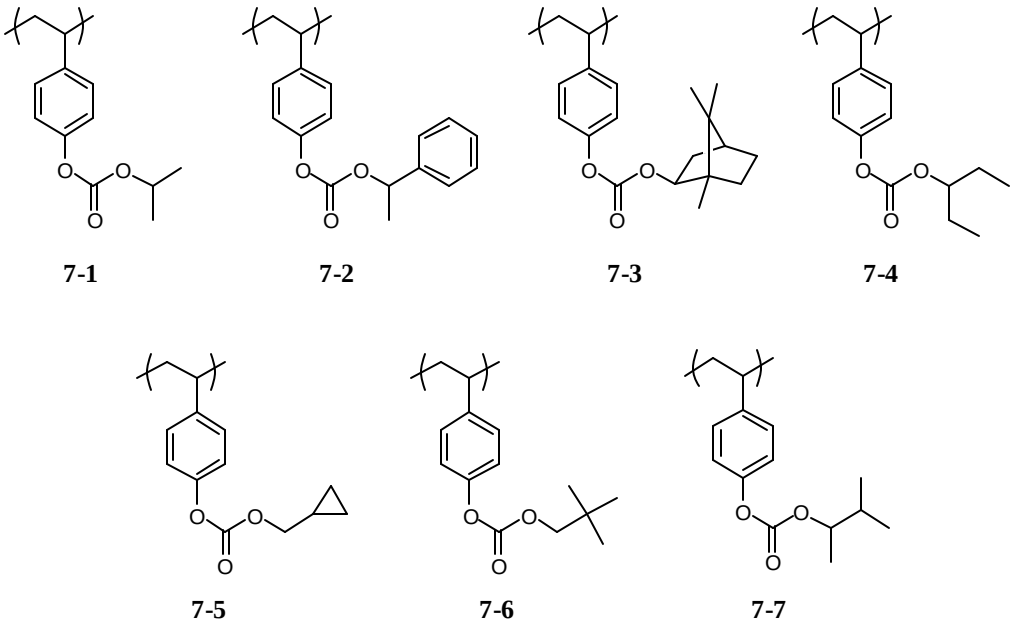

Figure 7.12: Structures of several polycarbonates screened as a detector layer for sandwich experiments.

stability of similar polymers would increase if the *t*-butyl group were replaced by groups that cleave to provide less stable carbocations. This trend is observed, more or less, with the polymers shown in Figure 7.12. Those polymers that cleave to form less stable primary carbocations are more thermally stable than those polymers that cleave to form more stable secondary carbocations (Figure

7.13). The same relationship applies to PTBOCST, which is the least thermally stable polymer because a stable tertiary carbocation is formed in the rate-determining step of the cleavage reaction.

Polymer **7-1** was first made because its thermal stability would be expected to be much higher due to the less stable secondary isopropyl cation that forms. The onset of thermal decomposition, shown in Figure 7.13, is higher than 250°C. However, when this polymer was blended with approximately

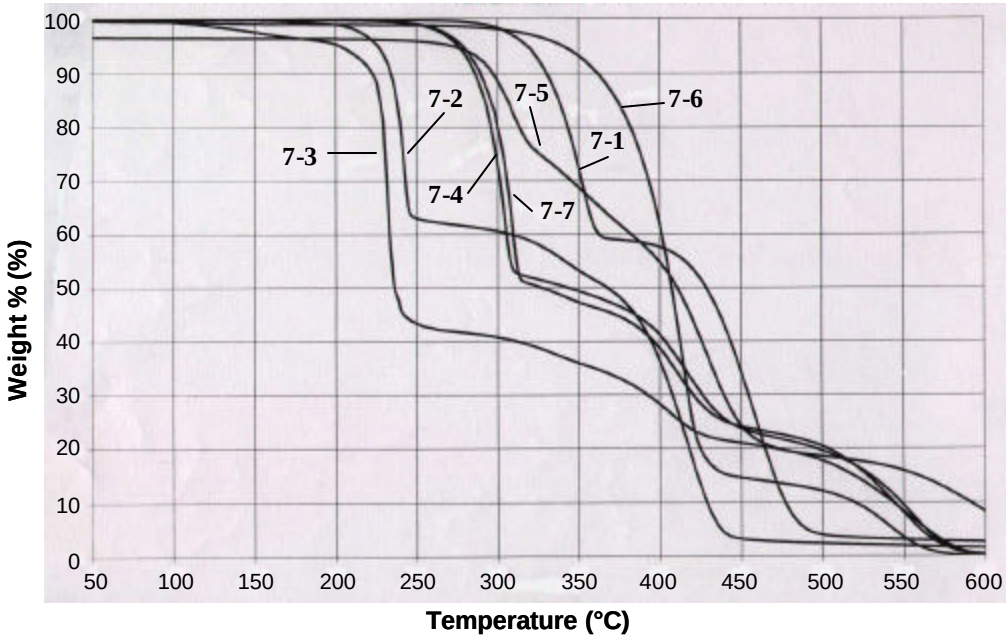

Figure 7.13: Thermogram of various carbonate polymers showing uncatalyzed thermal decomposition temperatures.

10 wt% of bis(4-*t*-butylphenyl)iodonium nonaflate (**7-8**), triphenylsulfonium nonaflate (**7-9**), or triphenylsulfonium heptaflate (**7-10**) and exposed with over 60 mJ/cm^2 of 248 nm radiation, no decrease in carbonyl absorbance was observed by infrared spectroscopy at 180°C (Figure 7.14, Table 7.1). However, when the

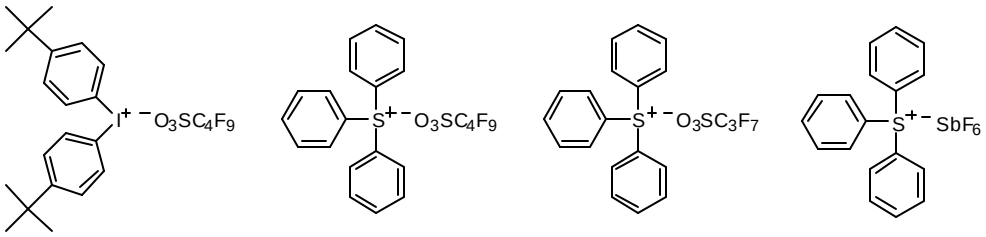

7-8 **7-9** **7-10** **7-11**

Figure 7.14: Structures of photoacid generators used to study the carbonate polymers shown in Figure 7.12.

same polymer was blended with triphenylsulfonium hexafluoroantimonate (**7-11**) and the mixture exposed, cleavage of the isopropyl group was immediately observed at the same temperature. These results suggest that perfluorobutanesulfonic acid and perfluoropropanesulfonic acid are not able to cleave the isopropyl carbonate group while hexafluoroantimonic acid cleaves the same group readily at 180°C. Since these fluorosulfonic acids are very strong, with pK_as that are less than -12, it is surprising that the isopropyl carbonate group is not cleaved. It is also surprising that antimonic acid cleaves this group while the others do not. These reactions take place in the solid phase and are therefore much different than those done in solution. More experiments need to be performed to understand these results, but for the current purpose we decided to look at other carbonates.

To increase the acid lability of the polycarbonate, more stable secondary and primary carbocations were examined. Polymer **7-2** was made because the carbocation formed could be stabilized by resonance into the aromatic ring, and polymer **7-3** was made because the secondary "norbornonium" cation could be

stabilized by Wagner-Meerwein shifts to relieve skeletal strain. As it turns out, all of the acids were able to cleave these two polymers at 180°C (Table 7.1). Unfortunately, neither of these polymers is thermally stable at 180°C, which precludes their use as a detector layer in our experiments. Polymers that could cleave to form less stable carbocations were next studied (**7-4** and **7-7**). Even though the carbocations that form from the cleavage of these groups are more stable than the isopropyl cation because of the extra sigma electron donation resulting from more alkyl groups, these carbocations are still less stable than the norbornonium cation and the benzyl cation. The thermal decomposition temperature of these two polymers are both similar, above 250°C. However, as shown in Table 7.1, both polymers were not cleaved using perfluorobutanesulfonic acid or perfluoropropanesulfonic acid at 180°C, but were cleaved with antimonic acid. Experiments were also performed on polymers **7-5** and **7-6**. The cation that forms resulting from the cleavage of **7-5** is stabilized by interaction with the higher energy electrons in the cyclopropyl C-C bonds. Although polymer **7-6** initially forms a primary neopentyl cation that initially cannot eliminate hydrogen to form an alkene, it may undergo a methyl shift and then eliminate, preserving the "chemical amplification" scheme that makes these detector layers so sensitive to the presence of acid. Polymer **7-5** is thermally stable up to 250°C, while polymer **7-6** is thermally stable up to 300°C. Both polymers were not cleaved with either perfluorobutanesulfonic acid or perfluoropropanesulfonic acid at 180°C. Polymer **7-5** is, however, slowly cleaved

with antimonic acid (50% deprotection in 10 min) while **7-6** is not (only 5% deprotection in 10 min).

Table 7.1: Data showing whether or not each polymer is cleaved with acid at 180°C.

Polymer	Thermally Stable (180°C)?	**7-8** BBI-109	**7-9** $Ph_3S^+ {}^-O_3SC_4F_9$	**7-10** $Ph_3S^+ {}^-SbF_6$	**7-11** $Ph_3S^+ {}^-O_3SC_3F_7$
7-1 PIPOCST	Yes	No	No	Yes	No
7-2 PAMBOCST	No	Yes	Yes	Yes	--- (Yes)
7-3 PISBOCST	No	Yes	Yes	Yes	--- (Yes)
7-4 P3POCST	Yes	No	No	Yes	No
7-5 PCPMOCST	Yes	No	No	Yes -- Slowly ~50% 10 min	No
7-6 PNPOCST	Yes	No	No	No ~5% 10 min	--- (No)
7-7 P3M2BOCST	Yes	--- (No)	No	Yes	No (10% total) Slow 5% 30 min

Of all the carbonate-protected polymers that were made, only **7-2** and **7-3** are cleaved with perfluorobutanesulfonic acid. Unfortunately, neither of these two polymers is thermally stable above 180°C, so other classes of polymers were investigated for detector layer applications. Ester-protected polymers such as those shown in Figure 7.15 were synthesized and evaluated. Polymers **7-12** and **7-13** start to decompose thermally at 180°C while polymer **7-14** is stable above 200°C (Figure 7.16). The rules for stability follow those seen with the polycarbonates earlier. That is, those polymers that cleave to form more stable carbocations are less stable thermally. Polymer **7-14** at first seemed like a good

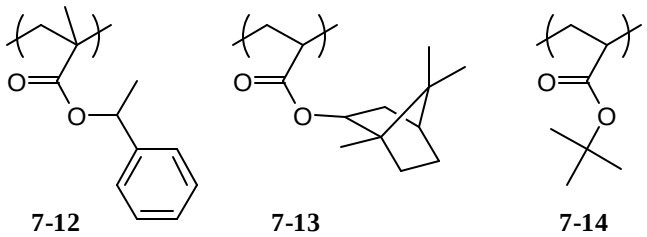

Figure 7.15: Structures of several polyesters screened as a detector layer for sandwich experiments.

candidate because its decomposition temperature is dramatically decreased in the presence of acid (Figure 7.16). However, these ester-protected polymers were found to be poor detector layers because the carbonyl peak of the protected ester is difficult to distinguish from the carbonyl peak of the unprotected acid.

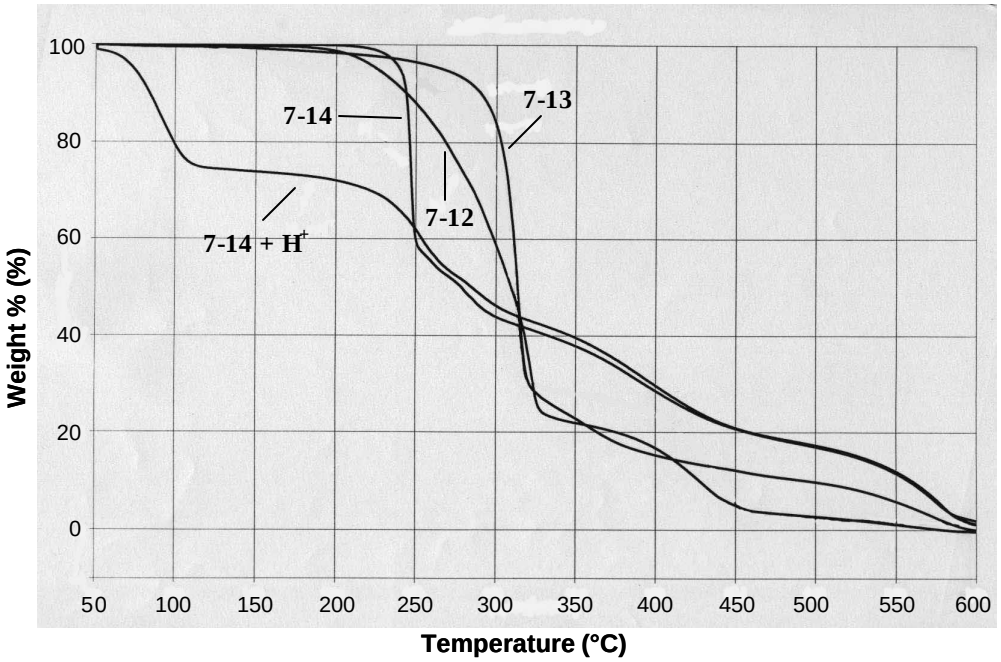

Figure 7.16: Thermogram of various ester polymers showing uncatalyzed and catalyzed thermal decomposition temperatures.

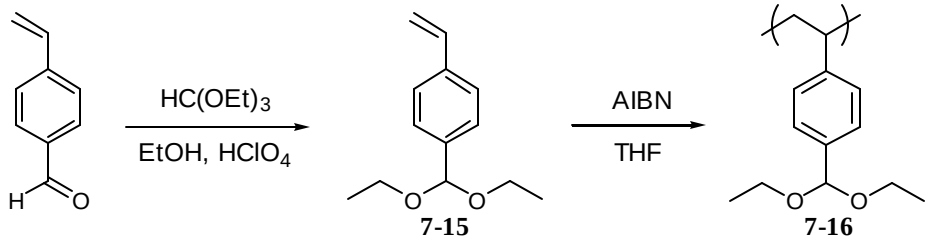

7-15 **7-16**

Figure 7.17: Synthesis of an acetal polymer for use as a detector layer in sandwich experiments.

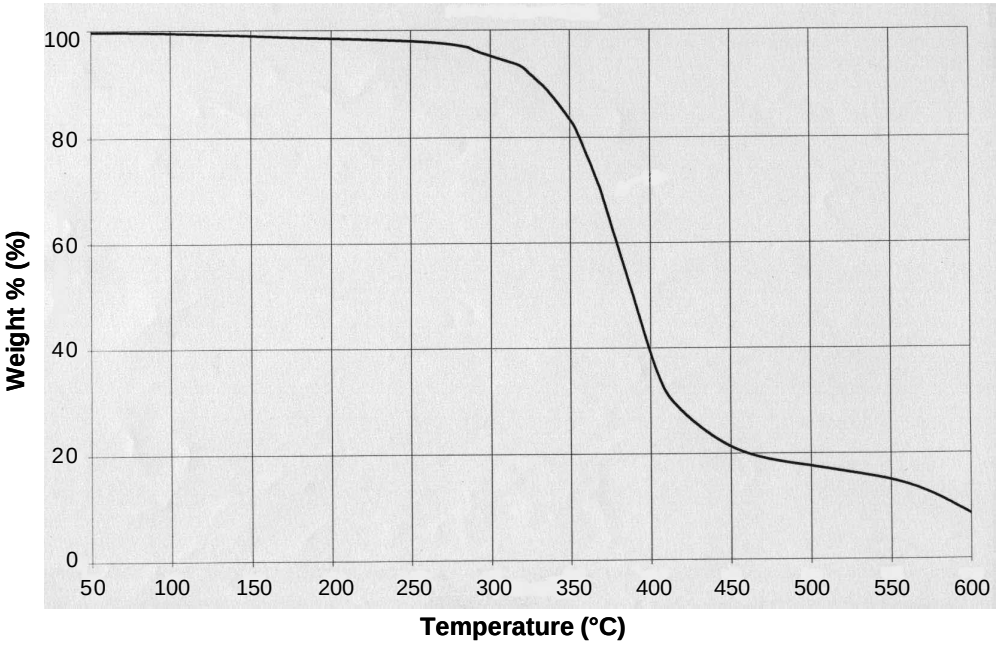

Figure 7.18: Thermogram of polymer **7-16** showing mass loss before 180°C.

For this reason, the ester polymers were abandoned and an acetal-protected polymer was next investigated (Figure 7.17). The hydrolysis of polymer **7-16** back to the starting aldehyde in the presence of acid may be monitored by infrared spectroscopy. Instead of monitoring the decrease of

absorbance of the carbonyl peak, as has been accomplished in the previous polymers, the increase in absorbance of the carbonyl peak was monitored. Unfortunately, at 180°C, there is not enough water present in the surrounding environment to allow hydrolysis. In addition, the polymer already starts to lose mass at 180°C (Figure 7.18). Therefore, this polymer was abandoned as well.

A suitable detector layer was found with polymer **7-18** (Figure 7.19). The pinacol rearrangement is a well-known example of an intramolecular cationic rearrangement. Under acidic conditions, a vicinal diol is converted to an aldehyde

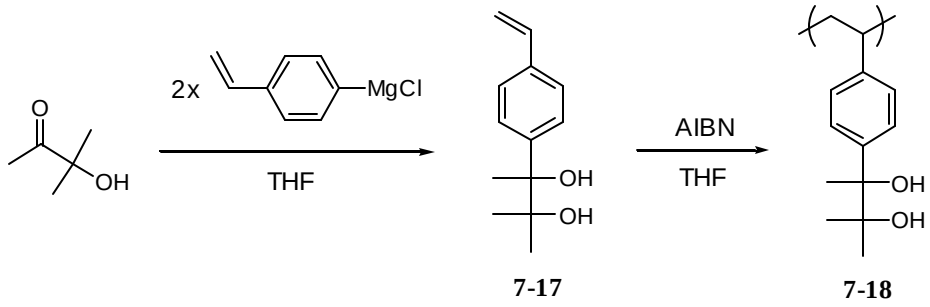

7-17 **7-18**

Figure 7.19: Synthesis of a polymer that can undergo the pinacol rearrangement in the presence of an acid catalyst.

or ketone. In this mechanism (Figure 7.20), water is not needed as in the case of the acid-catalyzed hydrolysis of the acetal polymer shown earlier. Water is instead eliminated, followed by a methyl shift. The carbocation closest to the aromatic ring forms preferentially to the other possible carboncation because it is more stable due resonance stabilization. Polymer **7-18** is thermally stable above 200°C (Figure 7.21), but undergoes the pinacol rearrangement at much lower temperatures when acid is present. The increase of absorbance of the carbonyl peak can be easily monitored in the infrared.

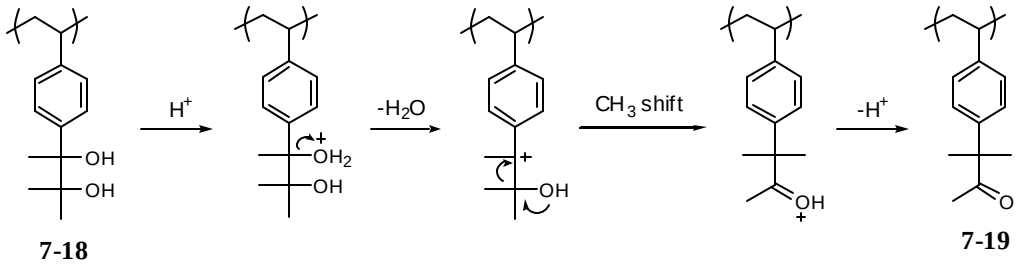

Figure 7.20: The formation of a ketone from a vicinal diol through the acid-catalyzed pinacol rearrangement.

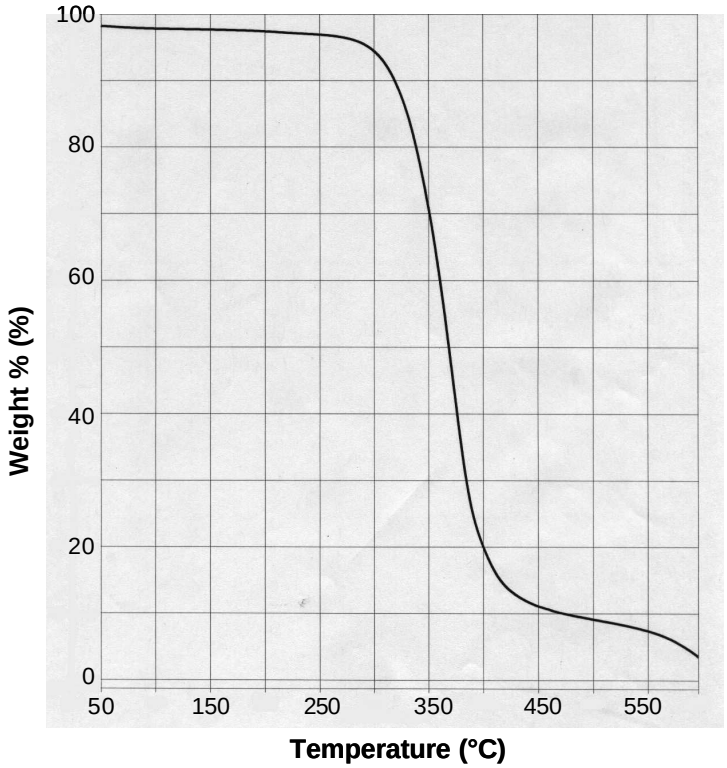

Figure 7.21: Thermogram of polymer **7-18** showing thermal decomposition above 200°C.

Polymer **7-18** is a good candidate for the infrared sandwich experiments, but needed to be modified in some way because the polymer is very difficult to float onto water in the floating process used to make the trilayer stacks (Figure 6.8). The film is brittle and cracks into many small pieces when it is floated onto water. In addition, it also possesses the undesirable property of tenacious adhesion to the glass substrate used to float polymers into water. Poly(4-hydroxystyrene) behaves in a similar way when it is floated onto water. However, this polymer is coated over the first acid reservoir layer by spinning from an alcohol solvent, so it does not need to be floated. Polymer **7-18** needs to be floated because a suitable solvent cannot be found that dissolves this polymer and not the underlying PHOST layer. Alcohol solvents dissolve the polymer, but would also dissolve the PHOST layer underneath. Considerable effort was spent on designing copolymer systems that have mechanical properties consistent with use in the floating process for making the trilayer stacks. The easiest approach is to copolymerize monomer **7-17** with another monomer that changes the properties of the final polymer in a positive way for floating. Another approach is to make a different polymer by another method and hope for favorable mechanical properties. To this end, several polymers were made and tested (Figure 7.22).

Copolymers **7-20** and **7-21** were made in an attempt to alleviate the tenacious adhesion to glass seen with polymer **7-18**. Both polymers are thermally stable up to 200°C. By incorporating more hydrophobic comonomers, it was hoped that the new polymers would better lift off the glass substrate.

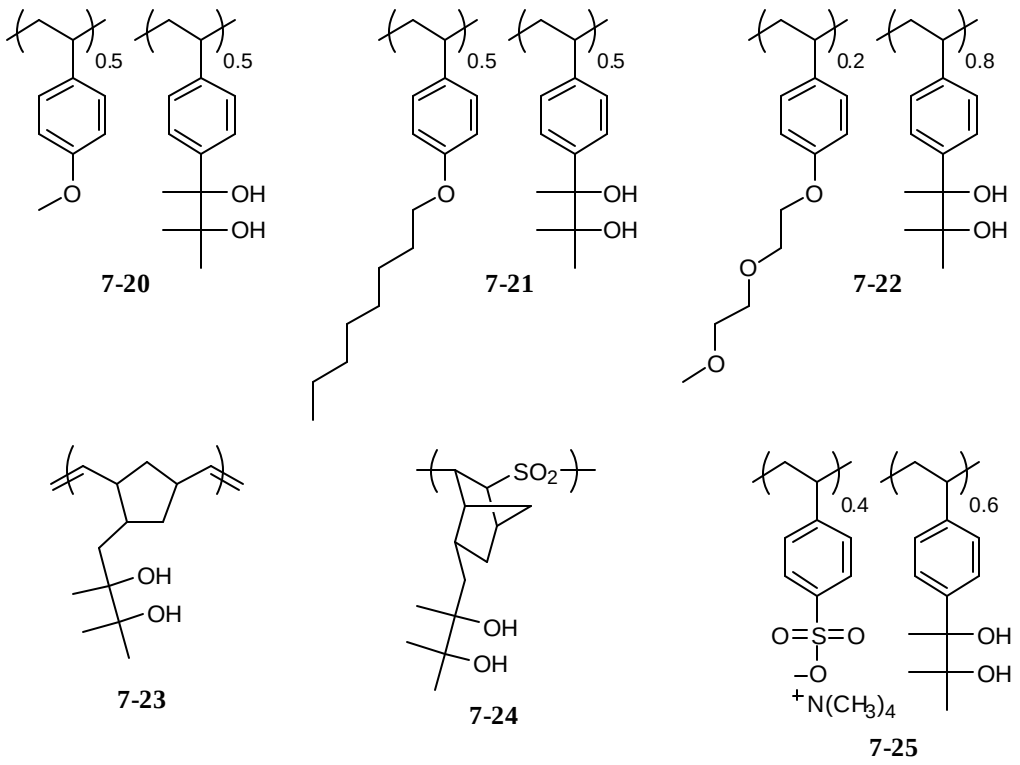

Figure 7.22: Other polymers synthesized and tested for the infrared sandwich experiments.

Unfortunately this was not the case, as the polymers did not peel off the glass substrate easily, and still cracked into several pieces when it eventually did release from the substrate. Polymer **7-22** was made next in an attempt to go the opposite direction – by making a more hydrophilic copolymer. This polymer is also stable up to 200°C, but did not peel easily from the glass substrate either. Polymer **7-23**, made from the ring-opening metathesis polymerization (ROMP) of the corresponding norbornene monomer, did not lift off the glass substrate. The norbornene monomer was instead radically polymerized with sulfur dioxide to

yield copolymer **7-24**. When this copolymer was evaluated at 180°C without PAG, however, the pinacol rearrangement was observed and one molecule of water was lost. After some investigation, it was concluded that residual acid from the polymerization involving SO_2 was the cause of the rearrangement. The polymer was dissolved in an organic solvent, washed with aqueous base, and isolated. Unfortunately, even in the absence of acid, the polymer was not thermally stable up to 180°C. Attention was therefore given to a water-soluble polymer (**7-25**) that could be spun from water and coated over the underlying PHOST layer. Water will not dissolve the PHOST layer, so this polymer was a good candidate. Much to our dismay, the polymer decomposed thermally even before reaching 180°C.

The mechanical properties of polymers are often improved by increasing their molecular weights. Since polymer **7-18** broke into pieces when floated onto water, a higher molecular weight polymer may not crack as easily. Monomer **7-17** was therefore polymerized with TEMPO (2,2,6,6-tetramethyl-1-piperidinyloxy) as the free radical initiator instead of AIBN. A much higher molecular weight polymer (Mw = 180,000 instead of Mw = 12,000) was obtained due to the "living" nature of the polymerization. The polymer was coated onto a glass substrate and attempts were made to float it into water. The polymer did not release from the substrate at all.

A solution to the floating problem came when a sodium chloride salt plate was used instead of the glass substrate. The polymer is first spun onto a polished NaCl disc, baked to remove residual solvent, and then the plate is submerged in a

water bath (Figure 7.23). As the salt plate starts to dissolve in water, the polymer film eventually lifts off and floats in the water above the plate. Complete dissolution of the salt plate was not necessary because the rapid dissolution of NaCl at the polymer/plate interface was enough to cause the polymer to lift off. Although this is an expensive solution, the plate can be removed from the water bath and could be polished for reuse.

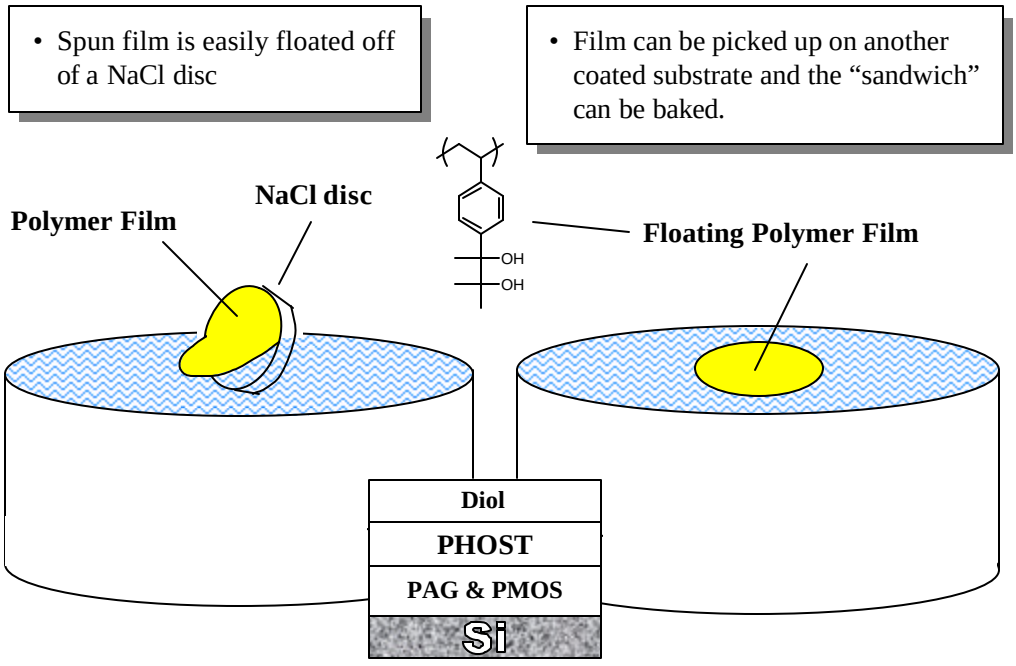

Figure 7.23: The use of a sodium chloride salt disc to float and lift the diol onto a sandwich stack for infrared experiments.

With this new technique in hand, diffusion measurements could be initiated to study the transport of acid through PHOST above the polymer's T_g. Several stacks with varying thicknesses of PHOST were made and monitored at

180°C using infrared spectroscopy. Diffusion of photogenerated acid through PHOST above its Tg is observed. As shown in Figure 7.24, the plot of thickness squared versus time shows a straight line with a slope of 1 x 10^{-4} $\mu m^2/s$. This diffusion coefficient is on the same order of magnitude as that of PEMA above its T_g. Since a straight line is obtained in this plot, this linear relationship between distance squared and time illustrates a diffusion mechanism based on concentration-dependent diffusion (Fickian diffusion). Figure 7.25 shows that diffusion is much more facile through PHOST when experiments are run above or near the polymer's T_g. Below this region, diffusion is so slow that it is not observed on the time scale of the experiment.

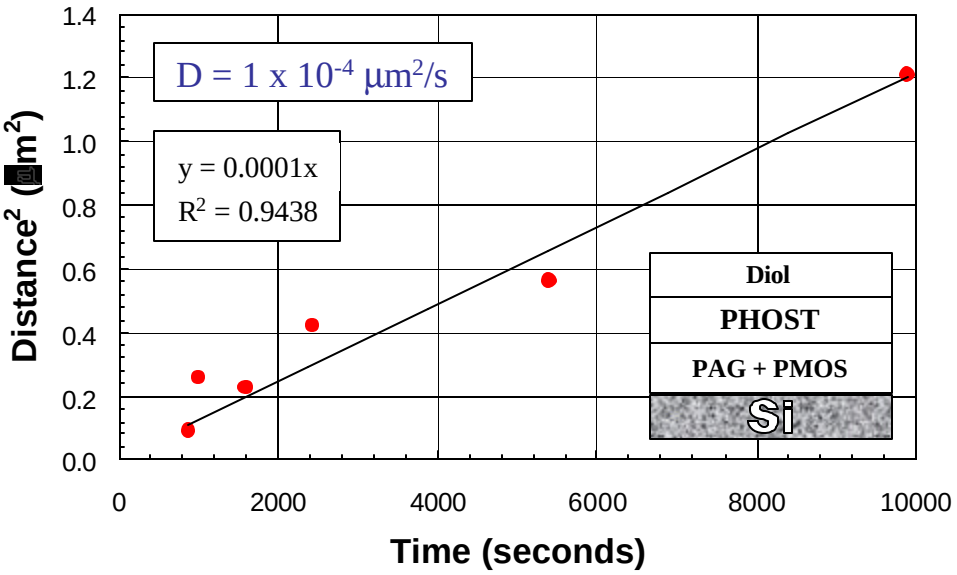

Figure 7.24: Plot of distance squared versus time for diffusion of perfluorobutanesulfonic acid through PHOST at 180°C.

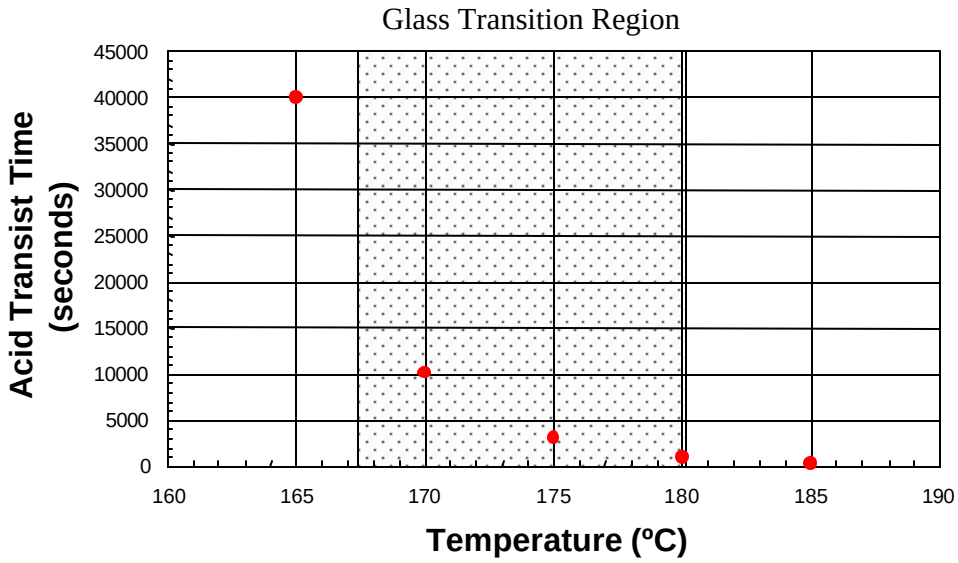

Figure 7.25: Acid diffusion through PHOST is observed at temperatures near or above the polymer's T_g.

CONCLUSIONS AND FUTURE WORK

These experiments bring to light several important observations and conclusions. Diffusion of photogenerated acid through PHOST at typical post-exposure baking temperatures (120-150°C) is too low to account for the observed linewidth spread. These temperatures are 30-60°C below the glass transition temperature of PHOST. We have shown that diffusion through PHOST more than 15°C below T_g is negligible at best. Above the T_g, however, diffusion of acid is observed. We have shown that diffusion in both PHOST and PEMA follows Fickian behavior above T_g. Although the model case of pure PHOST is informative, it is too simple to capture what transpires in actual resist systems, even though a typical 248 nm resist (APEX-E) is composed of a hydroxystyrene

unit as a main component. In an actual resist system such as APEX-E, diffusion is coupled with the deprotection reaction kinetics, and a better model must be invoked to explain the acid transport mechanism. Such a model is the reaction front propagation model. This model not only explains the mechanism of acid transport, but also predicts the decreasing rate of diffusion due to lost of acid molecules.

In order to fully understand acid diffusion through resist polymers, more polymers that are closer in structure to actual resist systems must be studied. The bilayer experiments should be performed on APEX-E and the extent of acid diffusion and deprotection reaction should be measured using infrared spectroscopy. The type of photoacid generator, amount of exposure (dose), and post-exposure baking temperature and time can be varied. Since diffusion is not decoupled from the reaction kinetics, diffusion coefficient numbers obtained from these studies may be entered in simulation models that can predict actual real-world processes.

CHAPTER 8: *DIFFUSION STUDIES WITH POLYMERIC PAGS*

In the last two chapters the diffusion of small acid molecules through both reactive and unreactive polymer films was discussed. The acid molecules were allowed to diffuse freely throughout the polymer matrix. In an unreactive polymer matrix, the free diffusion of acid followed Fickian behavior above the T_g of the polymer. In a reactive polymer matrix, diffusion is coupled with the reaction kinetics and significantly affects the reaction rates. The deprotection reaction rate of a chemically-amplified resist system is reaction-rate limited when acids with very large diffusion coefficients (i.e., very mobile acids) are used. On the other hand, the deprotection reaction rate is diffusion-limited when acids with low diffusion coefficients are used. It would be very interesting to study the extent of reaction in a catalytic, non-diffusing system. One way to make this possible is to bind the photoacids to a polymer backbone to limit its diffusion. This chapter describes our synthetic efforts to make polymer-bound photoacid generators. With these polymers in hand, experiments can be done to answer several important questions. How far can the proton travel away from its counteranion if that anion is bound to a polymer backbone? If diffusion is essentially zero, how does this change the deprotection reaction kinetics? What would be the new catalytic chain length of polymer-bound photoacids?

In addition to shedding light on some of these questions, the polymer-bound PAGs may be an important component in the design of future resists that do not outgas volatile byproducts during exposure. Current photoresists are

purposely designed to release volatile products in the deprotection reaction, but some of these byproducts are problematic because they tend to contaminate the expensive lens system in the stepper. It has been shown that a major component of outgassed products originates from the photodecomposition of the PAGs used in resist formulations.[108] By covalently linking the volatile component of the PAG (aromatic ring) to a polymer system, the amount of outgased product should be minimized.

Two polymeric PAGs and one monomeric PAG were made for the acid diffusion studies. Their structures are shown in Figure 8.1. All three produce very acidic molecules upon exposure. Polymer **8-1** was designed so that the anion component of the acid is covalently bound to the styrene polymer backbone. In

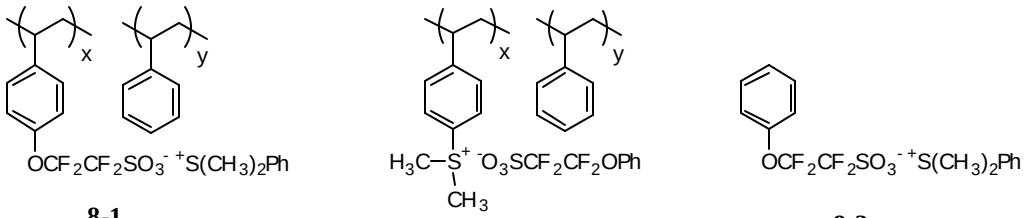

Figure 8.1: Structures of two PAG polymers and one PAG molecule synthesized for acid diffusion studies.

this configuration, the acidic proton would most likely not diffuse too far away from its counteranion. Polymer **8-2** was made as a control polymer to compare its results with the first polymer. In this case, the cation component of the PAG is bound to a polymer backbone. Irradiation causes the production of $PhOCF_2CF_2SO_3H$ acid, which is an unbound analogue of the acid produced from

polymer **8-1**. Polymer **8-2** is also the most likely candidate for a PAG with minimum outgased products because irradiation would cleave the aromatic-sulfur bond. Since the benzene ring is bound to the polymer backbone, it will not evaporate into the atmosphere. Compound **8-3** was made for use in more control experiments to determine the extent of diffusion of this type of acid when it is not bound to any polymer structure.

ANIONIC POLYMERIC PAG (8-1)

Much of the elegant synthetic work up to the lithium salt, **8-9**, has been described previously by Feiring *et al.* in two publications.[160,161] Polymers with pendant fluoroalkylsulfonate groups have been of interest due to their current and potential application as membranes for chloroalkali cells, batteries and fuel cells, and strong solid acid catalysts.[162,163] We are interested in these perfluoroalkylsulfonate monomers because they provide a route to the polymeric PAGs shown in Figure 8.1. The lithium salt that has been reported was made in good yield (Figure 8.2). Reaction of the potassium salt of 4-bromophenol (**8-4**) with 1,2-dibromotetrafluoroethylene affords the ether **8-5**.[164,165] This ether is transformed to the sulfinate salt (**8-6**) in high yield on reaction with sodium dithionite and sodium bicarbonate in aqueous acetonitrile. Oxidation with chlorine gas in water provides the sulfonyl chloride **8-7**, which was converted to

---

160 Feiring, A. E.; Wonchoba, E. R. *J. Fluor. Chem.* **2000**, *105*, 129-135.

161 Feiring, A. E.; Choi, S. K.; Doyle, M.; Wonchoba, E. R. *Macromolecules* **2000**, *33*, 9262-9271.

162 Meyer, W. H. *Adv. Mater. (Weinheim, Ger.)* **1998**, *10*, 439-448.

163 Savadogo, O. *J. New Mater. Electrochem. Syst.* **1998**, *1*, 47-66.

164 Rico, I.; Wakselman, C. *J. Fluor. Chem.* **1982**, *20*, 759.

165 Babb, D. A.; Ezzell, B. R.; Clement, K. S.; Richey, W. F.; Kennedy, A. P. *J. Polym. Sci., Part A: Polym. Chem.* **1993**, *31*, 3465.

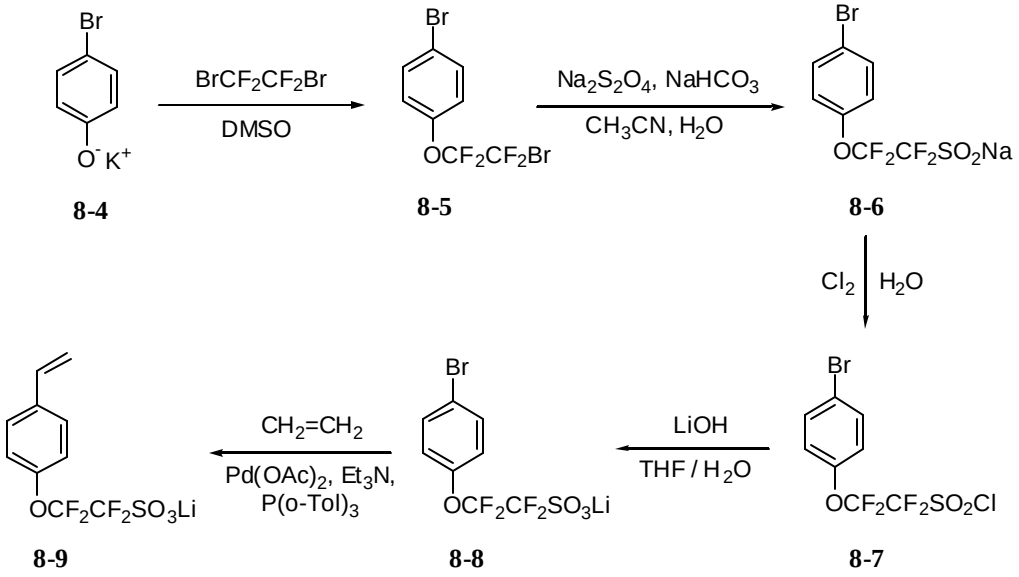

Figure 8.2: Synthesis of a fluorinated lithium sulfonate salt using known reactions and readily-available starting material.

the lithium sulfonate **8-8** by reaction with lithium hydroxide in aqueous THF. The styrene (**8-9**) is obtained from the corresponding lithium sulfonate and ethylene under typical Heck reaction conditions in the presence of a Pd catalyst.

Many attempts were made to convert the lithium salt **8-9** to the desired, photoactive sulfonium salt **8-12**. The synthesis of **8-12** was more difficult than anticipated due to problems with metathesis and unwanted polymerization, as described in the next two sections. This monomer is desired because it can be copolymerized with a variety of other monomers to form copolymers possessing a pendant photoactive group that produces strong acid upon irradiation. The next two sub-sections will describe our efforts to make this salt.

Pathway A

Starting with the previously synthesized styrene lithium salt (**8-9**), the pathway to the desired PAG monomer (**8-12**) is difficult for several reasons (Figure 8.3). Slowly passing the lithium compound down a strongly acidic ion exchange column such as Aldrich's Amberlite IR-120(plus) ion exchange resin using water as the eluent did not provide the desired sulfonic acid hydrate (**8-10**). The desired product could not be isolated because the styrene unit is polymerized cationically by the strongly acidic sulfonic acid. This is not surprising, since the product (**8-10**) should have a similar acidity to triflic acid, which is known to polymerize styrenes. Therefore, the pathway to the silver salt (**8-11**) and then to the desired product (**8-12**) could not be realized. The starting lithium salt was

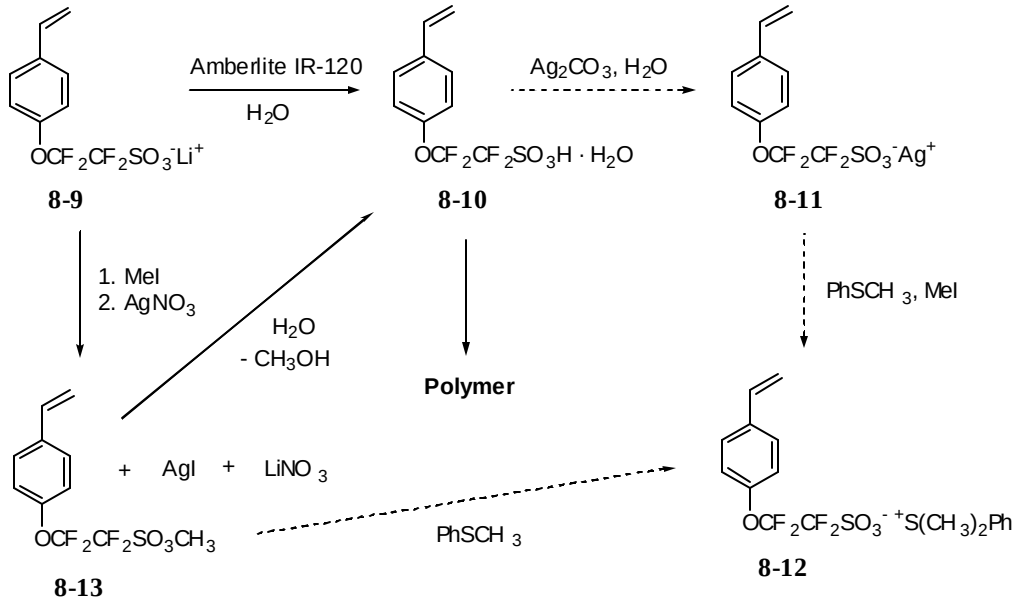

Figure 8.3: Attempted synthesis of the desired monomer from the starting fluorinated lithium sulfonate salt.

also reacted with iodomethane and silver nitrate in hope of obtaining the methyl sulfonate (**8-13**), which, when reacted with thioanisole should lead to the desired product. However, the methyl sulfonate is exceptionally water sensitive, and easily converts to the sulfonic acid form that can self-catalyze the production of undesirable polymer. The extent of methyl sulfonate formation was not investigated when iodomethane and silver nitrate were added to the lithium salt. Precipitation of yellow silver iodide is apparent in the reaction, but it was not clear if starting material (the lithium salt) was formed in addition to methyl nitrate or if the methyl sulfonate was formed with lithium nitrate. In any case, the methyl sulfonate is too hygroscopic to isolate. When thioanisole was added *in situ* to this reaction, the desired product could not be isolated.

Pathway B

This pathway was explored because it was thought that the methyl sulfonate **8-14** could be isolated and purified in good yield (Figure 8.4). Therefore, the lithium sulfonate **8-8** was reacted with dimethylsulfonate, but the methylated product was not obtained because it was difficult to isolate the product from excess dimethylsulfonate and lithium salt byproducts. The boiling points of **8-14** and dimethylsulfonate seemed to be close enough to render distillation difficult. In addition, product may not have been obtained because the product is a more powerful alkylating agent than dimethylsulfonate. Excess dimethylsulfonate was used, but this may not have helped at all.

The sulfonyl chloride, **8-7**, was reacted with methanol in sodium bicarbonate, the product could not be isolated, most likely due to water

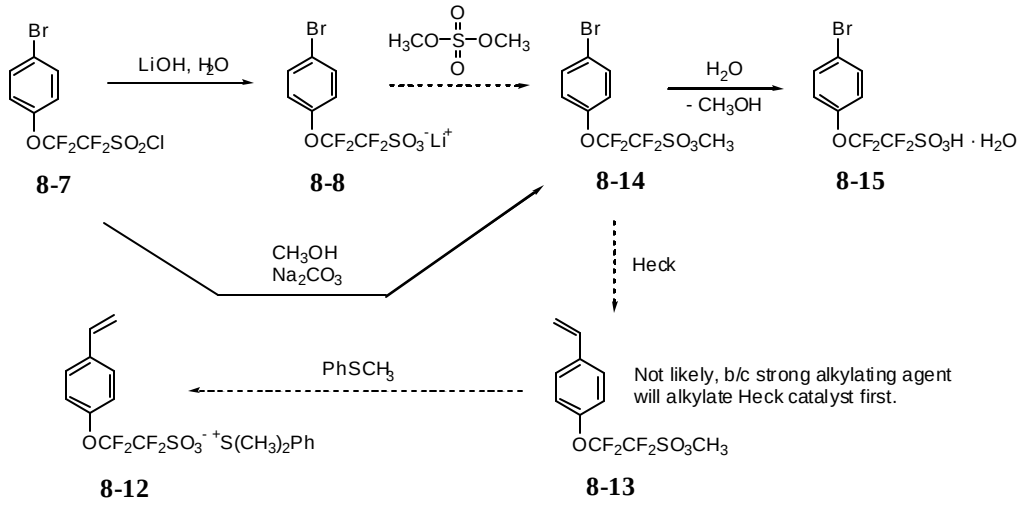

Figure 8.4: Another attempted synthesis of the desired monomer from available compounds.

contamination which spontaneously converts the product to the sulfonic acid, **8-15**. No methyl resonances were observed in the ^{1}H-NMR spectrum of the crude product. The same reaction was performed using triethylamine instead of sodium bicarbonate as the base, but a sulfinic acid or sulfinate salt (**8-6**) was formed in greater yield, possibly due to some electron transfer chemistry. This phenomenon is documented in the paper published by Feiring *et al.*[160] A control experiment demonstrated that triethylamine alone rapidly reduces **8-7** to **8-6**. Interestingly, the sulfonyl fluoride analogue of **8-7** is not reduced by triethylamine, which indicates a major difference in chemistry of perfluoroalkylsulfonyl chlorides and fluorides. If the methyl sulfonate **8-14** could be isolated and purified in good yield, it was thought that a Heck reaction, followed by addition of thioanisole, would provide the final product. However, the methyl sulfonate, a very powerful

alkylating agent, would most likely alkylate the Heck catalyst before its reaction with the bromide, killing the catalyst.

Successful Pathway

Since the synthesis of the monomeric PAG, **8-12**, was not realized, the only other choice was to polymerize the lithium salt (**8-9**) and then perform metathesis reactions on the polymer (Figure 8.5). This pathway was avoided in

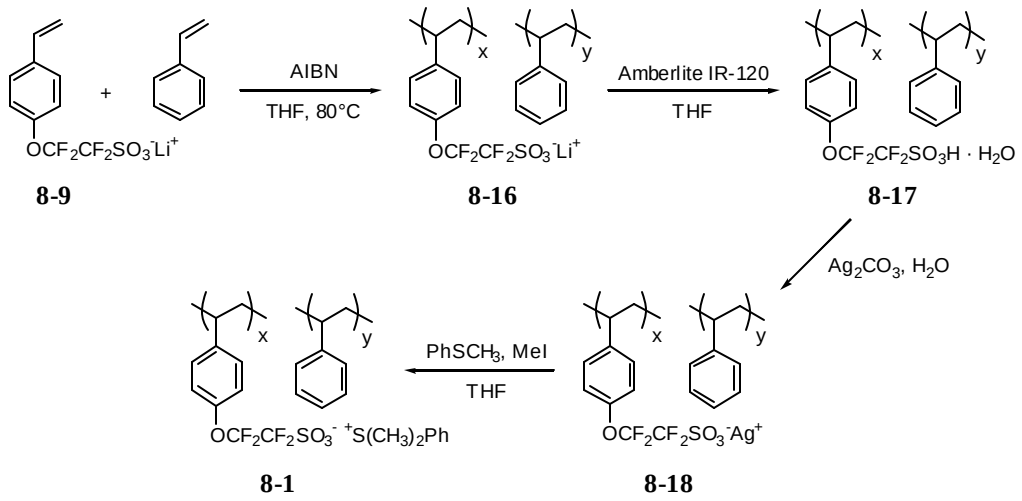

8-9 **8-16** **8-17**

8-1 **8-18**

Figure 8.5: Successful synthesis of **8-1** by performing metathesis on the polymer.

the early stages because it was thought that metathesis on a polymer structure would be difficult at best, and the extent of reaction would be difficult to determine. The lithium salt (**8-9**) was therefore polymerized radically with styrene in a 1 to 9 feed ratio. The polymer was precipitated into hexanes and washed several times with water to remove unreacted lithium monomer. This polymer was then passed through an acidic ion exchange column and immediately

converted to the silver salt by stirring with silver carbonate. The resulting polymer was dissolved in THF, and converted to the final product by addition of thioanisole and iodomethane. It can only be inferred, at this point, the extent of the metathesis reaction because it is difficult to determine by NMR (^{1}H and ^{19}F) how much silver is still attached to the polymer. Elemental analysis of the polymer was performed to determine the amount, if any, of silver that is left. The reported amount was < 0.11% of silver in the polymer.

By comparing the integration of the fluorine resonances from the polymer to the fluorine resonances of a known amount of additive (AgO_2CCF_3), it was calculated that x = 10 and y = 90 in structure **8-1**. This result supports the previous result from elemental analysis showing that most, if not all, of the silver had reacted because the starting lithium salt polymer most likely had a ratio of 1 to 9 also, due to the feed ratio of the polymerization, which was 1 to 9. The calculation of the copolymer ratio, when compared to the internal standard AgO_2CCF_3, is as follows:

Amount of AgO_2CCF_3 added: 8.5 mg
Amount of Polymer added: 8.9 mg

Molecular weight of AgO_2CCF_3: 220.88 g/mol
Molecular weight of Monomer X: 439.31 g/mol
Molecular weight of Monomer Y: 104 g/mol

Ratio of AgO_2CCF_3 peak to Polymer CF_2 peak: 6.14

Therefore 8.5 mg / 220.88 g/mol = 38.5 µmol AgO_2CCF_3
38.5 µmol / 6.14 = 6.27 µmol Monomer X
0.00000627 mol * 439.31 g/mol = 2.75 mg Monomer X
8.9 mg Polymer – 2.75 mg Monomer X = 6.15 mg Monomer Y
0.00615 g Monomer Y / 104 g/mol = 59.1 µmol Monomer Y

Finally, 6.27 mmol Monomer X / (6.27 mmol Monomer X + 59.1 mmol Monomer Y) = 9.6% Monomer X, so Monomer Y = 100% - 9.6% = 90.4%.

CATIONIC POLYMERIC PAG (8-2)

The cationic version of the polymeric PAG was much easier to make, as outlined in Figure 8.6. In the beginning, the sulfonyl chloride, **8-22**, was reacted

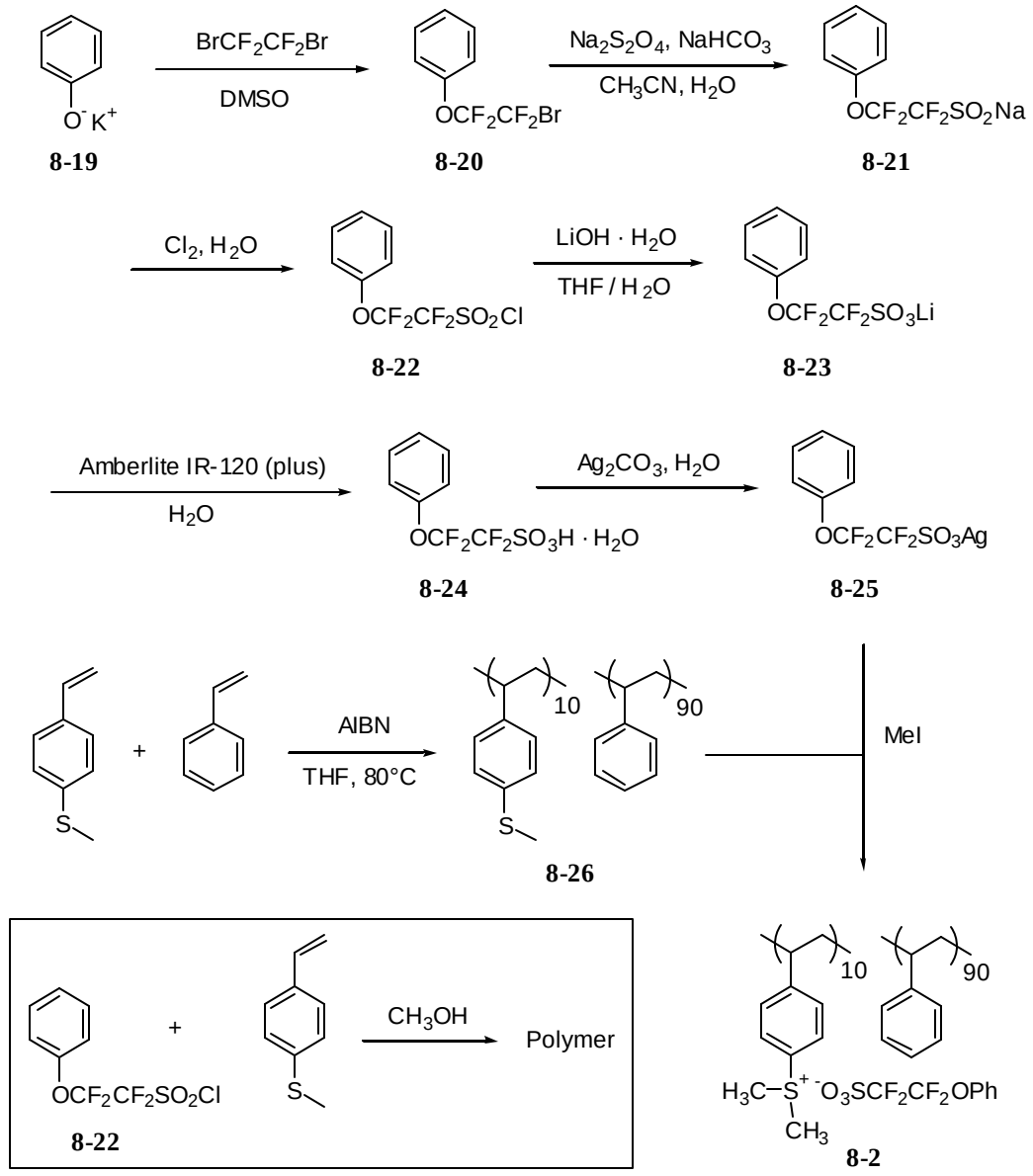

Figure 8.6: Synthesis of **8-2** by performing metathesis on the polymer.

with 4-methylthiostyrene in methanol. However, this did not yield the desired monomer. Instead, a polymer was obtained because the liberation of HCl as byproduct caused polymerization of the styrene unit. Sodium methoxide was later used instead of methanol to form sodium chloride as a much more inert byproduct, but the desired monomer still could not be obtained because of problems in crystallization of the product. Finally, the synthesis of the monomer was abandoned and metathesis was performed on the polymer backbone instead.

The lithium salt, **8-23**, was made in the same way as **8-8**. Compound **8-23** was converted to the acid form (**8-24**) by elution through an acidic ion exchange column. Reaction with silver carbonate provided the silver salt (**8-25**). Several copolymers with varying comonomer ratios were made using 4-methylthiostyrene and styrene. The polymer shown (Figure 8.6), in which x = 10 and y = 90 (confirmed by ^{1}H-NMR because the S-CH_3 peak can be integrated against the aromatic peaks), was reacted with the silver salt (**8-25**) and iodomethane to yield the desired polymer (**8-2**). ^{1}H-NMR analysis of the final polymer showed that all of the S-CH_3 resonances had shifted further downfield to form $^{+}$S-CH_3 resconances. Therefore, it was concluded that all of the methyl sulfide groups on the polymer backbone was converted to sulfonium groups. The 1 to 9 ratio, therefore, did not change and should be the same as the starting polymer (**8-26**). Elemental analysis of polymer **8-2** showed that there was not much elemental silver (< 0.05%) left in the polymer.

UNBOUND PAG (8-3)

The synthesis of compound **8-3** was necessary to compare its diffusion results to that of the polymeric versions (Figure 8.7). Purification of this compound was not trivial, however. When the silver salt, **8-25**, was reacted with thioanisole and iodomethane in acetonitrile, the formation of silver iodide was apparent due to the yellow precipitate that formed. After filtering out this yellow salt, the acetonitrile solution was concentrated to half its original volume and precipitated into hexanes. However, the desired compound does not form crystals but oils out of solution. Precipitation of the acetonitrile solution into diethyl ether results in the formation of very fine white powder that cannot be filtered because the powder passes straight through the filter paper. Attempts to recrystallize the compound from isopropanol was unsuccessful, but when recrystallized from a solution of acetonitrile and diethyl ether, white crystals were obtained.

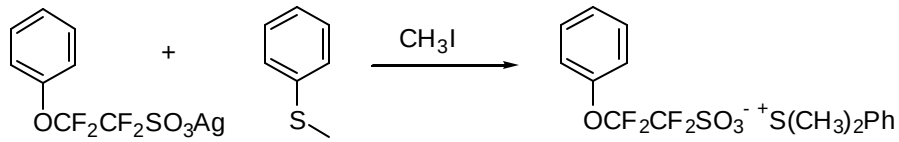

8-25 **8-3**

Figure 8.7: Synthesis of an unbound PAG that is similar to the polymeric versions.

INITIAL DIFFUSION STUDIES WITH POLYMERIC PAGS

Preliminary experiments using **8-1**, **8-2**, and **8-3** in our sandwich experiments showed interesting results. When each was blended in a 1:1 mass ratio with PTBOCST, coated onto a silicon wafer, exposed, and monitored by

infrared spectroscopy, the plot shown in Figure 8.8 was obtained. Compound **8-3** is the control because the PAG is unbound and should behave in a similar manner to other unbound PAGs used in manufacturing. The polymeric PAG with the cationic component bound to the polymer backbone (**8-2**) shows a larger diffusion range than that of the polymeric PAG with the anionic component bound to the polymer backbone (**8-1**). Assuming that the amount of acid generated is the same in each case because the dose of 5.9 mW for 120 sec (708 mJ/cm^2, flood exposed) and amount of PAG in the copolymer is the same, the results are expected. The acid in which the weak conjugate base is bound to the polymer backbone would not be expected to diffuse much, if at all. This is shown in the figure, where the acid path length is much lower.

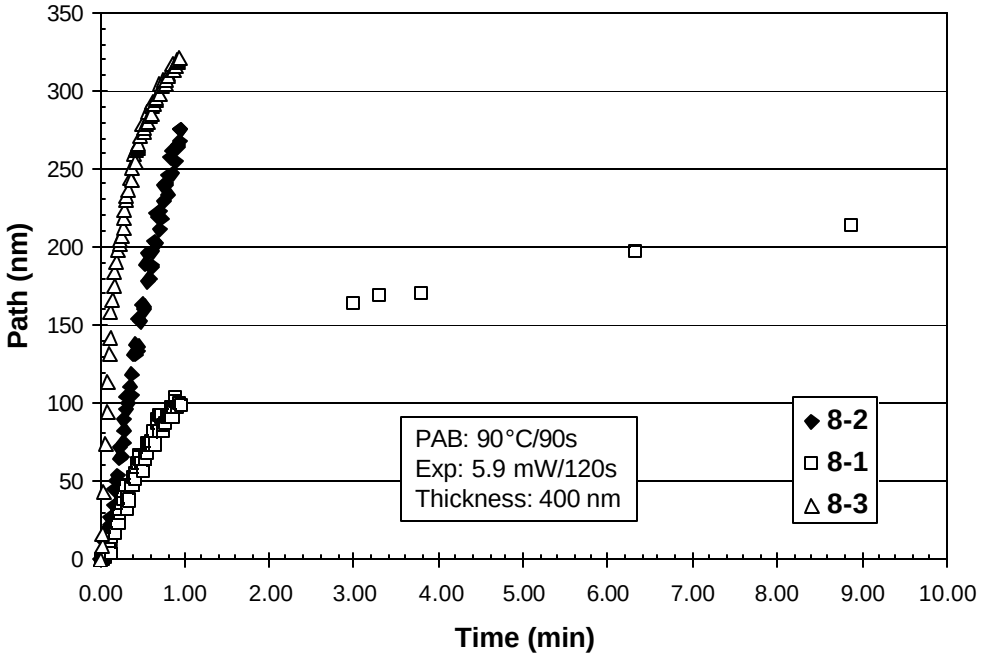

Figure 8.8: Diffusion range of bound and unbound PAGs in blends with PTBOCST at 90°C.

In another set of experiments, bilayer stacks, instead of the blended stacks shown earlier, were made to test acid diffusion length. The bottom layer consisted of either polymeric PAG **8-1** or **8-2** that was coated by spinning from diglyme onto the silicon wafer. A thin layer of PTBOCST was floated onto the first layer. These bilayer stacks were post-apply baked, exposed, and monitored under the infrared at 90°C. Figure 8.9 and Figure 8.10 shows the curves that were

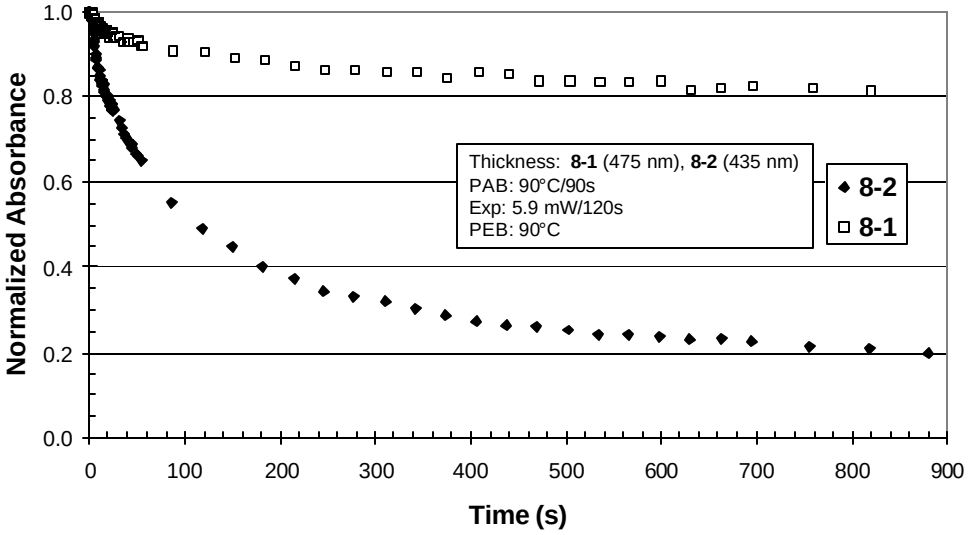

Figure 8.9: Absorbance curves for two polymeric PAGs tested in a bilayer stack experiment.

obtained. As expected, the polymer-bound PAG that has the weak conjugate base of the photogenerated acid bound to the polymer backbone has a much lower diffusion length. The absorbance of the detector layer only decreased down to about 80%. On the other hand, the absorbance of the detector layer in the other stack decreased to 20%. This result is expected because the photogenerated acid is not bound to the polymer backbone. Only the photoactive component of the

PAG is bound to the polymer structure, which makes little impact on the diffusion length of the photogenerated acid.

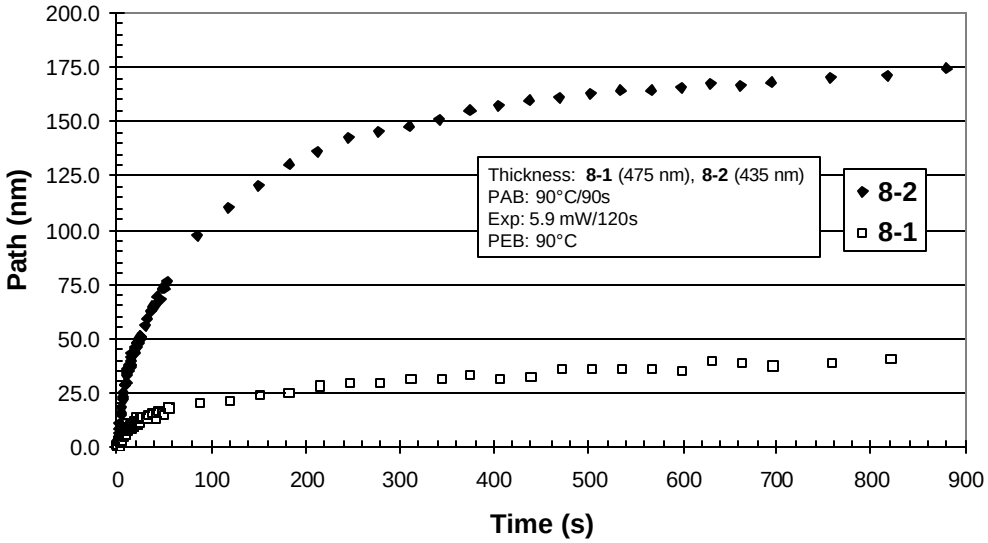

Figure 8.10: Path length curves for two polymeric PAGs tested in a bilayer stack experiment.

The initial results of these experiments, especially those experiments using the polymer-bound PAG **8-1**, imply that the diffusion of photogenerated acid is limited if the anion component is bound to a polymer backbone. If we assume that the diffusion path length is zero or very close to zero for the anion, then that would imply that the proton migrates at most 40 nm from the anion to cause the catalytic deprotection of TBOC groups on PTBOCST (Figure 8.10). This is a very difficult number to believe, and calculations show that the Coulombic interactions are very unfavorable due to this large charge separation.[129] The large path length shown by both polymeric PAGs **8-1** and **8-2** are much higher than

expected, but these are preliminary results. More diffusion studies will be done to determine why the diffusion lengths seen are so high. One explanation may be mixing at the polymer-polymer interface.

FUTURE WORK

Many more experiments should be performed to fully answer the questions presented at the beginning of this chapter. For example, if a trilayer stack was made in which PHOST is the intermediate layer and the polymeric PAG **8-1** was the feeder layer, would we see diffusion of the bound acid through PHOST above its T_g? One would not expect to see the migration of acid through the intermediate layer because the proton would not travel so far away from its counteranion as to cause such a large Coulombic potential energy. The diffusion of acid generated from **8-3** also needs to be compared to that of other PAGs in order to understand and calibrate differences in diffusion lengths seen with the polymeric PAGs. In addition, would a polymeric PAG such as **8-1** help in controlling linewidth variations when used in an actual photoresist formulation? Experiments with this PAG, when blended with current photoresists, would be very interesting indeed.

APPENDIX A: *EXPERIMENTAL SECTION*

REAGENTS AND CHEMICALS

All starting chemicals and reagents were procured from Aldrich Chemical (for many organic compounds), Strem Chemicals (catalysts), United Chemical Technologies or Gelest (silicon-containing compounds and platinum catalysts) and used as received unless noted otherwise. Solvents that needed to be dry were refluxed over the appropriate drying agent[166] and distilled under a nitrogen or argon atmosphere. The fluorinated norbornene alcohol (**2-1**), dinorbornene alcohol (**3-21**), and allylhexafluoroalcohol (**4-1**) were donated by Japan Synthetic Rubber Company (JSR). 1,2-Dibromotetrafluoroethane was purchased from Crescent Chemical Co. Hydrogen silsesquioxane polymer was donated by Dow Corning. Most of the photoacid generators used in the acid diffusion experiments were obtained from Midori Kagaku Company, except for triphenylsulfonium perfluorobutanesulfonate, which was donated by AZ Clariant or made in house.

CHARACTERIZATION TECHNIQUES

^{1}H-NMR (250 MHz) spectra were collected on a Bruker *AMX300* spectrometer. ^{1}H-NMR (300 MHz), ^{12}C-NMR (75 MHz), and ^{19}F-NMR (282 MHz) were recorded on a Varian *Unity Plus 300* spectrometer. ^{29}Si-NMR spectra were collected on a Bruker *DRX400* spectrometer. All spectra were referenced to either the deuterated solvent, tetramethylsilane (TMS), or fluorotrichloromethane

166 Perrin, D. D.; Armarego, W. L. F. *Purification of Laboratory Chemicals*, 3rd ed.; Butterworth-Heinemann Ltd: Oxford, 1994.

($FCCl_3$). FT-IR spectra of products were measured from KBr or NaCl pellets (solids) or salt plates (liquids) on a Nicolet *Avatar 360* IR spectrometer. FT-IR spectra of the sandwich stacks used in the acid diffusion experiments were recorded on a Nicolet *Magna 550* IR spectrometer. Fluorescence spectra were measured on a SPEX fluorescence spectrophotometer. UV-Vis spectra were measured on a Varian *Cary-1E* spectrophotometer. Gas chromatographs were recorded on a Hewlett Packard *5890 Series II* with an *HP-5* (crosslinked 5% PH ME siloxane) capillary column and flame ionization detector (FID). Mass spectra were measured using a Finnigan *MAT TSQ-700* spectrometer. Molecular weights (Mw) and polydispersity indices (PDI) were measured from THF solutions using a Viscotek GPC equipped with a set of two 5 mm crosslinked polystyrene columns (linear mix and 100 Å) from American Polymer Standards and are reported relative to polystyrene standards. Polymers containing acidic functional groups were pretreated with either diazomethane or iodomethane/DBU before GPC measurement, unless noted otherwise. Gas-phase vacuum UV measurements were made on an Acton *CAMS-507* spectrophotometer fitted with a custom-made gas cell attachment. The details of the cell design and implementation have been documented elsewhere.[53] Vacuum UV spectra of polymer films were measured and calculated on a J. A. Woollam *VU301* variable angle scanning ellipsometer (VASE) and/or measured with an Acton *CAMS-507* spectrophotometer. The films were cast on either silicon wafers (VASE) or calcium fluoride disks (Acton) from solutions in propylene glycol methyl ether acetate (PGMEA), cyclohexanone, or THF and baked at 100-130°C for at least 5

min prior to analysis. All absorbance data reported are in base 10. Differential scanning calorimetry (DSC) measurements and thermal gravimetric analysis (TGA) were performed on a Perkin Elmer *Series-7* thermal analysis system. Elemental analyses were performed either by Atlantic Microlabs of Norcross, GA or by Galbraith Laboratories of Knoxville, TN.

IMAGING TECHNIQUES AND INSTRUMENTATION

Contact printing was performed using a Headway spin coater, JBA *LS65* 1 kW exposure system with a 248 nm bandpass filter from Acton Research, and an Optoline quartz mask. Projection imaging work was performed on an Exitech 157 nm small field (1.5 x 1.5 mm^2) mini-stepper (0.6 NA) using a binary mask (σ 0.7) at International SEMATECH in Austin, TX. Scanning electron micrographs were collected on a JEOL *JWS-7550*. Coating, baking, and development of resist films at SEMATECH were performed using an FSI *Polaris 2000* track. Thickness measurements were made on a Prometrix interferometer. A typical resist formulation was prepared by mixing the polymer with 5 wt% (relative to polymer) photoacid generator (triphenylsulfonium nonaflate) and 0.3 wt% tetrabutylammonium hydroxide (TBAH) as the base to control acid diffusion and reduce T-topping. Dissolution inhibitors were mixed with the polymer to the desired ratio. The entire mixture was diluted in PGMEA to provide a viscosity that provides resist thicknesses of approximately 100-200 nm after spinning the resist at 2500 rpm onto a silicon wafer that may have been previously coated with ~80 nm BARC (bottom anti-reflective coating, Shipley AR19). The post-apply bake was usually 90-140°C for 60 sec and the post-exposure bake was 90-140°C

for 90 sec, unless stated otherwise. The exposed resists were developed in the industry-standard 0.26 *N* tetramethylammonium hydroxide (TMAH) developer.

SYNTHESIS

Diphenyldiethoxysilane: Into an argon-purged 500 mL round-bottom flask equipped with a magnetic stirrer, condenser, and addition funnel was added phenyltriethoxysilane (30.0 g, 125 mmol) in 200 mL anhydrous THF. Phenylmagnesium bromide (27.7 mL, 83.2 mmol, 3M in ether) was added dropwise. The resulting solution was stirred at reflux overnight. The THF was evaporated from the reaction mixture into a liquid nitrogen cooled trap. Anhydrous hexanes (200 mL) was added to the reaction flask to dissolve the product and precipitate the magnesium salt. This mixture was filtered (via cannula, through an enclosed fritted funnel) to another argon-purged 500 mL round-bottom flask equipped with a magnetic stirrer. The solvent was evaporated into a cold trap (liquid nitrogen cooled), yielding a yellow oil. This oil was distilled under vacuum (90-98°C / 0.03 mm Hg) to afford pure product (18.6 g, 82%). ^{1}H-NMR (ppm, $CDCl_3$): δ 7.69-7.67 (d, 4H, Ar-H); 7.42-7.35 (m, 6H, Ar-H); 3.91-3.86 (q, 4H, CH_3CH_2O); 1.28-1.25 (t, 6H, CH_3CH_2O).

1-Bromo-4-(tert-butoxy)benzene (Method A): In a Parr pressure bomb was placed a solution of 4-bromophenol (8.65 g, 50 mmol) in dichloromethane (150 mL). After cooling to -40°C, isobutene (112 mL) and concentrated sulfuric acid (0.5 mL) were added. After closing the pressure bomb, the reaction mixture was stirred for 66 h at room temperature. The bomb was recooled to -10°C and a solution of sodium hydroxide (1.25 g) in water (50 mL) was added carefully with

stirring to remove unreacted 4-bromophenol and to neutralize remaining sulfuric acid. After transferring the contents of the bomb to a precooled flask, the isobutene was removed (distillation into a cold trap, cooled to -60°C) and the dichloromethane phase was separated from the NaOH phase. The organic layer was washed with water and brine, dried with $MgSO_4$ and evaporated. Vacuum distillation of the crude product afforded pure 1-bromo-4-(*tert*-butoxy)benzene (55°C / 0.08 mm Hg, 10.6 g, 93%). ^{1}H-NMR (ppm, $CDCl_3$): δ 7.36-7.34 (d, 2H, Ar-H); 6.86-6.84 (d, 2H, Ar-H); 1.31 (s, 9H, CH_3). GC: 99% (6.56 min).

1-Bromo-4-(tert-butoxy)benzene (Method B): An oven-dried 100 mL three-neck flask equipped with a magnetic stir bar, thermometer, and nitrogen inlet was charged with CH_2Cl_2 (30 mL) and cooled to -30°C through the aid of a dry ice-CH_3OH/H_2O slush bath. To the flask were added liquefied isobutene (23 mL) and 4-bromophenol (5.00 g, 28.9 mmol). To the vigorously stirred reaction mixture was added trifluoromethanesulfonic acid (347 mg, 2.31 mmol). After completion of the addition, the resultant mixture was stirred for an additional 4 h at -78°C. Triethylamine (234 mg, 2.31 mmol) was then added, and the reaction mixture was then allowed to warm to room temperature. The solvents were evaporated. The oily residue was triturated with 100 mL petroleum ether and the solids were filtered. The organic solution was washed once with 1 M NaOH (100 mL) to remove unreacted 4-bromophenol, washed with saturated NaCl (100 mL), and dried over $MgSO_4$. Evaporation of the solvent, followed by vacuum distillation (53°C / 0.08 mm Hg), yielded pure product as a colorless liquid (5.31

g, 80%). ^{1}H-NMR (ppm, $CDCl_3$): δ 7.36-7.34 (d, 2H, Ar-H); 6.86-6.84 (d, 2H, Ar-H); 1.31 (s, 9H, CH_3). GC: 99% (6.56 min).

4-(tert-butoxyphenyl)phenyldiethoxysilane (**3-6**): Oven-dried magnesium filings (0.584 g, 24.0 mmol) were added to an argon-purged 100 mL three-neck round-bottom flask fitted with a magnetic stirrer, condenser, and an addition funnel containing 25 mL distilled THF. The protected bromide (5.00 g, 21.8 mmol) was dissolved in a minimum amount of THF and slowly added dropwise to the magnesium filings. One crystal of iodine was added and the flask was heated with a heat gun to help initiate the formation of the Grignard reagent. After initiation (the dark brown color of the iodine solution turns clear after heating) the rest of the THF was added to the reaction mixture so as to maintain a gentle reflux. The solution was heated at reflux for an additional 2 h and then allowed to cool to room temperature. Phenyltriethoxysilane (10.5 g, 43.7 mmol) was added to 100 mL THF in a separate 250 mL three-neck round-bottom flask fitted with a magnetic stirrer, reflux condenser, and addition funnel. The Grignard reagent prepared before was added to the addition funnel via a cannula. This was then added dropwise to the phenyltriethoxysilane solution. The reaction mixture was stirred at reflux overnight. The THF was evaporated from the reaction mixture into a liquid nitrogen cooled trap. Anhydrous hexanes (100 mL) was added to the reaction flask to dissolve the product and precipitate the magnesium salt. This mixture was filtered (via cannula, through an enclosed fritted funnel) to another argon-purged 250 mL round-bottom flask equipped with a magnetic stirrer. The solvent was evaporated into a cold trap (liquid nitrogen

cooled), yielding a yellow oil. This oil was distilled under vacuum (130-135°C / 0.03 mm Hg) to afford pure product (4.30 g, 57%). ^{1}H-NMR (ppm, $CDCl_3$): δ 7.67-7.65 (d, 2H, Ph-H); 7.55-7.53 (d, 2H, t-BuO-Ph-H); 7.40-7.34 (m, 3H, Ph-H); 6.98-6.96 (d, 2H, t-BuO-Ph-H); 3.88-3.82 (q, 4H, CH_3CH_2O); 1.34 (s, 9H, CH_3); 1.25-1.22 (t, 6H, CH_3CH_2O). ^{13}C-NMR (ppm, $CDCl_3$): δ 157.4, 135.6, 134.6, 133.3, 129.9, 127.6, 126.7, 122.8 (Ar-C); 78.1 ($C(CH_3)_3$); 58.6 (CH_3CH_2O); 28.7 (CH_3CH_2O); 18.1 ($C(CH_3)_3$). ^{29}Si-NMR (ppm, $CDCl_3$/TMS): -32.2 (Si).

Poly[4-(tert-butoxyphenyl)phenylsiloxane] (**3-7**): General polymerization procedure: The appropriate aqueous base (1 *M* NaOH, 30% NH_4OH, or 40% $N(Bu)_4OH$) (50 mg water content, 2.76 mmol water) was added to the diethoxy monomer (0.50 g, 1.84 mmol) dissolved in methanol (2 mL) in a capped scintillation vial containing a magnetic stirrer. The reaction mixture was stirred vigorously overnight at room temperature or with gentle heating (50°C). The polymer was precipitated into water, filtered, washed with water several times to remove excess base, and dried *in vacuo*. Yields ranged from 80 to 90%. ^{1}H-NMR (ppm, $CDCl_3$): δ 7.47-6.74 (bm, 9H, Ar-H); 1.31 (bs, 9H, CH_3). ^{13}C-NMR (ppm, $CDCl_3$): δ 157.1, 135.2, 134.6, 134.2, 129.7, 129.5, 128.3, 127.3, 122.6 (Ar-C); 78.3 ($C(CH_3)_3$); 28.7 (CH_3). ^{29}Si-NMR (ppm, $CDCl_3$/TMS): -40.0 (Si). GPC (THF): M_w = 40,000; M_n = 17,000; DPI = 2.3. TGA: Onset ~150°C.

4-(tert-butoxyphenyl)dichlorosilane (**3-8**): Oven-dried magnesium filings (0.584 g, 24.0 mmol) were added to an argon-purged 100 mL three-neck round-bottom flask fitted with a magnetic stirrer, condenser, and an addition funnel

containing 25 mL distilled THF. 1-Bromo-4-(*tert*-butoxy)benzene (5.00 g 21.8 mmol) was dissolved in a minimum amount of THF and slowly added dropwise to the magnesium filings. One crystal of iodine was added and the flask was heated with a heat gun to help initiate the formation of the Grignard reagent. After initiation (the dark brown color of the iodine solution turns clear after heating) the rest of the THF was added to the reaction mixture so as to maintain a gentle reflux. The solution was heated at reflux for an additional 2 h and then allowed to cool to room temperature. Trichlorosilane (5.92 g, 43.7 mmol) was added to 100 mL THF in a separate 250 mL three-neck round-bottom flask fitted with a magnetic stirrer, reflux condenser, and addition funnel. The Grignard reagent prepared before was added to the addition funnel via a cannula. This was then added dropwise to the trichlorosilane solution. The reaction mixture was stirred at 0°C for 3 h. The THF and excess trichlorosilane was evaporated from the reaction mixture into a liquid nitrogen cooled trap. Anhydrous hexanes (100 mL) was added to the reaction flask to dissolve the product and precipitate the magnesium salt. This mixture was filtered (via cannula, through an enclosed fritted funnel) to another argon-purged 250 mL round-bottom flask equipped with a magnetic stirrer. The solvent was evaporated into a cold trap (liquid nitrogen cooled), yielding a yellow oil. This oil was distilled under vacuum (67-70°C / 0.10 mm Hg) to afford pure product (2.61 g, 48%). ^{1}H-NMR (ppm, Benzene-d_6): δ 7.39-7.37 (d, 2H, Ar-H); 6.86-6.84 (d, 2H, Ar-H); 5.81 (s, 1H, SiH); 1.14 (s, 9H, CH_3). ^{13}C-NMR (ppm, Benzene-d_6): δ 160.1, 134.9, 124.2, 122.9 (Ar-C); 78.9 ($C(CH_3)_3$); 28.7 ($C(CH_3)_3$).

4-(tert-butoxyphenyl)triethoxysilane (**3-11**): Oven-dried magnesium filings (0.584 g, 24.0 mmol) were added to an argon-purged 100 mL three-neck round-bottom flask fitted with a magnetic stirrer, condenser, and an addition funnel containing 25 mL distilled THF. 1-Bromo-4-(*tert*-butoxy)benzene (5.00 g, 21.8 mmol) was dissolved in a minimum amount of THF and slowly added dropwise to the magnesium filings. One crystal of iodine was added and the flask was heated with a heat gun to help initiate the formation of the Grignard reagent. After initiation (the dark brown color of the iodine solution turns clear after heating) the rest of the THF was added to the reaction mixture so as to maintain a gentle reflux. The solution was heated at reflux for an additional 2 h and then allowed to cool to room temperature. Tetraethylorthosilicate (9.09 g, 43.7 mmol) was added to 100 mL THF in a separate 250 mL three-neck round-bottom flask fitted with a magnetic stirrer, reflux condenser, and addition funnel. The Grignard reagent prepared before was added to the addition funnel via a cannula. This was then added dropwise to the tetraethylorthosilicate solution. The reaction mixture was stirred at reflux overnight. The THF was evaporated from the reaction mixture into a liquid nitrogen cooled trap. Anhydrous hexanes (100 mL) was added to the reaction flask to dissolve the product and precipitate the magnesium salt. This mixture was filtered (via cannula, through an enclosed fritted funnel) to another argon-purged 250 mL round-bottom flask equipped with a magnetic stirrer. The solvent was evaporated into a cold trap (liquid nitrogen cooled), yielding a yellow oil. This oil was distilled under vacuum (110-115°C / 0.22 mm Hg) to afford pure product (2.50 g, 37%). ^{1}H-NMR (ppm, $CDCl_3$): δ

7.50-7.46 (d, 2H, Ar-H); 6.91-6.86 (d, 2H, Ar-H); 3.83-3.78 (q, 6H, CH_3CH_2O); 1.31 (s, 9H, CH_3); 1.20-1.17 (t, 9H, CH_3CH_2O). ^{13}C-NMR (ppm, $CDCl_3$): δ 157.3, 135.2, 124.3, 122.5 (Ar-C); 77.7 ($C(CH_3)_3$); 58.0 (CH_3CH_2O); 28.4 (CH_3CH_2O); 17.7 ($C(CH_3)_3$). ^{29}Si-NMR (ppm, $CDCl_3$/TMS): -57.6 (Si).

Poly[4-(tert-butoxyphenyl)silsesquioxane] (**3-12**): Ammonium hydroxide (30% in water, 51 mg water content, 2.82 mmol water) was added to 4-(*tert*-butoxyphenyl)triethoxysilane (0.50 g, 1.88 mmol) in 2 mL methanol in a capped scintillation vial containing a magnetic stirrer. The reaction mixture was stirred vigorously overnight at room temperature. The polymer was precipitated into water, filtered, washed with water several times to remove excess base, and dried *in vacuo*. ^{1}H-NMR (ppm, $CDCl_3$): δ 7.75-7.05 (bs, 2H, Ar-H); 7.05-6.40 (bs, 2H, Ar-H); 1.31 (bs, 9H, CH_3). ^{13}C-NMR (ppm, $CDCl_3$): δ 157.7, 135.2, 125.5, 122.9 (Ar-C); 78.2 ($C(CH_3)_3$); 28.9 (CH_3). GPC (THF): M_w = 3,650; M_n = 2,359; DPI = 1.5. TGA: Onset ~220°C.

4-(tert-butoxybenzyl)triethoxysilane (**3-13**): To a stirred mixture of lithium powder (2.59 g, 373 mmol, 0.5% sodium content) in 15 mL of anhydrous THF cooled to -10°C was added 4-(*tert*-butoxybenzyl)methyl ether (4.83 g, 24.9 mmol) dissolved in 7.5 mL diethyl ether at a rate of 30 drops per minute. Ten minutes after the addition was begun, the solution became green, slowly turning to dark brown as the addition was continued. The internal temperature of the reaction mixture was maintained between -5 and -15°C by manipulation of a dry ice-acetone bath used for cooling, while the rate of addition was kept constant. Subsequent to the addition, the mixture was stirred for another hour at -10°C.

The resulting benzyllithium solution was filtered through glass wool into an addition funnel provided with an outer glass shell into which a cooling mixture of dry ice and acetone at -10°C was placed. The solution was then added dropwise to a solution of tetraethylorthosilicate (7.78 g, 37.4 mmol) dissolved in 100 mL anhydrous THF cooled to -10°C. The stirred reaction mixture was allowed to warm to room temperature and then refluxed overnight. The THF and ether were evaporated from the reaction mixture into a liquid nitrogen cooled trap. Anhydrous hexanes (100 mL) was added to the reaction flask to dissolve the product and precipitate the lithium salt. This mixture was filtered (via cannula, through an enclosed fritted funnel covered with a layer of Celite) to another argon-purged 250 mL round-bottom flask equipped with a magnetic stirrer. The solvent was evaporated into a cold trap (liquid nitrogen cooled), yielding a yellow oil. This oil was distilled under vacuum (105-110°C / 0.50 mm Hg) to afford pure product (1.04 g, 13%). ^{1}H-NMR (ppm, $CDCl_3$): δ 7.05-7.03 (d, 2H, Ar-H); 6.84-6.82 (d, 2H, Ar-H); 3.74-3.68 (q, 6H, CH_3CH_2O); 2.14 (s, 2H, $ArCH_2$); 1.28 (s, 9H, CH_3); 1.14-1.11 (t, 9H, CH_3CH_2O). ^{13}C-NMR (ppm, $CDCl_3$): δ 152.2, 132.4, 129.1, 124.2 (Ar-C); 77.9 ($C(CH_3)_3$); 58.6 (CH_3CH_2O); 28.8 (CH_3CH_2O); 19.4 ($ArCH_2$); 18.1 ($C(CH_3)_3$). ^{29}Si-NMR (ppm, $CDCl_3$/TMS): -52.0 (Si).

Poly[4-(tert-butyoxybenzyl)silsesquioxane] (**3-14**): Ammonium hydroxide (30% in water, 43 mg water content, 2.40 mmol water) was added to 4-(*tert*-butoxybenzyl)triethoxysilane (0.50 g, 1.60 mmol) in 2 mL ethanol in a capped scintillation vial containing a magnetic stirrer. The reaction mixture was stirred vigorously overnight at room temperature. The polymer was precipitated into

water, filtered, washed with water several times to remove excess base, and dried *in vacuo*. ^{1}H-NMR (ppm, $CDCl_3$): δ 7.10-6.40 (bs, 4H, Ar-H); 2.00-1.30 (bs, 2H, CH_2); 1.23 (bs, 9H, CH_3). ^{13}C-NMR (ppm, $CDCl_3$): δ 152.5, 131.4, 129.1, 124.0 (Ar-C); 77.7 ($C(CH_3)_3$); 28.7 (CH_3), 20.9 (CH_2). ^{29}Si-NMR (ppm, $CDCl_3$/TMS): -73.0 (Si). GPC (THF): M_w = 2,760; M_n = 2,220; DPI = 1.2. TGA: Onset ~150°C.

Poly[methyl 3-(bicyclo[2.2.1]heptan-2-yl)-1,1,1-trifluoro-2-(trifluoro-methyl)propan-2-ol-6-yl siloxane] (**3-20**): Into a 100 mL round-bottom flask equipped with a magnetic stir bar and reflux condenser was added 3-(bicyclo[2.2.1]hept-5-en-2-yl)-1,1,1-trifluoro-2-(trifluoromethyl)propan-2-ol (**2-1**, NBHFA, 4.57 g, 16.7 mmol) to poly(methylhydridosiloxane) (1.00 g, 16.7 mmol) in 50 mL toluene. The condenser was fitted with a drying tube loaded with Drierite ($CaSO_4$) such that the reaction was exposed to dry air (oxygen accelerates the reaction). Hexachloroplatinic acid (0.34 g, 0.83 mmol) was then added to the stirred solution. The reaction mixture was stirred at 100°C overnight, at which time the solution turned a clear dark brown color (formation of colloidal platinum). Activated carbon (~10 g) was added to adsorb platinum. The mixture was filtered through Dicalite (diatomaceous earth) using a fritted funnel and washed with dichloromethane (~100 mL). The resulting solution was subjected to rotary evaporation to remove excess dichloromethane and toluene. The polymer was again dissolved in dichloromethane, stirred with activated carbon, and filtered through Dicalite. The resulting solution was precipitated into hexanes, at which point the polymer oiled out of solution. The hexanes was decanted, and the

polymer was dried at 50°C under vacuum to yield a yellowish-brown powder (1.20 g, 22%). ^{1}H-NMR (ppm, DMSO-d_6): δ 7.58 (bs, 1H, O<u>H</u>); 2.20-0.35 (m, 12H, norbornyl-<u>H</u>); 0.02 (s, 3H, Si-C<u>H</u>$_3$). ^{19}F-NMR (ppm, DMSO-d_6): δ -76.12 (m, 6F, C<u>F</u>$_3$). FTIR (cm^{-1}, KBr): 3596, 3479, 2963, 2870, 1457, 1261, 1214, 1107, 1017, 938, 906, 867, 770, 716, 663. GPC (THF): M_w = 19,600; M_n = 10,500; P_d = 1.87. A_{157} = 2.51 μm^{-1}. DSC: 43°C.

Poly[methyl 3-(tetracyclo[4.4.0.1^{2,5}.1^{7,10}]dodecan-2-yl)-1,1,1-trifluoro-2-(trifluoromethyl)propan-2-ol-8-yl siloxane] (**3-22**): Into a 100 mL round-bottom flask equipped with a magnetic stir bar and reflux condenser was added 3-(tetracyclo[4.4.0.1^{2,5}.1^{7,10}]dodec-7-en-2-yl)-1,1,1-trifluoro-2-(trifluoromethyl)propan-2-ol (**3-21**, DNBHFA, 5.67 g, 16.7 mmol) to poly(methylhydridosiloxane) (1.00 g, 16.7 mmol) in 50 mL toluene. The condenser was fitted with a drying tube loaded with Drierite ($CaSO_4$) such that the reaction was exposed to dry air (oxygen accelerates the reaction). Hexachloroplatinic acid (0.34 g, 0.83 mmol) was then added to the stirred solution. The reaction mixture was stirred at 100°C overnight, at which time the solution turned a clear dark brown color (formation of colloidal platinum). Activated carbon (~10 g) was added to adsorb platinum. The mixture was filtered through Dicalite (diatomaceous earth) using a fritted funnel and washed with dichloromethane (~100 mL). The resulting solution was subjected to rotary evaporation to remove excess dichloromethane and toluene. The polymer was again dissolved in dichloromethane, stirred with activated carbon, and filtered through Dicalite. The resulting solution was precipitated into hexanes, at which point the polymer oiled out of solution. The hexanes was

decanted, and the polymer was dried at 50°C under vacuum to yield a yellowish-brown powder (2.90 g, 44%). ^{1}H-NMR (ppm, DMSO-d_6): δ 7.54 (bs, 1H, O<u>H</u>); 2.40-0.30 (m, 18H, dinorbornyl-<u>H</u>); 0.02 (s, 3H, Si-C<u>H</u>$_3$). ^{19}F-NMR (ppm, DMSO-d_6): δ -76.06 (m, 6F, C<u>F</u>$_3$). FTIR (cm^{-1}, KBr): 3604, 3487, 3048, 2951, 2889, 1487, 1460, 1258, 1208, 1150, 1115, 1091, 1006, 917, 897, 773, 718, 703, 664. GPC (THF): M_w = 45,400; M_n = 16,100; DPI = 2.82. A_{157} = 3.63 μm^{-1}. DSC: 105°C.

Poly[methyl DNHFA siloxane-co-methyl DNHFATBOC siloxane] (**3-23**): Into an argon-purged 100 mL round-bottom flask containing the siloxane polymer (**3-22**, 1.07 g, 2.68 mmol) in 20 mL freshly distilled THF (K/Na alloy) was added 4-(dimethylamino)pyridine (DMAP, 32.7 mg, 0.268 mmol). After stirring for 5 min, di-*tert*-butyldicarbonate (0.117 g, 0.535 mmol) was added (slight bubbling occurs). The reaction mixture was stirred at room temperature overnight. Dichloromethane (50 mL) was added to dilute the solution, and the organic layer was washed with mild acid (3 wt% HCl, 50 mL), water (50 mL), brine (50 mL), and dried with $MgSO_4$. The dichloromethane was evaporated to 10 mL, and the polymer was precipitated into hexanes and dried *in vacuo* to yield a slightly yellow powder (0.90 g, 84%). ^{1}H-NMR (ppm, DMSO-d_6): δ 7.54 (bs, 1H, O<u>H</u>); 2.40-0.30 (m, 36H, dinorbornyl-<u>H</u>); 0.02 (s, 6H, Si-C<u>H</u>$_3$); 1.50 (s, 3H, *t*-butyl-<u>H</u>). ^{19}F-NMR (ppm, DMSO-d_6): δ -76.1 (m, 12F, C<u>F</u>$_3$). FTIR (cm^{-1}, KBr): 3592, 3483, 3041, 2944, 2885, 1775 (C=O), 1464, 1383, 1258, 1216, 1142, 1118, 1091, 1014, 920, 893, 773, 718, 703, 664. GPC (THF): M_w = 26,200; M_n = 9,510; DPI = 2.76. TGA: Onset ~120°C. According to TGA mass loss, x = 77, y = 23.

2-Ethoxymethoxy-1,1,1-trifluoro-2-trifluoromethyl-pent-4-ene (**4-2**): 1,1,1-Trifluoro-2-trifluoromethyl-pent-4-en-2-ol (**4-1**, 20.0 g, 96.2 mmol) was added to an argon-purged 500 mL round-bottom flask containing sodium hydride (2.77 g, 115 mmol) in 200 mL anhydrous THF. After the bubbling of hydrogen gas had ceased, ethyl chloromethyl ether (9.54 g, 101mmol) was added dropwise to the reaction mixture. The resulting mixture was stirred at reflux overnight and then diluted with 200 mL diethyl ether. The organic layer was washed with dilute base (0.01 *N* NaOH, 100 mL), brine (100 mL), and dried with $MgSO_4$. The crude product was distilled under reduced pressure (72-74°C / 52 mm Hg) to afford a colorless oil (16.0 g, 63%). ^{1}H-NMR (ppm, $CDCl_3$): δ 5.93-5.76 (m, 1H, CH_2=C<u>H</u>R); 5.27-5.17 (m, 2H, C<u>H$_2$</u>=CHR); 5.00 (s, 2H, OC<u>H$_2$</u>O); 3.73-3.64 (q, 2H, OC<u>H$_2$</u>CH_3); 2.85 (d, 2H, CH_2=CHC<u>H$_2$</u>); 1.21 (t, 3H, OCH_2C<u>H$_3$</u>).

2-Ethoxymethoxy-1,1,1-trifluoro-2-trifluoromethyl-pent-5-yl triethoxy-silane (**4-3**): Into a 50 mL three-neck flask equipped with a magnetic stir bar and reflux condenser was added triethoxysilane (2.00 g, 12.2 mmol) in anhydrous toluene (25 mL). The condenser was fitted with a drying tube loaded with Drierite such that the reaction was exposed to dry air (oxygen accelerates the reaction). Dichlorodicyclopentadienyl platinum (II) (48.6 mg, 122 μmol) was then added to the stirred solution. 2-Ethoxymethoxy-1,1,1-trifluoro-2-trifluoromethyl-pent-4-ene (**4-2**, 3.41 g, 12.8 mmol) was added dropwise via syringe. The reaction mixture was stirred at reflux overnight, at which time the solution turned a clear dark brown color (formation of colloidal platinum). The solvent and any excess triethoxysilane was removed by vacuum distillation. The

resulting oil was then distilled under vacuum to afford a clear, colorless liquid (130-134°C / 10 mm Hg, 2.00 g, 38%). ^{1}H-NMR (ppm, $CDCl_3$): δ 4.94 (s, 2H, $OC\underline{H}_2O$); 3.85-3.76 (q, 6H, $SiOC\underline{H}_2CH_3$); 3.72-3.63 (q, 2H, $OC\underline{H}_2CH_3$); 2.10-2.04 (t, 2H, $OC(CF_3)_2C\underline{H}_2$); 1.67 (p, 2H, $CH_2C\underline{H}_2CH_2$); 1.25-1.17 (t, $SiOCH_2C\underline{H}_3$); 1.25-1.17 (t, $OCH_2C\underline{H}_3$); 0.63 (t, 2H, $C\underline{H}_2Si$).

2-(tert-butoxycarbonyloxy)-3-(tetracyclo[4.4.0.1^{2,5}.1^{7,10}]dodec-7-en-2-yl)-1,1,1-trifluoro-2-(trifluoromethyl)propane (**4-5**): Into an argon-purged 250 mL round-bottom flask containing 3-(tetracyclo[4.4.0.1^{2,5}.1^{7,10}]dodec-7-en-2-yl)-1,1,1-trifluoro-2-(trifluoromethyl)propan-2-ol (8.60 g, 25.3 mmol) in 100 mL freshly distilled THF (K/Na alloy) was added 4-(dimethylamino)pyridine (DMAP, 0.309 g, 2.53 mmol). After stirring for 5 min, di-*tert*-butyldicarbonate (6.07 g, 27.8 mmol) was added (slight bubbling occurs). The reaction mixture was stirred at room temperature overnight. Dichloromethane (100 mL) was added to dilute the solution, and the organic layer was washed with mild acid (3 wt% HCl, 100 mL), water (100 mL), brine (100 mL), and dried with $MgSO_4$. The dichloromethane was evaporated and the brown oil was filtered through a plug of silica gel using hexanes as the solvent. This removes the dark color and other impurities to give a clear light yellow oil (10.65 g, 96%). ^{1}H-NMR (ppm, $CDCl_3$): δ 5.98-5.90 (m, 2H, $C\underline{H}=C\underline{H}$); 2.82 (bs, 2H, $C\underline{H}_2CR_2O$); 2.74 (bs, 1H, $C\underline{H}CH_2CR_2O$); 2.24-0.53 (m, 12H, aliphatic-$\underline{H}$); 1.49 (s, 9H, $C\underline{H}_3$). FTIR (cm^{-1}, KBr): 3047, 2960, 2873, 1772 (C=O), 1475, 1373, 1286, 1245 (C-F), 1210, 1127, 1086, 974, 866, 753.

2-(tert-butoxycarbonyloxy)-3-(8-triethoxysilyl tetracyclo[4.4.0.1^{2,5}.1^{7,10}] dodecan-2-yl)-1,1,1-trifluoro-2-(trifluoromethyl)propane (**4-6**): This compound was not isolated in pure form because it could not be distilled due to its high boiling point and could not be chromatographed because the ethoxysilane group is labile when exposed to silica gel.

2-(tert-butoxycarbonyloxy)-3-(bicyclo[2.2.1]hept-5-en-2-yl)-1,1,1-trifluoro-2-(trifluoromethyl)propane (**2-3**): Into an argon-purged 250 mL round-bottom flask containing NBHFA (**2-1**, 15.0 g, 54.7 mmol) in 100 mL freshly distilled THF (K/Na alloy) was added 4-(dimethylamino)pyridine (DMAP, 0.669 g, 5.47 mmol). After stirring for 5 min, di-*tert*-butyldicarbonate (13.1 g, 60.2 mmol) was added (slight bubbling occurs). The reaction mixture was stirred at room temperature overnight. Dichloromethane (100 mL) was added to dilute the solution, and the organic layer was washed with mild acid (3 wt% HCl, 100 mL), water (100 mL), brine (100 mL), and dried with $MgSO_4$. The dichloromethane was evaporated and the crude oil was distilled under reduced pressure to yield a clear, colorless oil (19.0 g, 93%). ^{1}H-NMR (ppm, $CDCl_3$): δ 6.21-6.17 (m, 1H, C<u>H</u>=CH); 5.97-5.93 (m, 1H, CH=C<u>H</u>); 2.82-2.77 (d, 2H, C<u>H</u>$_2$CR$_2$O); 2.70-0.60 (m, 7H, aliphatic-<u>H</u>); 1.49 (s, 9H, C<u>H</u>$_3$). FTIR (cm^{-1}, KBr): 2976, 2868, 1767 (C=O), 1286, 1240, 1209, 1127, 1081, 974, 871, 702.

3-(5-triethoxysilyl bicycle[2.2.1]heptan-2-yl)-1,1,1-trifluoro-2-(trifluoromethyl)-2-(tert-butoxycarbonyloxy)propane (**4-7**): Into a 100 mL three-neck flask equipped with a magnetic stir bar and reflux condenser was added triethoxysilane (3.29 g, 20.1 mmol) in anhydrous toluene (50 mL). The condenser was fitted with

a drying tube loaded with Drierite such that the reaction was exposed to dry air. Dichlorodicyclopentadienyl platinum (II) (53.2 mg, 134 μmol) was then added to the stirred solution. 2-(*tert*-Butoxycarbonyloxy)-3-(bicyclo[2.2.1]hept-5-en-2-yl)-1,1,1-trifluoro-2-(trifluoromethyl)propane (**2-3**, 5.00 g, 13.4 mmol) was added dropwise via syringe. The reaction mixture was stirred at reflux overnight, at which time the solution turned a clear dark brown color (formation of colloidal platinum). Activated carbon was added to adsorb platinum and the mixture was filtered through a bed of Dicalite and washed with hexanes. Evaporation of solvent and excess starting material *in vacuo* afforded product. ^{1}H-NMR (ppm, $CDCl_3$): δ 3.85-3.76 (q, 6H, $SiOC\underline{H}_2CH_3$); 2.82-2.77 (d, 2H, $C\underline{H}_2CR_2O$); 2.70-0.60 (m, 10H, aliphatic-H); 1.50 (s, 9H, $C\underline{H}_3$); 1.25-1.17 (t, $SiOCH_2C\underline{H}_3$).

3-(5-triethoxysilyl bicycle[2.2.1]heptan-2-yl)-1,1,1-trifluoro-2-(trifluoro-methyl)propan-2-ol (**4-8**): Into a 100 mL three-neck flask equipped with a magnetic stir bar and reflux condenser was added triethoxysilane (5.00 g, 30.5 mmol) in anhydrous toluene (50 mL). The condenser was fitted with a drying tube loaded with Drierite such that the reaction was exposed to dry air. Hexachloroplatinic acid (125 mg, 305 μmol) and NBHFA (**2-1**, 8.35 g, 30.5 mmol) were then added to the stirred solution. The reaction mixture was stirred at reflux overnight, at which time the solution turned a clear dark brown color (formation of colloidal platinum). Activated carbon was added to adsorb platinum and the mixture was filtered through a bed of Dicalite and washed with hexanes. Evaporation of solvent and excess starting material *in vacuo* afforded product. ^{1}H-NMR (ppm, $CDCl_3$): δ 3.85 (q, 6H, $OC\underline{H}_2CH_3$); 2.76 (d, 2H,

$C\underline{H}_2CR_2OH$); 2.20-0.60 (m, 10H, norbornyl-$\underline{H}$); 1.18 (t, 9H, $OCH_2C\underline{H}_3$). FTIR (cm^{-1}, KBr): 3351 (OH), 2951, 2870, 1460, 1402, 1219, 1170, 1150, 963, 800, 734.

tert-Butyl 5-(triethoxysilyl)bicycle[2.2.1]heptan-2-carboxylate (**4-9**): Into a 50 mL three-neck flask equipped with a magnetic stir bar and reflux condenser was added triethoxysilane (2.03 g, 12.4 mmol) in anhydrous toluene (25 mL). The condenser was fitted with a drying tube loaded with Drierite such that the reaction was exposed to dry air. Dichlorodicyclopentadienyl platinum (II) (41.1 mg, 103 μmol) was then added to the stirred solution. *tert*-Butyl bicyclo[2.2.1]hept-5-en-2-carboxylate (NBTBE, 2.00 g, 10.3 mmol) was added dropwise via syringe. The reaction mixture was stirred at reflux overnight, at which time the solution turned a clear dark brown color (formation of colloidal platinum). The solvent and any excess triethoxysilane was removed by vacuum distillation. The resulting oil was then distilled under vacuum to afford a clear, colorless liquid (97-102°C / 2 mm Hg, 1.50 g, 41%). ^{1}H-NMR (ppm, $CDCl_3$): δ 3.85-3.74 (q, 6H, $OC\underline{H}_2CH_3$); 2.67-0.60 (m, 10H, norbornyl-$\underline{H}$); 1.42 (s, 9H, t-butyl-$\underline{H}$); 1.19 (t, 9H, $OCH_2C\underline{H}_3$).

tert-Butyl 2-(trifluoromethyl)acrylate: To a 300 mL Parr pressure reactor containing a stir bar was added 2-(trifluoromethyl)acrylic acid (15.0 g, 94.9 mmol) in diethyl ether (35 mL). This solution was cooled to -40°C with a dry ice/isopropanol bath. Isobutene (35 mL) was condensed into the pressure reactor. To this solution was added conc. H_2SO_4 (1 mL), and the bomb was securely sealed. The reaction was stirred at room temperature overnight, cooled to -40°C,

and poured into ice-cold 1 *N* NaOH (150 mL). The organic layer was separated and the aqueous layer was extracted two times with diethyl ether (35 mL). The combined organic solutions were washed with water until neutral, dried over $MgSO_4$, and dried *in vacuo* to give a clear liquid (20.3 g, 99%). The product was further purified by vacuum distillation (73°C / 100 mm Hg). ^{1}H NMR ($CDCl_3$, 300 MHz, ppm): d 1.50 (s, 9H, t-Bu), 6.30-6.31 (m, 1H, C<u>H</u>=CH_2), 6.57-6.59 (m, 2H, CH=C<u>H</u>$_2$). ^{19}F NMR ($CDCl_3$, 282 MHz, ppm): d -66.1. IR (NaCl, cm^{-1}): 2980, 2934, 1731 (C=O), 1405, 1365, 1348, 1268 (C-F), 1113, 849. HRMS-CI (*m/z*): $[M + H]^+$ calcd for $C_8H_{11}F_3O_2$, 195.063; found, 195.063.

tert-Butyl 2-(trifluoromethyl)bicyclo[2.2.1]hept-5-en-2-carboxylate (**2-5**): Freshly cracked cyclopentadiene (5.05 g, 76.5 mmol) was added dropwise to *tert*-butyl 2-(trifluoromethyl)acrylate (5.00 g, 25.5 mmol) stirred in a 50 mL round-bottom flask equipped with a magnetic stir bar and reflux condenser. The solution became warm after 5 min. The reaction was stirred at room temperature overnight under an argon atmosphere. The crude product was vacuum distilled to give a clear colorless oil (80-85°C / 10 mm Hg, 4.20 g, 63%). ^{1}H-NMR (ppm, $CDCl_3$): δ 6.28 (m, 1H, CH=C<u>H</u>); 6.03 (m, 1H, CH=C<u>H</u>); 3.38-1.28 (m, 6H, norbornyl-<u>H</u>); 1.54 (s, 9H, *exo*-t-butyl-<u>H</u>); 1.41 (s, 9H, *endo*-t-butyl-<u>H</u>). GC: 99+%, 4.89-4.97 min.

tert-Butyl 5-(triethoxysilyl)-2-(trifluoromethyl)bicyclo[2.2.1]heptan-2-carboxylate (**4-10**), Method A: Into a 50 mL three-neck flask equipped with a magnetic stir bar and reflux condenser was added triethoxysilane (2.07 g, 12.6 mmol) in anhydrous toluene (25 mL). The condenser was fitted with a drying

tube loaded with Drierite such that the reaction was exposed to dry air. Dichlorodicyclopentadienyl platinum (II) (45.6 mg, 115 μmol) was then added to the stirred solution. tert-Butyl 2-(trifluoromethyl)bicyclo[2.2.1]hept-5-en-2-carboxylate (3.00 g, 11.5 mmol) was added dropwise via syringe. The reaction mixture was stirred at reflux overnight, at which time the solution turned a clear dark brown color (formation of colloidal platinum). The solvent and any excess triethoxysilane was removed by vacuum distillation. The resulting oil was then distilled under vacuum to afford a clear, colorless liquid (95-107°C / 0.35 mm Hg, 1.70 g, 35%). ^{1}H-NMR (ppm, $CDCl_3$): δ 3.81 (q, 6H, $OC\underline{H}_2CH_3$); 2.80-0.70 (m, 9H, norbornyl-H); 1.44 (s, 9H, t-butyl-H); 1.17 (t, 9H, $OCH_2C\underline{H}_3$).

tert-Butyl 5-(triethoxysilyl)-2-(trifluoromethyl)bicyclo[2.2.1]heptan-2-carboxylate (**4-10**), Method B: Into a 100 mL three-neck flask equipped with a magnetic stir bar and reflux condenser was added triethoxysilane (12.5 g, 76.3 mmol) to tert-Butyl 2-(trifluoromethyl)bicyclo[2.2.1]hept-5-en-2-carboxylate (10.0 g, 38.2 mmol). The condenser was fitted with a drying tube loaded with Drierite ($CaSO_4$) such that the reaction was exposed to dry air. Karstedt's catalyst (2% Pt(0) complexed with divinylsiloxane in a xylene solution, 7.44 mg, 38 μmol) was then added to the stirred solution. The reaction mixture was stirred at 100°C overnight, at which time the solution turned a clear dark brown color (formation of colloidal platinum). Activated carbon (~10 g) was added to adsorb platinum. The mixture was filtered through Dicalite (diatomaceous earth) using a fritted funnel and washed with hexane (~100 mL). The resulting solution was subjected to rotary evaporation to remove excess hexane and triethoxysilane to

yield a clear oil (14.35 g, 88%). ^{1}H-NMR (ppm, $CDCl_3$): δ 3.85-3.74 (q, 6H, $OC\underline{H}_2CH_3$); 2.90-0.76 (m, 9H, norbornyl-H); 1.45 (s, 9H, t-butyl-H); 1.24-1.16 (t, 9H, $OCH_2C\underline{H}_3$). FTIR (cm^{-1}, KBr): 2974, 2925, 2890, 1735 (C=O), 1456, 1391, 1367, 1282, 1262, 1118, 958, 784.

tert-Butyl 5-(triethoxysilyl)-3-(trifluoromethyl)bicyclo[2.2.1]heptan-2-carboxylate (**4-11**): Into a 50 mL three-neck flask equipped with a magnetic stir bar and reflux condenser was added triethoxysilane (0.689 g, 4.20 mmol) in anhydrous toluene (10 mL). The condenser was fitted with a drying tube baded with Drierite such that the reaction was exposed to dry air. Dichlorodicyclopentadienyl platinum (II) (15.2 mg, 38 μmol) was then added to the stirred solution. tert-Butyl 3-(trifluoromethyl)bicyclo[2.2.1]hept-5-en-2-carboxylate (1.00 g, 3.82 mmol) was added dropwise via syringe. The reaction mixture was stirred at reflux overnight, at which time the solution turned a clear dark brown color (formation of colloidal platinum). The solvent and any excess triethoxysilane was removed by vacuum distillation. The resulting oil was then distilled under vacuum to afford a clear, colorless liquid (92-95°C / 0.25 mm Hg, 0.70 g, 43%). ^{1}H-NMR (ppm, $CDCl_3$): δ 3.83 (q, 6H, $OC\underline{H}_2CH_3$); 3.10-0.75 (m, 9H, norbornyl-H); 1.42 (s, 9H, t-butyl-H); 1.18 (t, 9H, $OCH_2C\underline{H}_3$).

Poly[tert-Butyl 2-(trifluoromethyl)bicyclo[2.2.1]heptan-2-carboxylate-5-yl silsesquioxane] (**4-12**), Method A: Into a 10 mL round-bottom flask equipped with a magnetic stir bar was added **4-10** (1.00 g, 2.35 mmol) in 2 mL THF. Oxalic acid dihydrate (29.6 mg, 0.235 mmol) in 0.500 mL water was added and the resulting mixture was stirred at 80°C for 4 h. The polymer was twice

precipitated into water, filtered, and dried *in vacuo* to give a clear-white powder (0.50 g, 63%). ^{1}H-NMR (ppm, $CDCl_3$): δ 2.83-0.70 (m, 9H, norbornyl-H); 1.45 (s, 9H, t-butyl-H). FTIR (cm^{-1}, KBr): 2986, 2889, 1737 (C=O), 1481, 1460, 1404, 1373, 1291, 1260, 1240, 1178, 1143, 1117, 1086, 1020, 907, 846. GPC (THF): M_w = 1,170; M_n = 980; PDI = 1.19.

Poly[tert-Butyl 2-(trifluoromethyl)bicyclo[2.2.1]heptan-2-carboxylate-5-yl silsesquioxane] (**4-12**), Method B: Into a 10 mL vial containing 1.2 mL MeOH was added **4-10** (0.5 g, 1.17 mmol). Sodium hydroxide (2.52 mg, 0.063 mmol) in 0.063 mL water was added and the resulting solution was shaken and allowed to stand without stirring overnight. The polymer was precipitated into water, filtered, and dried *in vacuo* to give a white powder (0.300 g, 81%). ^{1}H-NMR (ppm, $CDCl_3$): δ 2.80-0.70 (m, 9H, norbornyl-H); 1.47 (s, 9H, t-butyl-H). FTIR (cm^{-1}, KBr): 2975, 2883, 1737 (C=O), 1456, 1398, 1369, 1292, 1253, 1171, 1151, 1118, 1079, 1016, 842. GPC (THF): M_w = 2550; M_n = 2200; PDI = 1.16.

Hydridodimethylsilyloxy-POSS capped with tert-Butyl 2-(trifluoromethyl)bicyclo[2.2.1]heptan-2-carboxylate (**4-16**): Into a 100 mL three-neck flask equipped with a magnetic stir bar and reflux condenser was added hydridodimethylsilyloxy-POSS (2.00 g, 2.05 mmol) to *tert*-butyl 2-(trifluoromethyl)bicyclo[2.2.1]hept-5-en-2-carboxylate (**2-5**, 4.35 g, 16.6 mmol) in 50 mL dry toluene. The condenser was fitted with a drying tube loaded with Drierite ($CaSO_4$) such that the reaction was exposed to dry air. Karstedt's catalyst (2% Pt(0) complexed with divinylsiloxane in a xylene solution, 4.00 mg, 20 μmol) was then added to the stirred solution. The reaction mixture was stirred at

100°C overnight, at which time the solution turned a clear dark brown color (formation of colloidal platinum). Activated carbon (~5 g) was added to adsorb platinum. The mixture was filtered through Dicalite (diatomaceous earth) using a fritted funnel and washed with hexane (~100 mL). The resulting solution was subjected to rotary evaporation to remove most of the hexane and toluene. The rest of the solution was precipitated into methanol, filtered, and collected to yield a white powder (3.70 g, 60%). ^{1}H-NMR (ppm, $CDCl_3$): δ 1.90-0.90 (m, 9H, norbornyl-H); 1.45 (s, 9H, t-butyl-H); 0.17-0.03 (m, 6H, Si-CH_3). ^{19}F-NMR (ppm, $CDCl_3$): δ -64.6, -65.1, -67.1, -68.0 (3F). FTIR (cm^{-1}, KBr): 2945, 2858, 1737 (C=O), 1450, 1368, 1281, 1255, 1122, 907, 835, 779, 503.

Hydridosilsesquioxane partially capped with 3-(bicyclo[2.2.1]hept-5-en-2-yl)-1,1,1-trifluoro-2-(trifluoromethyl)propan-2-ol (**4-19**): Into a 250 mL round-bottom flask equipped with a magnetic stir bar and reflux condenser was added NBHFA (**2-1**, 27.1 g, 98.8 mmol) to Dow Corning's FOx-16 (Flowable Oxide, hydridosilsesquioxane, which is obtained as a solution in methylisobutyl ketone, MIBK – evaporated to dryness before use) (4.77 g, 89.8 mmol) in 100 mL toluene. The condenser was fitted with a drying tube loaded with Drierite ($CaSO_4$) such that the reaction was exposed to dry air. Hexachloroplatinic acid (1.84 g, 4.49 mmol) was then added to the stirred solution. The reaction mixture was stirred at 100°C overnight, at which time the solution turned a clear light brown color (formation of colloidal platinum). FT-IR analysis of the reaction mixture indicated incomplete hydrosilylation by the presence of an Si-H peak. The reaction mixture was stirred at 100°C for another 4 days. FT-IR analysis still

indicates the presence of Si-H. The reaction was stopped and worked up nevertheless. Activated carbon (~20 g) was added to adsorb platinum. The mixture was filtered through Dicalite (diatomaceous earth) using a fritted funnel and washed with dichloromethane (~100 mL). The resulting solution was subjected to rotary evaporation to remove excess dichloromethane and toluene. The polymer was again dissolved in dichloromethane, and hydrogen was bubbled through the solution for 30 min. The mixture was stirred with activated carbon and filtered through Dicalite. The resulting solution was precipitated into hexanes, filtered, and dried at 50°C under vacuum to yield a yellowish-brown powder (4.12 g, 14%). Excess NBHFA was recovered by distillation. ^{1}H-NMR (ppm, DMSO-d_6): δ 7.60 (bs, 1H, O<u>H</u>); 3.59 (bs, 1H, Si-<u>H</u>); 2.40-0.30 (m, 12H, norbornyl-<u>H</u>). ^{19}F-NMR (ppm, DMSO-d_6): δ -76.02 (m, 6F, C<u>F</u>$_3$). FTIR (cm^{-1}, KBr): 3592, 3383, 2951, 2882, 2237 (Si-H), 1460, 1204, 1138, 1049, 967, 932, 882, 711, 664. GPC (THF): M_w = 7,470; M_n = 3,010; DPI = 2.482. A_{157} = 1.85 μm^{-1}. DSC: ~77°C.

4-Phthalimidomethylacridine (**6-5**): *N*-hydroxymethylphthalimide (9.67 g, 54.6 mmol) was added to a solution of acridine (9.78 g, 54.6 mmol) in 95% H_2SO_4 (125 mL) and stirred at room temperature overnight. The reaction mixture was diluted by dropwise addition to ice water (125 mL), and 15% NH_4OH (250 mL) was added, with ice cooling, to the resulting solution until a pH of 8-9 was obtained. The precipitate (a mixture of acridine, 4-phthalimidomethylacridine, and 4,5-diphthalimidomethylacridine) was collected by vacuum filtration, washed with water, and dried. The desired product, 4-phthalimidomethylacridine, was

separated by collecting the first band (of three) in a silica gel column using a 95:5 v/v toluene:ethyl acetate solution. After evaporation, drying, and recrystallization (same solvent mixture), light yellow powder (3.58 g, 19%) was obtained and its melting point determined (196-198°C, *lit*.[149] = 199-201°C). ^{1}H-NMR (ppm, $CDCl_3$): δ 5.75 (s, 2H, $C\underline{H}_2$); 7.40-7.7.99 (m, 9H, Ar-$\underline{H}$); 8.22 (d, 1H, C_5-$\underline{H}$); 8.72 (s, 1H, C_9-$\underline{H}$).

4-Aminomethylacridine (**6-6**): Concentrated hydrochloric acid (6 M, 200 mL) was added to 4-phthalimidomethylacridine (**6-5**, 3.58 g, 10.6 mmol) and the reaction mixture was stirred at 100°C for 2 hrs. After cooling, the precipitate (phthalic anhydride) was filtered and set aside. The filtrate was collected and the solvent evaporated, yielding a bright yellow powder (amine in its salt form). The amine salt was dissolved in water and neutralized with 5% NaOH. Extraction (toluene) and evaporation yielded the free amine (2.90 g, 93%). ^{1}H-NMR (ppm, $CDCl_3$): δ 2.23 (s, 2H, $N\underline{H}_2$); 4.51 (s, 2H, $C\underline{H}_2$); 7.41-7.99 (m, 6H, Ar-$\underline{H}$); 8.22 (d, 1H, C_5-$\underline{H}$); 8.73 (s, 1H, C_9-$\underline{H}$).

N-(Acridin-4-ylmethyl)-4-vinylbenzamide (**6-7**): Under a blanket of N_2, 4-aminomethylacridine (1.00 g, 4.81 mmol) was added to 10 mL of THF cooled to 0°C. Diisopropylethylamine (620 mg, 4.81 mmol) and 4-vinylbenzoic acid (712 mg, 4.81 mmol) was then added to the solution, followed by the addition of dicyclohexylcarbodiimide (1.09 g, 5.29 mmol) dissolved in 5 mL THF. The reaction mixture was stirred under N_2 at 25°C for 3 hrs. The mixture was then diluted with 15 mL of THF, and the white precipitate (dicyclohexylurea) was separated by gravity filtration. The filtrate was washed with water (3 x 20 mL),

10% $NaHCO_3$ solution (20 mL), and finally with saturated NaCl (20 mL). The organic layer was dried over $MgSO_4$. Evaporation *in vacuo* yielded crude product (955 mg, 59%). Column chromatography (silica, 9:1 toluene:ethyl acetate) was used to obtain pure product (180 mg, 11%). ^{1}H-NMR (ppm, $CDCl_3$): δ 5.26 (d, 1H, *trans*-C$\underline{H}_2$=CHR); 5.28 (d, 2H, C$\underline{H}_2$); 5.76 (d, 1H, *cis*-C$\underline{H}_2$=CHR); 6.61-6-73 (dd, 1H, CH_2=C$\underline{H}$R); 7.38,7.74 (dd, 4H, phenyl-$\underline{H}$); 7.43-8.03 (m, 6H, acridine-$\underline{H}$); 8.25 (d, 1H, C_5-H); 8.51 (t, 1H, N$\underline{H}$); 8.78 (s, 1H, C_9-H).

Poly[styrene-co-N-(acridin-4-ylmethyl)-4-vinylbenzamide] (**6-8**): Styrene (2.75 g, 26.4 mmol), AIBN (43.7 mg, 266 μmol), and *N*-(acridin-4-ylmethyl)-4-vinylbenzamide (**6-7**, 90 mg, 266 μmol) was added to tetrahydrofuran (10 mL). The solution was frozen in liquid N_2, evacuated to 5 torr for 5 min, flushed with N_2, and warmed to room temperature to remove O_2 by equilibration. This process was repeated two more times. The solution was then stirred overnight under N_2 at 80°C. The product was precipitated by dropwise addition of the reaction mixture to a stirred solution of methanol (100 mL). The solid was filtered and dried to give a light-yellow powder (1.80 g, 63%). ^{1}H-NMR (ppm, $CDCl_3$): δ 7.00-6.20 (m, Ar-$\underline{H}$); 1.9-0.9 (m, aliphatic-$\underline{H}$). GPC (THF): M_n = 10,400; M_w = 18,600; PDI = 1.788; λ_{max} (acridine) = 357 nm.

9-Methylacridine (**6-9**): Powdered $ZnCl_2$ (1.69 g, 12.41 mmol) was added to a stirred mixture of diphenylamine (1.00 g, 5.91 mmol) and glacial acetic acid (0.60 mL, 10.34 mmol). The resulting mixture was refluxed at 220°C for 14 hrs. A melt formed which was treated with hot water (10 mL). The aqueous phase was decanted and 20 mL acetone was added to the residue. After 15 min stirring

the mixture was filtered and the remaining dark green crystals were carefully washed with a small amount of acetone. The raw crystals were extracted several times with boiling water (100 mL altogether). By addition of ammonium hydroxide to the aqueous dark brown solution the product precipitated as yellow flakes. They were filtered off, washed with water, and dried at 50°C (*Yield* = 0.53 g, 46%; *mp* = 113-115°C, *lit*.[152] = 115-116°C). ^{1}H-NMR (ppm, $CDCl_3$): δ 3.10 (s, 3H, C<u>H</u>$_3$); 7.52-7.56 (m, 2H, Ar-<u>H</u>); 7.71-7.78 (m, 2H, Ar-<u>H</u>); 8.19-8.25 (m, 4H, Ar-<u>H</u>). FTIR (cm^{-1}, KBr): 3050 (ArH), 2930 (CH alkyl). MS (CI+) *m/z* 194 (M^+).

9-Bromomethylacridine (**6-10**): 9-Methylacridine (**6-9**, 0.20 g, 1.04 mmol) was added to 10 mL carbon tetrachloride. *N*-bromosuccinimide (0.22 g, 1.24 mmol) and benzoyl peroxide (5 mg) was added and the resulting mixture stirred under reflux for 24 hrs. The solution was filtered hot to remove succinimide. The filtrate was allowed to cool to crystallize product. The precipitated crystals were filtered and washed with cold water to remove any excess succinimide and *N*-bromosuccinimide (*Yield* = 0.15 g, 53%; *mp* = 164-168°C, *lit*.[167] = 169-170°C). ^{1}H-NMR (ppm, $CDCl_3$): δ 5.42 (s, 2H, -C<u>H</u>$_2$-); 7.64-8.29 (m, 8H, Ar-<u>H</u>).

4-Vinylbenzoic acid acridin-9-ylmethyl ester (**6-11**): 4-Vinylbenzoic acid (0.25 g, 1.69 mmol) and 1,8-diazobicyclo[7.4.0]undec-7-ene (0.26 g, 1.69 mmol) was added to 20 mL benzene. 9-Bromomethylacridine (0.46 g, 1.69 mmol) was dissolved in 10 mL benzene and slowly added to the reaction mixture. The

---

[167] Lehr, R. E.; Kaul, P. N. *J. Pharm. Sci.* **1975**, *64(6)*, 950-953.

resulting solution was stirred at room temperature for 15 hrs. The DBU-HBr salt was removed by filtration and the filtrate was washed with water (3 x 30 mL). The organic layer was dried with $MgSO_4$ and evaporated to yield desired product (*Yield* = 0.40 g, 70%). ^{1}H-NMR (ppm, $CDCl_3$): δ 5.33 (d, 1H, *trans*-C$\underline{H}_2$=CHR); 5.79 (d, 1H, *cis*-C$\underline{H}_2$=CHR); 6.34 (s, 2H, CH_2); 6.62-6-73 (dd, 1H, CH_2=C$\underline{H}$R); 7.37,7.91 (dd, 4H, phenyl-$\underline{H}$); 7.60-7.82, 8.25-8.45 (m, 8H, acridine-$\underline{H}$).

Poly[styrene-co-4-vinylbenzoic acid acridin-9-ylmethyl ester] (**6-12**): A solution of 4-Vinylbenzoic acid acridin-9-ylmethyl ester (44.6 mg, 0.132 mmol), styrene (1.36 g, 13.0 mmol) and AIBN (32.4 mg, 0.197 mmol) in 10 mL dry THF was heated at 80°C under N_2 for 24 hours. The polymer was twice precipitated into methanol, collected by filtration and dried under vacuo to yield a white powder (1.08 g, 77%). ^{1}H-NMR (ppm, $CDCl_3$): δ 7.24-6.85 (bs, Ar-$\underline{H}$), 6.70-6.25 (bs, Ar-$\underline{H}$), 2.04-1.60 (m, aliphatic-$\underline{H}$), 1.60-1.20 (m, aliphatic-$\underline{H}$). IR (cm^{-1}, KBr): 3024, 2920, 1600, 1491, 1451, 1262, 1023, 759, 695. GPC (THF): M_n = 8,500; M_w = 17,300; DPI = 2.0.

9-(2-Hydroxyethyl)acridine (**6-13**): 9-Methylacridine (**6-9**, 0.50 g, 2.59 mmol) was added to 10 mL of 36.5-38% formaldehyde solution and the resulting mixture stirred under reflux (110°C) for 4 hrs. The solution was allowed to cool overnight. The precipitated crystals were filtered and washed with water. Additional product was obtained by filtering the yellow solid formed in the filtrate after the addition of water. The crude crystals were recrystallized from 75% ethanol/water (*Yield* = 0.21g, 36%; *mp* = 155-157°C, *lit.*[152] = 155-156°C). ^{1}H-NMR (ppm, $CDCl_3$): δ 2.32 (s, 1H, O$\underline{H}$); 3.92 (t, 2H, Acr-C$\underline{H}_2$); 4.17 (t, 2H, C$\underline{H}_2$-

OH); 7.49-7.55 (m, 2H, Ar-H); 7.65-7.72 (m, 2H, Ar-H); 8.11 (d, 2H, Ar-H); 8.27 (d, 2H, Ar-H). FTIR (cm^{-1}, KBr): 3242 (OH), 2945 (ArH), 2858 (CH alkyl). MS (CI^+) *m/z* 223 (M^+); 206 ($M^+ - H_2O$).

9-[2-(4-Vinylbenzyloxy)ethyl]acridine (**6-14**): Potassium carbonate (62 mg, 448 µmol) and 9-(2-hydroxyethyl)acridine (**6-13**, 100 mg, 448 µmol) was added to 20 mL dried (CaH_2) dimethylsulfoxide. To this mixture was added 4-vinylbenzylchloride (68 mg, 448 µmol). The reaction mixture was stirred under nitrogen at room temperature for 24 hrs. Benzene (10 mL) was added to dilute the reaction mixture, and the entire mixture was washed with water (3 x 30 mL) and 10% sodium bicarbonate (30 mL). The organic layer was dried with $MgSO_4$ and evaporated to yield desired product (*Yield* = 50 mg, 33%). ^{1}H-NMR (ppm, $CDCl_3$): δ 3.90 (t, 2H, acridine-CH_2); 4.19 (t, 2H, acridine-CH_2-CH_2-O); 4.56 (s, 2H, phenyl-CH_2-O); 5.25 (d, 1H, *trans*-CH_2=CHR); 5.74 (d, 1H, *cis*-CH_2=CHR); 6.63-6.75 (dd, 1H, CH_2=CHR); 7.30-7.40 (dd, 4H, phenyl-H); 7.44-8.26 (m, 8H, acridine-H).

Poly[styrene-co-9-[2-(4-vinylbenzyloxy)ethyl]acridine] (**6-15**): A solution of 9-[2-(4-vinylbenzyloxy)ethyl]acridine (**6-14**, 49.0 mg, 0.145 mmol), styrene (1.49 g, 14.3 mmol) and AIBN (23.8 mg, 0.145 mmol) in 10 mL dry THF was heated at 80°C under N_2 for 24 hours. The polymer was twice precipitated into methanol, collected by filtration and dried *in vacuo* to yield a white powder (1.29 g, 84%). ^{1}H-NMR (ppm, $CDCl_3$): δ 7.24-6.88, 6.72-6.30, 2.15-1.60, 1.60-1.20. IR (cm^{-1}, KBr): 3024, 2915, 1600, 1491, 1451, 1366, 1028, 908, 749, 695. GPC (THF): M_n = 7,550; M_w = 17,700; PDI = 2.3.

General procedure for the preparation of polymers **7-1** *to* **7-7**: Chloroformates of primary alcohols were prepared by adding the alcohol to a cold (5°C) 20 wt% solution of phosgene (2.0 equiv) in benzene. The solution was warmed to room temperature and stirred overnight. Excess phosgene was carefully removed by bubbling a stream of dry argon through the reaction mixture, and the solvent was evaporated to give the crude chloroformate. The chloroformate could be distilled under vacuum, but was used in the next step without further purification. For the preparation of chloroformates of secondary alcohols, triethylamine (1.2 equiv) was added dropwise to the reaction mixture described above. The excess phosgene was removed as before, and the solution was diluted with dry ether and filtered over celite. Evaporate of the solvent gave the crude chloroformate, which was added (1.2 equiv) dropwise to a solution of poly(4-hydroxystyrene) (1 equiv) and triethylamine (1.2 equiv) in dry THF, following the procedure for **7-1** below. The solution was stirred at room temperature for 24 h, and the polymer was twice precipitated into methanol, collected by vacuum filtration, and dried *in vacuo*.

Poly(4-isopropyloxycarbonyloxystyrene) (**7-1**): Isopropyl chloroformate (1M solution in toluene, 12.1 g, 100 mmol) was added dropwise to a solution of poly(4-hydroxystyrene) (M_w = 29,200, 10.00 g, 83.3 mmol) from Hoechst Celanese and triethylamine (10.1 g, 100 mmol) in 500 mL dry THF. The solution was stirred at room temperature for 24 hrs. The polymer was twice precipitated into methanol, collected by filtration, and dried *in vacuo* to yield a white powder (10.2 g, 60%). ^{1}H-NMR (ppm, $CDCl_3$): δ 7.00-6.63, 6.63-6.17, 5.02-4.83, 2.00-

1.50, 1.55-1.10. FTIR (cm^{-1}, KBr): 2984, 2929, 1755, 1506, 1262, 1212, 1098, 913. TGA: Onset at 240°C.

Poly(1-phenylethyloxycarbonyloxystyrene) (**7-2**): ^{1}H-NMR (ppm, $CDCl_3$): δ 7.45-7.20, 6.90-6.60, 6.60-6.10, 5.85-5.68, 1.70-1.55, 1.50-1.10. FTIR (cm^{-1}, KBr): 3033, 2979, 2921, 1760, 1504, 1253, 1204, 1064, 1016, 899, 832, 755, 697. TGA: Onset at ~180°C.

Poly(1,7,7-trimethylbicyclo[2.2.1]hept-2-yloxycarbonyloxystyrene) (**7-3**): ^{1}H-NMR (ppm, $CDCl_3$): δ?7.00-6.65, 6.60-6.20, 4.70-4.55, 2.00-0.80. FTIR (cm^{-1}, KBr): 2955, 2878, 1756, 1504, 1456, 1388, 1258, 1214, 1185, 1059, 1015, 958, 832, 774. TGA: Onset at ~100°C.

Poly(1-ethylpropyloxycarbonyloxystyrene) (**7-4**): ^{1}H-NMR (ppm, $CDCl_3$): δ 7.05-6.65, 6.65-6.10, 4.73-4.55, 1.80-1.55, 1.55-1.10, 1.07-0.80. FTIR (cm^{-1}, KBr): 2965, 2931, 2878, 1751, 1504, 1461, 1257, 1219, 1103, 1011, 914, 822, 774. TGA: Onset at ~220°C.

Poly(cyclopropylmethyloxycarbonyloxystyrene) (**7-5**): ^{1}H-NMR (ppm, $CDCl_3$): δ **7**.10-6.65, 6.65-6.20, 4.15-4.00, 1.90-1.10, 0.70-0.50, 0.49-0.25. FTIR (cm^{-1}, KBr): 3081, 3013, 2921, 2849, 1756, 1504, 1451, 1403, 1345, 1253, 1214, 1050, 1011, 948, 827, 779. TGA: Onset at ~250°C.

Poly(2,2-dimethylpropyloxycarbonyloxystyrene) (**7-6**): ^{1}H-NMR (ppm, $CDCl_3$): δ?7.20-6.68, 6.68-6.20, 4.05-3.85, 2.0-1.10, 1.10-0.80. FTIR (cm^{-1}, KBr): 3037, 2955, 2868, 1761, 1601, 1509, 1480, 1369, 1248, 1209, 1050, 1016, 958, 914, 832, 779. TGA: Onset at ~300°C.

Poly(1,2-dimethylpropyloxycarbonyloxystyrene) (**7-7**): ^{1}H-NMR (ppm, $CDCl_3$): δ 7.00-6.65, 6.65-6.17, 4.75-4.55, 2.00-1.80, 1.80-1.50, 1.50-1.20, 1.05-0.80. FTIR (cm^{-1}, KBr): 2960, 2926, 2873, 1756, 1601, 1504, 1456, 1369, 1262, 1214, 1088, 1016, 914, 779. TGA: Onset at ~230°C.

General procedure for the synthesis of polymers **7-12** *to* **7-14**: The acrylate or methylacrylate (1 equiv) was dissolved in dry THF and AIBN (0.01 equiv) was added to the solution. After several freeze-pump-thaw cycles, the solution was refluxed at 80°C for 24 h. Precipitation of the polymer into methanol, followed by vacuum filtration and drying (50°C) *in vacuo*, yielded the desired polymer. Both acrylates of **7-13** and **7-14** are available commercially. The methylacrylate used to make polymer **7-12** was prepared by adding methacryloyl chloride (1.2 equiv) to a solution of 1-phenylethyl alcohol (1 equiv) and dry (CaH_2) pyridine (1.2 equiv) in dry benzene. The solution was heated for 5 h at 50°C. The reaction was poured into water, the layers were separated, and the aqueous layer was extracted with ether (3x). The combined organic layers were washed with 2*M* HCl (3x), water, 1*M* NaOH, water, and brine. The organic layer was dried over MgSO4, filtered, and evaporated to yield crude monomer which was polymerized in the next step without further purification.

Poly(1-phenylethyl methacrylate) (**7-12**): ^{1}H-NMR (ppm, $CDCl_3$): δ **7**.40-7.10, 5.70-5.40, 2.00-1.60, 1.60-1.20, 0.90-0.30. FTIR (cm^{-1}, KBr): 3086, 3033, 2984, 2926, 1712, 1475, 1446, 1287, 1156, 1108, 1059, 1030, 759, 682. TGA: Onset at ~170°C.

Poly(1,7,7-trimethylbicyclo[2.2.1]hept-2-yl acrylate) (**7-13**): ^{1}H-NMR (ppm, $CDCl_3$): δ?4.50-4.20, 2.10-1.50, 1.50-1.20, 1.20-0.70. FTIR (cm^{-1}, KBr): 2950, 2873, 1717, 1673, 1630, 1480, 1451, 1388, 1291, 1161, 1108, 1050, 1006, 938, 677. TGA: Onset at ~100°C.

Poly(t-butyl acrylate) (**7-14**): TGA: Uncatalyzed onset at ~200°C, Catalyzed onset at ~50°C.

4-Diethoxymethylstyrene (**7-15**): A trace amount of $HClO_4$ (in the tip of a capillary) was added to a mixture of 4-vinylbenzaldehyde (2.50 g, 18.9 mmol), triethylorthoformate (3.09 g, 20.8 mmol), and ethanol (2 mL). The mixture was stirred for 30 min at 45°C. When the reaction was completed the mixture was cooled and neutralized with an alcohol solution of KOH. Vacuum distillation (127°C at 1.7 torr) of the mixture yielded 2.00 g (51%) of product. ^{1}H-NMR (ppm, $CDCl_3$): δ 7.45-7.35 (m, 4H, Ar-H), 6.85-6.65 (dd, 1H, CH_2=CHR); 5.77-5.71 (d, 1H, *cis*-CH_2=CHR); 5.48 (s, 1H, Ar-CH); 5.25-5.21 (d, 1H, *trans*-CH_2=CHR); 3.65-3.47 (m, 4H, CH_2); 1.25-1.19 (t, 6H, CH_3). MS (CI+) *m/z* 207 (M+) – Calculated: 207.138505, Found: 207.138347. GC: 97.6% purity.

Poly(4-diethoxymethylstyrene) (**7-16**): A solution of 4-diethoxymethylstyrene (**7-15**, 2.00 g, 9.71 mmol) and AIBN (19.0 mg, 117 μmol) in dry THF (50 mL) was heated at 80°C for 24 hrs. The polymer was twice precipitated into methanol, collected by filtration, and dried *in vacuo* to yield product (0.60 g, 30%). ^{1}H-NMR (ppm, $CDCl_3$): δ 7.80-7.30, 6.80-6.40, 1.80-1.20. FTIR (cm^{-1}, KBr): 2970, 2921, 2868, 1915, 1615, 1509, 1446, 1340, 1296, 1450, 914, 846, 808. TGA: Onset at ~100°C.

4-(2,3-Hydroxy-3-methylbutan-2-yl)styrene (**7-17**): Oven-dried magnesium filings (5.00 g, 206 mmol) were charged to a 500 mL round-bottom flask containing 200 mL distilled THF. The reaction mixture was cooled to 0°C and 4-chlorostyrene (27.2 g, 196 mmol) was added dropwise over 30 min. The solution was heated at reflux for 1 hr and then allowed to cool to room temperature. 3-Hydroxy-3-methyl-2-butanone (10.00 g, 98.0 mmol) was added dropwise and the solution was stirred for 16 h under a nitrogen atmosphere. The resulting mixture was diluted with 200 mL diethyl ether. Hydrogen chloride (6 *N*) was added with stirring until the pH was slightly acidic (pH = 6). The phases were separated and the organic phase was washed with several small portions of deionized water followed by brine. The solution was dried over Na_2SO_4 and the solvent removed *in vacuo*. The product was purified by recrystallization from hexanes to give 11.10 g (55 %) of the desired compound as white crystals, mp = 74-75°C. ^{1}H-NMR (ppm, $CDCl_3$): δ 7.46-7.34 (m, 4H, Ar-H); 6.76-6.64 (dd, 1H, CH_2=CHR); 5.77-5.70 (d, 1H, *cis*-CH_2=CHR); 5.25-5.20 (dd, 1H, *trans*-CH_2=CHR); 2.53 (s, 1H, OH); 1.91 (s, 1H, OH); 1.62 (s, 3H, CH_3); 1.25 (s, 3H, CH_3); 1.07 (s, 3H, CH_3). FTIR (cm^{-1}, KBr): 3378, 2089, 2969, 2935, 1625, 1506, 1446, 1401, 1367, 1158, 1088, 1053, 988, 919, 839.

Poly[4-(2,3-hydroxy-3-methylbutan-2-yl)styrene] (**7-18**): A solution of 4-(2,3-hydroxy-3-methylbutan-2-yl)styrene (**7-17**, 1.00 g, 4.85 mmol) and AIBN (8.77 mg, 53 μmol) in dry THF was heated at 80°C for 24 hrs. The polymer was twice precipitated in diethyl ether, collected by filtration, and dried *in vacuo* to yield a white powder (0.225 g, 23%). ^{1}H-NMR (ppm, DMSO-d_6): δ 7.40-7.00

(bs, Ar-H); 6.70-6.10 (bs, Ar-H); 4.49 (bs, ArCRCH$_3$OH); 4.09 (bs, RCCH$_3$CH$_3$OH); 3.34 (bm, CH$_3$); 1.90-0.70 (m, aliphatic-H). FTIR (cm^{-1}, KBr): 3437 (OH), 2974, 2924, 1506, 1451, 1416, 1367, 1337, 1167, 1083, 1013, 958, 914, 839, 799, 590. TGA: Onset ~270-280°C. GPC (THF): M_n = 7,560; M_w = 12,000; PDI = 1.59.

4-(Methoxy)styrene: 4-Acetoxystyrene (10.00 g, 61.7 mmol) was added to a solution of potassium hydroxide (7.80 g, 139 mmol) in methanol (100 mL) at 0°C. The reaction mixture was stirred at 0°C for 5 hrs. Methyl iodide (19.7 g, 139 mmol) was added and the resulting solution was stirred at room temperature for 18 hrs. The reaction mixture was diluted with 100 mL water and extracted with diethyl ether (3 x 100 mL). The combined organic extracts were washed with 1 M NaOH, deionized water, and brine, dried with $MgSO_4$, and finally concentrated under reduced pressure to yield pure product as a clear light yellow oil (6.20 g, 75%). ^{1}H-NMR (ppm, $CDCl_3$): δ 7.36-7.32 (d, 2H, Ar-H); 6.88-6.82 (d, 2H, Ar-H); 6.71-6.60 (dd, 1H, CH$_2$=CHR); 5.63-5.56 (d, 1H, cis-CH$_2$=CHR); 5.14-5.09 (dd, 1H, trans-CH$_2$=CHR); 3.80 (s, 3H, OCH$_3$). FTIR (cm^{-1}, KBr): 3007, 2955, 2832, 1609, 1511, 1460, 1301, 1250, 1173, 1112, 1035, 989, 830.

Poly[4-(methoxy)styrene-co-4-(2,3-hydroxy-3-methylbutan-2-yl)styrene] (**7-20**): A solution of 4-(2,3-hydroxy-3-methylbutan-2-yl)styrene (**7-17**, 1.00 g, 4.85 mmol), 4-methoxystyrene (0.65 g, 4.85 mmol) and AIBN (17.5 mg, 107 μmol) in dry THF was heated at 80°C for 24 hrs. The polymer was twice precipitated in a 50:50 solution of diethyl ether:hexanes, collected by filtration, and dried *in vacuo* to yield a white powder (0.32 g, 19%). ^{1}H-NMR (ppm,

$CDCl_3$): δ 7.40-6.90 (bs, Ar-H); 6.90-6.20 (bs, Ar-H); 3.72 (bs, OCH_3); 2.20-0.70 (bm, aliphatic-H). FTIR (cm^{-1}, KBr): 3457 (OH), 2986, 2925, 2848, 1609, 1511, 1455, 1368, 1245, 1086, 1035, 963, 825, 805, 595. TGA: Onset ~240°C. GPC (THF): M_n = 7,170; M_w = 12,700; PDI = 1.77.

4-(n-octoxy)benzaldehyde: 1-Iodooctane (10.00 g, 41.6 mmol) was added to a mixture of 4-hydroxybenzaldehyde (5.59 g, 45.8 mmol) and potassium carbonate (11.51 g, 83.3 mmol) in acetone (200 mL). The reaction mixture was stirred under reflux for 48 h and then allowed to cool to room temperature. Diethyl ether (200 mL) was added and the resulting mixture was washed with water (2 x 100 mL), 10 wt % aqueous Na_2CO_3 (100 mL), and brine (100 mL). The solution was dried over $MgSO_4$ and the solvent removed *in vacuo*. The product was isolated by flash column chromatography (100% dichloromethane) to yield the desired compound as a clear oil (6.00 g, 62%). ^{1}H-NMR (ppm, $CDCl_3$): δ 9.86 (s, 1H, HCOR); 7.82-7.79 (d, 2H, Ar-H); 6.99-6.95 (d, 2H, Ar-H); 4.01 (t, 2H, $ArOCH_2$); 1.76 (m, 2H, $ArOCH_2CH_2$); 1.50-1.23 (m, 10H, CH_2); 0.87 (t, 3H, CH_3). FTIR (cm^{-1}, KBr): 2920, 2850, 2731, 1690, 1596, 1571, 1501, 1461, 1426, 1387, 1312, 1257, 1212, 1158, 1108, 1013, 824, 615.

4-(n-octoxy)styrene: Potassium *t*-butoxide (3.11 g, 27.8 mmol) was slowly added to a solution of triphenylmethylphosphonium bromide (9.15 g, 25.6 mmol) in anhydrous (distilled from $CaSO_4$) benzene. 4-(n-Octoxy)benzaldehyde (5.00 g, 21.4 mmol) was slowly added and the reaction mixture was stirred at room temperature for 2 h. Flash column chromatography using silica gel and dichloromethane as eluent yielded product (3.85g, 78%). ^{1}H-NMR (ppm,

$CDCl_3$): δ 7.35-7.30 (d, 2H, Ar-H); 6.86-6.81 (d, 2H, Ar-H); 6.70-6.58 (dd, 1H, CH_2=CHR); 5.62-5.55 (d, 1H, *cis*-CH_2=CHR); 5.12-5.07 (d, 1H, *trans*-CH_2=CHR); 3.93 (t, 2H, $ArOCH_2$); 1.79-1.70 (m, 2H, $ArOCH_2CH_2$); 1.50-1.25 (m, 10H, CH_2); 0.87 (t, 3H, CH_3). FTIR (cm^{-1}, KBr): 2925, 2850, 1606, 1506, 1466, 1297, 1247, 1167, 1113, 1018, 988, 894, 834.

Poly[4-(n-octoxy)styrene-co-4-(2,3-hydroxy-3-methylbutan-2-yl)styrene] (**7-21**): A solution of 4-(2,3-hydroxy-3-methylbutan-2-yl)styrene (**7-17**, 1.00 g, 4.85 mmol), 4-octoxystyrene (1.13 g, 4.85 mmol) and AIBN (18.0 mg, 107 μmol) in dry THF was heated at 80°C for 24 hrs. The polymer was twice precipitated in hexanes, collected by filtration, and dried *in vacuo* to yield a white powder (0.60 g, 26%). ^{1}H-NMR (ppm, $CDCl_3$): δ 7.20-6.90 (bs, Ar-H); 6.90-6.20 (bs, Ar-H); 3.80 (bs, OCH_2CH_2); 1.90-0.870 (bm, aliphatic-H). FTIR (cm^{-1}, KBr): 3437 (OH), 2930, 2850, 1606, 1511, 1461, 1367, 1242, 1172, 1093, 1018, 953, 914, 829. TGA: Onset ~200°C. GPC (THF): M_n = 10,400; M_w = 19,400; PDI = 1.87.

4-(2-(2-methoxyethoxy)ethoxy)benzaldehyde: 1-Bromo-2-(2-methoxy-ethoxy)ethane (9.00 g, 49.2 mmol) was added to a mixture of 4-hydroxybenzaldehyde (6.60 g, 54.1 mmol) and potassium carbonate (13.6 g, 98.3 mmol) in acetone (200 mL). The reaction mixture was stirred under reflux for 48 h and then allowed to cool to room temperature. Diethyl ether (200 mL) was added and the resulting mixture was washed with water (2 x 100 mL), 10 wt % aqueous Na_2CO_3 (100 mL), and brine (100 mL). The solution was dried over $MgSO_4$ and the solvent removed *in vacuo*. The product was isolated by flash column chromatography (100% dichloromethane) to yield the desired compound

as a clear oil (6.70 g, 61%). ^{1}H-NMR (ppm, $CDCl_3$): δ 9.84 (s, 1H, HCOR); 7.81-7.77 (d, 2H, Ar-H); 7.00-6.97 (d, 2H, Ar-H); 4.21-4.19 (t, 2H, $ArOCH_2$); 3.87-3.84 (t, 2H, $ArOCH_2CH_2$); 3.71-3.66 (t, 2H, OCH_2CH_2O); 3.56-3.53 (t, 2H, OCH_2CH_2O); 3.35 (s, 3H, CH_3). FTIR (cm^{-1}, KBr): 3052, 2986, 2930, 2879, 2822, 1696 (CHO), 1598, 1578, 1506, 1306, 1265, 1163, 1107, 1050, 835, 738, 702.

4-(2-(2-methoxyethoxy)ethoxy)styrene: Potassium *t*-butoxide (4.36 g, 38.9 mmol) was slowly added to a solution of triphenylmethylphosphonium bromide (12.8 g, 35.9 mmol) in anhydrous (distilled from $CaSO_4$) benzene. 4-(2-(2-Methoxyethoxy)ethoxy)benzaldehyde (6.70 g, 29.9 mmol) was slowly added and the reaction mixture was stirred at room temperature for 2 h. Flash column chromatography using silica gel and dichloromethane as eluent yielded product (4.41 g, 66%). ^{1}H-NMR (ppm, $CDCl_3$): δ 7.34-7.28 (d, 2H, Ar-H); 6.88-6.83 (d, 2H, Ar-H); 6.69-6.58 (dd, 1H, CH_2=CHR); 5.62-5.55 (d, 1H, *cis*-CH_2=CHR); 5.12-5.08 (d, 1H, *trans*-CH_2=CHR); 4.15-4.11 (t, 2H, $ArOCH_2$); 3.86-3.82 (t, 2H, $ArOCH_2CH_2$); 3.72-3.69 (t, 2H, OCH_2CH_2O); 3.58-3.54 (t, 2H, OCH_2CH_2O); 3.37 (s, 3H, CH_3). FTIR (cm^{-1}, KBr): 3047, 2986, 2925, 2884, 1721, 1696, 1614, 1516, 1455, 1266, 1245, 1112, 1061, 825, 733, 702. MS (CI^+): *m/z* 223 (M^+), Calculated: 223.133420, Found: 223.133337.

Poly[4-(2-(2-methoxyethoxy)ethoxy)styrene-co-4-(2,3-hydroxy-3-methyl-butan-2-yl)styrene] (**7-22**): A solution of 4-(2,3-hydroxy-3-methylbutan-2-yl)styrene (**7-17**, 1.00 g, 4.85 mmol), 4-(2-(2-methoxyethoxy)ethoxy)styrene (216 mg, 0.971 mmol) and AIBN (10.5 mg, 64 μmol) in dry THF was heated at 80°C

for 24 h. The polymer was twice precipitated in diethyl ether, collected by filtration, and dried *in vacuo* to yield a white powder (0.31 g, 25%). TGA: Onset ~270°C. GPC: M_n = 13,400, M_w = 105,500, PDI = 7.87.

ROMP polymer of 1-bicyclo[2.2.1]hept-5-en-2-yl-2,3-dimethyl-2,3-dihydroxybutane (**7-23**): A solution of 1-bicyclo[2.2.1]hept-5-en-2-yl-2,3-dimethyl-2,3-dihydroxybutane (0.51 g, 2.43 mmol) and Grubb's ruthenium phenyl carbene (30 mg, 36 umol, 1.5 mol %) in dry THF (50 mL) was stirred at room temperature for 3 h. The polymer was twice precipitated in hexanes, collected by filtration, and dried in vacuo to yield polymer (0.30 g, 59%). ^{1}H-NMR (ppm, $CDCl_3$): δ 5.50-4.80 (C<u>H</u>=C<u>H</u>); 3.75-3.55 (CH=CHC<u>H</u>); 2.80-1.40 (C<u>H</u>$_2$); 1.40-1.00 (C<u>H</u>$_3$). FTIR (cm^{-1}, KBr): 3442, 2974, 2940, 2860, 1715, 1635, 1446, 1367, 1138, 963. GPC: M_n = 4,380, M_w = 7,540, PDI = 1.72.

Alternating copolymer of sulfur dioxide and 1-bicyclo[2.2.1]hept-5-en-2-yl-2,3-dimethyl-2,3-dihydroxybutane (**7-24**): Sulfur dioxide (1.22 g, 19.1 mmol) was condensed into a flask with THF (50 mL) cooled to -45°C (dry ice in acetonitrile). 1-Bicyclo[2.2.1]hept-5-en-2-yl-2,3-dimethyl-2,3-dihydroxybutane (2.00 g, 9.52 mmol) and *t*-butyl hydroperoxide (9.00 mg, 100 µmol, 1 mol%) was added and the solution was stirred at -45°C for 4 hrs. Hydroquinone (80 mg) in 5 mL THF was added to the reaction mixture to stop the polymerization. Any excess sulfur dioxide was evaporated upon cooling the reaction mixture to room temperature. The mixture was diluted with 20 mL THF and the polymer was twice precipitated in a 2% solution of triethyl amine in diethyl ether (300 mL). Drying *in vacuo* gave desired polymer (4.55 g). FTIR (cm^{-1}, KBr): 3422, 2974,

2935, 2735, 2676, 2487, 1720, 1640, 1476, 1431, 1396, 1297, 1187, 1128, 1028, 894, 600. TGA: Onset < 100°C.

Poly[tetramethylammonium-4-styrenesulfonate-co-4-(2,3-hydroxy-3-methyl-butan-2-yl)styrene] (**7-25**): This polymer was obtained from a previous graduate student. The details and synthesis of this polymer has been described previously.[168]

1-Bromo-2-(4-bromophenoxy)tetrafluoroethane (**8-5**): 4-Bromophenol (45.4 g, 262 mmol) was dissolved in 265 mL of 1.033 *N* potassium hydroxide in methanol. This solution was evaporated to dryness on a rotary evaporator and the resulting solid was dried at 140°C and 0.1 mm Hg. The solid (**8-4**) was mixed with 500 mL of DMSO under argon. 1,2-Dibromotetrafluoroethane (75.0 g, 289 mmol) was added dropwise at 30-40°C. The resulting mixture was heated to 60°C for 6 h. It was cooled to room temperature and diluted to 1 L with ice and water. The organic layer was separated and the aqueous solution was extracted with 2x50 mL of methylene chloride. The methylene chloride extracts were concentrated on a rotary evaporator and the residue combined with the original organic layer. This material was washed with 2x200 mL of water, dried over anhydrous magnesium sulfate, and filtered. The filtrate was distilled under reduced pressure giving 51.6 g (56%) of product, bp 60-65°C at 0.25 mm Hg. ^{1}H-NMR (ppm, $CDCl_3$): δ 7.51 (d, 2H, Ar-H); 7.08 (d, 2H, Ar-H). ^{19}F-NMR (ppm, $CDCl_3$): δ -68.5 (2F); -86.5 (2F).

---

[168] Medeiros, D. R. Ph.D. Dissertation, University of Texas at Austin, 1998.

Sodium 2-(4-bromophenoxy)tetrafluoroethanesulfinate (**8-6**): 1-Bromo-2-(4-bromophenoxy)tetrafluoroethane (**8-5**, 43.0 g, 122 mmol) was added under argon to a stirred mixture of 150 mL of distilled and deoxygenated water, sodium bicarbonate (21.6 g, 257 mmol), 150 mL of acetyl nitrile, and sodium dithionite (44.7 g, 257 mmol). This mixture was heated to 65°C resulting in a rapid gas evolution. Gas evolution ceased after about 1 h and the mixture was heated to 70-75°C for 3 h. It was cooled to about 10°C in an ice water bath and 200 mL of ethyl acetate was added. The mixture was filtered and the solid was washed with ethyl acetate. The combined filtrates were separated into aqueous and organic layers and the organic layer was washed with 4x25 mL of saturated aqueous sodium chloride solution. The organic layer was concentrated on a rotary evaporator to about ¼ its initial volume and filtered. The solid was washed with ethyl acetate. The combined organic solutions were concentrated to dryness on a rotary evaporator giving 37.5 g (86%) of white solid which was converted to the sulfonyl chloride without further purification. ^{1}H-NMR (ppm, CD_3OD): δ 7.47 (d, 2H, Ar-H); 7.11 (d, 2H, Ar-H). ^{19}F-NMR (ppm, CD_3OD): δ -83.9 (2F); -134.6 (2F).

2-(4-Bromophenoxy)tetrafluoroethanesulfonyl chloride (**8-7**): Sodium 2-(4-bromophenoxy)tetrafluoroethanesulfinate (**8-6**, 35.5 g, 98.9 mmol) was dissolved in a mixture of 70 mL distilled and deoxygenated water and 35 mL of 1,1,2-trichlorotrifluoroethane (CFC-113) in a round bottom flask equipped with a dry-ice condenser and cooled to 5-15°C. Chlorine gas (14.0 g, 198 mmol) was bubbled into this mixture over about 1 h. The resulting yellow mixture was

stirred 1 h without external cooling. It was warmed to 20°C and an additional 35 mL of CFC-113 was added. The organic layer was separated and the aqueous solution was extracted with 30 mL of CFC-113. The combined organic solutions were dried over anhydrous magnesium sulfate and concentrated on a rotary evaporator. The residue was distilled through a short Vigreux column giving 25.2 g (69%) of product, bp 80-87°C at 0.40 mm Hg. ^{1}H-NMR (ppm, $CDCl_3$): δ 7.52 (d, 2H, Ar-H); 7.10 (d, 2H, Ar-H). ^{19}F-NMR (ppm, $CDCl_3$): δ -78.9 (2F); -107.8 (2F).

*Lithium 2-(4-bromophenoxy)tetrafluoroethanesulfonat*e (**8-8**): Lithium hydroxide monohydrate (5.93 g, 141.3 mmol) was dissolved in 70 mL deoxygenated distilled water. THF (18 mL) was added and this solution was heated to 35°C. The heat source was removed and 2-(4-bromophenoxy)tetrafluoroethanesulfonyl chloride (**8-7**, 25.0 g, 67.3 mmol) was added dropwise over 45 min at a rate so that the exotherm maintained the solution at about 55°C. After the addition was complete, the solution was held at 55°C for an additional 1.5 h. The solution was cooled to room temperature. Its pH was adjusted to 7 by addition of concentrated hydrochloric acid and the aqueous solution was evaporated to dryness on the rotary evaporator. The solid was slurried with ether and filtered. The ether solution was treated with three volumes of hexane resulting in deposition of a white solid. The solid was filtered off and washed with hexane. The filtrate was evaporated and the residue was again precipitated from ether solution by addition of hexane. The combined precipitates were recrystallized from acetonitrile with cooling in the refrigerator with the

filtrate concentrated several times to collect additional fractions. The combined recrystallized product was dissolved in ether, filtered, and concentrated on a rotary evaporator. The product was dried at 100°C and 0.1 mm Hg giving 20.3 g (84%) of product as a white solid. ^{1}H-NMR (ppm, CD_3OD): δ 7.46 (d, 2H, Ar-H); 7.10 (d, 2H, Ar-H). ^{19}F-NMR (ppm, $CDCl_3$): δ -83.7 (2F); -119.0 (2F).

Lithium 2-(4-ethenylphenoxy)tetrafluoroethanesulfonate (**8-9**): A 1 L autoclave was charged with lithium 2-(4-bromophenoxy)tetrafluoroethane-sulfonate (10.0 g, 27.9 mmol), acetonitrile (30 mL), $Pd(OAc)_2$ (125 mg, 0.557 mmol), tri-*o*-tolylphosphine (339 mg, 1.11 mmol), and triethylamine (30 mL). The autoclave was closed, cooled, evacuated, and charged with ethylene to 150 psi. The mixture was heated with stirring to 85°C for 24 h, holding the gas pressure at 200 psi by venting or adding ethylene as needed. The mixture was cooled to room temperature and vented to atmospheric pressure. The autoclave contents were recovered using a mixture of acetonitrile and ether to rinse. The mixture was treated with lithium hydroxide monohydrate (1.5 g) in 25 mL water with vigorous stirring and filtered through celite. The celite was washed with acetonitrile and ether. The combined filtrates were evaporated to dryness at 75-80°C and 5 mm Hg. The residue was extracted with 100 mL ether and filtered. The filtrate was diluted with 100 mL hexane and the resulting precipitate was collected, precipitated a second time from a mixture of ether and hexane and dried at 65°C and 0.20 mm Hg. Additional product was obtained by concentrating the above ether and hexane filtrates and reprecipitating the residue for a total yield of 4.62 g (54%) of product. ^{1}H-NMR (ppm, Acetone-d_6): δ 7.51 (d, 2H, Ar-H);

7.22 (d, 2H, Ar-H); 6.82-6.71 (dd, 1H, ArCH=CH_2); 5.84-5.77 (d, 1H, *cis*-ArCH=CH_2); 5.28-5.23 (d, 1H, *trans*-ArCH=CH_2). ^{19}F-NMR (ppm, CD_3CN): δ -82.4 (2F); -118.2 (2F).

Poly[styrene-co-lithium 2-(4-ethenylphenoxy)tetrafluoroethanesulfonate] (**8-16**): Into a 50 mL round-bottom flask equipped with a magnetic stir bar and reflux condenser was added lithium 2-(4-ethenylphnoxy)tetrafluoroethane-sulfonate (**8-9**, 0.50 g, 1.63 mmol), styrene (1.53 g, 14.7 mmol), and AIBN (27.0 mg, 0.16 mmol) in 15 mL THF. The solution was frozen, evacuated, purged with argon, and thawed several times and then heated under argon at 80°C overnight. The polymer was twice precipitated into hexanes, filtered, washed with water (to remove unreacted lithium salt monomer), and dried *in vacuo* to give a white powder (1.82 g, 90%). ^{1}H-NMR (ppm, DMSO-d_6): δ 7.30-6.30 (m, 9H, aromatic-H); 2.00-1.00 (m, 6H, aliphatic-H). ^{19}F-NMR (ppm, DMSO-d_6): δ -80.5 (2F); -117.8 (2F).

Poly[styrene-co-2-(4-ethenylphenoxy)tetrafluoroethanesulfonic acid hydrate] (**8-17**) and *poly[styrene-co-silver 2-(4-ethenylphenoxy)tetrafluoro-ethanesulfonate]* (**8-18**): Poly[styrene-co-lithium 2-(4-ethenylphenoxy)tetra-fluoroethanesulfonate] (**8-16**, 1.28 g) was dissolved in 5 mL THF and slowly passed through Amberlite IR-120 (plus) ion exchange resin (previously washed several times with dilute HCl, water, and THF) using THF as the eluent. The THF fractions were concentrated to about 20 mL, and excess silver carbonate (~2.0 g) was added. The resulting mixture was stirred overnight in the dark, filtered through a bed of celite, and washed with THF. The filtrate was

concentrated to about 5 mL, precipitated into hexanes, and dried *in vacuo* to yield white powder (1.52 g, 94%). ^{1}H-NMR (ppm, DMSO-d_6): δ 7.30-6.30 (m, 9H, Ar-H); 2.00-1.10 (m, 6H, aliphatic-H). ^{19}F-NMR (ppm, DMSO-d_6): δ -81.5 (2F); -117.2 (2F).

Poly[styrene-co-dimethylphenylsulfonium 2-(4-ethenylphenoxy)tetra-fluoroethanesulfonate] (**8-1**): Thioanisole (0.100 g, 0.797 mmol) was added to poly[styrene-co-silver 2-(4-ethenylphenoxy)tetrafluoro-ethanesulfonate] (**8-18**, 1.07 g, 7.97 mmol) dissolved in freshly distilled THF (20 mL). The solution was cooled to 0°C with an ice water bath. Iodomethane (0.565 g, 3.98 mmol) was added dropwise, and silver iodide precipitated immediately. The resulting mixture was stirred in the dark at room temperature for 20 h, filtered through a bed of celite, and then filtered through a 0.45 μm filter. The filtrate was concentrated to half its initial volume, precipitated into hexanes, and dried *in vacuo* to yield a white powder (0.61 g, 57%). ^{1}H-NMR (ppm, $CDCl_3$): δ 7.60-6.20 (m, 14H, Ar-H); 3.39 (bs, 6H, SCH_3); 2.00-0.80 (m, 6H, aliphatic-H). ^{19}F-NMR (ppm, $CDCl_3$): δ -81.7 (2F); -117.2 (2F).

1-Bromo-2-phenoxytetrafluoroethane (**8-20**): Phenol (50.0 g, 531 mmol) was dissolved in 500 mL of 1.062 *N* potassium hydroxide in methanol. This solution was evaporated to dryness on a rotary evaporator and the resulting solid was dried at 140°C and 0.1 mm Hg. The solid (**8-19**) was mixed with 1 L of DMSO under argon. 1,2-Dibromotetrafluoroethane (152 g, 584 mmol) was added dropwise at 30-40°C. The resulting mixture was heated to 60°C for 6 h. It was cooled to room temperature and diluted to 2 L with ice and water. The organic

layer was separated and the aqueous solution was extracted with 2x100 mL of methylene chloride. The methylene chloride extracts were concentrated on a rotary evaporator and the residue combined with the original organic layer. This material was washed with 2x400 mL of water, dried over anhydrous magnesium sulfate, and filtered. The filtrate was distilled under reduced pressure giving 77.8 g (51%) of product, bp 81-85°C at 40 mm Hg. ^{1}H-NMR (ppm, $CDCl_3$): δ 7.41-7.18 (m, 5H, Ar-H). ^{19}F-NMR (ppm, $CDCl_3$): δ -68.4 (2F); -86.3 (2F).

Sodium 2-phenoxytetrafluoroethanesulfinate (**8-21**): 1-Bromo-2-phenoxytetrafluoroethane (**8-20**, 74.0 g, 271 mmol) was added under argon to a stirred mixture of 250 mL of distilled and deoxygenated water, sodium bicarbonate (47.8 g, 569 mmol), 250 mL of acetyl nitrile, and sodium dithionite (94.4 g, 542 mmol). This mixture was heated to 65°C resulting in a rapid gas evolution. Gas evolution ceased after about 1 h and the mixture was heated to 70-75°C for 3 h. It was cooled to about 10°C in an ice water bath and 300 mL of ethyl acetate was added. The mixture was filtered and the solid was washed with ethyl acetate. The combined filtrates were separated into aqueous and organic layers and the organic layer was washed with 4x50 mL of saturated aqueous sodium chloride solution. The organic layer was concentrated on a rotary evaporator to about ¼ its initial volume and filtered. The solid was washed with ethyl acetate. The combined organic solutions were concentrated to dryness on a rotary evaporator giving 44.0 g (58%) of white solid, which was converted to the sulfonyl chloride without further purification. ^{1}H-NMR (ppm, DMSO-d_6): δ 7.46-7.19 (m, 5H, Ar-H). ^{19}F-NMR (ppm, DMSO-d_6): δ -81.6 (2F); -132.5 (2F).

2-Phenoxytetrafluoroethanesulfonyl chloride (**8-22**): Sodium 2-phenoxytetrafluoroethanesulfinate (**8-21**, 44.0 g, 157 mmol) was dissolved in a mixture of 100 mL distilled and deoxygenated water and 50 mL of 1,1,2-trichlorotrifluoroethane (CFC-113) in a round-bottom flask equipped with a dry-ice condenser and cooled to 5-15°C. Chlorine gas (22.3 g, 314 mmol) was bubbled into this mixture over about 1 h. The resulting yellow mixture was stirred 1 h without external cooling. It was warmed to 20°C and an additional 50 mL of CFC-113 was added. The organic layer was separated and the aqueous solution was extracted with 50 mL of CFC-113. The combined organic solutions were dried over anhydrous magnesium sulfate and concentrated on a rotary evaporator. The residue was distilled through a short Vigreux column giving 20.4 g (44%) of product, bp 48-55°C at 0.80 mm Hg. ^{1}H-NMR (ppm, $CDCl_3$): δ 7.43-7.18 (m, 5H, Ar-H). ^{19}F-NMR (ppm, $CDCl_3$): δ -78.6 (2F); -107.8 (2F).

Lithium 2-phenoxytetrafluoroethanesulfonate (**8-23**): Lithium hydroxide monohydrate (4.30 g, 103 mmol) was dissolved in 50 mL deoxygenated distilled water. THF (15 mL) was added and this solution was heated to 35°C. The heat source was removed and 2-phenoxytetrafluoroethanesulfonyl chloride (**8-22**, 15.0 g, 51.3 mmol) was added dropwise over 45 min at a rate so that the exotherm maintained the solution at about 55°C. After the addition was complete, the solution was held at 55°C for an additional 1.5 h. The solution was cooled to room temperature. Its pH was adjusted to 7 by addition of concentrated hydrochloric acid and the aqueous solution was evaporated to dryness on the rotary evaporator. The solid was slurried with ether and filtered. The ether

solution was treated with three volumes of hexane resulting in deposition of a white solid. The solid was filtered off and washed with hexane. The filtrate was evaporated and the residue was again precipitated from ether solution by addition of hexane. The combined precipitates were recrystallized from acetonitrile with cooling in the refrigerator with the filtrate concentrated several times to collect additional fractions. The combined recrystallized product was dissolved in ether, filtered, and concentrated on a rotary evaporator. The product was dried at 100°C and 0.1 mm Hg giving 14.3 g (99%) of white solid. ^{1}H-NMR (ppm, DMSO-d_6): δ 7.49-7.18 (m, 5H, Ar-H). ^{19}F-NMR (ppm, DMSO-d_6): δ -81.3 (2F); -117.2 (2F).

2-Phenoxytetrafluoroethanesulfonic acid hydrate (**8-24**): Lithium 2-phenoxytetrafluoroethanesulfonate (**8-23**, 14.4 g, 51.3 mmol) was dissolved in 20 mL water and slowly passed through Amberlite IR-120 (plus) ion exchange resin (previously washed several times with THF, dilute HCl, and water) using water as the eluent. The water fractions were concentrated to dryness, yielding a white solid (13.50 g, 90%). ^{1}H-NMR (ppm, DMSO-d_6): δ 7.49-7.18 (m, 5H, Ar-H); 4.82 (bs, H, H_2O and SO_3H). ^{19}F-NMR (ppm, DMSO-d_6): δ -81.2 (2F); -117.2 (2F).

Silver 2-phenoxytetrafluoroethanesulfonate (**8-25**): 2-Phenoxytetrafluoroethanesulfonic acid hydrate (**8-24**, 13.5 g, 46.2 mmol) was dissolved in 100 mL water. Silver carbonate (25.5 g, 92.4 mmol) was slowly added to the solution, at which time bubbling was immediately observed due to the formation of water and carbon dioxide. The mixture was stirred overnight in the dark and filtered to

remove unreacted silver carbonate. The filtrate was concentrated and dried under vacuum at 50°C for 5 h to yield a grayish powder (15.5 g, 88%). ^{1}H-NMR (ppm, D_2O): δ 7.40-7.15 (m, 5H, Ar-H). ^{19}F-NMR (ppm, D_2O): δ -82.2 (2F); -118.0 (2F).

Poly[styrene-co-4-methylsulfanylstyrene] (**8-26**): The same procedure was used to make three different copolymer ratios (x = 10, 20, 30; y = 90, 80, 70). Into a 100 mL round-bottom flask equipped with a magnetic stir bar and reflux condenser were added 1-(methylsulfanyl)-4-vinylbenzene (0.721 g, 4.81 mmol), styrene (5.00 g, 43.3 mmol), and AIBN (0.103 g, 0.625 mmol) in 50 mL freshly distilled THF. The solution was frozen, evacuated, thawed, and purged with argon three times before being heated at 80°C for 18 h. The polymer was twice precipitated into methanol, filtered, and dried *in vacuo* to yield white powder (5.50 g, 94%). ^{1}H-NMR (ppm, $CDCl_3$): δ 7.20-6.25 (m, 9H, aromatic-H); 2.41 (bs, 3H, S-CH_3); 2.10-0.85 (m, 6H, aliphatic-H). GPC (THF): M_w = 14,600; M_n = 6,330; DPI = 2.306.

Poly[styrene-co-dimethyl-4-vinylphenylsulfonium 2-phenoxytetrafluro-ethanesulfonate] (**8-2**): Silver 2-phenoxytetrafluoroethanesulfonate (**8-25**, 0.735 g, 1.93 mmol) was added to a solution of poly[styrene-co-4-methylsulfanylstyrene] (**8-26**, 2.00 g, 18.4 mmol) in freshly distilled THF (50 mL). The resulting solution was cooled to 0°C using an ice water bath. Iodomethane (0.223 g, 1.57 mmol) was added dropwise to the cooled solution. The formation of yellow precipitate (AgI) was immediately observed. The mixture was stirred in the dark at room temperature for an additional 20 h, filtered

through a bed of celite, and then filtered through a 0.45 μm filter. The filtrate was concentrated to half its initial volume, precipitated into hexanes, and dried *in vacuo* to yield a white powder (2.22 g, 88%). ^{1}H-NMR (ppm, $CDCl_3$): δ 7.40-6.25 (m, 14H, Ar-H); 3.40-3.15 (bs, 6H, SCH_3); 2.10-1.10 (m, 6H, aliphatic-H). ^{19}F-NMR (ppm, $CDCl_3$): δ -81.6 (2F); -117.2 (2F). GPC (THF): M_w = 14,600; M_n = 6,330; PDI = 2.306.

Dimethylphenylsulfonium 2-phenoxytetrafluoroethanesulfonate (**8-3**): Silver 2-phenoxytetrafluoroethanesulfonate (**8-25**, 2.00 g, 5.25 mmol) was added to a solution of thioanisole (0.652 g, 5.25 mmol) in dry acetonitrile (20 mL). The resulting solution was cooled to 0°C using an ice water bath. Iodomethane (0.819 g, 5.77 mmol) was added dropwise to the cooled solution. The formation of yellow precipitate (AgI) was immediately observed. The mixture was stirred in the dark at room temperature for an additional 20 h, filtered through a bed of celite, and then filtered through a 0.45 μm filter. The solvent was evaporated, and the crude solid was redissolved in a minimum amount of acetonitrile. Diethyl ether was added dropwise to this solution until a persistent cloudiness was observed in the solution. The resulting solution was cooled in the refrigerator for 24 h, and filtration provided pure, crystallized product (0.96 g, 89%). ^{1}H-NMR (ppm, Acetone-d_6): δ 8.20-7.25 (m, 10H, Ar-H); 3.49 (s, 6H, SCH_3). ^{19}F-NMR (ppm, Acetone-d_6): δ -82.3 (2F); -118.0 (2F).

APPENDIX B: *SYNTHESIS OF 1-(DIMETHYLAMINO)-1,2-DIMETHYLDISILANE*

Significant effort was expended in synthesizing a silylating agent for use in a top-surface imaging (TSI) approach to pattern small features on a silicon substrate. In this thin film imaging technique (Figure B.1), only the top surface (100-200 nm) of the resist is exposed. Exposure causes the generation of a photoacid that catalyzes the deprotection of a polymer such as PTBOCST. The

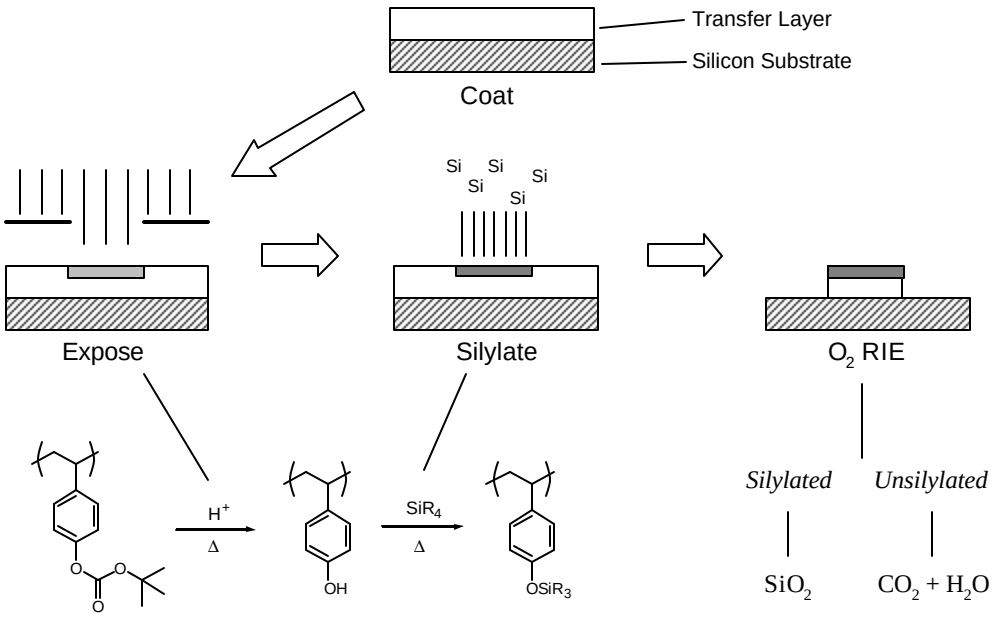

Figure B.1: The top-surface imaging technique used for high-resolution imaging.

free hydroxyl groups are then selectively silylated with a silylating agent. During an anisotropic etch step using oxygen plasma as the etchant, the resulting imaged

top layer is transferred into the thicker underlying layer to produce three-dimenional patterns. In regions where silicon is present, a silicon oxide layer is formed that resists further etching while the other areas form only volatile oxides.

1-(Dimethylamino)-1,2-dimethyldisilane was chosen as the silylating agent because the molecular weight of the functionality that is transferred by this reagent [-$SiH(CH_3)SiH_2(CH_3)$] is closer to the molecular weight of the gaseous byproducts lost (CO_2 and isobutylene) than other silylating agents such as dimethylaminodimethylsilane. The film thickness lost from evaporation of carbon dioxide and isobutylene, therefore, is compensated by adding a silylating agent with a similar molecular weight. This minimizes distortion of latent images.

Two methods were used to make 1-(dimethylamino)-1,2-dimethyldisilane.[169] The first method involved one extra synthetic step, but it is a much safer route. The second route involved the reduction of 1,1,2,2-tetrachloro-1,2-dimethyldisilane to 1,2-dimethyldisilane, which may spontaneously disproportionate into silane gas, which is pyrophoric.

PATHWAY A

The first synthetic scheme is shown in Figure B.2. 1-Chloro-1,1,2,2,2-pentamethyldisilane (**B-1**) was subjected to Friedel-Crafts acylation conditions ($AlCl_3$ and acetyl chloride) to make 1,1,2,2-tetrachloro-1,2-dimethyldisilane (**B-2**). Hexamethyldisilane may also be used with the correct amount of $AlCl_3$ and acetyl chloride to make the same product, but a large quantity of the starting **B-1**

[169] Both syntheses were generously provided by Dr. David Wheeler of Sandia National Laboratories.

compound was available, so it was used instead. 1,1,2,2-Tetrachloro-1,2-dimethyldisilane was then treated with 4-methylnaphthyl Grignard reagent to make 1,1,2-trichloro-1,2-dimethyl-2-(4-methyl-naphthalen-1-yl)-disilane (**B-3**). Reduction by lithium aluminum hydrided afforded 1,2-dimethyl-1-(4-methyl-naphthalen-1-yl)-disilane (**B-4**). Bromination with hydrogen bromide (to give **B-5**), followed by dimethylamination, provided the desired target compound, 1-(dimethylamino)-1,2-dimethyldisilane (**B-6**). The overal yield from 1,1,2,2-tetrachloro-1,2-dimethyldisilane to the product is 51%.

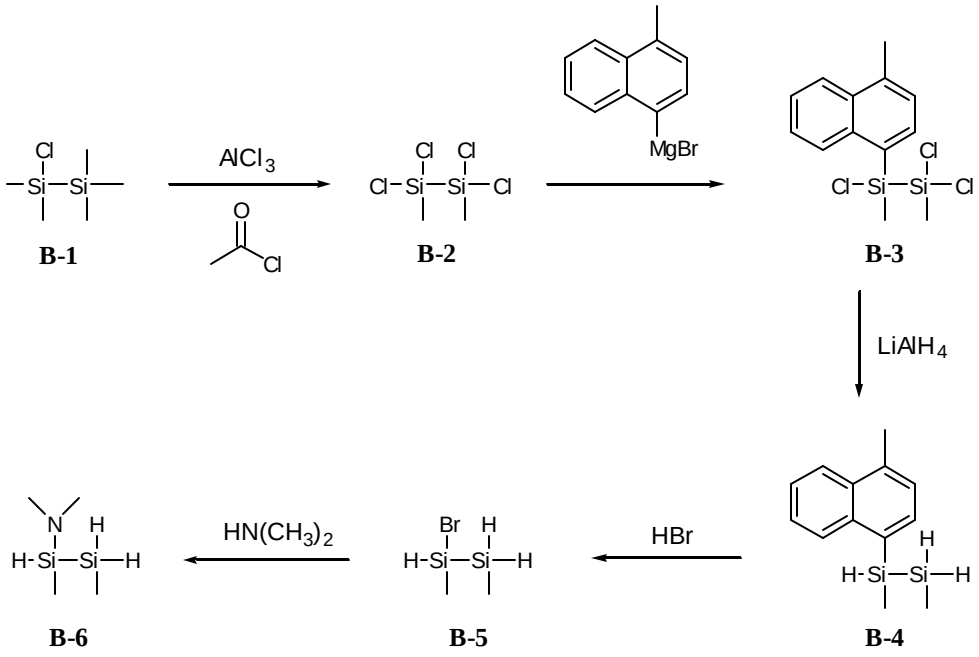

Figure B.2: The first synthetic route for making 1-(dimethylamino)-1,2-dimethyldisilane.

PATHWAY B

An alternative route to the product involved first the reduction of 1,1,2,2-tetrachloro-1,2-dimethyldisilane (**B-2**) with lithium aluminum hydride (Figure B.3). The resulting product, 1,2-dimethyldisilane (**B-7**) was converted directly to 1-chloro-1,2-dimethyldisilane (**B-8**) by reaction with copper chloride and UV light. Dimethylamination provided the desired product (**B-6**). The overal yield of this path from 1,1,2,2-tetrachloro-1,2-dimethyldisilane is 35%, which is somewhat lower than the first path even though a step was eliminated.

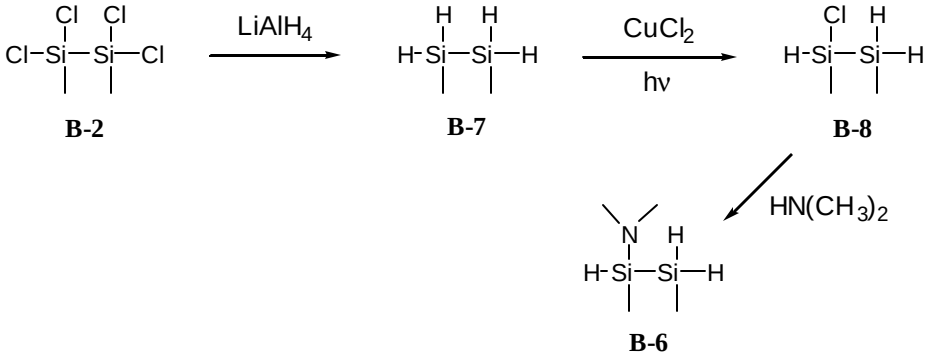

Figure B.3: An alternative route to 1-(dimethylamino)-1,2-dimethyldisilane.

EXPERIMENTAL SECTION

1,1,2,2-Tetrachloro-1,2-dimethyldisilane (**B-2**): Into an argon purged 500 mL three-neck flask equipped with a magnetic stir bar, condenser and an addition funnel was added aluminum chloride (139 g, 1.04 mol). Into this same flask was added (all at once) 1-chloro-1,1,2,2,2-pentamethyldisilane (52.51 g, 0.315 mol)

(slightly exothermic). Acetyl chloride (81.72 g, 1.04 mol) was then added to the addition funnel and added dropwise (exothermic!) to the solution in the flask. The flask was vigorously stirred and shaken for the first 30 min of addition. The acetyl chloride was added over a period of 2 h, at which time the solution became dark red. The resulting mixture was heated at 130°C for 20 h under an argon atmosphere. A ^{1}H-NMR ($CDCl_3$) of an aliquot of the mixture was taken to determine the amount of conversion. Based on the integrations, about 80% of starting material was converted to 1,1,2,2-tetrachloro-1,2-dimethyldisilane, while 20% was 1,1,2-trichloro-1,2,2-trimethyldisilane. Therefore, additional calculated amounts (based on the starting disilane in moles – 20% more) of aluminum chloride (8.20 g, 61 mmol) and acetyl chloride (4.82 g, 61 mmol) were added. The reaction mixture was stirred for an additional 2 h. The resulting mixture was then vacuum distilled (quickly, through a short-path distillation setup without using water to cool – just air) from the reaction flask into a flask cooled with a liquid nitrogen trap. It is important to keep the reaction mixture warm and to not let it solidify in the flask. Disposal of the leftover mixture should also be done when the liquid is warm. A clear liquid was collected in the flask (66.58 g, 93%) and stored under an argon atmosphere in the refrigerator. ^{1}H-NMR (ppm, $CDCl_3$): δ 0.992 (s, 6H, $C\underline{H}_3$). Based on ^{1}H-NMR integrations: 98% of 1,1,2,2-tetrachloro-1,2-dimethyldisilane, 2% 1,1,2-trichloro-1,2,2-trimethyldisilane.

1,1,2-Trichloro-1,2-dimethyl-2-(4-methyl-naphthalen-1-yl)-disilane (**B-3**) and *1,2-Dimethyl-1-(4-methyl-naphthalen-1-yl)-disilane* (**B-4**): Oven-dried magnesium filings (4.36 g, 0.180 mol) were added to a 500 mL round-bottom

flask fitted with a magnetic stirrer and an addition funnel containing 150 mL distilled ether. 1-Bromo-4-methylnaphthalene (27.5 g, 0.120 mol) was slowly added dropwise over 30 min to the magnesium filings and a minimum amount of ether (10 mL). One crystal of iodine was added to help initiate the formation of the Grignard reagent. After initiation the rest of the ether was added to the reaction mixture so as to maintain gentle reflux. The solution was heated at reflux for an additional 2 h and then cooled to room temperature. At this point the methylnaphthyl Grignard phase separated. This is normal. 1,1,2,2-Tetrachloro-1,2-dimethyldisilane (30.00 g, 0.132 mol) was added to 150 mL anhydrous ether in a separate 500 mL round-bottom flask fitted with a magnetic stirrer, reflux condenser, and addition funnel. The flask was cooled to 0°C, and the freshly prepared Grignard reagent was added to the addition funnel via a cannula. This was then added dropwise to the disilane solution. The reaction mixture was stirred at 0°C for 4 h. Lithium aluminum hydride (3.75 g, 99 mmol) was dissolved in 50 mL THF and this solution was added dropwise to the reaction mixture (exothermic!). After stirring for an additional 1 h at 0°C, saturated ammonium chloride (200 mL) was added dropwise (violent bubbling!) until the bubbling stopped. The ether layer was separated, washed with saturated ammonium chloride (2 x 100 mL), dried with $MgSO_4$, and concentrated *in vacuo*. The crude product was vacuum distilled to yield a colorless liquid (110°C / 0.20 mm Hg, 18.65 g, 61%). ^{1}H-NMR (ppm, Cyclohexane-d_{12}): δ 8.04-7.15 (m, 6H, Ar-H); 4.80 (t/m, 1H, R_2Si-H); 3.69 (d/m, 2H, $RSiH_2$); 2.61 (s, 3H, Ar-CH_3); 0.56 (d, 3H, $RHSiCH_3$); 0.10 (t, 3H, H_2SiCH_3). (Note: One must run the NMR in a

nonchlorinated solvent because these solvents will react, by a radical mechanism initiated by radiation, with the disilane – the Si-H bond is cleaved.)

1-Bromo-1,2-dimethyldisilane (**B-5**) and *1-(Dimethylamino)-1,2-dimethyldisilane* (**B-6**): Into an argon purged 500 mL three-neck flask equipped with a magnetic stir bar and reflux condenser was added 1,2-dimethyl-1-(4-methyl-naphthalen-1-yl)-disilane (18.65 g, 81 mmol) in anhydrous pentane (200 mL). The solution was cooled to -78°C and hydrogen bromide (approximately 13.1 g, 0.162 mol, measured by difference by using the weight before and after of the gas cylinder) was bubbled into the solution through a glass tube. The solution turned yellow-brown at this point. After completion of the addition, the reaction mixture was warmed to -20°C and dimethylamine (approximately 14.6 g, 0.324 mol) was bubbled into the solution. In the first 2 equivalents of addition the entire flask is filled with white precipitate (Dimethylamine/hydrogen bromide salt), but afterwards the white precipitate settles into the solution. Vigorous stirring is necessary. The reaction mixture was stirred at room temperature overnight under an argon atmosphere. The solution was filtered into another 500 mL three-neck flask by Schlenck techniques and washed with additional anhydrous pentane. The pentane was distilled out using a Vigreaux column and a short-path distillation setup at normal pressure under argon. 1-(Dimethylamino)-1,2-dimethyldisilane was then distilled under vacuum into a pre-weighed flask cooled with liquid nitrogen. (Some methylnaphthalene also distills out with the disilane.) The resulting solution was then distilled again to remove the rest of the pentane and 4-methylnaphthalene. This afforded the desired colorless liquid (8.91 g, 83%). ^{1}H-

NMR (ppm, Cyclohexane-d_{12}): δ 4.64 (t/m, 1H, R_2SiH); 3.50 (d/m, 2H, $RSiH_2$); 2.49 (s, 6H, CH_3NCH_3); 0.26 (d, 3H, $RHSiCH_3$); 0.13 (t, 3H, H_2SiCH_3).

1,2-Dimethyldisilane (**B-7**): Into an argon purged 500 mL three-neck flask equipped with a magnetic stir bar, addition funnel and reflux condenser was added lithium aluminum hydride (6.00 g, 0.158 mol) in *n*-butyl ether (150 mL). To this vigorously stirred mixture was added dropwise 1,1,2,2-tetrachloro-1,2-dimethyldisilane (30.0 g, 0.132 mol) (exothermic!). The resulting mixture was stirred 30 min while hot and then vacuum distilled (quickly, through a short-path distillation setup) from the reaction flask into a flask cooled with liquid nitrogen. A colorless solution was collected that is composed of both the product and some *n*-butyl ether. This solution was then redistilled under an argon atmosphere to collect pure 1,2-dimethyldisilane (35-40°C, 9.15 g, 77%). ^{1}H-NMR (ppm, Benzene-d_6): δ 3.68 (t/m, 4H, SiH); 0.02 (t/m, 6H, $SiCH_3$).

1-Chloro-1,2-dimethyldisilane (**B-8**) and *1-(Dimethylamino)-1,2-dimethyldisilane* (**B-6**): Into an argon purged 250 mL three-neck flask equipped with a magnetic stir bar, powder addition funnel and a reflux condenser was added 1,2-dimethyldisilane (9.00 g, 0.100 mol) in 100 mL anhydrous pentane. The solution was cooled to 15°C (manipulation of an ice bath), and copper chloride (6.05 g, 45 mmol) was added through a powder addition funnel. The reaction mixture was kept at 15-20°C with stirring under an argon atmosphere. The reaction was irradiated with 366 nm light until commencement of hydrogen evolution and the simultaneous appearance of black copper metal precipitate. After continuous stirring for 2 h (or until hydrogen evolution ceases), the reaction

mixture was filtered into another argon purged 500 mL three-neck flask equipped with a magnetic stir bar, reflux condenser and glass tube. The black copper residue was washed twice with additional anhydrous pentane (100 mL total) and the combined solution was stirred at -20°C. Dimethylamine (approximately 11.25 g, 0.250 mol) was bubbled into the solution through the glass tube. In the first 2 equivalents of addition the entire flask was filled with white precipitate (Dimethylamine/hydrogen chloride salt), but afterwards the white precipitate settled into the solution. Vigorous stirring was necessary. The reaction mixture was stirred at room temperature overnight under an argon atmosphere. The solution was filtered into another 500 mL three-neck flask by Schlenck techniques and washed with additional anhydrous pentane. The pentane was distilled out using a Vigreaux column and a short-path distillation setup at normal pressure under argon. 1-(Dimethylamino)-1,2-dimethyldisilane was then distilled under vacuum into a pre-weighed flask cooled with liquid nitrogen. The resulting solution was then distilled again under argon to remove the rest of the pentane and other impurities. This afforded the desired colorless liquid (105-110°C, 6.16 g, 46%). ^{1}H-NMR (ppm, Cyclohexane-d_{12}): δ 4.64 (t/m, 1H, R_2SiH); 3.50 (d/m, 2H, $RSiH_2$); 2.49 (s, 6H, CH_3NCH_3); 0.26 (d, 3H, $RHSiCH_3$); 0.13 (t, 3H, H_2SiCH_3).

REFERENCES

Silicon Compounds (Silicones), In *Kirk-Othmer Encyclopedia of Chemical Technology*; 4th ed.; Kroschwitz, J. I.; Howe-Grant, M., Eds.; Wiley: New York, 1997; Vol. 22, p 1.

Agaskar, P. A. *Colloids and Surfaces* **1992**, *63*, 131-138.

Agaskar, P. A. *J. Chem. Soc., Chem. Commun.* **1992**, *63*, 131.

Allen, R. D.; Wallraff, G. M.; Hinsberg, W. D.; Conley, W. *J. Photopolym. Sci. Technol.* **1993**, *6*, 575.

Allen, R. D.; Wallraff, G. M.; Hinsberg, W. D.; Simpson, L. *J. Vac. Sci. Technol. B* **1991**, *9*, 3357.

Allen, R. D.; Wallraff, G. M.; Hinsberg, W. D.; Simpson, L.; Kunz, R. *Polymers for Microelectronics*, In *ACS Symposium Series 537*; Thompson, L. F.; Willson, C. G.; Tagawa, S., Eds.; American Chemical Society: Washington, DC, 1994; Chapter 11.

Allen, R. D.; Wallraff, G. M.; Hofer, D. C.; Kunz, R. R. *IBM J. Res. Develop.* **1997**, *41*, 95.

Arkles, B. *Silanes*, In *Handbook of Grignard Reagents*; Silverman, G.; Rakita, P., Eds.; Marcel Dekker: New York, 1996; Chap. 32; p 667.

Asakawa, K.; Ushirogouchi, T.; Nakase, M. *Proc. SPIE Int. Soc. Opt. Eng.* **1995**, *2438*, 563.

Atkins, P. W. *Physical Chemistry*, 5th ed.; W. H. Freeman and Company: New York, 1994; p 851.

Babb, D. A.; Ezzell, B. R.; Clement, K. S.; Richey, W. F.; Kennedy, A. P. *J. Polym. Sci., Part A: Polym. Chem.* **1993**, *31*, 3465.

Bernthsen, A. *Liebigs Ann. Chem.* **1884**, *224*, 1.

Bloomstein, T. M.; Horn, M. W.; Rothschild, M.; Kunz, R. R.; Palmacci, S. T.; Goodman, R. B. *J. Vac. Sci. Technol., B* **1997**, *15*, 2112-2116.

Bloomstein, T. M.; Rothschild, M.; Kunz, R. R.; Hardy, D. E.; Goodman, R. B.; Palmacci, S. T. *J. Vac. Sci. Technol., B* **1998**, *16*, 3154-3157.

Born, M.; Wolf, E. *Principles of Optics*, 6th ed.; Pergamon Press: Oxford, 1983; pp 415, 441.

Bowen, E. J.; Holder, N. J.; Woodger, G. B. *J. Phys. Chem*. **1962**, *66*, 2491.

Breunig, S.; Risse, W. *Makromol. Chem.* **1992**, *193*, 2915.

Brodsky, C.; Byers, J.; Conley, W.; Hung, R.; Yamada, S.; Patterson, K.; Somervell, M.; Trinque, B.; Tran, H. V.; Cho, S.; Chiba, T.; Lin, S. H.; Jamieson, A.; Johnson, H.; Vander Heyden, A.; Willson, C. G. *J. Vac. Sci. Technol. B* **2000**, *18*, 3396-3401.

Brook, M. A. *Hydrosilanes as Reducing Agents*, In *Silicon in Organic, Organometallic, and Polymer Chemistry*; Wiley: New York, 2000; Chap. 7.

Brook, M. A. *Silicones*, In *Silicon in Organic, Organometallic, and Polymer Chemistry*; Wiley: New York, 2000; Chap. 9.

Brook, M. A. *Formation of Si-C Bonds: The Synthesis of Functional Organosilanes*, In *Silicon in Organic, Organometallic, and Polymer Chemistry*; Wiley: New York, 2000; Chap. 12.

Brown, J. F., Jr.; Vogt, J. H., Jr.; Katchman, A.; Eustance, J. W.; Kiser, K. M.; Krantz, D. W. *J. Am. Chem. Soc.* **1960**, *82*, 6194.

Burger, C.; Kreuzer, F. H. *Polysiloxanes and Polymers Containing Siloxane Groups*, In *Silicon in Polymer Synthesis*; Kricheldorf, H. R., Ed.; Springer: Berlin, 1996; Chap. 3; p 113.

Cameron, J. F.; Mori, J. M.; Zydowsky, T. M.; Kang, D.; Sinta, R.; King, M.; Scaiano, J.; Pohlers, G.; Virdee, S.; Connolly, T. *Proc. SPIE-Int. Soc. Opt. Eng.* **1998**, *3333*, 680-691.

Chalk, A. J.; Harrod, J. F. *J. Am. Chem. Soc.* **1965**, *87*, 16.

Chiba, T.; Hung, R.; Yamada, S.; Trinque, B.; Yamachika, M.; Brodsky, C.; Patterson, K.; Vander Heyden, A.; Jamieson, A.; Lin, S. H.; Somervell,

M.; Byers, J.; Conley, W.; Willson, C. G. *J. Photopolym. Sci. Technol.* **2000**, *13*, 657-664.

Clarson, S. J.; Semlyen, J. A. *Siloxane Polymers*; Prentice Hall: Englewood Cliffs, 1993.

Coenjarts, C.; Cameron, J. F.; Deschamps, N.; Hambly, D.; Pohlers, G.; Scaiano, J. C.; Sinta, R. F.; Virdee, S.; Zampini, A. *Proc. SPIE-Int. Soc. Opt. Eng.* **1999**, *3678*, 1062-1073.

Connolly, J.; Chen, K. R.; Kwong, R.; Lawson, M.; Linehan, L.; Moreau, W. *Proc. SPIE Int. Soc. Opt. Eng.* **1998**, *3333*, 1124.

Crank, J.; Park, G. *Diffusion in Polymers*; Academic Press: New York, 1968.

Crivello, J. V., In *Radiation Curing in Polymer Science and Technology: Photoinitiating Systems*; Fouassier, J. P.; Rabek, J. F., Eds.; Elsevier: New York, 1993; Vol. II, Chapter 8.

Crivello, J. V. *J. Polym. Sci., Part A: Polym. Chem.* **1999**, *37*, 4241-4254.

Crivello, J. V.; Lam, J. H. W. *Macromolecules* **1977**, *10*, 1307.

Crivello, J. V.; Lam, J. H. W. *J. Org. Chem.* **1978**, *43*, 305.

Crivello, J. V.; Malik, R. *J. Polym. Sci., Part A: Polym. Chem.* **1997**, *35*, 407-425.

Cronin, M. F.; Adams, M.; Fedynyshyn, T. H.; Georger, J.; Mori, J. M.; Sinta, R.; Thackeray, J. W. *Proc. SPIE Int. Soc. Opt. Eng.* **1994**, *2195*, 214.

Dammel, R. *Diazonaphthoquinone-based Resists*; Tutorial Texts in Optical Engineering, v. TT 11; SPIE Optical Engineering Press: Bellingham, WA, 1993.

Davidson, I. M. T.; Thompson, J. F. *J. Chem. Soc., Chem. Commun.* **1971**, 251.

DeBroer, T. J.; Backer, H. J. *Org. Synth., Coll. Vol. 4* **1963**, 250.

Dentinger, P. M.; Lu, B.; Taylor, J. W.; Bukofsky, S. J.; Feke, G. D.; Hessman, D.; Grober, R. D. *J. Vac. Sci. Technol., B* **1998**, *16*, 3767-3772.

Diverdi, L. A.; Topp, M. R. *J. Phys. Chem.* **1984**, *88*, 3447-3451.

Drake, R.; MacKinnon, I.; Taylor, R. *Recent Advances in the Chemistry of Siloxane Polymers and Copolymers*, In *The Chemistry of Organic Silicon Compounds*; Rappoport, Z.; Apeloig, Y., Eds.; Wiley: Chichester, UK, 1998; Vol. 2, Chap. 38, p 2217.

Eaborn, C.; Bott, R. W. *Synthesis and Reaction of the Silicon-Carbon Bond*, In *The Bond to Carbon*; MacDiarmid, A. G., Ed.; Dekker: New York, 1968; Vol. 1, p 105.

Eckert, A. R.; Moreau, W. M. *Proc. SPIE-Int. Soc. Opt. Eng.* **1997**, *3049*, 879-887.

Eddy, V. J.; Hallgren, J. E. *J. Org. Chem.* **1987**, *52*, 1903.

Fasce, D. P.; Williams, R. J. J.; Mechin, F.; Pascault, J. P.; Llauro, M. F.; Petiaud, R. *Macromolecules* **1999**, *32*, 4757-4763.

Fedynyshyn, T. H.; Kunz, R. R.; Doran, S. P.; Goodman, R. B.; Lind, M. L.; Curtin, J. E. *Proc. SPIE Int. Soc. Opt. Eng.* **2000**, *3999*, 335.

Fedynyshyn, T. H.; Thackeray, J. W.; Georger, J. H.; Denison, M. D. *J. Vac. Sci. Technol. B* **1994**, *12*, 3888.

Feher, F. J.; Budzichowski, T. A.; Blanski, R. L.; Weller, K. J.; Ziller, J. W. *Organometallics* **1991**, *10*, 2526-2528.

Feher, F. J.; Weller, K. J. *Inorg. Chem.* **1991**, *30*, 880.

Feher, F. J.; Weller, K. J.; Ziller, J. W. *J. Am. Chem. Soc.* **1992**, *114*, 9686.

Feiring, A. E.; Choi, S. K.; Doyle, M.; Wonchoba, E. R. *Macromolecules* **2000**, *33*, 9262-9271.

Feiring, A. E.; Wonchoba, E. R. *J. Fluor. Chem.* **2000**, *105*, 129-135.

Feke, G. D.; Grober, R. D.; Pohlers, G.; Moore, K.; Cameron, J. F. *Analytical Chemistry* **2001**, *73*, 3472-3480.

Frechet, J. M. J.; Ito, H.; Willson, C. G. *Proc. Microcircuit. Eng.* **1982**, *82*, 260.

Frye, C. L.; Collins, W. T. *J. Am. Chem. Soc.* **1970**, *92*, 5586.

Frye, C. L.; Klosowski, J. M. *J. Am. Chem. Soc.* **1971**, *93*, 4599.

Gilman, H.; McNinch, H. A. *J. Org. Chem.* **1961**, *26*, 3723-3729.

Gokan, H.; Esho, S.; Ohnishi, Y. *J. Electrochem. Soc.: Solid State Sci. Tech.* **1983**, *130*, 143.

Goodall, B. L.; Benedikt, G. M.; McIntosh, L. H.; Barns, D. A. *U. S. Patent* **1995**, 5468819.

Grandler, J. R.; Jencks, W. P. *J. Am. Chem. Soc.* **1982**, *104*, 1937.

Gray, D. E., Ed. *American Institute of Physics Handbook*; McGraw-Hill: New York, 1972.

Hacker, N., In *Radiation Curing in Polymer Science and Technology: Photoinitiating Systems*; Fouassier, J. P.; Rabek, J. F., Eds.; Elsevier: New York, 1993; Vol. II, Chapter 9.

Hall, D. B.; Torkelson, J. M. *Macromolecules* **1998**, *31*, 8817-8825.

Harkness, B. R.; Takeuchi, K.; Tachikawa, M. *Macromolecules* **1998**, *31*, 4798-4805.

Hennis, A. D.; Polley, J. D.; Long, G. S.; Sen, A.; Yandulov, D.; Lipian, J.; Benedikt, G. M.; Rhodes, L. F.; Huffman, J. *Organometallics* **2001**, *20*, 2802-2812.

Hess, F.; Cullen, E.; Grozinger, K. *Tet. Let.* **1971**, *28*, 2591-2594.

Hien, S.; Angood, S.; Ashworth, D.; Basset, S.; Bloomstein, T. M.; Dean, K. R.; Kunz, R. R.; Miller, D. A.; Patel, S.; Rich, G. *Proc. SPIE Int. Soc. Opt. Eng.* **2001**, *4345*, 439-447.

Hinsberg, W.; Houle, F. A.; Hoffnagle, J.; Sanchez, M.; Wallraff, G.; Morrison, M.; Frank, S. *J. Vac. Sci. Technol., B* **1998**, *16*, 3689-3694.

Hinsberg, W.; MacDonald, S.; Clecak, N.; Snyder, C. *J. Photopolym. Sci. Technol.* **1993**, *6*, 535-546.

Hinsberg, W. D.; MacDonald, S. A.; Clecak, N. J.; Snyder, C. D. *Chem. Mater.* **1994**, *6*, 481-488.

Hinsberg, W. D.; MacDonald, S. A.; Clecak, N. J.; Snyder, C. D.; Ito, H. *Proc. SPIE-Int. Soc. Opt. Eng.* **1993**, *1925*, 43-52.

Hiyama, T.; Kusumoto, T. *Hydrosilylation of C=C and C? C*, In *Comprehensive Organic Synthesis*; Trost, B. M.; Fleming, I., Eds.; Pergamon: Oxford, 1991; Vol. 8, Chap. 3.12, p 763.

Homberger, A. W.; Jensen, H. *J. Am. Chem. Soc.* **1926**, *48*, 800-801.

Houlihan, F. M.; Kometani, J. M.; Timko, A. G.; Hutton, R. S.; Gabor, A.; Medina, A.; Biafore, J.; Slater, S. *Proc. SPIE Int. Soc. Opt. Eng.* **1998**, *3333*, 73.

Hung, R. J. Ph.D. Dissertation, University of Texas at Austin, 2001.

Hung, R. J.; Tran, H. V.; Trinque, B. C.; Chiba, T.; Yamada, S.; Sanders, D. P.; Connor, E. F.; Grubbs, R. H.; Kopp, J.; Frechet, J. M. J.; Thomas, B. H.; Shafer, G. J.; DesMarteau, D. D.; Conley, W.; Willson, C. G. *Proc. SPIE* **2001**, *4345*, 385-395.

Itani, T.; Yoshino, H.; Fujimoto, M.; Kasama, K. *J. Vac. Sci. Technol. B* **1995**, *13*, 3026.

Ito, H. *IBM J. Res. Develop.* **1997**, *41*, 69-80.

Ito, H.; Allen, R. D.; Opitz, J.; Wallow, T. I.; Truong, H. D.; Hofer, D. C.; Varanasi, P. R.; Jordhamo, G. M.; Jayaraman, S.; Vicari, R. *Proc. SPIE* **2000**, *3999*, 2-12.

Ito, H.; Breyta, G.; Sooriyakumaran, R.; Hofer, D. C. *J. Photopolym. Sci. Technol.* **1995**, *8*, 505.

Ito, H.; Willson, C. G. *Polym. Eng. Sci.* **1982**, *23*, 1021.

Jessop, J. L. P.; Goldie, S. N.; Scranton, A. B.; Blanchard, G. J. *Polym. Mater. Sci. Eng.* **2000**, *82*, 48-49.

Jessop, J. L. P.; Goldie, S. N.; Scranton, A. B.; Blanchard, G. J.; Rangarajan, B.; Capodieci, L.; Subramanian, R.; Templeton, M. K. *Proc. SPIE-Int. Soc. Opt. Eng.* **1999**, *3678*, 914-922.

Kaimoto, Y.; Nozaki, K.; Takechi, S.; Abe, N. *Proc. Soc. Photo-Opt. Instrum. Eng.* **1992**, *1672*, 66.

Klabunde, K. J.; Anderson, B. B.; Bader, M. *Inorg. Synth.* **1979**, *19*, 72.

Knunyants, I. L. *et al*. *J. Fluor. Chem.* **1975**, *6*, 227-240.

Koros, W. J.; Hellums, M. W. *Transport Properties*, In *Encyclopedia of Polymer Science and Engineering*; 2nd ed., 1989.

Krasnoperova, A. A.; Khan, M.; Rhyner, S.; Taylor, J. W.; Zhu, Y.; Cerrina, F. *J. Vac. Sci. Technol. B* **1994**, *12*, 3900.

Kunz, R.; Allen, R. D.; Hinsberg, W. D.; Wallraff, G. M. *Proc. Soc. Photo-Opt. Instrum. Eng.* **1993**, *1925*, 167.

Kunz, R. R.; Bloomstein, T. M.; Hardy, D. E.; Goodman, R. B.; Downs, D. K.; Curtin, J. E. *J. Vac. Sci. Technol., B* **1999**, *17*, 3267-3272.

Lackowicz, J. R. *Principles of Fluorescence Spectroscopy*; Plenum Press: New York, 1986; Chapters 1-2.

Laine, R. M.; Sellinger, A. *Chem. Mater.* **1996**, *8*, 1592-1593.

Laine, R. M.; Sellinger, A. *Macromolecules* **1996**, *29*, 2327-2330.

Laine, R. M.; Zhang, C. *J. Organomet. Chem.* **1996**, *521*, 199-201.

Lehr, R. E.; Kaul, P. N. *J. Pharm. Sci.* **1975**, *64(6)*, 950-953.

Lin, E. K.; Wu, W.-l.; Satija, S. K. *Macromolecules* **1997**, *30*, 7224-7231.

Lin, S. T.; Narske, R. N.; Klabunde, K. J. *Organometallics* **1985**, *4*, 571-574.

Loy, D. A.; Shea, K. J. *Chem. Rev. (Washington, D. C.)* **1995**, *95*, 1431-1442.

MacDonald, S. A.; Hinsberg, W. D.; Wendt, H. R.; Clecak, N. J.; Willson, C. G.; Snyder, C. D. *Chem. Mater.* **1993**, *5*, 348-356.

MacDonald, S. A.; Willson, C. G.; Frechet, J. M. J. *Acc. Chem. Res.* **1994**, *27*, 151-158.

Maercker, A. *Angew. Chem. Int. Ed. Engl.* **1987**, *26*, 972-989.

Malone, M. S. *The Big Score: The Billion Dollar Story of Silicon Valley*; Doubleday: New York, 1985; p 141.

Malone, M. S. *The Microprocessor: A Biography*; Springer-Verlag: New York, 1995; p 10-20.

Marciniec, B.; Gulinski, J.; Urbaniak, W.; Kornetka, Z. W. *Comprehensive Handbook on Hydrosilylation Chemistry*; Pergamon: Oxford, 1992.

Mark, J. E. *Polym. Prepr. (Am. Chem. Soc., Div. Polym. Chem.)* **1998**, *39*, 437-438.

Martynova, T. N.; Korchkov, V. P.; Smyannikov, P. P. *J. Organomet. Chem.* **1983**, *258*, 277.

Maruno, T.; Nakamura, K.; Murata, N. *Macromolecules* **1996**, *29*, 2006-2010.

Mataga, N.; Kaifu, Y.; Koizumi, M. *Bull. Chem. Soc. Jpn.* **1956**, *29*, 373.

Mathew, J. P.; Reinmuth, A.; Melia, J.; Swords, N.; Risse, W. *Macromolecules* **1996**, *29*, 2755-2763.

McAdams, C. L.; Tsiartas, P.; Willson, C. G. *Polym. Mater. Sci. Eng.* **1997**, *77*, 437-438.

McGrath, M.; Sall, E.; Tremont, S. *Chem. Rev.* **1995**, *95*, 381.

McKean, D.; Schaedili, U.; MacDonald, S. *Polymers in Microlithography*, In *ACS Symposium Series 412*; Reichmanis, E.; MacDonald, S.; Iwayanagi, T., Eds.; American Chemical Society: Washington, DC, 1989; p 27.

McKean, D. R.; Schaedeli, U.; MacDonald, S. A. *J. Polym. Sci., Part A: Polym. Chem.* **1989**, *27*, 3927.

Medeiros, D. R. Ph.D. Dissertation, University of Texas at Austin, 1998.

Meyer, W. H. *Adv. Mater. (Weinheim, Ger.)* **1998**, *10*, 439-448.

Moller, U.; Cech, D.; Schubert, F. *Liebigs Ann. Chem.* **1990**, *12*, 1221-1225.

Moore, G. E. *Electronics* **1965**, *38*, 1.

Mucha, J. A.; Hess, D. W.; Aydil, E. S., In *Introduction to Microlithography*; 2nd ed.; Thompson, L. F.; Willson, C. G.; Bowden, M. J., Eds.; American Chemical Society: Washington, DC, 1994; Chapter 5.

Mueller, K. E.; Koros, W. J.; Mack, C. A.; Willson, C. G. *Proc. SPIE Int. Soc. Opt. Eng.* **1997**, *3049*, 706.

Nakamura, J.; Ban, H.; Deguchi, K.; Tanaka, A. *Jpn. J. Appl. Phys.* **1991**, *10*, 6065.

Nakamura, J.; Ban, H.; Tanaka, A. *Jpn. J. Appl. Phys.* **1992**, *31*, 4294-4300.

Nakano, K.; Maeda, K.; Iwasa, S.; Hasegawa, E. *Proc. SPIE Int. Soc. Opt. Eng.* **1995**, *2438*, 433.

Namatsu, H.; Takahashi, Y.; Yamazaki, K.; Yamaguchi, T.; Nagase, M.; Kurihara, K. *J. Vac. Sci. Technol. B* **1998**, *16*, 69-76.

Namatsu, H.; Yamaguchi, T.; Nagase, M.; Yamazaki, K.; Kurihara, K. *Microelectron. Eng.* **1998**, *41/42*, 331-334.

Noll, W. *Chemistry and Technology of Silicones*; Academic Press: New York, 1968.

Oikawa, A.; Hatakenaka, Y.; Ikeda, Y.; Kokubo, Y.; Miyata, S.; Santoh, N.; Abe, N. J. *J. Photopolym. Sci. Technol.* **1995**, *8*, 519.

Ojima, I. *The Hydrosilylation Reaction*, In *The Chemistry of Organic Silicon Compounds*; Patai, S.; Rappoport, Z., Eds.; Wiley: Chichester, UK, 1989; Vol. 1, Chap. 25, p 1479.

Ojima, I.; Li, Z.; Zhu, J. *Recent Advances in the Hydrosilylation and Related Reactions*, In *The Chemistry of Organic Silicon Compounds*; Rappoport, Z.; Apeloig, Y., Eds.; Wiley: Chichester, UK, 1998; Vol. 2, Chap. 29, p 1687.

Okoroanyanwu, U.; Byers, J.; Shimokawa, T.; Willson, C. G. *Chem. Mater.* **1998**, *10*, 3328-3333.

Okoroanyanwu, U.; Shimokawa, T.; Byers, J.; Medeiros, D. R.; Willson, C. G. *Proc. SPIE Int. Soc. Opt. Eng.* **1997**, *3049*, 92.

Okoroanyanwu, U.; Shimokawa, T.; Byers, J.; Willson, C. G. *Chem. Mater.* **1998**, *10*, 3319-3327.

Patterson, K. Ph.D. Dissertation, University of Texas at Austin, 2000.

Patterson, K.; Okoroanyanwu, U.; Shimokawa, T.; Cho, S.; Byers, J.; Willson, C. G. *Proc. SPIE Int. Soc. Opt. Eng.* **1998**, *3333*, 425-437.

Patterson, K.; Yamachika, M.; Hung, R.; Brodsky, C.; Yamada, S.; Somervell, M.; Osborn, B.; Hall, D.; Dukovic, G.; Byers, J.; Conley, W.; Willson, C. G. *Proc. SPIE Int. Soc. Opt. Eng.* **2000**, *3999*, 365-374.

Perkins, F. K.; Dobisz, E. A.; Marrian, C. R. K. *J. Vac. Sci. Technol. B* **1993**, *11*, 2597.

Perrin, D. D.; Armarego, W. L. F. *Purification of Laboratory Chemicals*, 3rd ed.; Butterworth-Heinemann Ltd: Oxford, 1994.

Petersen, J. S.; Byers, J. D. *Proc. SPIE Int. Soc. Opt. Eng.* **1996**, *2724*, 164.

Petersen, J. S.; Mack, C. A.; Sturtevant, J.; Byers, J. D.; Miller, D. A. *Proc. SPIE Int. Soc. Opt. Eng.* **1995**, *2438*, 167.

Petrov, A. D.; Mironov, B. F.; Ponomarenko, V. A.; Chernyshev, E. A. *Synthesis of Organosilane Monomers*; Consultants Bureau: New York, 1964.

Pohlers, G.; Virdee, S.; Scaiano, J. C.; Sinta, R. *Chem. Mater.* **1996**, *8*, 2654-2658.

Postnikov, S. V. Ph.D. Dissertation, University of Texas at Austin, 1999.

Postnikov, S. V.; Stewart, M. D.; Tran, H. V.; Nierode, M. A.; Medeiros, D. R.; Cao, T.; Byers, J.; Webber, S. E.; Wilson, C. G. *J. Vac. Sci. Technol., B* **1999**, *17*, 3335-3338.

Przybilla, K. J.; Kinoshita, Y.; Kudo, T.; Masuda, S.; Okazaki, H.; Padmanaban, M.; Pawlowski, G.; Roeschert, H.; Spiess, W.; Suehiro, N. *Proc. SPIE Int. Soc. Opt. Eng.* **1993**, *1925*, 76.

Quirk, M.; Serda, J. *Semiconductor Manufacturing Technology*; Prentice-Hall: Upper Saddle River, 2001; p 373.

Rahimian, K.; Assink, R. A.; Loy, D. A. *Polym. Prepr. (Am. Chem. Soc., Div. Polym. Chem.)* **2000**, *41*, 512-513.

Rau, N.; Neureuther, A. R.; Ogawa, T.; Kubena, R.; Stratton, F.; Fields, C.; Willson, C. G. *Proc. SPIE Int. Soc. Opt. Eng.* **1998**, *3333*, 1413.

Raulins, N. R., In *Acridines*; 2nd ed.; Acheson, R. M., Ed.; John Wiley & Sons: New York, 1973; Chapter 1.

Reichmanis, E.; Houlihan, F.; Nalamasu, O.; Neehan, T. *Chem. Mater.* **1991**, *3*, 394.

Reiser, A. *Photoreactive Polymers: The Science and Technology of Resists*; John Wiley & Sons: New York, 1989.

Rhodes, L. F.; Bell, A.; Jayaraman, S.; Lipian, J.; Goodall, B. L.; Shick, R. A. *International Patent* **1999**, WO 9914256.

Rico, I.; Wakselman, C. *J. Fluor. Chem.* **1982**, *20*, 759.

Rothschild, M.; Bloomstein, T. M.; Curtin, J. E.; Downs, D. K.; Fedynyshyn, T. H.; Hardy, D. E.; Liberman, V.; Sedlacek, J. H. C.; Uttaro, R. S.; Bates, A. K.; Van Peski, C. *J. Vac. Sci. Technol. B* **1999**, *17*, 3262-3266.

Rothschild, M.; Bloomstein, T. M.; Fedynyshyn, T. H.; Kunz, R. R.; Liberman, V.; Switkes, M. *J. Photopolym. Sci. Technol.* **2000**, *13*, 369-372.

Sakamizu, T.; Arai, T.; Yamaguchi, H.; Shiraishi, H. *Proc. SPIE Int. Soc. Opt. Eng.* **1997**, *3049*, 448.

Sanders, D. P.; Connor, E. F.; Grubbs, R. H.; Hung, R. J.; Osborn, B. P.; Tran, H. V.; MacDonald, S.; Willson, C. G. *Macromolecules* **2002**, submitted for publication.

Savadogo, O. *J. New Mater. Electrochem. Syst.* **1998**, *1*, 47-66.

Schlegel, L.; Ueno, T.; Hayashi, N.; Iwayanagi, T. *J. Vac. Sci. Technol. B* **1991**, *9*, 278.

Sen, A.; Hennis, A. D.; Polley, J. D.; Long, G. S.; Yandulov, D.; Lipian, J.; Benedikt, G. M.; Rhodes, L. F.; Huffman, J. *Organometallics* **2001**, *20*, 2802-2812.

Stark, F. O.; Falender, J. R.; Wright, A. P. *Silicones*, In *Comprehensive Organometallic Chemistry*; Wilkinson, G.; Stone, F. G. A.; Abel, E. W., Eds.; Pergamon: Oxford, 1982; Chap. 9.3; p 305.

Stewart, M. D.; Postnikov, S. V.; Tran, H. V.; Medeiros, D. R.; Nierode, M. A.; Cao, T.; Byers, J.; Webber, S. E.; Willson, C. G. *Polym. Mater. Sci. Eng.* **1999**, *81*, 58-59.

Stewart, M. D.; Somervell, M. H.; Tran, H. V.; Postnikov, S. V.; Willson, C. G. *Proc. SPIE Int. Soc. Opt. Eng.* **2000**, *3999*, 665-674.

Thackeray, J. W.; Denison, M. D.; Fedynyshyn, T. H.; Kang, D.; Sinta, R. *Microelectronics Technology, Polymers for Advanced Imaging and Packaging*, In *ACS Symposium Series 614*; Reichmanis, E.; Ober, C.; MacDonald, S.; Iwayanagi, T.; Nishikubo, T., Eds.; American Chemical Society: Washington, DC, 1995; p 84.

Thompson, L. F.; Willson, C. G.; Bowden, M. J. *Introduction to Microlithography*, 2nd ed.; American Chemical Society: Washington DC, 1994.

Tran, H. V.; Hung, R. J.; Chiba, T.; Yamada, S.; Mrozek, T.; Hsieh, Y. T.; Chambers, C. R.; Osborn, B. P.; Trinque, B. C.; Pinnow, M. J.; MacDonald, S. A.; Willson, C. G. *Macromolecules* **2002**, submitted for publication.

Tran, H. V.; Hung, R. J.; Chiba, T.; Yamada, S.; Mrozek, T.; Hsieh, Y. T.; Chambers, C. R.; Osborn, B. P.; Trinque, B. C.; Pinnow, M. J.; Sanders, D. P.; Connor, E. F.; Grubbs, R. H.; Conley, W.; MacDonald, S. A.; Willson, C. G. *J. Photopolym. Sci. Technol.* **2001**, *14*, 669-674.

Trinque, B. C.; Chiba, T.; Hung, R. J.; Chambers, C. R.; Pinnow, M. J.; Tran, H. V.; Wunderlich, J.; Hsieh, Y. T.; Thomas, B. H.; Shafer, G. J.;

DesMarteau, D. D.; Conley, W.; Willson, C. G. *J. Vac. Sci. Technol. B* **2001**, in press.

Uchino, S.; Yamamoto, J.; Migitaka, S.; Kojima, K.; Hashimoto, M.; Murai, F.; Shiraishi, H. *J. Photopolym. Sci. Technol.* **1998**, *11*, 555.

Uenishi, K.; Kawabe, Y.; Kokubo, T.; Slater, S.; Blakeney, A. *Proc. SPIE Int. Soc. Opt. Eng.* **1991**, *1466*, 102.

Van Amergedon, G. J. *Rubber Chem. Technol.* **1951**, *24*, 109.

van Delft, F. C. M. J. M.; Weterings, J. P.; van Langen-Suurling, A. K.; Romijn, H. *J. Vac. Sci. Technol. B* **2000**, *18*, 3419-3423.

Voronkov, M. G.; Yuzhelevskii, Y. A.; Mileshkevich, V. P. *Russ. Chem. Rev.* **1975**, *44*, 355.

Vrentas, J. S.; Liu, H. T.; Lau, M. K. *J. Appl. Polym. Sci.* **1982**, *27*, 3987.

Wakefield, B. J. *Organolithium Methods*; Academic Press: London, 1988; p 47-49.

Wallow, T. I.; Houlihan, F. M.; Nalamasu, O.; Chandross, E. A.; Neenan, T. X.; Reichmanis, E. *Proc. SPIE Int. Soc. Opt. Eng.* **1996**, *2724*, 255.

Wallraff, G. M.; Hinsberg, W. D. *Chem. Rev.* **1999**, *99*, 1801-1821.

Willson, C. G.; Yueh, W.; Leeson, M. J.; Steinhausler, T.; McAdams, C. L.; Dammel, R. R.; Sounik, J. R.; Aslam, M.; Vicari, R.; Sheehan, M. T. *Proc. SPIE-Int. Soc. Opt. Eng.* **1997**, *3049*, 226-237.

Woods, R. L.; Lyons, C. F.; Mueller, R.; Conway, J. *Proceedings of the KTI Microelectronics Seminar* **1988**, 341-359.

Yamada, S. Ph. D. Dissertation, University of Texas at Austin, 2000.

Yoshiyuki, T.; Nakayama, Y.; Okazaki, S. *J. Vac. Sci. Technol. B* **1992**, *10*, 2615.

Zhang, P. L.; Webber, S.; Mendenhall, J.; Byers, J. D.; Chao, K. *Proc. SPIE Int. Soc. Opt. Eng.* **1998**, *3333*, 794.

Zheng, L; Farris, R. J.; Coughlin, E. B. *J. Polym. Sci., Part A: Polym. Chem.* **2001**, *39*, 2920-2928.

Zuniga, M.; Neureuther, A. R. *J. Vac. Sci. Technol. B* **1995**, *13*, 2957.

VITA

Hoang Vi Tran was born on March 27, 1974 in Saigon, Vietnam to Vi Ba and Thi Rot Tran. He grew up in Roanoke, Virginia with his three sisters, Hue Linh, Tuyet Linh, and Ai Linh. After graduating from Patrick Henry High School, he enrolled in the College of William and Mary in Williamsburg, Virginia. He received a Bachelors of Science in Chemistry in May 1996 with a minor in Computer Science. During the summer and next academic year, he studied polymer chemistry under the supervision of Professor William H. Starnes and received his Master of Arts in Chemistry in August 1997. Shortly afterwards, he enrolled in the Doctor of Philosophy program at the University of Texas at Austin, working in the Organic Division of the Department of Chemistry and Biochemistry under the supervision of Professor C. Grant Willson.

Permanent address: 2327 Broadway Avenue, Roanoke, VA 24014

This dissertation was typed by the author.